

University of Nebraska - Lincoln

DigitalCommons@University of Nebraska - Lincoln

---

Theses, Dissertations, and Student Research from  
Electrical & Computer Engineering

Electrical & Computer Engineering, Department of

---


Spring 5-19-2011

# WIRELESS COMMUNICATIONS AND COGNITIVE RADIO TRANSMISSIONS UNDER QUALITY OF SERVICE CONSTRAINTS AND CHANNEL UNCERTAINTY

Sami Akin

*University of Nebraska-Lincoln*, [samiakin@huskers.unl.edu](mailto:samiakin@huskers.unl.edu)

Follow this and additional works at: <http://digitalcommons.unl.edu/elecengtheses>

 Part of the [Other Electrical and Computer Engineering Commons](#), [Signal Processing Commons](#),  
and the [Systems and Communications Commons](#)

---

Akin, Sami, "WIRELESS COMMUNICATIONS AND COGNITIVE RADIO TRANSMISSIONS UNDER QUALITY OF SERVICE CONSTRAINTS AND CHANNEL UNCERTAINTY" (2011). *Theses, Dissertations, and Student Research from Electrical & Computer Engineering*. 18.

<http://digitalcommons.unl.edu/elecengtheses/18>

This Article is brought to you for free and open access by the Electrical & Computer Engineering, Department of at DigitalCommons@University of Nebraska - Lincoln. It has been accepted for inclusion in Theses, Dissertations, and Student Research from Electrical & Computer Engineering by an authorized administrator of DigitalCommons@University of Nebraska - Lincoln.

WIRELESS COMMUNICATIONS AND COGNITIVE RADIO TRANSMISSIONS  
UNDER QUALITY OF SERVICE CONSTRAINTS AND CHANNEL  
UNCERTAINTY

by

Sami Akin

A DISSERTATION

Presented to the Faculty of  
The Graduate College at the University of Nebraska  
In Partial Fulfilment of Requirements  
For the Degree of Doctor of Philosophy

Major: Engineering

Under the Supervision of Mustafa Cenk Gursoy

Lincoln, Nebraska

May, 2011

WIRELESS COMMUNICATIONS AND COGNITIVE RADIO TRANSMISSIONS  
UNDER QUALITY OF SERVICE CONSTRAINTS AND CHANNEL  
UNCERTAINTY

Sami Akin, Ph. D.

University of Nebraska, 2011

Adviser: Mustafa Cenk Gursoy

In this thesis, we study wireless communications and cognitive radio transmissions under quality of service (QoS) constraints and channel uncertainty. Initially, we focus on a time-varying Rayleigh fading channel and assume that no prior channel knowledge is available at the transmitter and the receiver. We investigate the performance of pilot-assisted wireless transmission strategies. In particular, we analyze different channel estimation techniques, including single-pilot minimum mean-square-error (MMSE) estimation, and causal and noncausal Wiener filters, and analyze efficient resource allocation strategies. Subsequently, we study the training-based transmission and reception schemes over a priori unknown, Rayleigh fading relay channels in which the fading is modeled as a random process with memory. In the second part of the thesis, we study the effective capacity of cognitive radio channels in order to identify the performance in the presence of statistical quality of service (QoS) constraints. The cognitive radio users are assumed to initially perform channel sensing to detect the activity of primary users and then transmit the data at two different average power levels depending on the presence or absence of active primary users. We conduct the performance analysis in both single-band and multi-band environments in the presence of interference constraints. Later, we consider a cognitive radio system in which the

cognitive secondary users operate under channel uncertainty and QoS constraints, and perform both channel estimation and sensing. In this setting, we analyze the effective capacity and determine efficient power and rate allocation policies. Finally, we study cognitive multiple-input multiple-output (MIMO) channels in the low-power regime, and investigate the energy efficiency.

COPYRIGHT

© 2011, Sami Akin

# Contents

<b>Contents</b>	<b>v</b>
<b>List of Figures</b>	<b>x</b>
<b>1 Introduction</b>	<b>1</b>
1.1 Channel Conditions Affecting Quality of Wireless Communications	1
1.2 Pilot-Assisted Transmission . . . . .	2
1.3 Cognitive Radio . . . . .	4
1.4 Spectrum Sensing . . . . .	5
1.5 Effective Capacity . . . . .	6
1.6 Interference Constraints and Spectrum Utilization . . . . .	7
1.7 Quality of Service Constraints in Cognitive Radio Systems . . . . .	8
1.8 Cognitive MIMO Radio Systems . . . . .	10
1.9 Overview . . . . .	12
<b>2 Training Optimization for Gauss-Markov Rayleigh Fading Channels</b>	<b>18</b>
2.1 Channel Model . . . . .	19
2.2 Pilot Symbol-Assisted Transmission . . . . .	20
2.3 Optimal Power Distribution and Training Period for BPSK Signals .	22
2.3.1 Problem Formulation . . . . .	22

2.3.2	Numerical Results . . . . .	23
2.4	Low Complexity Training Optimization . . . . .	29
2.5	Conclusion . . . . .	35
<b>3</b>	<b>Pilot-Symbol-Assisted Communications with Noncausal and Causal Wiener Filters</b>	<b>36</b>
3.1	Channel Model . . . . .	37
3.2	Pilot Symbol-Assisted Transmission and Reception . . . . .	37
3.3	Achievable Rates . . . . .	38
3.4	Optimizing Training Parameters in Gauss-Markov Channels . . . . .	42
3.5	Numerical Results . . . . .	45
3.5.1	Optimal Parameters and Effects of Aliasing . . . . .	45
3.5.2	Causal Filter Performance in the Absence of Aliasing . . . . .	49
3.6	Conclusion . . . . .	53
<b>4</b>	<b>Achievable Rates and Training Optimization for Fading Relay Channels with Memory</b>	<b>54</b>
4.1	Channel Model . . . . .	55
4.2	Network Training Phase . . . . .	55
4.3	Data Transmission Phase . . . . .	58
4.3.1	Non-overlapped Case . . . . .	59
4.3.2	Overlapped Case . . . . .	60
4.4	Achievable Rates for AF Relaying . . . . .	60
4.5	Achievable Rates for DF Relaying . . . . .	63
4.6	Optimizing Training Parameters . . . . .	65
4.7	Numerical Results . . . . .	67
4.8	Conclusion . . . . .	70

<b>5</b>	<b>Effective Capacity Analysis of Cognitive Radio Channels for Quality of Service Provisioning</b>	<b>72</b>
5.1	System and Cognitive Channel Model . . . . .	73
5.2	Channel Sensing . . . . .	75
5.3	State Transition Model and Effective Capacity with CSI at the Receiver only . . . . .	77
5.3.1	State Transition Model . . . . .	77
5.3.2	Effective Capacity . . . . .	82
5.3.3	Numerical Results . . . . .	85
5.4	State Transition Model and Effective Capacity with CSI at Both the Receiver and Transmitter . . . . .	89
5.4.1	State Transition Model . . . . .	91
5.4.2	Effective Capacity . . . . .	94
5.4.3	Numerical Results . . . . .	96
5.5	Conclusion . . . . .	98
<b>6</b>	<b>Cognitive Radio Transmission under QoS Constraints and Interference Limitations</b>	<b>100</b>
6.1	Cognitive Channel Model and Channel Sensing . . . . .	101
6.2	State Transition Model . . . . .	105
6.3	Interference Power Constraints . . . . .	110
6.4	Effective Capacity . . . . .	114
6.5	Numerical Results . . . . .	119
6.5.1	Rayleigh Fading . . . . .	120
6.5.2	Nakagami Fading . . . . .	125
6.6	Conclusion . . . . .	126



<b>7</b>	<b>Performance Analysis of Cognitive Radio Systems under QoS Constraints and Channel Uncertainty</b>	<b>129</b>
7.1	Cognitive Channel Model . . . . .	130
7.2	Channel Sensing . . . . .	132
7.3	Pilot Symbol-Assisted Transmission . . . . .	134
7.3.1	Training Phase . . . . .	137
7.3.2	Data Transmission Phase . . . . .	141
7.4	State Transition Model . . . . .	143
7.5	Effective Capacity . . . . .	149
7.6	Numerical Results . . . . .	150
7.7	Conclusion . . . . .	157
<b>8</b>	<b>On the Transmission Capacity Limits of Cognitive MIMO Channels</b>	<b>160</b>
8.1	Channel Model and Power Constraint . . . . .	160
8.2	State Transition Model and Channel Throughput Metrics . . . . .	164
8.2.1	State Transition . . . . .	164
8.2.2	Effective Capacity . . . . .	169
8.2.3	Ergodic Capacity . . . . .	172
8.3	Effective Capacity in the Low-Power Regime . . . . .	172
8.3.1	First and Second Derivative of the Effective Capacity . . . . .	172
8.3.2	Energy Efficiency in the Low-Power Regime . . . . .	180
8.4	Numerical Results . . . . .	183
8.5	Conclusion . . . . .	186
<b>A</b>	<b>Proof of Theorem 1</b>	<b>188</b>
<b>B</b>	<b>Proof of Theorem 2</b>	<b>190</b>

<b>C Proof of Theorem 3</b>	<b>191</b>
<b>D Proof of Theorem 4</b>	<b>193</b>
<b>E Proof of Theorem 5</b>	<b>195</b>
<b>F Proof of Theorem 6</b>	<b>197</b>
<b>G Proof of Theorem 7</b>	<b>200</b>
<b>H Proof of Theorem 8</b>	<b>203</b>
<b>Bibliography</b>	<b>205</b>

# List of Figures

2.1	Achievable data rates vs. training period $T$ for $\alpha = 0.99, 0.90, 0.80,$ and $0.70$ . $SNR = \frac{P}{\sigma_n^2} = 0$ dB . . . . .	24
2.2	Optimal power distribution among the pilot and data symbols when $\alpha = 0.99$ and $SNR = 0$ dB. The optimal period is $T = 23$ . . . . .	25
2.3	Optimal power distribution among the pilot and data symbols when $\alpha = 0.90$ and $SNR = 0$ dB. The optimal period is $T = 7$ . . . . .	26
2.4	Optimal power distribution among the pilot and data symbols when $\alpha = 0.90$ and $SNR = 0$ dB. The suboptimal period is $T = 23$ . . . . .	27
2.5	Bit energy $\frac{E_b}{N_0}$ vs. $SNR$ dB when $\alpha = 0.99$ . . . . .	28
2.6	Optimal training period $T$ vs. $SNR$ for $\alpha = 0.99, 0.90, 0.80,$ and $0.70$ . . . . .	29
2.7	Optimal power distribution for the pilot and data symbols when $\alpha = 0.99$ and $SNR = -7$ dB. The optimal period is $T = 65$ . . . . .	30
2.8	Achievable data rates vs. training period $T$ for $\alpha = 0.99, 0.90, 0.80,$ and $0.70$ . $SNR = 5$ dB . . . . .	31
2.9	Achievable data rates for BPSK signals vs. training period $T$ for $\alpha = 0.90$ . $SNR = 0$ dB. . . . .	33

2.10	Achievable data rates for BPSK signals vs. $\alpha$ for $T = 6$ and $10$ . $SNR = 0$ dB. "+ and solid line" and "+ and dotted line" are plotting rates achieved with power allocation from (2.27) and (2.15), respectively, when $T = 10$ . "o and solid line" and "o and dotted line" are plotting rates achieved with power allocation from (2.27) and (2.15), respectively, when $T = 6$ . . . . .	34
3.1	The power spectral density of Gauss-Markov channels for $\alpha = 0.99$ , $0.95$ , and $0.90$ when $\sigma_h^2 = 1$ . . . . .	43
3.2	Achievable rates when $\alpha = 0.99$ for $SNR = 0, 5, 10$ , and $20$ dB. The dotted lines provide rates when aliasing is taken into account, and the solid lines give the rates when aliasing is ignored. . . . .	45
3.3	Achievable rates when $\alpha = 0.90$ for $SNR = 0, 5, 10$ , and $20$ dB. The dotted lines provide rates when aliasing is taken into account, and the solid lines give the rates when aliasing is ignored. . . . .	46
3.4	The optimal power distribution among the pilot and data symbols when $\alpha = 0.99$ and $SNR = 0$ dB. The optimal period is $16$ . . . . .	47
3.5	The optimal power distribution among the pilot and data symbols when $\alpha = 0.90$ and $SNR = 0$ dB. The optimal period is $5$ . . . . .	48
3.6	Achievable rates vs. training period when noncausal and causal filters are employed at the receiver. $\alpha = 0.99$ and $SNR = 0, 5, 10$ , and $20$ dB. The red lines give the rates when a noncausal filter is used and the blue lines show the rates when a causal filter is used. . . . .	49

3.7 Achievable rates vs. *SNR* when noncausal and causal filters are employed at the receiver.  $\alpha = 0.99$ . The dashed line gives the rate when a noncausal filter is used and the solid line shows the rate when a causal filter is used. . . . . 50

3.8 Bit energy  $\frac{E_b}{N_0}$  vs. *SNR* dB when  $\alpha = 0.99$ . . . . . 51

3.9 Optimal period vs. *SNR* dB for causal and noncausal filters when  $\alpha = 0.99$ . . . . . 52

4.1 The optimal achievable rates vs. *SNR* for the Gauss-Markov fading model ( $\alpha = 0.99$ ) and different relaying techniques.  $\sigma_{sd}^2 = 1, \sigma_{sr}^2 = 16$  and  $\sigma_{rd}^2 = 16$ . (S: single-pilot estimation. W: Wiener filter.) . . . . . 64

4.2 The optimal achievable rates vs. *SNR* for the lowpass fading model when noncausal Wiener filter is employed.  $\sigma_{sd}^2 = 1, \sigma_{sr}^2 = 4$  and  $\sigma_{rd}^2 = 4$ . 65

4.3 Normalized bit energies  $\frac{E_b}{N_0}$  vs. *SNR* for the lowpass fading model when noncausal Wiener filter is employed.  $\sigma_{sd}^2 = 1, \sigma_{sr}^2 = 4$  and  $\sigma_{rd}^2 = 4$ . 68

4.4 The optimal achievable rates vs. training period *M* for the Gauss-Markov fading model. Single-pilot MMSE estimation is employed. The dashed lines are obtained when  $\sigma_{sd}^2 = 1, \sigma_{sr}^2 = 4$  and  $\sigma_{rd}^2 = 4$  and solid lines are obtained when  $\sigma_{sd}^2 = 1, \sigma_{sr}^2 = 16$  and  $\sigma_{rd}^2 = 16$  . . . . . 69

4.5 Optimal power distribution among the pilot and data symbols when  $\sigma_{sd}^2 = 1, \sigma_{sr}^2 = 4, \sigma_{rd}^2 = 4, SNR = 0$  dB. Fading is a Gauss-Markov process with  $\alpha = 0.99$ . Single-pilot MMSE estimation is employed. The optimal period is  $M = 30$ . Note that the first 15 symbols belong to the source and the last 15 bars belong to the relay . . . . . 70

4.6	Optimal power distribution among the pilot and data symbols when $\sigma_{sd}^2 = 1$ , $\sigma_{sr}^2 = 16$ , $\sigma_{rd}^2 = 16$ , $SNR = 0$ dB. Fading is a Gauss-Markov process with $\alpha = 0.99$ . Wiener filter is employed. The optimal period is $M = 12$ . Note that the first 6 symbols belong to the source and the last 6 bars belong to the relay . . . . .	71
5.1	State transition model for the cognitive radio channel. The numbered label for each state is given on the bottom-right corner of the box representing the state. . . . .	80
5.2	Effective Capacity and $P_f - P_d$ v.s. Channel Detection Threshold $\lambda$ . $\theta = 0.01$ . . . . .	85
5.3	Effective Capacity and $P_f - P_d$ v.s. Channel Detection Threshold $\lambda$ . $\theta = 1$ .	87
5.4	Effective Capacity and $P_f - P_d$ v.s. Channel Sensing Duration, $N$ . $\theta = 0.01$ . . . . .	88
5.5	Optimal Data Transmission Rates and $P_f - P_d$ v.s. Channel Sensing Duration $N$ . $\theta = 0.01$ . . . . .	90
5.6	Effective Capacity and Optimal Data Transmission Rates v.s. QoS exponent $\theta$ . . . . .	90
5.7	Effective Capacity and $P_f - P_d$ for different schemes v.s. Energy Detection Threshold, $\lambda$ . $\theta = 0.01$ . . . . .	97
5.8	Effective Capacity for different schemes v.s. QoS exponent $\theta$ . . . . .	97
6.1	Probability of Detection $P_d$ and False Alarm $P_f$ vs. Energy Detection Threshold . . . . .	104
6.2	State transition model for the cognitive radio channel. The numbered label for each state is given on the lower-right corner of the box representing the state. . . . .	108

6.3	Probability of different scenarios vs. probability of detection $P_d$ for different number of channels $M$ . . . . .	120
6.4	Effective capacity vs. probability of detection $P_d$ for different number of channels $M$ when $\bar{I}_{avg} = 0$ dB. . . . .	122
6.5	Effective capacity vs. probability of detection $P_d$ for different number of channels $M$ when $\bar{I}_{avg} = -10$ dB. . . . .	123
6.6	Effective capacity vs. $\bar{I}_{avg}$ for different values of $M$ when $P_d = 0.9$ and $P_f = 0.2$ in the Rayleigh fading channel. . . . .	124
6.7	$P_{int}$ vs. correct detection probability $P_d$ for different number of channels $M$ in the upper figure. False alarm probability $P_f$ vs. correct detection probability $P_d$ in the lower figure. . . . .	126
6.8	Effective capacity vs. $\bar{I}_{avg}$ for different values of $M$ when $P_d = 0.9$ and $P_f = 0.2$ in the Nakagami- $m$ fading channel with $m = 3$ . . . . .	127
7.1	Transmission frame consisting of channel sensing, channel training and data transmission. Total frame duration is $T$ . First $N$ seconds is allocated to channel sensing. Following channel sensing, a single pilot symbol is sent in the training phase. Under the assumption that the symbol rate is $B$ complex symbols per second, a single pilot has a duration of $1/B$ seconds, where $B$ denotes the bandwidth. The remaining time of $T - N - 1/B$ seconds is used for data transmission. . . . .	131
7.2	Two-state Markov model for the primary user activity. . . . .	140
7.3	Upper Figure: Effective capacity vs. detection probability $P_d$ for different values of $\bar{P}_{avg}$ . Lower Figure: False alarm probability $P_f$ vs. $P_d$ . . . . .	151
7.4	Optimal values of $\bar{P}_1$ and $\bar{P}_2$ vs. detection probability $P_d$ for different values of $\bar{P}_{avg}$ . . . . .	152

- 7.5 Optimal values of  $r_1$  and  $r_2$  vs. detection probability  $P_d$  for different values of  $\bar{P}_{avg}$ . . . . . 153
- 7.6 Effective capacity vs.  $\eta$ , the fraction of total power allocated to the pilot symbol, for different values of  $\bar{P}_{avg}$ . . . . . 154
- 7.7 Optimal values of  $r_1$  and  $r_2$  vs.  $\eta$ , the fraction of total power allocated to the pilot symbol, for different values of  $\bar{P}_{avg}$ . . . . . 155
- 7.8 Optimal values of  $\bar{P}_1$  and  $\bar{P}_2$  vs.  $\eta$ , the fraction of total power allocated to the pilot symbol, for different values of  $\bar{P}_{avg}$ . . . . . 156
- 7.9  $\eta$ , the fraction of total power allocated to the pilot symbol, vs detection probability  $P_d$ .  $\mathbf{P}_{avg} = 5$  dB. . . . . 157
- 7.10 Effective Capacity vs.  $\bar{P}_{avg}$  when  $m - mmse$  and  $l - mmse$  estimation techniques are employed. . . . . 158
- 7.11 Effective capacity vs. detection probability  $P_d$  for different values of  $\bar{P}_{avg}$  when  $m - mmse$  and  $l - mmse$  estimation techniques are employed. 159
  
- 8.1 State transition model for the cognitive radio channel. The numbered label for each state is given on the bottom-right corner of the box representing the state. . . . . 166
- 8.2 Two-state Markov model for the primary user activity. . . . . 167
- 8.3 Effective Rate and  $\nu$  v.s.  $\mu$  for different Decay Rate,  $\theta$ , values. . . . . 183
- 8.4 Effective Rate v.s. Decay Rate,  $\theta$  for different Number of Antennas,  $M$ . . 185
- 8.5 Effective Rate v.s. SNR for different values of Decay Rate,  $\theta$   $M = 1$ . . . . 186
- 8.6 Effective Rate v.s. SNR for different values of Decay Rate,  $\theta$   $M = 3$ . . . . 187



# Chapter 1

## Introduction

### 1.1 Channel Conditions Affecting Quality of Wireless Communications

One of the key characteristics of wireless communications that most greatly impact system design and performance is the time-varying nature of the channel conditions, experienced due to mobility and changing physical environment. This has led mainly to three lines of work in the performance analysis of wireless systems. A considerable amount of effort has been expended in the study of cases in which the perfect channel state information (CSI) is assumed to be available at either the receiver or the transmitter or both. With the perfect CSI available at the receiver, the authors in [25] and [49] studied the capacity of fading channels. The capacity of fading channels is also studied in [32] and [31] with perfect CSI at both the receiver and the transmitter. A second line of work has considered fast fading conditions, and assumed that neither the receiver nor the transmitter is aware of the channel conditions (see e.g., [79], [55], [64]). On the other hand,

most practical wireless systems attempt to learn the channel conditions but can only do so imperfectly. Hence, it is of great interest to study the performance when only imperfect CSI is available at the transmitter or the receiver. When the channel is not known a priori, one technique that provides imperfect receiver CSI is to employ pilot signals in the transmission to estimate the channel.

## 1.2 Pilot-Assisted Transmission

Pilot-Assisted Transmission (PAT) multiplexes known training signals with the data signals. These transmission strategies and pilot symbols known at the receiver can be used for channel estimation, receiver adaptation, and optimal decoding [68]. One of the early studies has been conducted by Cavers in [17], [18] where an analytical approach to the design of PATs is presented. [78] has shown that the data rates are maximized by periodically embedding pilot symbols into the data stream. The more pilot symbols are transmitted and the more power is allocated to the pilot symbols, the better estimation quality we have, but the more time for transmission of data is missed and the less power we have for data symbols. Hassibi and Hochwald [37] has optimized the power and duration of training signals by maximizing a capacity lower bound in multiple-antenna Rayleigh block fading channels. Adirredy *et al.* [78] investigated the optimal placement of pilot symbols and showed that the periodical placement maximizes the data rates. In general, the amount, placement, and fraction of pilot symbols in the data stream have considerable impact on the achievable data rates. An overview of pilot-assisted wireless transmission techniques is presented in [68].

In [56], considering adaptive coding of data symbols without requiring feedback to the transmitter, Abou-Faycal *et al.* studied the data rates achieved with

PSAM over Gauss-Markov Rayleigh fading channels. In their studies, the training period is optimized by maximizing the achievable rates. The authors in [1] also considered pilot symbol-assisted transmission over Gauss-Markov Rayleigh channels and analyzed the optimal power allocation among data symbols while the pilot symbol has fixed power. They have shown that the power distribution has a decreasing character with respect to the distance to the last sent pilot, and that data power adaptation improves the rates. The authors in [70] considered a similar setting and analyzed training power adaptation but assumed that the power is uniformly distributed among data symbols.

Ohno and Giannakis [60] considered general slowly-varying fading processes. Employing a noncausal Wiener filter for channel estimation at the receiver, they obtained a capacity lower bound and optimized the spacing of training symbols and training power. Baltersee *et al.* in [14] and [13] have also considered using a noncausal Wiener filter to obtain a channel estimate, and they optimized the training parameters by maximizing achievable rates in single and multiple antenna channels.

Furthermore, cooperative wireless communications has attracted much interest. Cooperative relay transmission techniques have been studied in [47] and [46] where Amplify-and-Forward (AF) and Decode-and-Forward (DF) models are considered. However, most of the studies have assumed that the channel conditions are perfectly known at the receiver and/or transmitter. In one of the recent studies, Wang *et al.* [16] considered wireless sensory relay networks where the conditions of the channels are learnt imperfectly only by the relay nodes.

### 1.3 Cognitive Radio

With the rapid growth in the wireless networks in the last two decades, the scarcity in spectrum has become a serious problem for spectrum sharing, since much of the prime wireless spectrum has been allocated for specific applications. However, recent measurements show that the licensed spectrum is severely underutilized. This has caused significant interest in using the spectrum dynamically by exploring the empty spaces in the spectrum without disturbing the primary users. In such systems, in order to avoid the interference to the primary users, it is very important for the cognitive secondary users (SUs) to detect the activity of the primary users. When the primary users are active, the secondary user should either avoid using the channel or transmit at low power in order not to exceed the noise power threshold of the primary users, whereas the SUs can use the channel without any constraints when the channel is free of the primary users. An overview of cognitive radio systems and the challenges in this area can be found in [39], [87] and [66].

With the above-mentioned motivation, recent years have witnessed a large body of work on channel sensing and dynamic spectrum sharing. Dynamically sharing the spectrum in the time-domain by exploiting whitespace between the bursty transmissions of a set of users, represented by an 802.11b based wireless LAN (WLAN), is considered by the authors in [27], where a model that describes the busy and idle periods of a WLAN is considered. The authors in [40], [86] and [22] focused on the problem of maximally utilizing the spectrum opportunities in cognitive radio networks with multiple potential channels and developed an optimal strategy for opportunistic spectrum access. In [45], Kim and Shin modeled the primary users' usage pattern of the channels as semi-Markov processes and

used a two-state transition model for each channel. They addressed the optimization of the sensing-period to achieve the maximum discovery of opportunities for cognitive users, and also the optimization of the sensing sequence of channels to minimize delay in locating an idle channel.

Cognitive operation is also studied from an information-theoretic perspective with the goal of identifying the fundamental performance limits (see e.g. [73], [23], [61] and [42]). In [73], the capacity of opportunistic secondary communication over a spectral pool of two independent channels is explored and it is shown that the benefits of spectral pooling are lost in dynamic spectral environments. In [23], [61] and [42], cognitive radio channel is modeled as an interference channel in which the cognitive transmitter has side information about the primary user's transmission. In [23], an achievable rate region for such a cognitive radio channel is constructed using information-theoretic arguments.

## 1.4 Spectrum Sensing

Note that spectrum sensing, which is crucial in the detection of the presence of primary users and hence in interference management, also induces a cost in terms of reduced time for data transmission. Motivated by this fact, the authors in [50] studied the tradeoff between channel sensing and throughput considering the Shannon capacity as the throughput metric. They formulated an optimization problem and identified the optimal sensing time which yields the highest throughput while providing sufficient protection in terms of interference to the primary users.

Initially, before using the channel, SUs have to detect the activities of the primary users. Among different channel detection techniques, sensing-based access

to the channel is favored because of its low employment cost and compatibility with the legacy of licensed systems [29]. The authors in [86] and [22] developed an optimal strategy for opportunistic spectrum access. Moreover, the authors in [40] focused on the optimal sensing order problem in multi-channel cognitive medium access control with opportunistic transmission, and studied the problem of maximally utilizing the spectrum opportunities in cognitive radio networks with multiple potential channels.

## 1.5 Effective Capacity

The maximum throughput levels achieved in wireless systems operating under such statistical QoS constraints can be identified through the notion of effective capacity. The effective capacity is defined in [83] as the maximum constant arrival rate that a given time-varying service process can support while meeting the QoS requirements. Effective capacity is defined as a dual concept to effective bandwidth which characterizes the minimum amount of constant transmission rate required to support a time-varying source in the presence of statistical QoS limitations [19]. The application and analysis of effective capacity in various settings have attracted much interest. In [52], [76], [75] and [74], authors focused on the problem of resource allocation in the presence of statistical QoS constraints. In [36], energy efficiency is investigated under QoS constraints by analyzing the normalized effective capacity in the low-power and wideband regimes. Moreover, we would like to note reference [71] which has also considered a cognitive radio system with buffer constraints. In this work, Simeone *et al.* followed a different approach and investigated the maximum throughput that can be achieved while keeping the queues at the primary and secondary transmitters stable.

## 1.6 Interference Constraints and Spectrum

### Utilization

In [12], Asghari and Aissa, under constraints on the average interference caused at the licensed user over Rayleigh fading channels, studied two adaptation policies at the secondary user's transmitter in a cognitive radio system one of which is variable power and the other is variable rate and power. They maximized the achievable rates under the above constraints and the bit error rate (BER) requirement in *m*-ary quadrature amplitude modulation (MQAM). The authors in [57] derived the fading channel capacity of a secondary user subject to both average and peak received-power constraints at the primary receiver. In addition, they obtained optimum power allocation schemes for three different capacity notions, namely, ergodic, outage, and minimum-rate. Ghasemi *et al.* in [28] studied the performance of spectrum-sensing radios under channel fading. They showed that due to uncertainty resulting from fading, local signal processing alone may not be adequate to meet the performance requirements. Therefore, to remedy this uncertainty they also focused on the cooperation among SUs and the tradeoff between local processing and cooperation in order to maximize the spectrum utilization. Furthermore, the authors in [50] focused on the problem of designing the sensing duration to maximize the achievable throughput for the secondary network under the constraint that the primary users are sufficiently protected. They formulated the sensing-throughput tradeoff problem mathematically, and use energy detection sensing scheme to prove that the formulated problem indeed has one optimal sensing time which yields the highest throughput for the secondary network. Moreover, Poor *et al.* introduced a novel wideband spectrum sensing technique, called as multiband joint detection in [67], that jointly detects

the signal energy levels over multiple frequency bands rather than considering one band at a time, which is proposed to be efficient in improving the dynamic spectrum utilization and reducing interference to the primary users.

## 1.7 Quality of Service Constraints in Cognitive Radio Systems

As described before, issues regarding channel sensing, spectrum sharing and throughput in cognitive radio networks have been extensively studied recently (see also, for instance, [24]). However, another critical concern of providing QoS guarantees over cognitive radio channels has not been sufficiently addressed yet. In many wireless communication systems, providing certain QoS assurances is crucial in order to provide acceptable performance and quality. However, this is a challenging task in wireless systems due to random variations experienced in channel conditions and random fluctuations in received power levels and supported data rates. Hence, in wireless systems, generally statistical, rather than deterministic, QoS guarantees can be provided. Note that the situation is further exacerbated in cognitive radio channels in which the access to the channel can be intermittent or transmission occurs at lower power levels depending on the activity of the primary users. Furthermore, cognitive radio can suffer from errors in channel sensing in the form of false alarms. Hence, it is of paramount interest to analyze the performance of cognitive radio systems in the presence of QoS limitations in the form of delay or buffer constraints.

As discussed above, the central challenge for the cognitive SUs is to control their interference levels. In general, interference management needs to be per-



formed under uncertainty as channel sensing done by the SUs may result in false alarms and miss-detections. In such an interference limited scenario, cognitive SUs should also satisfy their own QoS requirements by transmitting at high rates and limiting the delay experienced by the data in the buffers. This, too, has to be achieved under channel uncertainty since wireless channel conditions, which vary over time randomly due to mobility and changing environment, can only be estimated imperfectly through training techniques. Note also that providing QoS guarantees is especially more challenging for SUs as they have to take into account both the changing channel conditions and varying primary user activity. These considerations are critical for the successful deployment of cognitive radio systems in practice.

In many wireless systems, it is very important to provide reliable communications while sustaining a certain level of QoS under time-varying channel conditions. These considerations have led to studies that investigate the cognitive radio performance under QoS constraints. Musavian and Aissa in [59] considered variable-rate, variable-power MQAM modulation employed under delay QoS constraints over spectrum-sharing channels. As a performance metric, they used the effective capacity to characterize the maximum throughput under QoS constraints. They assumed two users sharing the spectrum with one of them having a primary access to the band. The other, known as secondary user, is constrained by interference limitations imposed by the primary user. Considering two modulation schemes, continuous MQAM and discrete MQAM with restricted constellations, they obtained the effective capacity of the secondary user's link, and derived the optimum power allocation scheme that maximizes the effective capacity in each case. Additionally, in [58], they proposed a QoS constrained power and rate allocation scheme for spectrum sharing systems in which the SUs are allowed to

use the spectrum under an interference constraint by which a minimum-rate of transmission is guaranteed to the primary user for a certain percentage of time. Moreover, applying an average interference power constraint which is required to be fulfilled by the secondary user, they obtained the maximum arrival-rate supported by a Rayleigh block-fading channel subject to satisfying a given statistical delay QoS constraint. We note that in these studies on the performance under QoS limitations, channel sensing is not incorporated into the system model. As a result, adaptation of the cognitive transmission according to the presence or absence of the primary users is not considered.

## 1.8 Cognitive MIMO Radio Systems

It is known that having multiple antenna at the receiver and the transmitter can improve the performance levels and can provide large increases in terms of throughput and reliability of data transmission. Therefore, there has been much interest in understanding and analyzing the MIMO channels, and many comprehensive studies have been conducted, and considerable effort and time have been expended [30], [77]. In most of the studies, ergodic Shannon capacity formulations are considered as the objective functions [54], [53], [69]. The authors, in [54] and [53], provided the analytical characterizations of the impacts on the multiple-antenna capacity of several features that fall outside the standard antenna model. Furthermore, focusing on a different approach in understanding MIMO channels, the author in [33] investigated MIMO systems in the presence of statistical queuing constraints which is not captured by Shannon's formulation.

Furthermore, recently cognitive MIMO radio models were also considered since MIMO cognitive models can provide much better performance levels for

the SUs. Modeling a channel setting with a single licensed user and a single cognitive user, that is equivalent to an interference channel with degraded message sets, the authors in [72] focused on the fundamental limits of operation of a MIMO cognitive radio network, and they showed that under certain conditions, the achievable region is optimal for a portion of the capacity region that includes sum capacity. Considering three scenarios, namely when the secondary transmitter has complete, partial, or no knowledge about the channels to the primary receivers, they aimed to maximize the throughput of the SU, while keeping the interference temperature at the primary receivers below a certain threshold [43]. Furthermore, in [26], the authors proposed a practical CR transmission strategy consisting of three major stages, namely, environment learning that applies blind algorithms to estimate the spaces that are orthogonal to the channels from the primary receiver, channel training that uses training signals applies the linear-minimum-mean-square-error (L-MMSE)-based estimator to estimate the effective channel, and data transmission. Considering imperfect estimations in both learning and training stages they derived a lower bound on the ergodic capacity that is achievable for the CR in the data-transmission stage. It was also shown in [62] that the asymptotes of the achievable transmission rates of the opportunistic (secondary) link are obtained in the regime of large numbers of antennas. Another study of cognitive MIMO channels was considered in [85]. Recently, the authors in [41] considered the maximization of the effective capacity in a single-user multi-antenna system with covariance knowledge, and Liu *et al.* in [51] studied the effective capacity of a class of multiple-antenna wireless systems subject to Rayleigh flat fading.

## 1.9 Overview

In this thesis, we considered training and data transmission in arbitrarily correlated fading channels (i.e., fading channels with memory). We jointly optimized training period, and data and training power allocations by maximizing the input-output mutual information. Furthermore, we characterized achievable rates and energy-per-bit requirements by using optimal training parameters. We employed both single-pilot MMSE estimators and Wiener filter estimators to learn the channel in time-selective Rayleigh fading channels. We showed that achievable rates obtained using causal and noncausal Wiener filters are almost same at high signal-to-noise ratio (SNR) values. We analyzed fast fading channels and investigated the impact upon the performance of aliasing due to under-sampling of the channel. We identified the performance limits of imperfectly known relay channels.

Moreover, we constructed a cognitive radio channel model, and considered both channel sensing and data transmission. Initially considering interference management and CSI at receiver, we set secondary users with two transmission power levels and rates. We studied energy detection methods and found probability of false alarm and misdetection. We identified a state-transition model by comparing transmission rates with instantaneous channel capacity values. We determined effective capacity of cognitive radio transmission by incorporating channel sensing results. We identified performance in the presence of statistical QoS constraints. We investigated interactions among effective capacity, QoS constraints, channel sensing duration, and channel detection threshold. Furthermore, considering perfect CSI at both the receiver and the transmitter, we obtained optimal power adaptation policies that maximize effective capacity. We incorporated multiband channel sensing. We identified optimal criterion to select a transmis-

sion channel out of the available channels. We imposed an average interference power to protect primary users. We obtained optimal transmission policies under average interference power constraint. Modeling activities of primary users as first order Markov process and imposing both average and peak power constraints, we used pilot symbols to eliminate channel uncertainty. Finally, we focused on cognitive MIMO under QoS constraints in low-power regime.

The organization of the rest of the thesis is as follows:

In Chapter 2, considering that no prior channel knowledge is available at the transmitter and the receiver, we focus on a time-varying Rayleigh fading channel. The channel is modeled by a Gauss-Markov model. Pilot symbols which are known by both the transmitter and the receiver are transmitted with a period of  $T$  symbols. In this setting, we seek to jointly optimize the training period, training power, and data power allocation by maximizing achievable rates. This chapter, as a conference paper, appeared in IEEE International Conference on Communications (ICC) in 2007 [4]. In Chapter 3, we study training-based transmission and reception schemes over a-priori unknown, time-selective Rayleigh fading channels. Since causal operation is crucial in real-time, delay-constrained applications, we consider the use of causal, as well as noncausal, Wiener filters for channel estimation. We optimize the training parameters by maximizing a capacity lower bound. Although the treatment is general initially, we concentrate on the Gauss-Markov channel model for numerical analysis. As another contribution, we analyze fast fading channels and the impact upon the performance of aliasing due to under-sampling of the channel. The results in this chapter, as a conference paper, appeared in 9th IEEE International Workshop on Signal Processing Advances in Wireless Communications (SPAWC) in 2008 [6]. In Chapter 4, we study the training-based transmission and reception schemes over a priori

unknown, Rayleigh fading relay channels in which the fading is modeled as a random process with memory. Unknown fading coefficients of the channels are estimated at the receivers with the assistance of the pilot symbols. We consider two channel estimation methods: single-pilot MMSE estimation and noncausal Wiener filter estimation. We study AF and DF relaying techniques with two different transmission protocols. We obtain achievable rate expressions and optimize the training parameters by maximizing these expressions. We concentrate on the Gauss-Markov and lowpass fading processes for numerical analysis. This chapter, as a conference paper, appeared at the 42nd Annual Conference on Information Sciences and Systems (CISS) in 2008 [5].

In Chapter 5, we study the effective capacity of cognitive radio channels in order to identify the performance in the presence of statistical QoS constraints. The cognitive radio is assumed to initially perform channel sensing to detect the activity of primary users and then transmit the data at two different average power levels depending on the presence or absence of active primary users. More specifically, we identify a state-transition model for cognitive transmission by comparing the transmission rates with the instantaneous channel capacity values, and incorporating the sensing decision and its correctness into the model, and we determine the effective capacity of cognitive transmission and provide a tool for the performance analysis in the presence of statistical QoS constraints. Furthermore, we investigate the interactions between the effective capacity, QoS constraints, channel sensing duration, and channel detection threshold through numerical analysis. We analyze both fixed-power/fixed-rate transmission schemes and variable schemes by considering different assumptions on the availability of CSI at the transmitter. We quantify the performance gains through power and rate adaptation. This chapter, as a journal paper, appeared in IEEE Transactions on Wireless

Communications in 2010 [2], and, as conference papers, appeared in the Proceedings of the IEEE Global Communications Conference (Globecom) in 2009 [10] and IEEE Wireless Communications and Networking Conference (WCNC) in 2010 [8].

In Chapter 6, we study the effective capacity of cognitive radio channels where the cognitive radio detects the activity of primary users in a multiband environment and then performs the data transmission in one of the transmission channels. Both the secondary receiver and the secondary transmitter know the fading coefficients of their own channel, and of the channel between the secondary transmitter and the primary receiver. The cognitive radio has two power allocation policies depending on the activities of the primary users and the sensing decisions. More specifically, we consider a scenario in which the cognitive system employs multi-channel sensing and uses one channel for data transmission thereby decreasing the probability of interference to the primary users. We identify a state-transition model for cognitive radio transmission in which we compare the transmission rates with instantaneous channel capacities, and also incorporate the results of channel sensing. We determine the effective capacity of the cognitive channel under limitations on the average interference power experienced by the primary receiver. We identify the optimal criterion to select the transmission channel out of the available channels and obtain the optimal power adaptation policies that maximize the effective capacity. We analyze the interactions between the effective capacity, QoS constraints, channel sensing duration, channel detection threshold, detection and false alarm probabilities through numerical techniques. This chapter, as a conference paper, appeared in Proceedings of IEEE ICC in 2010 [11].

In Chapter 7, considering that no prior channel knowledge is available at the secondary transmitter and the secondary receiver, we study the effective capacity of cognitive radio channels in order to identify the performance limits under

channel uncertainty and QoS constraints. Below, we delineate the operation of the cognitive SUs. We assume that, following channel sensing, SUs perform channel estimation to learn the channel conditions. Due to interactions and interdependencies between channel sensing and estimation, we are faced with a challenging scenario. For instance, not detecting the activities of primary users reliably can lead to degradations in the estimation of the channel conditions, e.g., if the primary users are active but detected as idle, the quality of the channel estimate will deteriorate. After performing the sensing and estimation tasks, SUs initiate the data transmission phase. We assume that SUs operate under QoS constraints in the form of limitations on the buffer length. In order to identify the maximum throughput under such constraints, we employ the effective capacity as a performance metric [83]. The activity of primary users is modeled as a two-state Markov process<sup>1</sup>. In this setting, we jointly optimize the training symbol power, data symbol power and transmission rates. This chapter, as a journal paper, has been submitted to IEEE Transactions on Wireless Communications for the second round [3], and, as conference paper, appeared in Proceedings of the IEEE Globecom in 2010 [7].

In Chapter 8, we focus on cognitive MIMO scenario under the QoS constraints. In particular, we consider the low-power regime and identify the impact of QoS limitations on the performance. Note that in reference [33], the author analyzed the MIMO wireless communications under QoS constraints, but the difference is that we've investigated the cognitive MIMO case with the presence of interference from the primary users, and we consider two different transmission policies

---

<sup>1</sup> In addition to having the assumption of no prior channel knowledge and explicitly considering channel estimation, Markovian modeling of primary user activity constitutes another significant departure from the setting considered in [11] where primary user activity is assumed to vary independently from one frame to another.



depending on the activities of primary users. Furthermore, in this chapter, we consider a general cognitive MIMO link model where fading coefficients have arbitrary distributions and are correlated. Not only the channel fading coefficients but also the received interference variables have arbitrary distributions and are possibly correlated. We assume that the secondary transmitter and receiver have perfect CSI. This chapter, as a conference paper, appeared in IEEE WCNC in 2011 [9].

## Chapter 2

# Training Optimization for Gauss-Markov Rayleigh Fading Channels

In this chapter, pilot-assisted transmission over Gauss-Markov Rayleigh fading channels is considered. A simple scenario, where a single pilot signal is transmitted every  $T$  symbols and  $T - 1$  data symbols are transmitted in between the pilots, is studied. First, it is assumed that binary phase-shift keying (BPSK) modulation is employed at the transmitter. With this assumption, the training period, and data and training power allocation are jointly optimized by maximizing an achievable rate expression. Achievable rates and energy-per-bit requirements are computed using the optimal training parameters. Secondly, a capacity lower bound is obtained by considering the error in the estimate as another source of additive Gaussian noise, and the training parameters are optimized by maximizing this lower bound.

## 2.1 Channel Model

We consider the following model in which a transmitter and a receiver are connected by a time-varying Rayleigh fading channel,

$$y_k = h_k x_k + n_k \quad k = 1, 2, 3, \dots \quad (2.1)$$

where  $y_k$  is the complex channel output,  $x_k$  is the complex channel input,  $h_k$  and  $n_k$  are the fading coefficient and additive noise component, respectively. We assume that  $h_k$  and  $n_k$  are independent zero mean circular complex Gaussian random variables with variances  $\sigma_h^2$  and  $\sigma_n^2$ , respectively. It is further assumed that  $x_k$  is independent of  $h_k$  and  $n_k$ .

While the additive noise samples  $\{n_k\}$  are assumed to form an independent and identically distributed (i.i.d.) sequence, the fading process is modeled as a first-order Gauss-Markov process, whose dynamics is described by

$$h_k = \alpha h_{k-1} + z_k \quad 0 \leq \alpha \leq 1, \quad k = 1, 2, 3, \dots, \quad (2.2)$$

where  $\{z_k\}$ 's are i.i.d. circular complex Gaussian variables with zero mean and variance equal to  $(1-\alpha^2)\sigma_h^2$ . In the above formulation,  $\alpha$  is a parameter that controls the rate of the channel variations between consecutive transmissions. For instance, if  $\alpha = 1$ , fading coefficients stay constant over the duration of transmission, whereas, when  $\alpha = 0$ , fading coefficients are independent for each symbol. For bandwidths in the 10 kHz range and Doppler spreads of the order of 100 Hz, typical values for  $\alpha$  are between 0.9 and 0.99 [56].

## 2.2 Pilot Symbol-Assisted Transmission

We consider pilot-assisted transmission where periodically embedded pilot symbols, known by both the sender and the receiver, are used to estimate the fading coefficients of the channel thereby enabling us to track the time-varying channel. We assume the simple scenario where a single pilot symbol is transmitted every  $T$  symbols while  $T - 1$  data symbols are transmitted in between the pilot symbols. The following average power constraint,

$$\frac{1}{T} \sum_{k=lT}^{(l+1)T-1} E \left[ |x_k|^2 \right] \leq P \quad l = 0, 1, 2, \dots, \quad (2.3)$$

is imposed on the input. Therefore, the total average power allocated to pilot and data transmission over a duration of  $T$  symbols is limited by  $PT$ .

Communication takes place in two phases. In the training phase, the pilot signal is sent and the channel output is given by

$$y_{lT} = h_{lT} \sqrt{P_t} + n_{lT} \quad l = 0, 1, 2, 3, \dots \quad (2.4)$$

where  $P_t$  is the power allocated to the pilot symbol. The fading coefficients are estimated via MMSE estimation, which provides the following estimate:

$$\hat{h}_{lT} = \frac{\sqrt{P_t} \sigma_h^2}{P_t \sigma_h^2 + \sigma_n^2} y_{lT}. \quad (2.5)$$

Following the transmission of the training symbol, data transmission phase starts and  $T - 1$  data symbols are sent. Since a single pilot symbol is transmitted, the estimates of the fading coefficients in the data transmission phase are obtained as

follows:

$$\hat{h}_k = \frac{\sqrt{P_t}\sigma_h^2}{P_t\sigma_h^2 + \sigma_n^2} \alpha^{k-lT} y_{lT} \quad lT + 1 < k \leq (l+1)T - 1. \quad (2.6)$$

Now, we can express the fading coefficients as

$$h_k = \hat{h}_k + \tilde{h}_k \quad (2.7)$$

where  $\tilde{h}_k$  is the estimation error. Consequently, the input-output relationship in the data transmission phase can be written as

$$y_k = \hat{h}_k x_k + \tilde{h}_k x_k + n_k \quad lT + 1 < k \leq (l+1)T - 1. \quad (2.8)$$

Note that  $\hat{h}_k$  and  $\tilde{h}_k$  for  $lT + 1 < k < (l+1)T$  are uncorrelated zero-mean circularly symmetric complex Gaussian random variables with variances

$$\sigma_{\hat{h}_k}^2 = \frac{P_t\sigma_h^4}{P_t\sigma_h^2 + \sigma_n^2} (\alpha^{k-lT})^2, \quad (2.9)$$

and

$$\sigma_{\tilde{h}_k}^2 = \sigma_h^2 - \frac{P_t\sigma_h^4}{P_t\sigma_h^2 + \sigma_n^2} (\alpha^{k-lT})^2, \quad (2.10)$$

respectively.

## 2.3 Optimal Power Distribution and Training Period for BPSK Signals

### 2.3.1 Problem Formulation

In this section, we consider that BPSK is employed at the transmitter to send the information. Since our main goal is to optimize the training parameters and identify the optimal power allocation, BPSK signaling is adopted due to its simplicity. In the  $k^{\text{th}}$  symbol interval, the BPSK signal can be represented by two equiprobable points located at  $x_{k,1} = \sqrt{P_{d,k}}$  and  $x_{k,2} = -\sqrt{P_{d,k}}$  on the constellation map. Note that  $P_{d,k}$  is the average power of the BPSK signal in the  $k^{\text{th}}$  symbol interval. In this interval, the input-output mutual information conditioned on the value  $y_{IT}$  is given by

$$I_k(x_k; y_k | y_{IT} = y_{IT}^*) = \frac{1}{2} \int p_{y_k|x_k}(y|x_{k,1}) \log \frac{p_{y_k|x_k}(y|x_{k,1})}{p_{y_k}(y)} dy + \frac{1}{2} \int p_{y_k|x_k}(y|x_{k,2}) \log \frac{p_{y_k|x_k}(y|x_{k,2})}{p_{y_k}(y)} dy \quad (2.11)$$

where

$$p_{Y_k|X_k}(y_k|x_k) = \frac{1}{\pi(\sigma_{\hat{h}_k}^2 |x_k|^2 + \sigma_n^2)} \exp\left(\frac{-|y_k - \hat{h}_k x_k|^2}{\sigma_{\hat{h}_k}^2 |x_k|^2 + \sigma_n^2}\right)$$

and

$$p_{y_k}(y_k) = \frac{1}{2} p_{y_k|x_k}(y_k|x_{k,1}) + \frac{1}{2} p_{y_k|x_k}(y_k|x_{k,2}).$$

We consider the following achievable rate expression, which acts as a lower bound to the channel capacity:

$$I_L(T, P_t, \mathbf{P}_d) = E \left[ \frac{1}{T} \sum_{k=lT+1}^{(l+1)T-1} I_k(x_k; y_k | y_{lT} = y_{lT}^*) \right] \quad (2.12)$$

$$= \frac{1}{T} \sum_{k=lT+1}^{(l+1)T-1} E [I_k(x_k; y_k | y_{lT} = y_{lT}^*)] \quad (2.13)$$

where the expectation is with respect to  $y_{lT}$ , and  $y_{lT}^*$  is a realization of the random variable  $y_{lT}$ . Note that the achievable rate is expressed as a function of the training period,  $T$ ; power of the pilot signal,  $P_t$ ; and the power allocated to  $T - 1$  data symbols transmitted in between the pilot symbols, which is described by the following vector

$$\mathbf{P}_d = [P_{d,1}, P_{d,2}, \dots, P_{d,T-1}]. \quad (2.14)$$

Our goal is to solve the joint optimization problem

$$(T^*, P_t^*, \mathbf{P}_d^*) = \arg \max_{\substack{T, P_t, \mathbf{P}_d \\ P_t + \sum_{k=1}^{T-1} P_{d,k} \leq PT}} I_L(T, P_t, \mathbf{P}_d) \quad (2.15)$$

and obtain the optimal training period, and optimal data and pilot power allocations. Since it is unlikely to reach to closed-form solutions, we have employed numerical tools to solve (2.15).

### 2.3.2 Numerical Results

In this section, we summarize the numerical results. Figure 2.1 plots the data rates achieved with optimal power allocations as a function of the training pe-

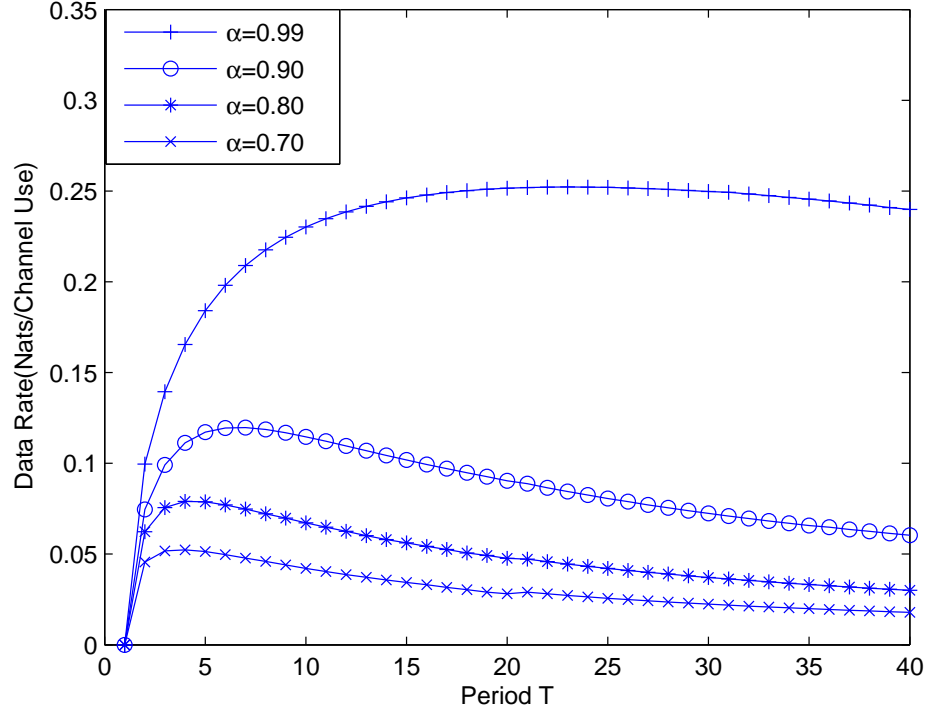


Figure 2.1: Achievable data rates vs. training period  $T$  for  $\alpha = 0.99, 0.90, 0.80,$  and  $0.70$ .  $SNR = \frac{P}{\sigma_n^2} = 0$  dB

riod for different values of  $\alpha$ . The power level is kept fixed at  $P = \sigma_n^2 = 1$ . It is observed that the optimal values of the training period,  $T$ , are 23, 7, 4, and 4 for  $\alpha = 0.99, 0.90, 0.80,$  and  $0.70$ , respectively. Note that the optimal  $T$  and optimal data rate are decreasing with the decreasing  $\alpha$ . This is expected because the faster the channel changes, the more frequently the pilot symbols should be sent. This consequently reduces the data rates which are already adversely affected by the fast changing and imperfectly known channel conditions. Figures 2.2 and 2.3 are the bar graphs providing the optimal training and data power allocation when the training period is at its optimal value. In the graphs, the first bar corresponds to the power of the training symbol while the remaining bars



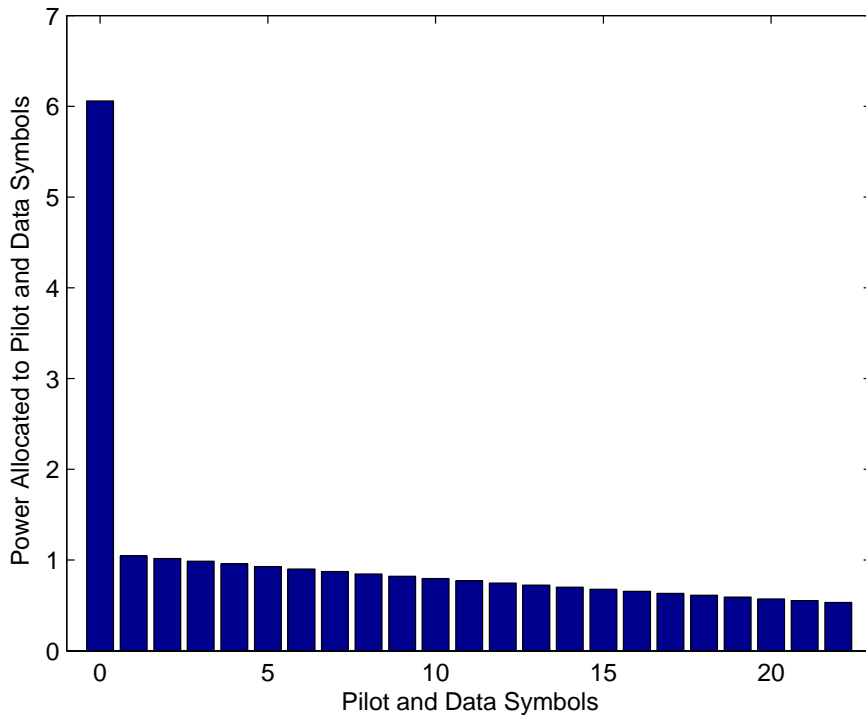


Figure 2.2: Optimal power distribution among the pilot and data symbols when  $\alpha = 0.99$  and  $SNR = 0$  dB. The optimal period is  $T = 23$ .

provide the power levels of the data symbols. We immediately observe from both figures that the data symbols, which are farther away from the pilot symbol, are allocated less power since channel gets noisier for these symbols due to poorer channel estimates. Moreover, comparing Fig. 2.2 and Fig. 2.3, we see that having a longer training period enables us to put more power on the pilot signal and therefore have better channel estimates. We also note that if  $\alpha$  is small as in Fig. 2.3, the power of the data symbols decreases faster as they move away from the pilot symbol. From these numerical results, it is evident that  $\alpha$  greatly affects the optimal power allocation and optimal  $T$ . Fig. 2.4 gives the power distribution when  $\alpha = 0.90$  and  $T = 23$ . Note that this value of the training period is subopti-

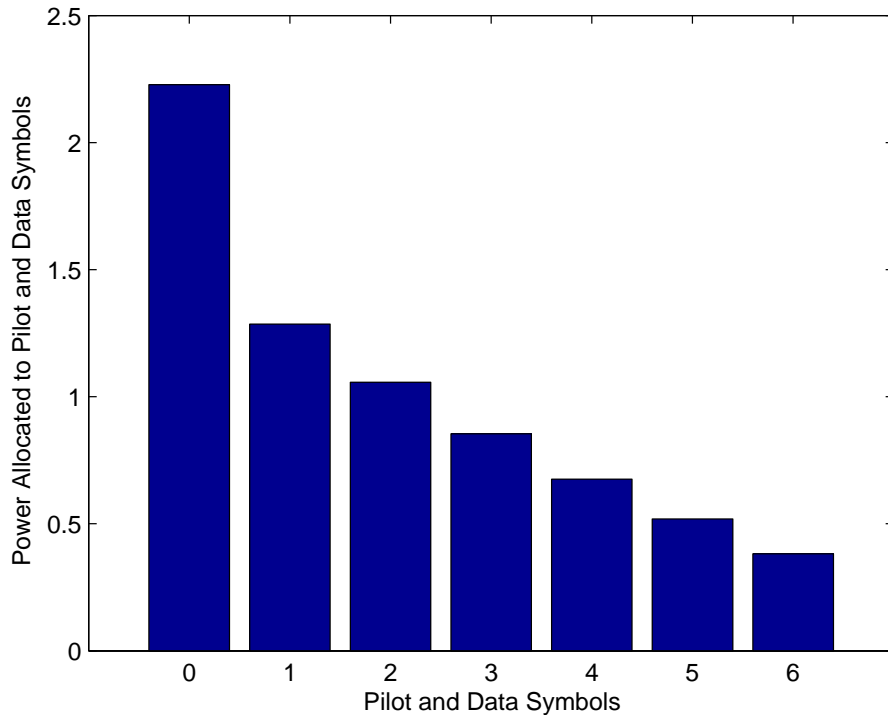


Figure 2.3: Optimal power distribution among the pilot and data symbols when  $\alpha = 0.90$  and  $SNR = 0$  dB. The optimal period is  $T = 7$ .

mal. The inefficiency of this choice is apparent in the graph. Since the channel is changing relatively fast and the quality of the channel estimate deteriorates rather quickly, data symbols after the 15<sup>th</sup> symbol interval are given little or no power, leading to a considerable loss in data rates.

In systems with scarce energy resources, energy required to send one information bit, rather than data rates, is a suitable metric to measure the performance. The least amount of normalized bit energy required for reliable communications is given by

$$\frac{E_b}{N_0} = \frac{SNR}{C(SNR)} \quad (2.16)$$

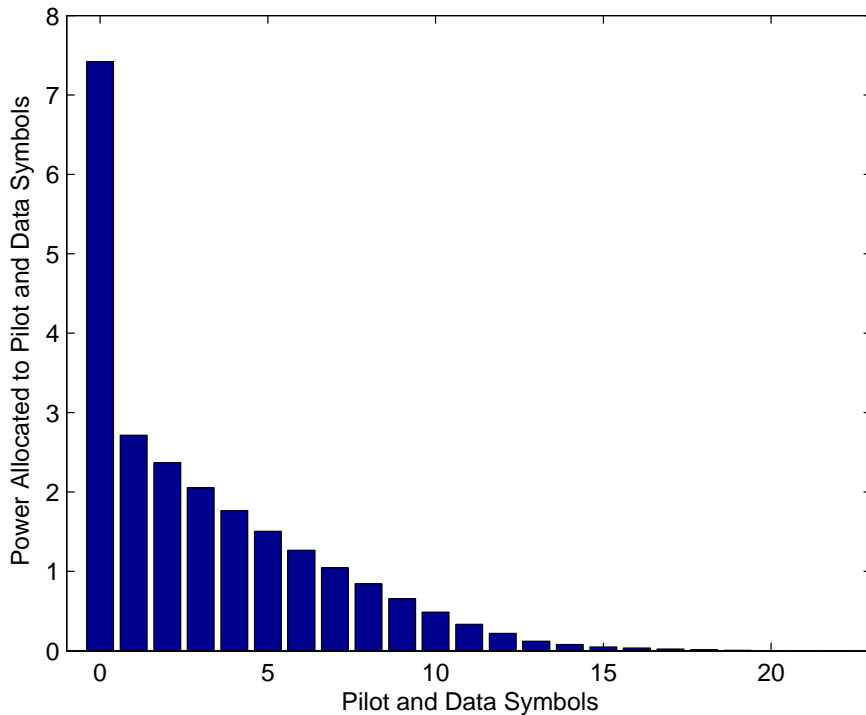


Figure 2.4: Optimal power distribution among the pilot and data symbols when  $\alpha = 0.90$  and  $SNR = 0$  dB. The suboptimal period is  $T = 23$ .

where  $C(SNR)$  is the channel capacity in bits/symbol. In our setting, the bit energy values found from

$$\frac{E_b}{N_0} = \frac{SNR}{I_L(T^*, P_t^*, \mathbf{P}_d^*)} \quad (2.17)$$

provide an upper bound on the values obtained from (2.16), and also gives us indications on the energy efficiency of the system. Fig. 2.5 plots the required bit energy values as a function of the SNR. The bit energy initially decreases as SNR decreases and achieves its minimum value at approximately  $SNR = -5.5$  dB below which the bit energy requirement starts increasing. Hence, it is extremely energy inefficient to operate below  $SNR = -5.5$  dB. In general, one needs to operate at low SNR levels for improved energy efficiency. From Fig. 2.6, which

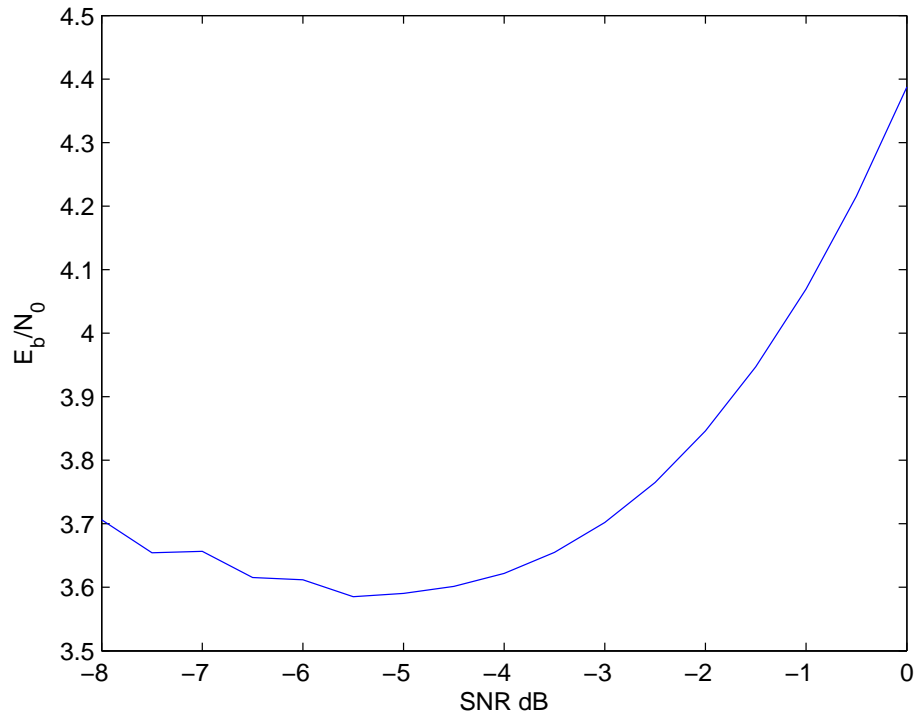


Figure 2.5: Bit energy  $\frac{E_b}{N_0}$  vs. SNR dB when  $\alpha = 0.99$ .

plots the optimal training period,  $T$ , as a function of the SNR, we observe that  $T$  increases as SNR decreases. Hence, training is performed less frequently in the low SNR regime. Fig. 2.7 provides the pilot and data power allocation when SNR =  $-7$  dB,  $\alpha = 0.99$ , and  $T = 65$ . It is interesting to note that although  $T$  is large, a considerable portion of the available time slots are not being used for transmission. This approach enables the system to put more power on the pilot symbol and nearby data symbols. Hence, although the system trains and transmits less frequently, a more accurate channel estimate is obtained and used in return.

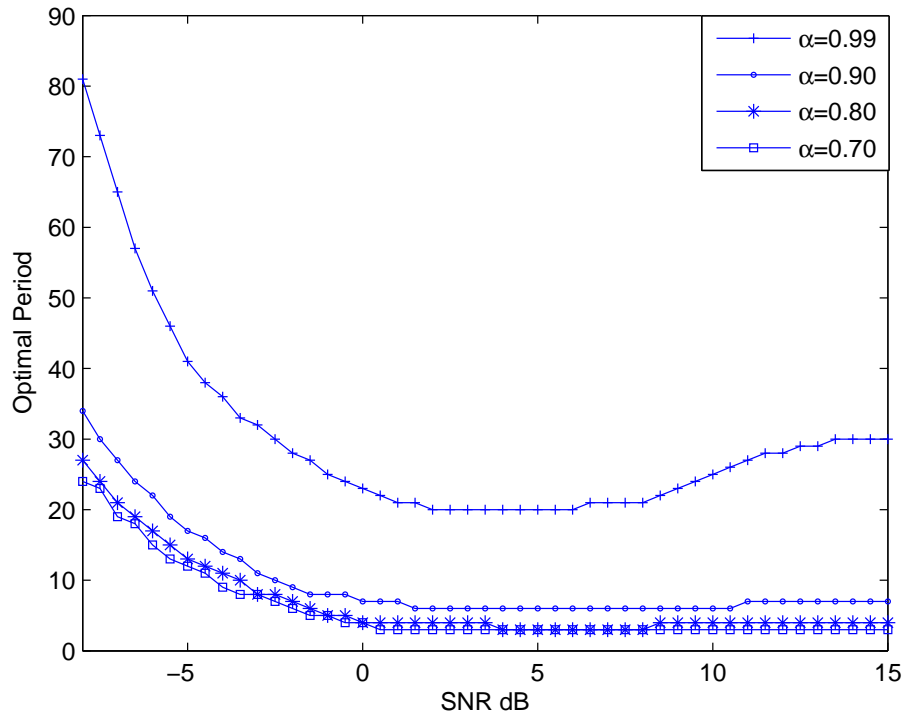


Figure 2.6: Optimal training period  $T$  vs.  $SNR$  for  $\alpha = 0.99, 0.90, 0.80,$  and  $0.70$ .

## 2.4 Low Complexity Training Optimization

Recall that the input-output relationship in the data transmission phase is given by<sup>1</sup>

$$y_k = \hat{h}_k x_k + \tilde{h}_k x_k + n_k \quad k = 1, 2, \dots, T-1. \quad (2.18)$$

In the preceding section, we fixed the modulation format and computed the input-output mutual information achieved in the channel (2.18). In this section, we pursue another approach akin to that in [37]. We treat the error in the channel

<sup>1</sup>It is assumed that a single pilot signal is transmitted at  $k = 0$ .

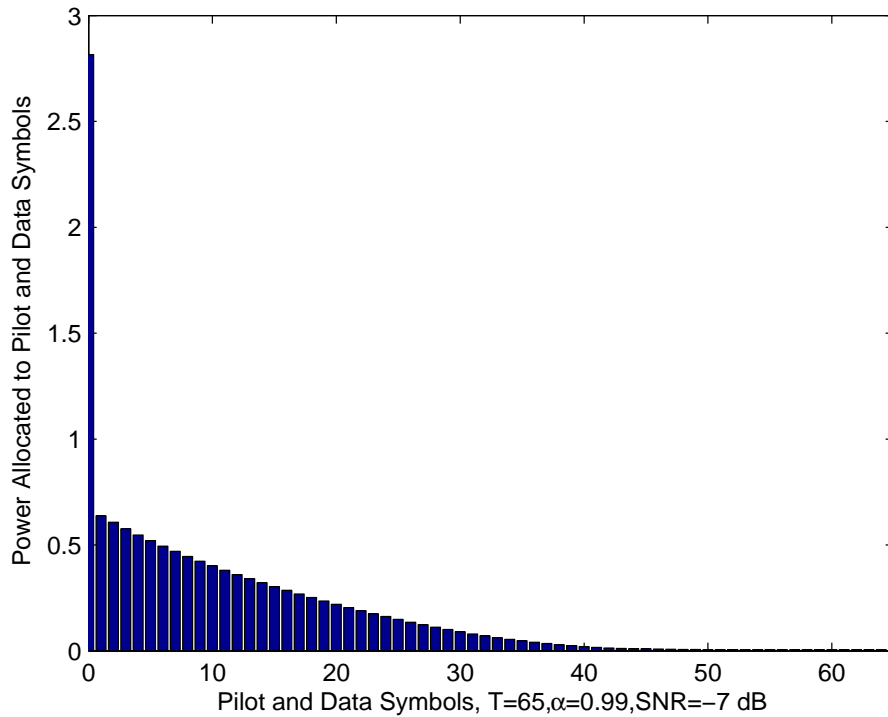


Figure 2.7: Optimal power distribution for the pilot and data symbols when  $\alpha = 0.99$  and  $SNR = -7$  dB. The optimal period is  $T = 65$ .

estimate as another source of additive noise and assume that

$$w_k = \tilde{h}_k x_k + n_k \quad (2.19)$$

is zero-mean Gaussian noise with variance

$$\sigma_{w_k}^2 = \sigma_{\tilde{h}_k}^2 P_{d,k} + \sigma_n^2. \quad (2.20)$$

where  $P_{d,k} = E[|x_k|^2]$  is the average power of the symbol  $x_k$  and  $\sigma_{\tilde{h}_k}^2$  is given in (2.10). Since the Gaussian noise is the worst case noise [37], the capacity of the

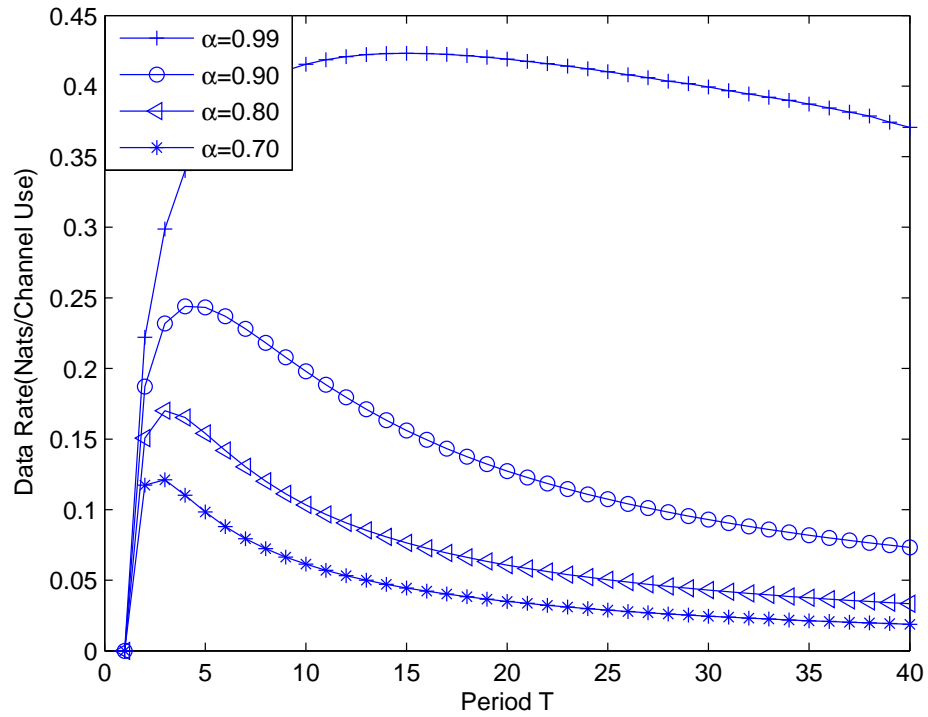


Figure 2.8: Achievable data rates vs. training period  $T$  for  $\alpha = 0.99, 0.90, 0.80,$  and  $0.70$ .  $SNR = 5$  dB

channel

$$y_k = \hat{h}_k x_k + w_k \quad k = 1, 2, \dots \quad (2.21)$$

is a lower bound to the capacity of the channel given in (2.18). An achievable rate expression for channel (2.21) is

$$I_{\text{worst}} = \max_{T, P_t} \max_{\mathbf{x} \in E[|\mathbf{x}|^2] \leq PT - P_t} \frac{1}{T} \sum_{k=1}^{T-1} I_k(x_k; y_k | \hat{h}_k) \quad (2.22)$$

$$= \max_{T, P_t} \max_{\substack{\mathbf{P}_d, \\ P_{d,k} \geq 0 \forall k \\ \sum_{k=1}^{T-1} P_{d,k} \leq PT - P_t}} \frac{1}{T} \sum_{k=1}^{T-1} \max_{x_k \in E[|x_k|^2] \leq P_{d,k}} I_k(x_k; y_k | \hat{h}_k) \quad (2.23)$$

$$= \max_{T, P_t, \mathbf{P}_d, \sum_{k=1}^{T-1} P_t + P_{d,k} \leq PT} \frac{1}{T} \sum_{k=1}^{T-1} E \left[ \log \left( 1 + \frac{\sigma_{\hat{h}_k}^2 P_{d,k}}{\sigma_{\hat{h}_k}^2 P_{d,k} + \sigma_n^2} |\tilde{\zeta}|^2 \right) \right]. \quad (2.24)$$

In (2.22),  $\mathbf{x} = (x_1, x_2, \dots, x_{T-1})$  denotes the vector of  $T - 1$  input symbols, and the inner maximization is over the space of joint distribution functions of  $\mathbf{x}$ . (2.23) is obtained by observing that once the data power distribution is fixed, the maximization over the joint distribution can be broken down into separate maximization problems over marginal distributions. (2.24) follows from the fact that Gaussian input maximizes the mutual information  $I(x_k; y_k | \hat{h}_k)$  when the channel in consideration is (2.21). Note that in (2.24),  $\tilde{\zeta}$  is a zero mean, unit variance, circular complex Gaussian random variable, and the expectation is with respect to  $\tilde{\zeta}$ . We can again numerically solve the above optimization and Fig. 2.8 plots the achievable data rates with optimal power allocation as a function of  $T$  for different values of  $\alpha$  when SNR = 5 dB. An even simpler optimization problem results if we seek to optimize the upper bound

$$\frac{1}{T} \sum_{k=1}^{T-1} E \left[ \log \left( 1 + \frac{\sigma_{\hat{h}_k}^2 P_{d,k}}{\sigma_{\hat{h}_k}^2 P_{d,k} + \sigma_n^2} |\tilde{\zeta}|^2 \right) \right] \leq \frac{1}{T} \sum_{k=1}^{T-1} \log \left( 1 + \frac{\sigma_{\hat{h}_k}^2 P_{d,k}}{\sigma_{\hat{h}_k}^2 P_{d,k} + \sigma_n^2} \right), \quad (2.25)$$



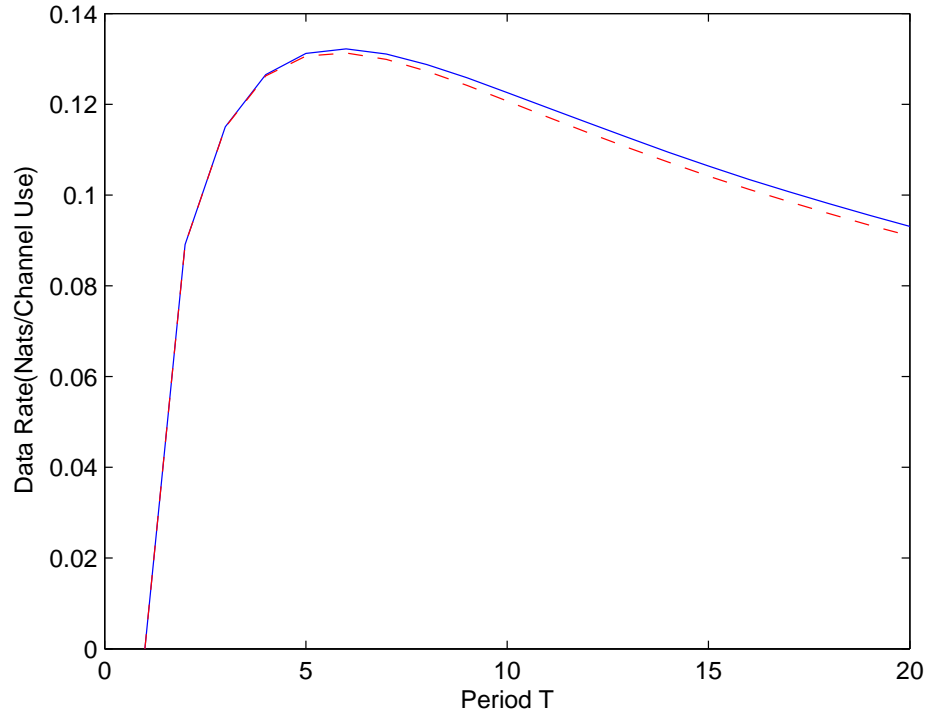


Figure 2.9: Achievable data rates for BPSK signals vs.training period  $T$  for  $\alpha = 0.90$ . SNR = 0 dB.

which is obtained by using the Jensen's inequality and noting that  $E[|\zeta|^2] = 1$ . In this case, the optimization problem becomes

$$\max_{\substack{T, P_t, P_d, \\ \sum_{k=1}^{T-1} P_t + P_{d,k} \leq PT}} \frac{1}{T} \sum_{k=1}^{T-1} \log \left( 1 + \frac{\sigma_{\tilde{h}_k}^2 P_{d,k}}{\sigma_{\tilde{h}_k}^2 P_{d,k} + \sigma_n^2} \right) = \max_{\substack{T, P_t, P_d, \\ \sum_{k=1}^{T-1} P_t + P_{d,k} \leq PT}} \frac{1}{T} \log \left( \prod_{k=1}^{T-1} \left( 1 + \frac{\sigma_{\tilde{h}_k}^2 P_{d,k}}{\sigma_{\tilde{h}_k}^2 P_{d,k} + \sigma_n^2} \right) \right). \quad (2.26)$$

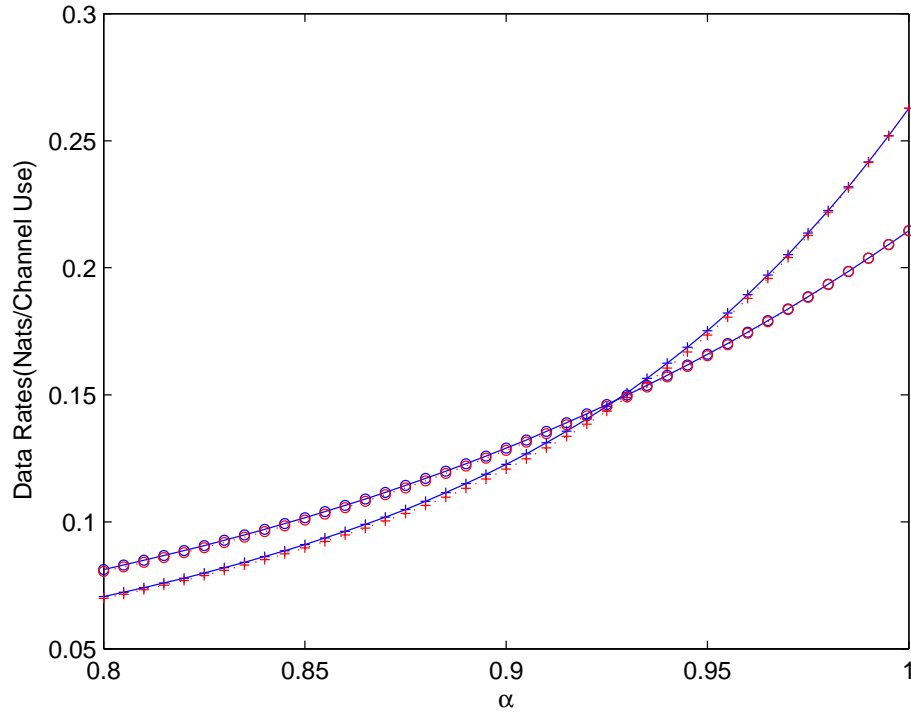


Figure 2.10: Achievable data rates for BPSK signals vs.  $\alpha$  for  $T = 6$  and  $10$ .  $SNR = 0$  dB. “+ and solid line” and “+ and dotted line” are plotting rates achieved with power allocation from (2.27) and (2.15), respectively, when  $T = 10$ . “o and solid line” and “o and dotted line” are plotting rates achieved with power allocation from (2.27) and (2.15), respectively, when  $T = 6$ .

Since logarithm is a monotonically increasing function, the optimal training and data power allocation for fixed  $T$  can be found by solving

$$\max_{\substack{P_t, P_d \\ \sum_{k=1}^{T-1} P_t + P_{d,k} \leq PT}} \prod_{k=1}^{T-1} \left( 1 + \frac{\sigma_{\hat{h}_k}^2 P_{d,k}}{\sigma_{\hat{h}_k}^2 P_{d,k} + \sigma_n^2} \right). \quad (2.27)$$

It is very interesting to note that the optimal power distribution found by solving (2.27) is very similar to that obtained from (2.15) where BPSK signals are considered. Figure 2.9 plots the achievable data rates as a function of training pe-

riod when BPSK signals are employed for transmission. Hence, the data rates are computed using (2.12). In the figure, the solid line shows the data rates achieved with power distribution found from (2.15) while the dashed line corresponds to rates achieved with power allocation obtained from (2.27). Note that both curves are very close and the training period is maximized at approximately the same value.

Fig. 2.10 plots the achievable rates for BPSK signals as a function of the parameter  $\alpha$  for  $T = 6$  and 10. The power distribution is again obtained from both (2.27) and (2.15). We again recognize that the loss in data rates is negligible when (2.27) is used to find the power allocation.

## 2.5 Conclusion

We have studied the problem of training optimization in pilot-assisted wireless transmissions over Gauss-Markov Rayleigh fading channels. We have considered a simple scenario where a single pilot is transmitted every  $T$  symbols for channel estimation and  $T - 1$  data symbols are transmitted in between the pilot symbols. MMSE estimation is employed to estimate the channel. We have jointly optimized the training period,  $T$ , and data and training power distributions by maximizing achievable rate expressions. We have provided numerical results showing the optimal parameters, power distributions, and maximized achievable rates. We have also studied the energy efficiency of pilot-assisted transmissions by analyzing the energy-per-bit requirements.

## Chapter 3

# Pilot-Symbol-Assisted Communications with Noncausal and Causal Wiener Filters

In this chapter, pilot-assisted transmission over time-selective flat fading channels is studied. It is assumed that noncausal and causal Wiener filters are employed at the receiver to perform channel estimation with the aid of training symbols sent periodically by the transmitter. For both filters, the variances of estimate errors are obtained from the Doppler power spectrum of the channel. Subsequently, achievable rate expressions are provided. The training period, and data and training power allocations are jointly optimized by maximizing the achievable rate expressions. Numerical results are obtained by modeling the fading as a Gauss-Markov process. The achievable rates of causal and noncausal filtering approaches are compared. For the particular ranges of parameters considered in this chapter, the performance loss incurred by using a causal filter as opposed to a noncausal filter is shown to be small. The impact of aliasing that occurs in the undersampled version of the channel Doppler spectrum due to fast fading is analyzed. Finally,

energy-per-bit requirements are investigated in the presence of noncausal and causal Wiener filters.

### 3.1 Channel Model

The time-selective Rayleigh channel is modeled as

$$y_k = h_k x_k + n_k \quad k = 1, 2, 3, \dots \quad (3.1)$$

where  $y_k$  is the complex channel output,  $x_k$  is the complex channel input,  $\{n_k\}$  is assumed to be a sequence of i.i.d. zero-mean Gaussian random variables with variance  $\sigma_n^2$ , and  $\{h_k\}$  is the sequence of fading coefficients.  $\{h_k\}$  is assumed to be a zero-mean stationary Gaussian random process with power spectral density  $S_h(e^{j\omega})$ . It is further assumed that  $x_k$  is independent of  $h_k$  and  $n_k$ . While both the transmitter and the receiver know the channel statistics, neither has prior knowledge of instantaneous realizations of the fading coefficients. Note that the discrete-time model is obtained by sampling the received signal every  $T_s$  seconds.

### 3.2 Pilot Symbol-Assisted Transmission and Reception

We consider pilot-assisted transmission where periodically inserted pilot symbols, known by both the sender and the receiver, are used to estimate the fading coefficients of the channel using a Wiener filter. We assume the simple scenario where a single pilot symbol is transmitted every  $M$  symbols while  $M - 1$  data symbols are transmitted in between the pilot symbols. We consider the following average

power constraint

$$\frac{1}{M} \sum_{k=lM}^{(l+1)M-1} E \left[ |x_k|^2 \right] \leq P \quad l = 0, 1, 2, \dots \quad (3.2)$$

on the input. Therefore, the total average power allocated to the pilot and data transmission over a duration of  $M$  symbols is limited by  $MP$ .

Communication takes place in two phases. In the training phase, the transmitter sends pilot symbols and the receiver estimates the channel coefficients. In this phase, the channel output is given by

$$y_{lM} = h_{lM} \sqrt{P_t} + n_{lM} \quad (3.3)$$

where  $P_t$  is the power allocated to the pilot symbol. In the data transmission phase, data symbols are transmitted. In this phase, the input-output relationship can be written as

$$y_k = \hat{h}_k x_k + \tilde{h}_k x_k + n_k \quad lM < k \leq (l+1)M - 1 \quad (3.4)$$

where  $\hat{h}_k$  and  $\tilde{h}_k$  are the estimated channel coefficient and the error in the estimate at sample time  $k$ , respectively. Note that  $\hat{h}_k$  and  $\tilde{h}_k$  for  $lM < k \leq (l+1)M - 1$  are uncorrelated zero-mean circularly symmetric complex Gaussian random variables with variances  $\sigma_{\hat{h}_k}^2$  and  $\sigma_{\tilde{h}_k}^2$ , respectively.

### 3.3 Achievable Rates

For the estimation of the fading coefficients, we assume that a Wiener filter, which is the optimum linear estimator in the mean-square sense, is employed at the

receiver. Note that since pilot symbols are sent with a period of  $M$ , the channel is sampled every  $MT_s$  seconds. Therefore we have to consider the under-sampled version of the channel's Doppler spectrum which is given by

$$S_{h,m}(e^{jw}) = \frac{1}{M} \sum_{k=0}^{M-1} e^{jm(w-2\pi k)/M} S_h \left( e^{j(w-2\pi k)/M} \right). \quad (3.5)$$

Also shown in [60], it can easily be seen from [44] that the channel MMSE for the noncausal Wiener filter at time  $Ml + m$  is given by

$$\sigma_{h_{Ml+m}}^2 = \sigma_h^2 - \frac{1}{2\pi} \int_{-\pi}^{\pi} \frac{P_t |S_{h,m}(e^{jw})|^2}{P_t S_{h,0}(e^{jw}) + \sigma_n^2} dw \quad (3.6)$$

where  $P_t$  again denotes the power allocated to one pilot symbol. On the other hand, from [44], we can also easily find that the channel MMSE at time  $Ml + m$  for the causal Wiener filter is given by

$$\sigma_{\tilde{h}_{Ml+m}}^2 = \sigma_h^2 - \frac{1}{2\pi} \int_{-\pi}^{\pi} \frac{P_t |S_{h,m}(e^{jw})|^2}{P_t S_{h,0}(e^{jw}) + \sigma_n^2} dw + \frac{1}{2\pi} \int_{-\pi}^{\pi} \frac{P_t}{r_e} \left| \left\{ \frac{S_{h,m}(e^{jw})}{L^*(e^{jw})} \right\}_- \right|^2 dw \quad (3.7)$$

where  $L^*(e^{jw})$  is obtained from the canonical factorization of the channel output's sampled power spectral density at  $m = 0$ , which is given by

$$P_t S_{h,0}(e^{jw}) + \sigma_n^2 = r_e L(e^{jw}) L^*(e^{jw}). \quad (3.8)$$

The operators  $\{\}_+$  and  $\{\}_-$  yield the causal and the anti-causal part of the function to which they are applied, respectively. Note that, using the orthogonality principle, we have

$$\sigma_{\tilde{h}_{Ml+m}}^2 = \sigma_h^2 - \sigma_{h_{Ml+m}}^2 \quad (3.9)$$

where  $\sigma_{\tilde{h}_{Ml+m}}^2$  is the variance of the channel estimate at time  $Ml + m$ . Similarly as in [4], treating the error in (3.4) as another source of additive noise and assuming that

$$w_k = \tilde{h}_k x_k + n_k \quad (3.10)$$

is zero-mean Gaussian noise with variance

$$\sigma_{w_k}^2 = \sigma_{\tilde{h}_k}^2 P_m + \sigma_n^2 \quad (3.11)$$

we obtain the following lower bound on the channel capacity:

$$C \geq \frac{1}{M} \sum_{m=1}^{M-1} E \left\{ \log \left( 1 + \frac{P_m \sigma_{\tilde{h}_m}^2}{P_m \sigma_{\tilde{h}_m}^2 + \sigma_n^2} |\tilde{\zeta}|^2 \right) \right\} \quad (3.12)$$

where  $\tilde{\zeta}$  is a zero-mean, unit-variance, circularly symmetric complex Gaussian random variable and  $P_m = E [|x_{Ml+m}|^2]$  denotes the power of the  $m^{\text{th}}$  data symbol after the pilot symbol. Note that the error variance  $\sigma_{\tilde{h}_{Ml+m}}^2$  depends in general on  $m$  and hence the location of the data symbol with respect to the pilot symbol. However, if the fading slowly varies and the channel is sampled sufficiently fast, we can satisfy  $2\pi f_D \leq \pi/M$  where  $f_D$  is the maximum Doppler frequency of the channel. In this case,  $M \leq \frac{1}{2f_D}$ . We can see from the Nyquist's Theorem that there is no aliasing in the under-sampled version of the channel's Doppler spectrum, and hence  $|S_{h,m}(e^{jw})| = |S_{h,0}(e^{jw})| = |S_h(e^{jw/M})|/M$ , for  $m \in [1, M-1]$  and  $-\pi \leq w \leq \pi$ . Therefore, (3.6) reduces to

$$\begin{aligned} \sigma_{\tilde{h}_{Ml+m}}^2 &= \sigma_h^2 - \frac{1}{2\pi} \int_{-\pi}^{\pi} \frac{P_t |S_{h,0}(e^{jw})|^2}{P_t S_{h,0}(e^{jw}) + \sigma_n^2} dw \\ &= \sigma_h^2 - \frac{1}{2\pi} \int_{-\pi/M}^{\pi/M} \frac{P_t |S_h(e^{jw})|^2}{P_t S_h(e^{jw}) + M\sigma_n^2} dw = \sigma_h^2, \end{aligned} \quad (3.13)$$



and also (3.7) can be expressed as

$$\begin{aligned}
\sigma_{\hat{h}_{Ml+m}}^2 &= \sigma_h^2 - \frac{1}{2\pi} \int_{-\pi}^{\pi} \frac{P_t |S_{h,0}(e^{jw})|^2}{P_t S_{h,0}(e^{jw}) + \sigma_n^2} dw + \frac{1}{2\pi} \int_{-\pi}^{\pi} \frac{P_t}{r_e} \left| \left\{ \frac{S_{h,0}(e^{jw})}{L^*(e^{jw})} \right\} \right|_-^2 dw \\
&= \sigma_h^2 - \frac{1}{2\pi} \int_{-\pi/M}^{\pi/M} \frac{P_t |S_h(e^{jw})|^2}{P_t S_h(e^{jw}) + M\sigma_n^2} dw + \frac{1}{2\pi} \int_{-\pi/M}^{\pi/M} \frac{P_t}{Mr_f} \left| \left\{ \frac{S_h(e^{jw})}{F^*(e^{jw})} \right\} \right|_-^2 dw \\
&= \sigma_{\hat{h}}^2,
\end{aligned} \tag{3.14}$$

where

$$\frac{P_t S_h(e^{jw})}{M} + \sigma_n^2 = r_f F(e^{jw}) F^*(e^{jw}). \tag{3.15}$$

Therefore, under this assumption, the error variances become independent of  $m$ . Since the estimate quality is the same for each data symbol regardless of its position with respect to the pilot symbol, uniform power allocation among the data symbols is optimal and we have

$$P_m = \frac{MP - P_t}{M - 1} = P_0. \tag{3.16}$$

Then, we can rewrite (3.12) as

$$C \geq \frac{M-1}{M} E \left\{ \log \left( 1 + \frac{P_0 \sigma_h^2}{P_0 \sigma_h^2 + \sigma_n^2} |\zeta|^2 \right) \right\}. \tag{3.17}$$

### 3.4 Optimizing Training Parameters in Gauss-Markov Channels

In this section, we assume that the fading process is modeled as a first-order Gauss-Markov process, whose dynamics is described by

$$h_k = \alpha h_{k-1} + z_k \quad 0 \leq \alpha \leq 1 \quad k = 1, 2, 3, \dots \quad (3.18)$$

where  $\{z_k\}$  are i.i.d. circular complex Gaussian variables with zero mean and variance equal to  $(1 - \alpha^2)\sigma_h^2$ . The power spectral density of the Gauss-Markov process with variance  $\sigma_h^2$  is given by

$$S_h(e^{jw}) = \frac{(1 - \alpha^2)\sigma_h^2}{1 + \alpha^2 - 2\alpha \cos(w)}. \quad (3.19)$$

Note that  $S_h(e^{jw})$  in (3.19) is not bandlimited and hence the condition  $2\pi f_D \leq \pi/M$  can only be satisfied when  $M = 1$  which is not a viable strategy. However if the fading is slowly-varying and hence the value of  $\alpha$  is close to 1, the Doppler spectrum  $S_h(e^{jw})$  decreases sharply for large frequencies and most of the energy is accumulated at low Doppler frequencies. Figure 3.1 plots  $S_h(e^{jw})$  for  $\alpha = 0.99, 0.95$ , and  $0.90$ , and verifies the above claim. We can easily find that the frequency ranges  $[-\pi/49, \pi/49]$ ,  $[-\pi/9, \pi/9]$  and  $[-\pi/4, \pi/4]$  contain more than 90 % of the power when  $\alpha = 0.99, 0.95$ , and  $0.90$ , respectively. Hence, if  $M \leq 49, 9$ , and  $4$ , respectively, in these cases, the impact of aliasing will be negligible. Otherwise, ignoring the effect of aliasing will decrease the error variance and hence the achievable rates under this assumption will be higher than those obtained when aliasing is considered.

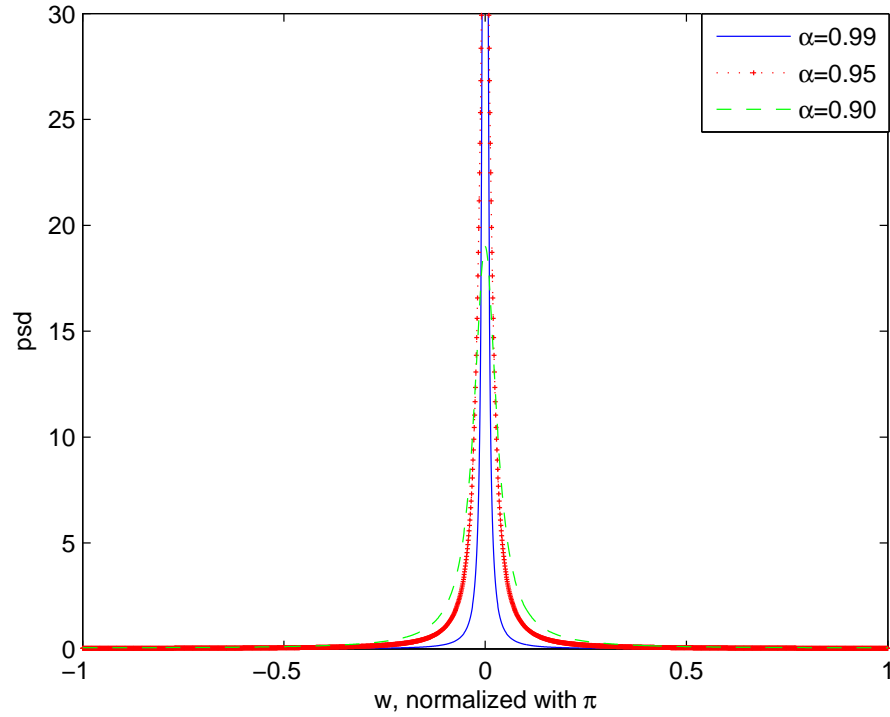


Figure 3.1: The power spectral density of Gauss-Markov channels for  $\alpha = 0.99$ , 0.95, and 0.90 when  $\sigma_h^2 = 1$ .

In the Gauss-Markov model, the error variance for the noncausal Wiener filter can easily be obtained from (3.6). In order to obtain the error variance for the causal filter in the absence of aliasing, we have to perform the canonical factorization. We begin with rewriting (3.8) as

$$\frac{P_t S_h(e^{jw/M})}{M} + \sigma_n^2 = r_f F(e^{jw/M}) F^*(e^{jw/M}) \quad (3.20)$$

where

$$F(e^{jw}) = \frac{1 - u e^{-jw}}{1 - \alpha e^{-jw}}.$$

From (3.20), we can deduce that

$$c + \sigma_n^2 \alpha (e^{jw/M} + e^{-jw/M}) = r_f (1 + u) + r_f u (e^{jw/M} + e^{-jw/M}) \quad (3.21)$$

where

$$c = \frac{P_t}{M} (1 - \alpha^2) \sigma_h^2 + (1 + \alpha^2) \sigma_n^2.$$

From (3.21), we can write

$$r_f = \frac{c + \sqrt{c^2 - 4\alpha^2 \sigma_n^4}}{2} \quad \text{and} \quad u = \frac{\alpha \sigma_n^2}{r_f} \quad (3.22)$$

where  $0 < u < 1$  and  $r_f > 0$ . After the canonical factorization, we can write

$$\begin{aligned} \frac{S_h(e^{jw/M})}{F^*(e^{jw/M})} &= \frac{(1 - \alpha^2) \sigma_h^2}{(1 - \alpha e^{-jw/M})(1 - \alpha e^{jw/M})} \frac{1 - \alpha e^{jw/M}}{1 - u e^{jw/M}} \\ &= \frac{(1 - \alpha^2) \sigma_h^2}{(1 - \alpha e^{-jw/M})(1 - u e^{jw/M})} \end{aligned} \quad (3.23)$$

$$= B \left[ \frac{u\alpha}{e^{jw/M} - \alpha} - \frac{1}{e^{jw/M} - 1/u} \right] \quad (3.24)$$

where

$$B = -\frac{(1 - \alpha^2) \sigma_h^2}{u(1 - u\alpha)}.$$

The anti-causal part can be written as

$$\left\{ \frac{S_h(e^{jw/M})}{F^*(e^{jw/M})} \right\}_- = \frac{(1 - \alpha^2) \sigma_h^2 u}{(1 - u\alpha)} \frac{e^{jw/M}}{(1 - u e^{jw/M})}. \quad (3.25)$$

After making a change of variables, we have

$$\left\{ \frac{S_h(e^{jw})}{F^*(e^{jw})} \right\}_- = \frac{(1 - \alpha^2) \sigma_h^2 u}{(1 - u\alpha)} \frac{e^{jw}}{(1 - u e^{jw})}. \quad (3.26)$$

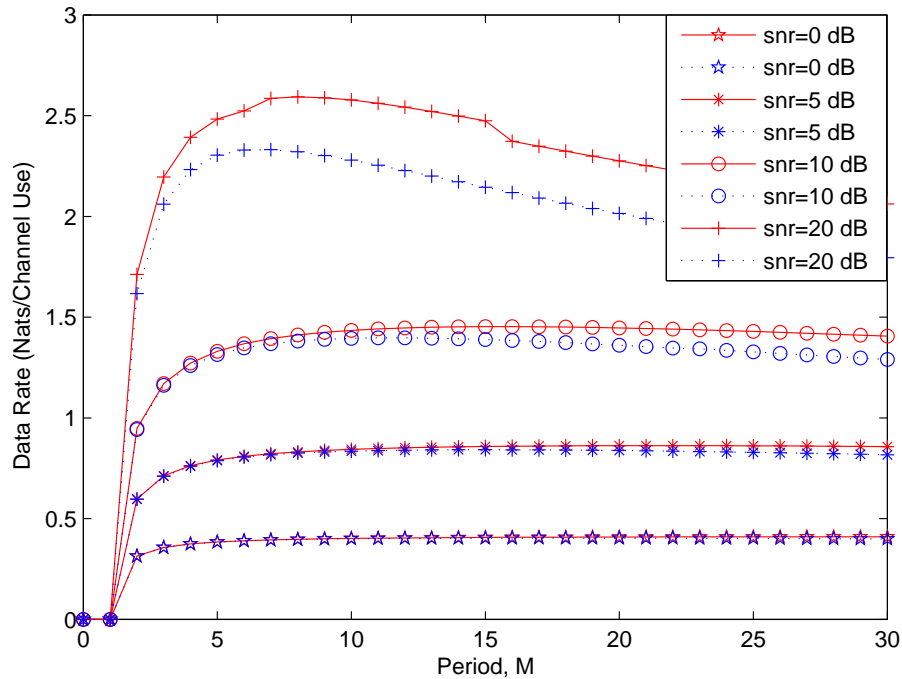


Figure 3.2: Achievable rates when  $\alpha = 0.99$  for  $SNR = 0, 5, 10,$  and  $20$  dB. The dotted lines provide rates when aliasing is taken into account, and the solid lines give the rates when aliasing is ignored.

## 3.5 Numerical Results

### 3.5.1 Optimal Parameters and Effects of Aliasing

In this section, we present our numerical results. Initially, we consider noncausal Wiener filtering and jointly optimize the training period, and data and pilot symbol power allocation. Moreover, we study the effects of aliasing in the under-sampled channel Doppler spectrum. In Figure 3.2, we plot the achievable rates as a function of the training period when  $\alpha = 0.99$ , i.e., when the channel is changing very slowly, for SNR values of 0, 5, 10 and 20 dB. In this figure, plotted curves are obtained with optimal pilot and data power allocation. The dotted lines give the

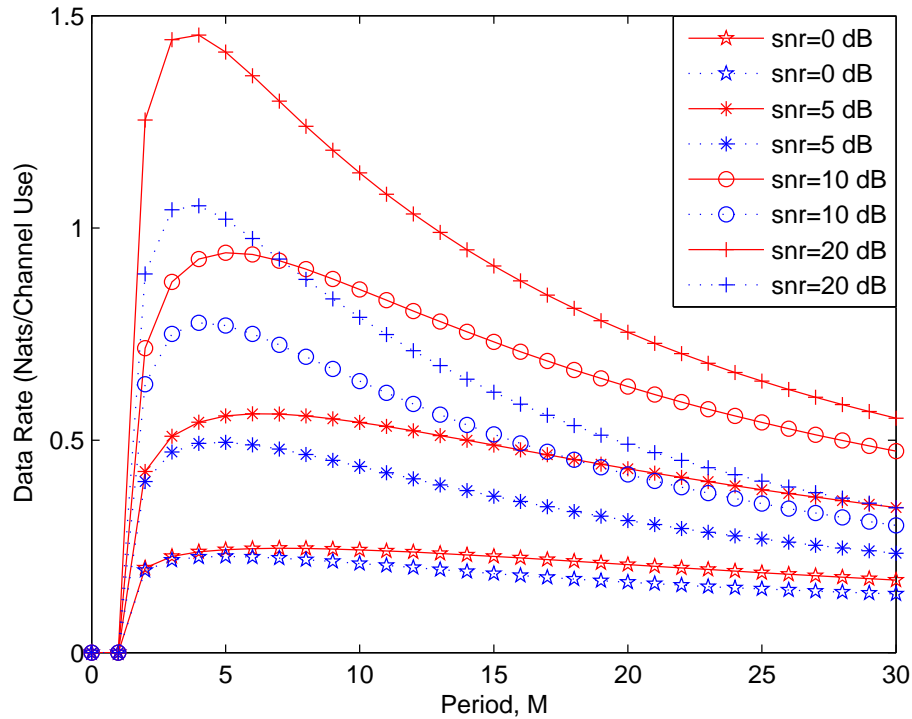


Figure 3.3: Achievable rates when  $\alpha = 0.90$  for  $SNR = 0, 5, 10,$  and  $20$  dB. The dotted lines provide rates when aliasing is taken into account, and the solid lines give the rates when aliasing is ignored.

data rates obtained when aliasing is taken into account. Solid lines show the rates when aliasing is ignored. As seen in Fig. 3.2, when SNR is small, the difference between the dotted and solid lines is negligible. As SNR increases, the difference between the lines is also increasing. From this, we can conceive that the effect of aliasing is more dominant with increasing SNR. When  $\alpha = 0.99$  and aliasing is taken into account, the optimal training periods are 16, 15, 12 and 7 for SNR values of 0, 5, 10 and 20 dB, respectively. On the other hand, when aliasing is ignored, we have optimal values as 25, 21, 16 and 8. Hence, the optimal training period decreases as SNR increases and aliasing is considered.

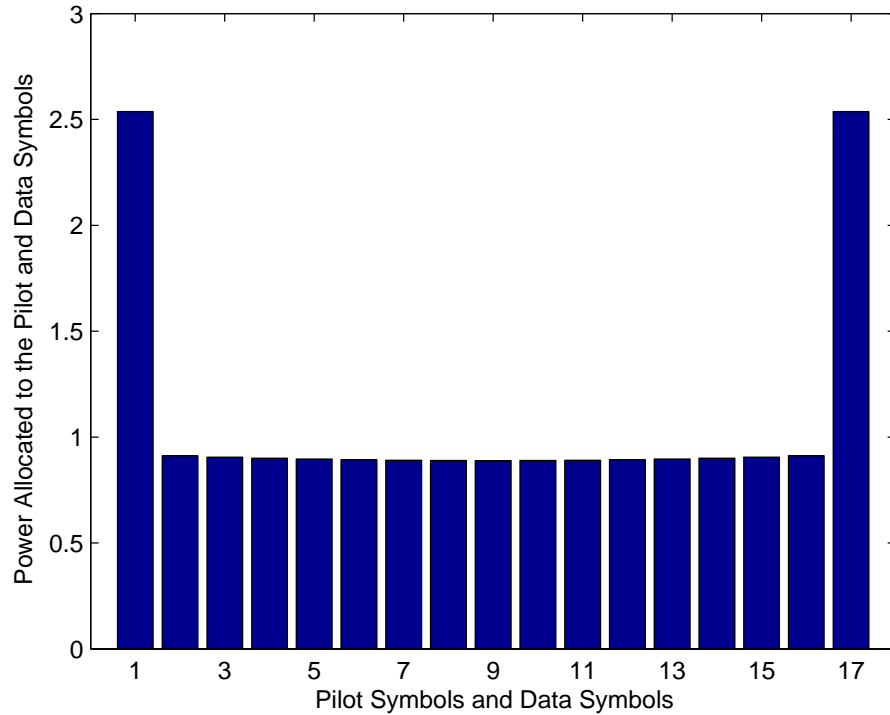


Figure 3.4: The optimal power distribution among the pilot and data symbols when  $\alpha = 0.99$  and  $SNR = 0$  dB. The optimal period is 16.

In Figure 3.3, we plot the achievable rates when  $\alpha = 0.90$ . Comparing Figs 3.2 and 3.3, we observe that aliasing has a more significant impact as  $\alpha$  decreases. This is expected since aliasing increases in a faster changing channel and hence ignoring aliasing provides a looser upper bound. When  $\alpha = 0.90$  and aliasing is taken into account, the optimal training periods are 7, 6, 5 and 4 for SNR values of 0, 5, 10 and 20 dB, respectively. When aliasing is ignored, the optimal values are 5, 5, 4 and 4, respectively. As before, the optimal period is decreasing and the effect of aliasing is increasing with the increasing SNR.

Figure 3.4 and Figure 3.5 are the bar graphs providing the optimal training and data power allocation for  $\alpha = 0.99$  and 0.90, respectively, when the training

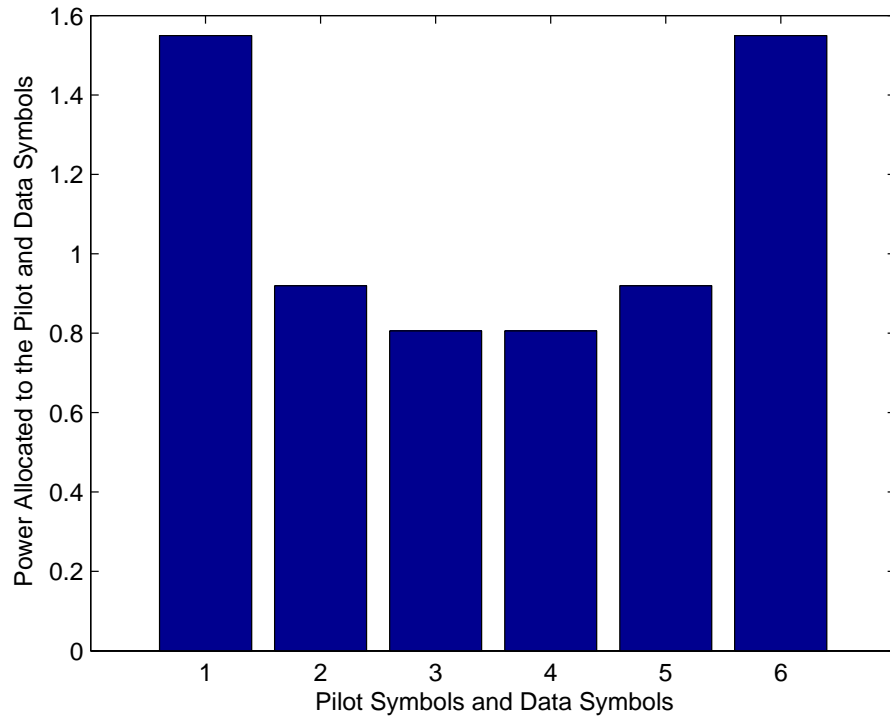


Figure 3.5: The optimal power distribution among the pilot and data symbols when  $\alpha = 0.90$  and  $SNR = 0$  dB. The optimal period is 5.

period is at its optimal value. In the graphs, the first and the last bars give the power of the pilot symbols and the ones in between represent the data symbol power levels. These bar graphs are obtained when the effect of aliasing on the channel estimation is taken into account. We can immediately observe from both graphs that the data symbols farther away from the pilot symbols are allocated less power because the error in the estimation increases with the distance to the pilot symbols. In Fig. 3.4, the decrease in the allocated power is small since the channel is very slowly varying and estimate error is almost independent of  $m$ . On the other hand, the decrease is more obvious when the channel changes faster as evidenced in Fig. 3.5. Furthermore, comparing Figs. 3.4 and 3.5, we see



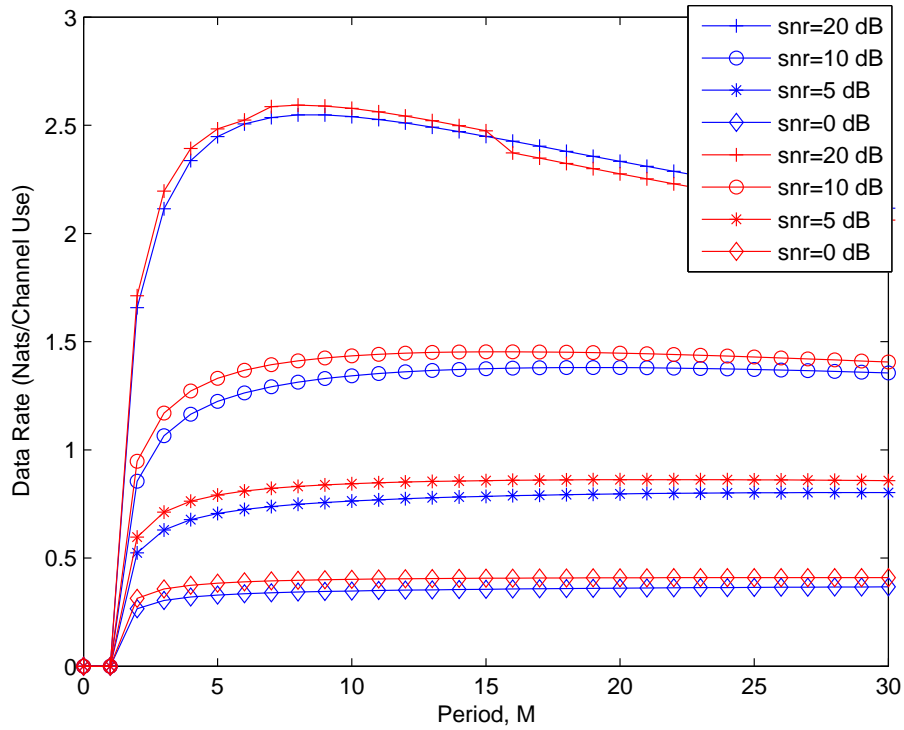


Figure 3.6: Achievable rates vs. training period when noncausal and causal filters are employed at the receiver.  $\alpha = 0.99$  and  $SNR = 0, 5, 10,$  and  $20$  dB. The red lines give the rates when a noncausal filter is used and the blue lines show the rates when a causal filter is used.

that when the training period value is high, more power is allocated to the pilot symbol, enabling the system to track the channel more accurately.

### 3.5.2 Causal Filter Performance in the Absence of Aliasing

In this section, we study the performance when a causal Wiener filter is employed at the receiver. Since it is rather difficult to obtain the canonical factorization of arbitrary spectrum, we only consider cases in which the channel is slowly varying and the aliasing effect can be ignored. In Figure 3.6, we plot the achievable rates as a function of the training period for  $\alpha = 0.99$  when noncausal and causal

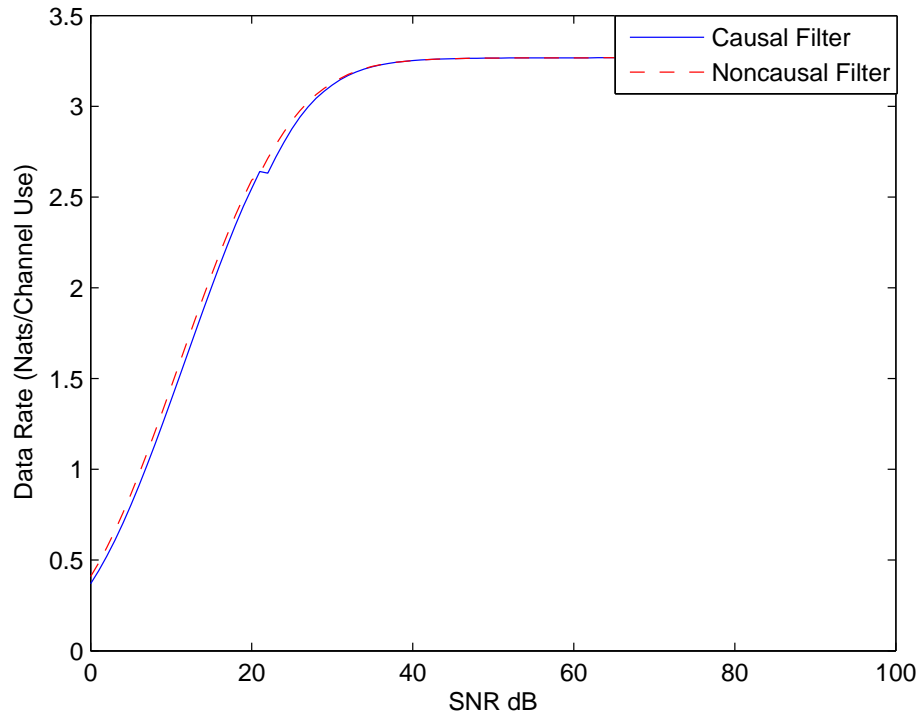


Figure 3.7: Achievable rates vs.  $SNR$  when noncausal and causal filters are employed at the receiver.  $\alpha = 0.99$ . The dashed line gives the rate when a noncausal filter is used and the solid line shows the rate when a causal filter is used.

Wiener filters are used. We compare the results when  $SNR = 0, 5, 10$  and  $20$  dB. The dotted lines provide the rates for the case of the causal filter and the solid lines show the results for the case of the noncausal filter. We observe that the optimal training periods are 44, 29, 19 and 9 for the causal filter when  $SNR = 0, 5, 10$  and  $20$ , respectively. For the noncausal filter, the optimal periods are 25, 21, 16 and 8 for the same  $SNR$  values. We observe from the plots that the performance of causal and noncausal filters are very close. In Figure 3.7, we plot the achievable rates as a function of  $SNR$  at optimal periods obtained by using causal and noncausal filters. Again the performances are very similar. Moreover, after 45 dB, the rates are the same for both filters. Therefore, for the ranges of

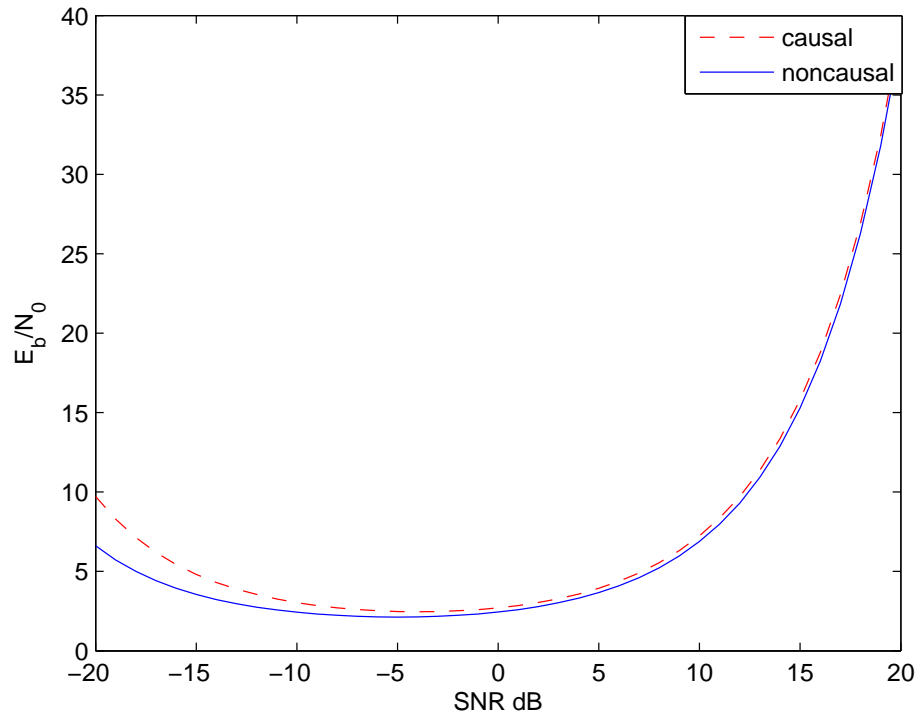


Figure 3.8: Bit energy  $\frac{E_b}{N_0}$  vs. SNR dB when  $\alpha = 0.99$ .

parameters considered in these figures, causal filter should be preferred over the noncausal one.

In systems where energy is at a premium, the energy required to send one bit of information is a metric that can be adopted to measure the efficiency of the system. The least amount of normalized bit energy required for reliable communications is given by  $\frac{E_b}{N_0} = \frac{SNR}{C(SNR)}$  where  $C(SNR)$  is the channel capacity in bits/symbol. In our setting, we use the achievable rates and analyze the required bit energy levels. In Figure 3.8, we plot the bit energy levels. The dashed and solid lines show the results for causal and noncausal filters. Note that the minimum bit energies are achieved at SNR = -4 dB and -3 dB for noncausal and causal filters, respectively. Operating below these SNR levels should be avoided as it

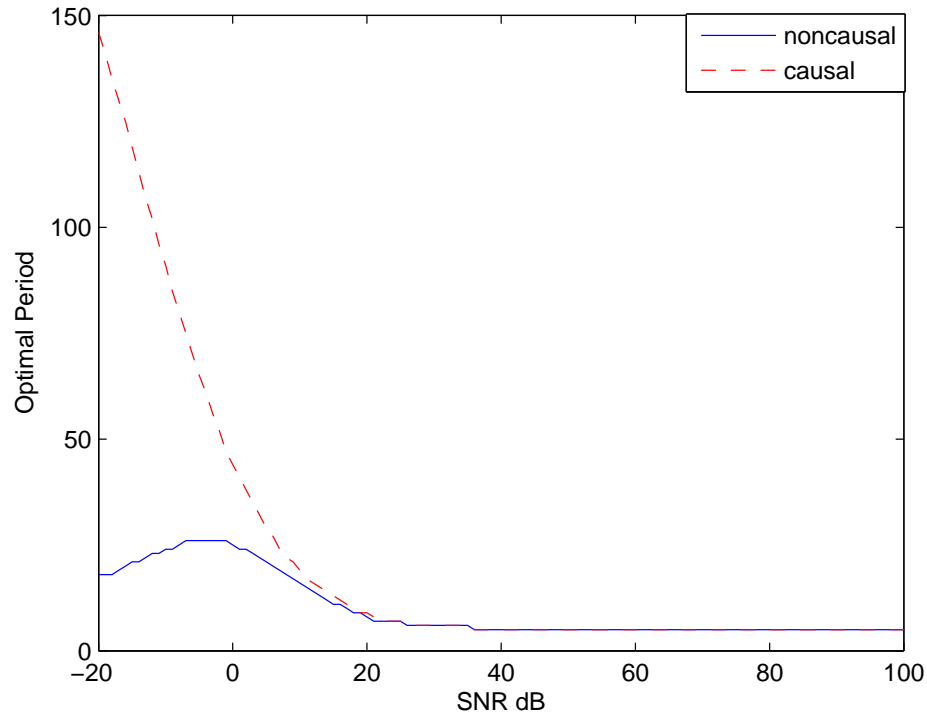


Figure 3.9: Optimal period vs.  $SNR$  dB for causal and noncausal filters when  $\alpha = 0.99$ .

only increases the required energy per bit. Figure 3.9 shows the optimal training period values as a function of SNR for both filters. Interestingly, the optimal period is increasing as SNR decreases for the causal filter while it first increases and then decreases when the noncausal filter is used. Since both past and future pilots are used when a noncausal filter is employed, having large training periods will diminish the benefits of future pilots especially for the data symbols in the middle. Therefore, this option is avoided in this case. On the other hand, having a larger period in the causal filter case enables the system to put more power to the pilot by not using data symbol slots farther away from the pilot and hence to obtain more accurate channel estimates. In both filters, as SNR increases the

optimal period value stays constant at 5.

### **3.6 Conclusion**

We have studied pilot-assisted communications when causal and noncausal Wiener filters are employed at the receiver for channel estimation. We have obtained achievable rate expressions by finding the error variances in both cases. Subsequently, we have jointly optimized the training period and power, and data power levels. We have analyzed the effects of aliasing on the data rates in Gauss-Markov Rayleigh fading channels when noncausal filters are used. We have provided numerical results showing the optimal parameters. We have compared the performances of causal and noncausal Wiener filters at different SNR values. We have also studied the energy-efficiency of pilot-assisted modulation with both filters.

## Chapter 4

# Achievable Rates and Training Optimization for Fading Relay Channels with Memory

In this chapter, transmission over time-selective, flat fading relay channels is studied. It is assumed that channel fading coefficients are not known a priori. Transmission takes place in two phases: network training phase and data transmission phase. In the training phase, pilot symbols are sent and the receivers employ single-pilot MMSE estimation or noncausal Wiener filter to learn the channel. AF and DF techniques are considered in the data transmission phase and achievable rate expressions are obtained. The training period, and data and training power allocations are jointly optimized by using the achievable rate expressions. Numerical results are obtained considering Gauss-Markov and lowpass fading models. Achievable rates are computed and energy-per-bit requirements are investigated. The optimal power distributions among pilot and data symbols are provided.

## 4.1 Channel Model

We consider a three-node-relay network which consists of one source node, one relay node and one destination node. Source-destination, source-relay and relay-destination channels are modeled as Rayleigh fading channels with fading coefficients denoted by  $h_{sd} \sim \mathcal{CN}(0, \sigma_{sd}^2)$ ,  $h_{sr} \sim \mathcal{CN}(0, \sigma_{sr}^2)$  and  $h_{rd} \sim \mathcal{CN}(0, \sigma_{rd}^2)$ <sup>1</sup>, respectively. Each channel is independent of others and exhibits memory with an arbitrary correlation structure. Hence  $\{h_{sd}\}$ ,  $\{h_{sr}\}$ , and  $\{h_{rd}\}$  are assumed to be mutually independent Gaussian random processes with power spectral densities  $S_{h_{sd}}(e^{jw})$ ,  $S_{h_{sr}}(e^{jw})$  and  $S_{h_{rd}}(e^{jw})$ , respectively. In this relay network, information is sent from the source to the destination with the aid of the relay. Transmission takes place in two phases: network training phase and data transmission phase. Over a duration of  $M$  symbols, the source and the relay are subject to the following power constraints:

$$\|\mathbf{x}_{s,t}\|^2 + E\{\|\mathbf{x}_s\|^2\} \leq MP_s \quad \text{and} \quad \|\mathbf{x}_{r,t}\|^2 + E\{\|\mathbf{x}_r\|^2\} \leq MP_r \quad (4.1)$$

where  $\mathbf{x}_{s,t}$  and  $\mathbf{x}_{r,t}$  are the source and relay pilot vectors, respectively, and  $\mathbf{x}_s$  and  $\mathbf{x}_r$  are the data vectors sent by the source and the relay, respectively.

## 4.2 Network Training Phase

In the network training phase, source and relay send pilot symbols in nonoverlapping intervals with a period of  $M$  symbols to facilitate channel estimation at the receivers. In a block of  $M$  symbols, transmission takes place in the following or-

---

<sup>1</sup> $x \sim \mathcal{CN}(m, \sigma^2)$  is used to denote that  $x$  is a proper complex Gaussian random variable with mean  $m$  and variance  $\sigma^2$ .

der. First, the source sends a single pilot symbol  $x_{s,t}$ , and the relay and destination receive

$$y_{r,t} = h_{sr}x_{s,t} + n_r \quad \text{and} \quad y_{d,t} = h_{sd}x_{s,t} + n_d, \quad (4.2)$$

and estimates  $h_{sr}$  and  $h_{sd}$ , respectively. Then, transmission enters the data transmission phase, and source sends an  $(M - 2)/2$ -dimensional data vector that is again received by the relay and destination terminals. Next, only the relay sends a single pilot symbol  $x_{r,t}$ , and the signal received at the destination node is

$$y_{d,t}^r = h_{rd}x_{r,t} + n_d^r, \quad (4.3)$$

which is used by the destination to estimate  $h_{rd}$ . In (4.2) and (4.3),  $n_r$ ,  $n_d$ , and  $n_d^r$  are assumed to be i.i.d. zero mean Gaussian random variables with variance  $\sigma_n^2$ , modeling the additive thermal noise present at the receivers. In the remaining duration of  $(M - 2)/2$  symbols, transmission again enters the data transmission phase. In this case, the relay transmits an  $(M - 2)/2$  dimensional data vector to the destination while the source either becomes silent or continues its transmission depending on the cooperation protocol. This order of transmission is repeated for the next block of  $M$  symbols.

As noted before, we consider two channel estimation methods. In the first method, only a single pilot symbol is used to obtain the MMSE estimate of the channel fading coefficients. As described in [35], MMSE estimates of the fading



coefficients and the variances of the estimate errors are given as follows<sup>2</sup>:

$$\hat{h}_{sr} = \frac{\sigma_{sr}^2 \sqrt{P_{x_{s,t}}}}{\sigma_{sr}^2 P_{x_{s,t}} + \sigma_n^2} y_{r,t}, \quad \sigma_{\hat{h}_{sr}}^2 = \frac{\sigma_{sr}^2 \sigma_n^2}{\sigma_{sr}^2 P_{x_{s,t}} + \sigma_n^2} \quad (4.4)$$

$$\hat{h}_{sd} = \frac{\sigma_{sd}^2 \sqrt{P_{x_{s,t}}}}{\sigma_{sd}^2 P_{x_{s,t}} + \sigma_n^2} y_{d,t}, \quad \sigma_{\hat{h}_{sd}}^2 = \frac{\sigma_{sd}^2 \sigma_n^2}{\sigma_{sd}^2 P_{x_{s,t}} + \sigma_n^2} \quad (4.5)$$

$$\hat{h}_{rd} = \frac{\sigma_{rd}^2 \sqrt{P_{x_{r,t}}}}{\sigma_{rd}^2 P_{x_{r,t}} + \sigma_n^2} y_{d,t}^r, \quad \sigma_{\hat{h}_{rd}}^2 = \frac{\sigma_{rd}^2 \sigma_n^2}{\sigma_{rd}^2 P_{x_{r,t}} + \sigma_n^2} \quad (4.6)$$

where  $P_{x_{s,t}}$  and  $P_{x_{r,t}}$  are the power of the pilot symbols sent by the source and the relay, respectively, and  $y_{r,t} \sim \mathcal{CN}(0, \sigma_{sr}^2 P_{x_{s,t}} + \sigma_n^2)$ ,  $y_{d,t} \sim \mathcal{CN}(0, \sigma_{sd}^2 P_{x_{s,t}} + \sigma_n^2)$  and  $y_{d,t}^r \sim \mathcal{CN}(0, \sigma_{rd}^2 P_{x_{r,t}} + \sigma_n^2)$ .

In the second method, we employ the noncausal Wiener filter which is the optimum linear estimator in the mean-square sense. The Wiener filter is employed at both the relay and the destination. Note that since pilot symbols are sent with a period of  $M$  symbols, the channels are sampled every  $MT_s$  seconds, where  $T_s$  is the sampling time. As described in [6], we have to consider the undersampled versions of the Doppler spectrums of the fading coefficients, which are given by

$$S_{h_{sr},m}(e^{jw}) = \frac{1}{M} \sum_{k=0}^{M-1} e^{jm(w-2\pi k)/M} S_{h_{sr}} \left( e^{j(w-2\pi k)/M} \right) \quad (4.7)$$

$$S_{h_{sd},m}(e^{jw}) = \frac{1}{M} \sum_{k=0}^{M-1} e^{jm(w-2\pi k)/M} S_{h_{sd}} \left( e^{j(w-2\pi k)/M} \right) \quad (4.8)$$

$$S_{h_{rd},m}(e^{jw}) = \frac{1}{M} \sum_{k=0}^{M-1} e^{jm(w-2\pi k)/M} S_{h_{rd}} \left( e^{j(w-2\pi k)/M} \right). \quad (4.9)$$

Then, the channel MMSE variances for the noncausal Wiener filter at time  $Ml + m$

---

<sup>2</sup> $\hat{h}$  and  $\tilde{h}$  are used to denote the estimate and error in the estimate of  $h$ , respectively. Hence, we can write  $h = \hat{h} + \tilde{h}$ .

are given by [44]

$$\sigma_{h_{sr}}^2(Ml + m) = \sigma_{sr}^2 - \frac{1}{2\pi} \int_{-\pi}^{\pi} \frac{P_{x_{s,t}} |S_{h_{sr},m}(e^{jw})|^2}{P_{x_{s,t}} S_{h_{sr},0}(e^{jw}) + \sigma_n^2} dw \quad (4.10)$$

$$\sigma_{h_{sd}}^2(Ml + m) = \sigma_{sd}^2 - \frac{1}{2\pi} \int_{-\pi}^{\pi} \frac{P_{x_{s,t}} |S_{h_{sd},m}(e^{jw})|^2}{P_{x_{s,t}} S_{h_{sd},0}(e^{jw}) + \sigma_n^2} dw \quad (4.11)$$

$$\sigma_{h_{rd}}^2(Ml + m) = \sigma_{rd}^2 - \frac{1}{2\pi} \int_{-\pi}^{\pi} \frac{P_{x_{r,t}} |S_{h_{rd},m}(e^{jw})|^2}{P_{x_{r,t}} S_{h_{rd},0}(e^{jw}) + \sigma_n^2} dw \quad (4.12)$$

for  $l = 0, 1, 2, \dots$  and  $m = 0, 1 \dots (M - 1)$ .

After obtaining the estimates, we can express the fading coefficients as

$$\begin{aligned} h_{sr}(Ml + m) &= \hat{h}_{sr}(Ml + m) + \tilde{h}_{sr}(Ml + m) \\ h_{sd}(Ml + m) &= \hat{h}_{sd}(Ml + m) + \tilde{h}_{sd}(Ml + m) \\ h_{rd}(Ml + m) &= \hat{h}_{rd}(Ml + m) + \tilde{h}_{rd}(Ml + m). \end{aligned} \quad (4.13)$$

### 4.3 Data Transmission Phase

Note that as described in the previous section, within a block of  $M$  symbols, two symbol durations are allocated for channel training while data transmission is performed in the remaining portion of the time. We assume that relay operates in half-duplex mode. Hence, the relay first listens and then transmits to the destination. We consider two transmission protocols: non-overlapped and overlapped transmissions.

### 4.3.1 Non-overlapped Case

In this protocol, the source and relay send data symbols in nonoverlapping intervals. The source, after sending the pilot symbol, sends its  $(M - 2)/2$  data symbols received by the relay and the destination as<sup>3</sup>

$$y_{r,d}(m) = h_{sr}(m)x_{s,d}(m) + n_r(m)$$

and

$$y_{d,d}(m) = h_{sd}(m)x_{s,d}(m) + n_d(m) \quad m = 2, \dots, \frac{M}{2}. \quad (4.14)$$

Next, the source stops transmission, and the relay sends first its pilot symbol and then  $(M - 2)/2$  data symbols which are generated from  $\mathbf{y}_{r,d} = [y_{r,d}(2), \dots, y_{r,d}(M/2)]$ . Thus the destination receives

$$y_{d,d}(j) = h_{rd}(j)x_{r,d}(j) + n_d(j) \quad j = m + M/2 \quad (4.15)$$

where again  $m = 2, \dots, M/2$ . After substituting (4.13) into (4.14) and (4.15), we obtain

$$\begin{aligned} y_{r,d}(m) &= \hat{h}_{sr}(m)x_{s,d}(m) + \tilde{h}_{sr}(m)x_{s,d}(m) + n_r(m) \\ y_{d,d}(m) &= \hat{h}_{sd}(m)x_{s,d}(m) + \tilde{h}_{sd}(m)x_{s,d}(m) + n_d(m) \\ y_{d,d}(j) &= \hat{h}_{rd}(j)x_{r,d}(j) + \tilde{h}_{rd}(j)x_{r,d}(j) + n_d(j) \end{aligned} \quad (4.16)$$

where  $m = 2, \dots, M/2$  and  $j = m + M/2$ .

---

<sup>3</sup>Since we consider transmission in a block of  $M$  symbols, we drop the block index for the sake of simplicity and use  $m$  instead of using  $Ml + m$ .

### 4.3.2 Overlapped Case

In this protocol, the source continues its transmission while the relay is sending its data symbols. The source becomes silent only when the relay is sending the pilot symbol. Therefore, the received signals in the data transmission phase can be written as

$$\begin{aligned} y_{r,d}(m) &= h_{sr}(m)x_{s,d}(m) + n_r(m) \\ y_{d,d}(m) &= h_{sd}(m)x_{s,d}(m) + n_d(m) \\ y_{d,d}(j) &= h_{sd}(j)x_{s,d}(j) + h_{rd}(j)x_{r,d}(j) + n_d(j) \end{aligned} \quad (4.17)$$

where  $m = 2, \dots, M/2$  and  $j = m + M/2$ . Similarly as in the non-overlapped case, we can integrate the estimation results to (4.17) and write

$$\begin{aligned} y_{r,d}(m) &= \hat{h}_{sr}(m)x_{s,d}(m) + \tilde{h}_{sr}(m)x_{s,d}(m) + n_r(m) \\ y_{d,d}(m) &= \hat{h}_{sd}(m)x_{s,d}(m) + \tilde{h}_{sd}(m)x_{s,d}(m) + n_d(m) \\ y_{d,d}(j) &= \hat{h}_{sd}(j)x_{s,d}(j) + \tilde{h}_{sd}(j)x_{s,d}(j) + \hat{h}_{rd}(j)x_{r,d}(j) + \tilde{h}_{rd}(j)x_{r,d}(j) + n_d(j). \end{aligned} \quad (4.18)$$

## 4.4 Achievable Rates for AF Relaying

In this section, we consider the AF relaying scheme in which the relay sends to the destination simply the scaled version of the signal received from the source.

An achievable rate expression for the AF relaying scheme is given by

$$I_{AF} = \frac{1}{M} \sum_{m=2}^{M/2} \sup_{p_{x_{s,d}}} I \left( x_{s,d}(m); y_{d,d}(m), y_{d,d}(m + M/2) \middle| \hat{h}_{sr}(m), \hat{h}_{sd}(m), \hat{h}_{sd}(m + M/2), \hat{h}_{rd}(m + M/2) \right) \quad (4.19)$$

where  $\{x_{s,d}(m)\}$  are components of the transmitted signal vector  $\mathbf{x}_{s,d}$ , and  $\{y_{d,d}(m)\}$  and  $\{y_{d,d}(m + M/2)\}$  are the components of the  $(M - 2)$ -dimensional received signal  $\mathbf{y}_{d,d} = [y_{d,d}(2), \dots, y_{d,d}(M/2), y_{d,d}(M/2 + 2), \dots, y_{d,d}(M)]$ , respectively.

Note that the above formulation supposes that the destination node also knows  $\{\hat{h}_{sr}\}$ . Hence, it is assumed that these estimates are reliably forwarded by the relay to the destination using reliable low rate links. A lower bound on  $I_{AF}$  can be obtained by assuming similarly as in [37] that the estimation errors are additional sources of worst-case Gaussian noise. We define the new noise random variables in non-overlapped and overlapped cases as

$$\begin{aligned} z_{r,d}(m) &= \tilde{h}_{sr}(m)x_{s,d}(m) + n_r(m) \\ z_{d,d}(m) &= \tilde{h}_{sd}(m)x_{s,d}(m) + n_d(m) \\ z_{d,d}(j) &= \tilde{h}_{rd}(j)x_{r,d}(j) + n_d(j) \end{aligned} \quad (4.20)$$

and

$$\begin{aligned} z_{r,d}(m) &= \tilde{h}_{sr}(m)x_{s,d}(m) + n_r(m) \\ z_{d,d}(m) &= \tilde{h}_{sd}(m)x_{s,d}(m) + n_d(m) \\ z_{d,d}(j) &= \tilde{h}_{sd}(j)x_{s,d}(j) + \tilde{h}_{rd}(j)x_{r,d}(j) + n_d(j) \end{aligned} \quad (4.21)$$

respectively. By assuming that the new noise components are Gaussian random

variables and using techniques similar to those in [84], we can obtain the following worst-case achievable rate expression for the non-overlapped case:

$$I_{nonover} = \frac{1}{M} E_{w_{sr}, w_{sd}, w_{rd}} \sum_{m=2}^{M/2} \log(1 + a_{1,m} + f(b_{1,m}, c_{1,j})) \quad (4.22)$$

where

$$a_{1,m} = \frac{P_{x_s,d(m)} \sigma_{\hat{h}_{sd}(m)}^2}{\sigma_{z_{d,d}(m)}^2} |w_{sd}|^2, \quad b_{1,m} = \frac{P_{x_s,d(m)} \sigma_{\hat{h}_{sr}(m)}^2}{\sigma_{z_{r,d}(m)}^2} |w_{sr}|^2, \quad (4.23)$$

$$c_{1,j} = \frac{P_{x_r,d(j)} \sigma_{\hat{h}_{rd}(j)}^2}{\sigma_{z_{d,d}(j)}^2} |w_{rd}|^2, \quad f(x, y) = \frac{xy}{1+x+y}$$

and  $w_{sd} \sim \mathcal{CN}(0, 1)$ ,  $w_{sr} \sim \mathcal{CN}(0, 1)$ ,  $w_{rd} \sim \mathcal{CN}(0, 1)$ .  $P_{x_s,d(m)}$  and  $P_{x_r,d(j)}$  are the powers of the  $m^{\text{th}}$  source symbol and  $j^{\text{th}}$  relay symbol, respectively, and  $\sigma_{\hat{h}_{sr}(m)}^2 = \sigma_{sr}^2 - \sigma_{\hat{h}_{sr}(m)}^2$ ,  $\sigma_{\hat{h}_{sd}(m)}^2 = \sigma_{sd}^2 - \sigma_{\hat{h}_{sd}(m)}^2$ ,  $\sigma_{\hat{h}_{rd}(m)}^2 = \sigma_{rd}^2 - \sigma_{\hat{h}_{rd}(m)}^2$ . Finally, note that  $j = m + M/2$ .

Similarly, we can find the following achievable rate expression for the overlapped case:

$$I_{over} = \frac{1}{M} E_{w_{sr}, w_{sd}, w_{rd}} \sum_{m=2}^{M/2} \log(1 + a_{2,m} + f(d_{2,m}, c_{2,j}) + q(a_{2,m}, b_{2,j}, c_{2,j}, d_{2,m})) \quad (4.24)$$

where

$$a_{2,m} = \frac{P_{x_s,d(m)} \sigma_{\hat{h}_{sd}(m)}^2}{\sigma_{z_{d,d}(m)}^2} |w_{sd}|^2, \quad b_{2,j} = \frac{P_{x_s,d(j)} \sigma_{\hat{h}_{sd}(j)}^2}{\sigma_{z_{d,d}(j)}^2} |w_{sd}|^2, \quad (4.25)$$

$$c_{2,j} = \frac{P_{x_s,d(m)} \sigma_{\hat{h}_{sr}(m)}^2}{\sigma_{z_{r,d}(m)}^2} |w_{sr}|^2, \quad d_{2,m} = \frac{P_{x_r,d(j)} \sigma_{\hat{h}_{rd}(j)}^2}{\sigma_{z_{d,d}(j)}^2} |w_{rd}|^2$$

and  $q(a, b, c, d) = \frac{(1+a)b(1+c)}{1+c+d}$  and  $j = m + M/2$ .

## 4.5 Achievable Rates for DF Relaying

The repetition coding and the parallel coding are two possible coding techniques used in DF schemes [47]. First, we consider the repetition coding, and for this case the achievable rate is given by

$$I_{RC} = \frac{1}{M} \sum_{m=2}^{M/2} \sup_{p_{x_s}} \left\{ \min \left[ I(x_{s,d}(m); y_{r,d}(m) | \hat{h}_{sr}(m)), \right. \right. \\ \left. \left. I(x_{s,d}(m); y_{d,d}(m), y_{d,d}(m + M/2) | \hat{h}_{sd}(m), \hat{h}_{sd}(m + M/2), \hat{h}_{rd}(m + M/2)) \right] \right\} \quad (4.26)$$

Employing the techniques used in the AF non-overlapped scheme, we obtain the following achievable rate expression for non-overlapped DF with repetition coding:

$$I_{nonover,rc} = \frac{1}{M} E_{w_{sr}, w_{sd}, w_{rd}} \sum_m \min(I_1, I_2) \quad (4.27)$$

where

$$I_1 = \log [1 + b_{1,m}], \quad I_2 = \log [1 + a_{1,m} + c_{1,j}],$$

and  $a_{1,m}$ ,  $b_{1,m}$  and  $c_{1,j}$  are given in (4.23). For the overlapped case of the DF repetition coding, (4.27) holds with  $I_1$  and  $I_2$  defined as

$$I_1 = \log [1 + c_{2,j}], \quad I_2 = \log [1 + a_{2,m} + b_{2,j} + d_{2,m} + a_{2,m}b_{2,j}]$$

where  $a_{2,m}$ ,  $b_{2,j}$ ,  $c_{2,j}$ , and  $d_{2,m}$  are given in (4.25).

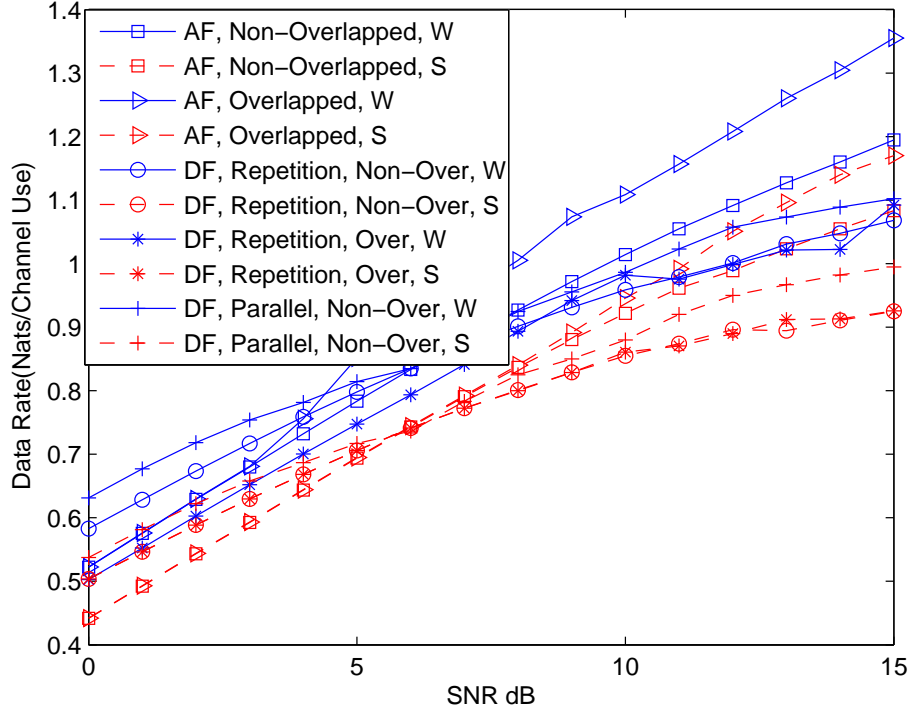


Figure 4.1: The optimal achievable rates vs.  $SNR$  for the Gauss-Markov fading model ( $\alpha = 0.99$ ) and different relaying techniques.  $\sigma_{sd}^2 = 1$ ,  $\sigma_{sr}^2 = 16$  and  $\sigma_{rd}^2 = 16$ . (S: single-pilot estimation. W: Wiener filter.)

When we employ the parallel coding, we have

$$I_{PC} = \frac{1}{M} \sum_{m=2}^{M/2} \sup_{P_{x_s}, \hat{P}_{x_r}} \left\{ \min \left[ I(x_{s,d}(m); y_{r,d}(m) | \hat{h}_{sr}(m)), \right. \right. \\ \left. \left. I(x_{s,d}(m); y_{d,d}(m) | \hat{h}_{sd}(m)) + I(x_{r,d}(m + M/2); y_{d,d}(m + M/2) | \hat{h}_{rd}(m + M/2)) \right] \right\}. \quad (4.28)$$

Similarly, we can find, for the nonoverlapping case, an achievable rate expression given by

$$I_{nonover,pc} = \frac{1}{M} E_{w_{sr}, w_{sd}, w_{rd}} \sum_m \min(I_1, I_2) \quad (4.29)$$



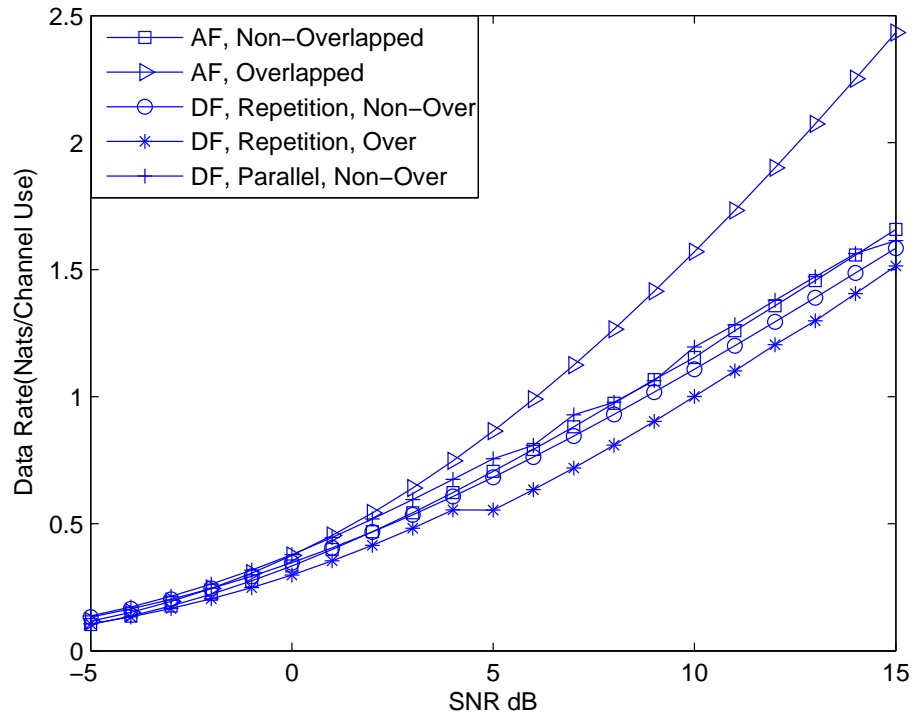


Figure 4.2: The optimal achievable rates vs.  $SNR$  for the lowpass fading model when noncausal Wiener filter is employed.  $\sigma_{sd}^2 = 1$ ,  $\sigma_{sr}^2 = 4$  and  $\sigma_{rd}^2 = 4$ .

where

$$I_1 = \log(1 + b_{1,m}), \quad I_2 = \log(1 + a_{1,m}) + \log(1 + c_{1,j}).$$

## 4.6 Optimizing Training Parameters

In this section, we consider two particular fading processes. In the first case, fading is modeled as a first-order Gauss-Markov process whose dynamics is described by

$$h_k = \alpha h_{k-1} + z_k \quad 0 \leq \alpha \leq 1 \quad k = 1, 2, 3, \dots$$

where  $\{z_k\}$  are i.i.d. circular complex Gaussian variables with zero mean and variance equal to  $(1-\alpha^2)\sigma_h^2$ . In the above formulation,  $\alpha$  is a parameter that controls the rate of the channel variations between consecutive transmissions. The power spectral density of the Gauss-Markov process with variance  $\sigma_h^2$  is given by

$$S_h(e^{jw}) = \frac{(1-\alpha^2)\sigma_h^2}{1+\alpha^2-2\alpha\cos(w)}. \quad (4.30)$$

We also model the fading as a lowpass Gaussian process whose power spectral density is given by

$$S_h(e^{jw}) = \begin{cases} \frac{\sigma_h^2}{2f_d}, & \text{for } |w| < w_d \\ 0, & \text{otherwise} \end{cases} \quad (4.31)$$

where  $w_d = 2\pi f_d$  is the maximum Doppler spread in radians.

In Gauss-Markov channels, it is difficult to find a closed-form expression for the variance of the estimate error when Wiener filter is used, because the channel's spectrum is not band limited. Therefore, there is always aliasing in the undersampled Doppler spectrums, which causes an increase in the variance of the error. On the other hand, when fading is modeled as a lowpass process, we can find an explicit solution for the error variance, and we can express it as

$$\sigma_h^2 = \frac{\sigma_h^2 \sigma_n^2}{P_{x,t} \sigma_h^2 + \sigma_n^2}.$$

In the lowpass case, if the channel is sampled sufficiently fast (i.e.,  $M < \frac{1}{2f_d}$ ), there is no aliasing and the power is distributed equally among data symbols. However, note that the power allocated to the data symbols of the source is not equal to the power allocated to the data symbols of the relay. In general, if there is aliasing or a single pilot is used for estimation, the power allocated to the data symbols will

differ depending on their distance to the pilot signals.

Having obtained achievable rate expressions, our next goal is to jointly optimize training period  $M$ , training power, and power allocated to the data symbols.

## 4.7 Numerical Results

In this section, we present numerical optimization results. In Figure 4.1, we plot the optimal achievable rates with respect to SNR for different relaying protocols by using two different methods of channel estimation. Fading is assumed to be a Gauss-Markov process. The solid lines indicate the optimal data rates obtained when noncausal Wiener filter is used, whereas the dashed lines show the optimal data rates obtained when a single pilot symbol is used for estimation. The rates are optimal in the sense that they are obtained with optimal training parameters and optimal power allocations. We can see that at low SNR values, DF provides higher rates and parallel non-overlapped DF scheme is the most efficient one. As expected, Wiener filter performance is better than that of the estimation that uses a single pilot. Moreover, at low SNR values non-overlapped and overlapped relaying schemes give the same optimal results, and optimal power distributions among data and pilot symbols are the same for both. Note that DF repetition Non-overlapped and Overlapped schemes do not give the same result when Wiener Filter is used for estimation. On the other hand, at high SNR values, we see a significant increase in the data rate of AF overlapped scheme compared to the other schemes.

In Figure 4.2, we plot the optimal data rates when we estimate the lowpass fading process using a noncausal Wiener filter. The channel variances are  $\sigma_{sd}^2 = 1$ ,  $\sigma_{sr}^2 = 4$  and  $\sigma_{rd}^2 = 4$ . Conclusions similar to that given for Fig. 4.1 are drawn

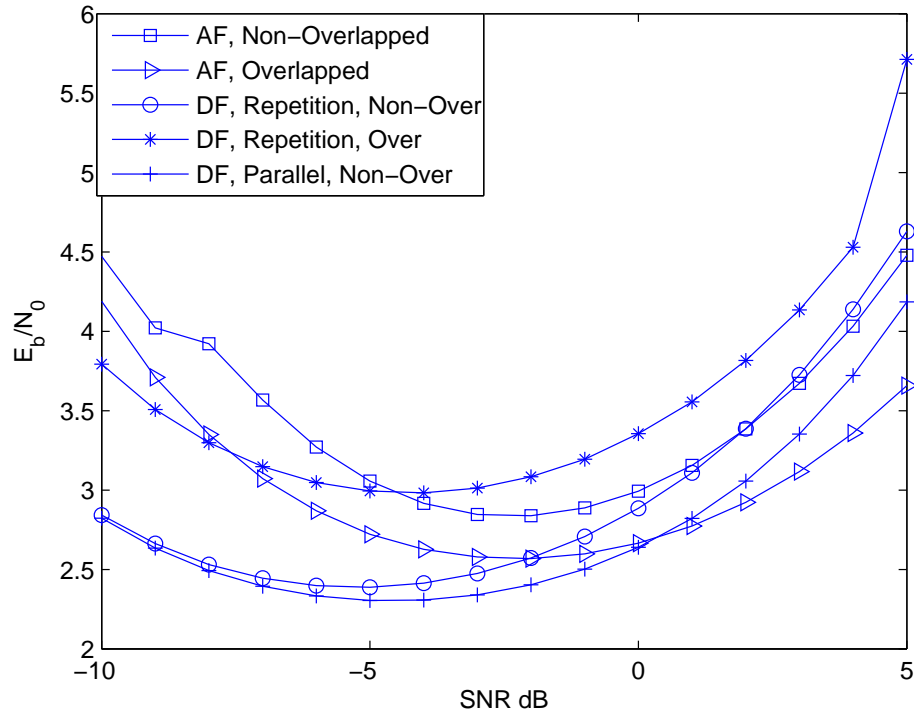


Figure 4.3: Normalized bit energies  $\frac{E_b}{N_0}$  vs.  $SNR$  for the lowpass fading model when noncausal Wiener filter is employed.  $\sigma_{sd}^2 = 1$ ,  $\sigma_{sr}^2 = 4$  and  $\sigma_{rd}^2 = 4$ .

again. In Fig. 4.3, the bit energy normalized by the noise variance,  $\frac{E_b}{N_0}$ , is plotted as a function of  $SNR$ . In all cases, we observe that minimum bit energy is achieved at a nonzero  $SNR$  value. If  $SNR$  is further decreased, higher bit energy values are required and hence, operation at these very low  $SNRs$  should be avoided.

In Figure 4.4, we plot the optimal data rates as a function of the training period,  $M$ , when  $SNR = 0$  dB for different relaying schemes and different channel variances. Single-pilot-symbol estimation is employed. Since a relatively low  $SNR$  value is considered, AF non-overlapped and AF overlapped schemes provide lowest rates. The highest performance is obtained when DF parallel non-overlapped scheme is used.

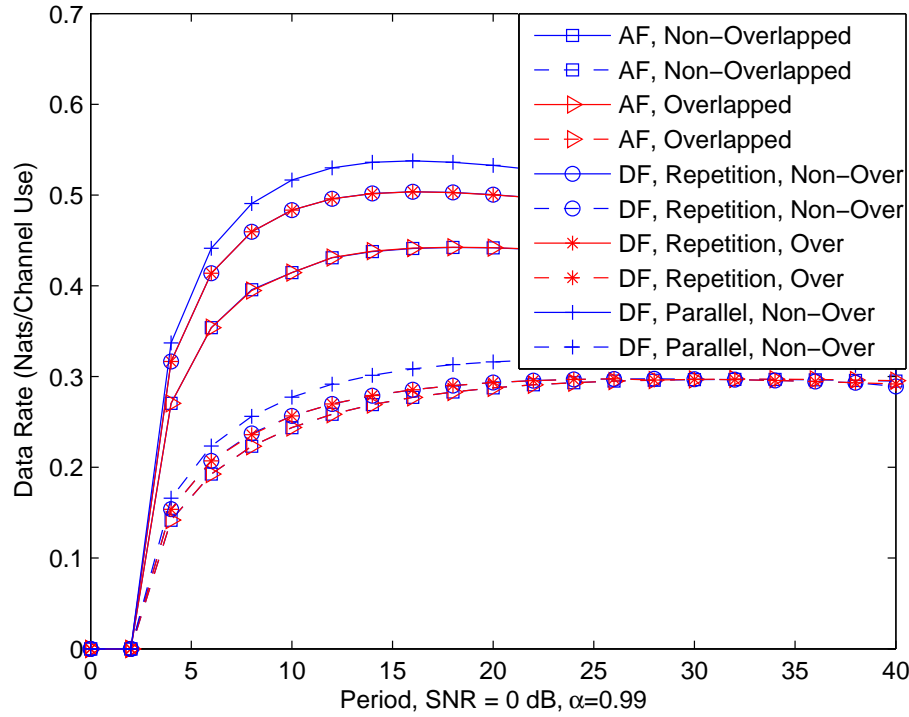


Figure 4.4: The optimal achievable rates vs. training period  $M$  for the Gauss-Markov fading model. Single-pilot MMSE estimation is employed. The dashed lines are obtained when  $\sigma_{sd}^2 = 1$ ,  $\sigma_{sr}^2 = 4$  and  $\sigma_{rd}^2 = 4$  and solid lines are obtained when  $\sigma_{sd}^2 = 1$ ,  $\sigma_{sr}^2 = 16$  and  $\sigma_{rd}^2 = 16$

In Fig. 4.5, power allocated to the pilot and data symbols is plotted when Gauss-Markov channel is considered and AF non-overlapped scheme is employed. The first half of the bars shows the power allocated to the source symbols and the rest shows the power allocated to the relay symbols. The first bar of the each group gives the power of the pilot symbols. Note that these power distributions are obtained when the period is at its optimal value when SNR=0 dB. The optimal period is 30 when  $\sigma_{sd}^2 = 1$ ,  $\sigma_{sr}^2 = 4$ ,  $\sigma_{rd}^2 = 4$ . In Figure 4.6, the optimal power distribution is displayed when noncausal Wiener filter is used for estimation at SNR = 0 dB. Note that the optimal period is 12.

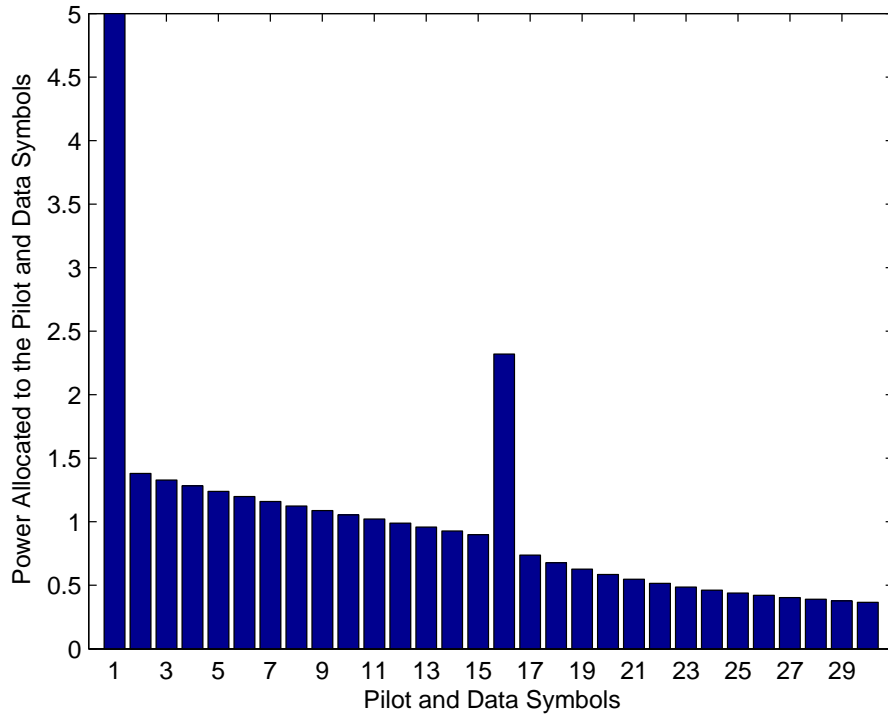


Figure 4.5: Optimal power distribution among the pilot and data symbols when  $\sigma_{sd}^2 = 1$ ,  $\sigma_{sr}^2 = 4$ ,  $\sigma_{rd}^2 = 4$ ,  $SNR = 0$  dB. Fading is a Gauss-Markov process with  $\alpha = 0.99$ . Single-pilot MMSE estimation is employed. The optimal period is  $M = 30$ . Note that the first 15 symbols belong to the source and the last 15 bars belong to the relay

## 4.8 Conclusion

We have studied transmission over imperfectly-known relay channels. The channels are learned using single-pilot MMSE estimation or noncausal Wiener filter. We have obtained achievable rate expressions for both AF and DF relaying schemes. Subsequently, we have jointly optimized the training period and power, and data power levels in Gauss-Markov and lowpass fading models. We have compared the performances of different relaying techniques at different SNR values and different channel variances.

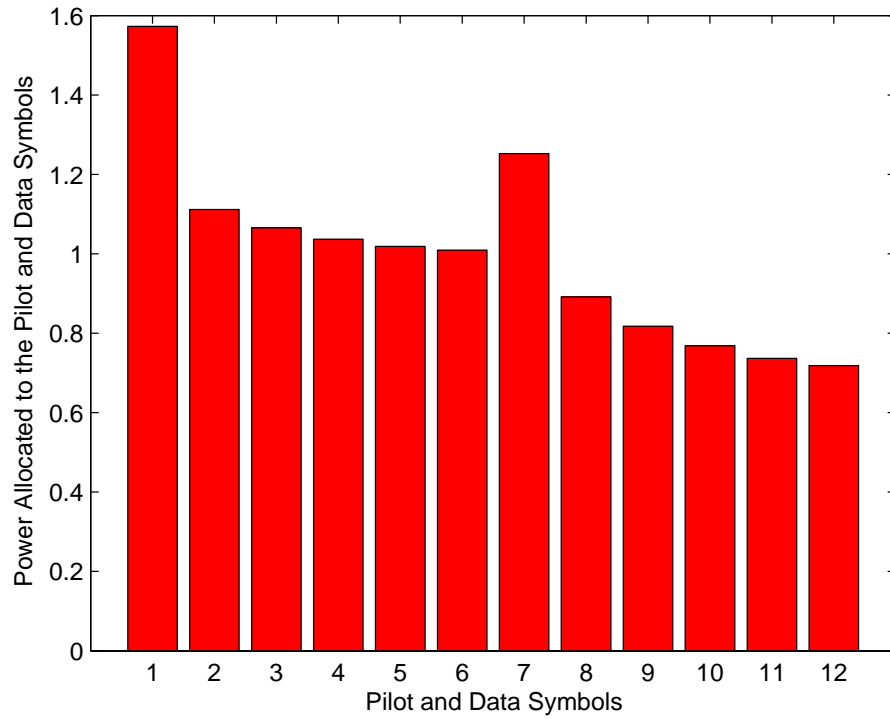


Figure 4.6: Optimal power distribution among the pilot and data symbols when  $\sigma_{sd}^2 = 1$ ,  $\sigma_{sr}^2 = 16$ ,  $\sigma_{rd}^2 = 16$ ,  $SNR = 0$  dB. Fading is a Gauss-Markov process with  $\alpha = 0.99$ . Wiener filter is employed. The optimal period is  $M = 12$ . Note that the first 6 symbols belong to the source and the last 6 bars belong to the relay

## Chapter 5

# Effective Capacity Analysis of Cognitive Radio Channels for Quality of Service Provisioning

In this chapter, the performance of cognitive radio systems is studied when the SUs operate under statistical QoS constraints. In the cognitive radio channel model, SUs initially perform channel sensing, and then engage in data transmission at two different average power levels depending on the channel sensing results. A state transition model is constructed to model this cognitive transmission channel. Statistical QoS constraints are imposed as limitations on buffer violation probabilities. Effective capacity of the cognitive radio channel, which provides the maximum throughput under such QoS constraints, is determined. This analysis is conducted for fixed-power/fixed-rate, fixed-power/variable-rate, and variable-power/variable-rate transmission schemes under different assumptions on the availability of CSI at the transmitter. The interactions and tradeoffs between the throughput, QoS constraints, and channel sensing parameters (e.g., sensing duration and threshold, and detection and false alarm probabilities) are investigated.



The performances of fixed-rate and variable-rate transmission methods are compared in the presence of QoS limitations. It is shown that variable schemes outperform fixed-rate transmission techniques if the detection probabilities are high. Performance gains through adapting the power and rate are quantified and it is shown that these gains diminish as the QoS limitations become more stringent.

## 5.1 System and Cognitive Channel Model

We consider a cognitive radio channel model in which a secondary transmitter attempts to send information to a secondary receiver possibly in the presence of primary users. Initially SUs perform channel sensing, and then depending on the primary users' activity, the secondary transmitter selects its transmission power and rate, i.e., when the channel is busy, the average symbol power is  $\bar{P}_1$  and the rate is  $r_1$ , and when the channel is idle, the average symbol power is  $\bar{P}_2$  and the rate is  $r_2$ . For instance, if  $\bar{P}_1 = 0$ , the secondary transmitter stops transmission in the presence of an active primary user. In the above model, the transmission rates  $r_1$  and  $r_2$  can be fixed or time-varying depending on whether the transmitter has CSI or not. Moreover, in general we assume  $\bar{P}_1 < \bar{P}_2$ .

We assume that the data generated by the source is initially stored in the data buffer before being transmitted in frames of duration  $T$  seconds over the cognitive wireless channel. During transmission, the discrete-time channel input-output relation in the  $i^{\text{th}}$  symbol duration is given by

$$y(i) = h(i)x(i) + n(i) \quad i = 1, 2, \dots \quad (5.1)$$

if the primary users are absent. On the other hand, if primary users are present

in the channel, we have

$$y(i) = h(i)x(i) + s_p(i) + n(i) \quad i = 1, 2, \dots \quad (5.2)$$

Above,  $x(i)$  and  $y(i)$  denote the complex-valued channel input and output, respectively. We assume that the bandwidth available in the system is  $B$  and the channel input is subject to the following average energy constraints:  $\mathbb{E}\{|x(i)|^2\} \leq \bar{P}_1/B$  and  $\mathbb{E}\{|x(i)|^2\} \leq \bar{P}_2/B$  for all  $i$ , when the channel is busy and idle, respectively. Since the bandwidth is  $B$ , symbol rate is assumed to be  $B$  complex symbols per second, indicating that the average power of the system is constrained by  $\bar{P}_1$  or  $\bar{P}_2$ . In (5.1) and (5.2),  $h(i)$  denotes the fading coefficient between the cognitive transmitter and the receiver. The fading coefficients can have arbitrary marginal distributions but they are assumed to have finite variances, i.e.,  $\mathbb{E}\{|h(i)|^2\} = \mathbb{E}\{z(i)\} = \sigma_h^2 < \infty$ . Note that, here and throughout the chapter, we have denoted the magnitude-square of the fading coefficients by  $z(i) = |h(i)|^2$ . Finally, we consider a block-fading channel model and assume that the fading coefficients stay constant for a block of duration  $T$  seconds and change independently from one block to another.

In (5.2),  $s_p(i)$  represents the sum of the active primary users' faded signals arriving at the secondary receiver. In the input-output relations (5.1) and (5.2),  $n(i)$  models the additive thermal noise at the receiver, and is a zero-mean, circularly symmetric, complex Gaussian random variable with variance  $\mathbb{E}\{|n(i)|^2\} = \sigma_n^2$  for all  $i$ . We further assume that  $\{n_i\}$  is an i.i.d. sequence.

## 5.2 Channel Sensing

We assume that the first  $N$  seconds of the frame duration  $T$  is allocated to sense the channel. If the transmission strategies of the primary users are not known, energy-based detection methods are well-suited for the detection of the activities of primary users. The channel sensing can be formulated as a hypothesis testing problem between the noise  $n(i)$  and the signal  $s_p(i)$  in noise. Noting that there are  $NB$  complex symbols in a duration of  $N$  seconds, this can mathematically be expressed as follows:

$$\begin{aligned}\mathcal{H}_0 & : y(i) = n(i), \quad i = 1, \dots, NB \\ \mathcal{H}_1 & : y(i) = s_p(i) + n(i), \quad i = 1, \dots, NB.\end{aligned}\tag{5.3}$$

We assume that  $s_p(i)$  has a circularly symmetric complex Gaussian distribution with zero-mean and variance  $\sigma_{s_p}^2$ . Note that this is an accurate assumption if the signals are being received in a rich multipath environment or the number of active primary users is large. Moreover, if, for instance the primary users are employing phase or frequency modulation,  $s_p(i)$  in the presence of even a single primary user in flat Rayleigh fading will be Gaussian distributed<sup>1</sup>. As in [50], we further assume that the signal samples  $\{s_p(i)\}$  are independent and identically distributed. Under these assumptions, the optimal Neyman-Pearson detector for the above hypothesis problem is given by [63]

$$Y = \frac{1}{NB} \sum_{i=1}^{NB} |y(i)|^2 \underset{\mathcal{H}_0}{\overset{\mathcal{H}_1}{\geq}} \lambda\tag{5.4}$$

---

<sup>1</sup>Note that zero-mean, circular, complex Gaussian distributions are invariant under rotation. For instance, if the fading coefficient  $h$  is zero-mean, circularly symmetric, complex Gaussian distributed, then so is  $he^{j\phi}$  for any random  $\phi$ .

where  $\lambda$  is the detection threshold. We can immediately conclude that the test statistic  $Y$  is chi-square distributed with  $2NB$  degrees of freedom. In this case, the probabilities of false alarm and detection can be established as follows:

$$P_f = Pr(Y > \lambda | \mathcal{H}_0) = 1 - P\left(\frac{NB\lambda}{\sigma_n^2}, NB\right) \quad (5.5)$$

$$P_d = Pr(Y > \lambda | \mathcal{H}_1) = 1 - P\left(\frac{NB\lambda}{\sigma_n^2 + \sigma_{s_p}^2}, NB\right) \quad (5.6)$$

where  $P(x, a)$  denotes the regularized lower gamma function and is defined as  $P(x, a) = \frac{\gamma(x, a)}{\Gamma(a)}$  where  $\gamma(x, a)$  is the lower incomplete gamma function and  $\Gamma(a)$  is the Gamma function.

Above, we have considered an i.i.d. scenario. If  $\{s_p(i)\}$  are correlated and if the correlation structure is known by the cognitive users, then the optimal detector computes, as the test statistic, the quadratic form  $\mathbf{y}^\dagger \mathbf{K} \mathbf{y}$  where  $\mathbf{y}$  is the vector of  $NB$  received signal samples  $\{y(i)\}_{i=1}^{NB}$ , and  $\mathbf{K}$  is a matrix that depends on the covariance matrix of the primary user signal samples  $\{s_p(i)\}_{i=1}^N$  [63, Case III.B.4]. If  $\{s_p(i)\}$  are identically distributed, then the false alarm and detection probabilities are again expressed in terms of the regularized lower gamma function and are in the same form as in (5.5) and (5.6) (see [63, Equation III.B.96]).

In the hypothesis testing problem given in (5.3), another approach is to consider  $Y$  as Gaussian distributed, which is accurate if  $NB$  is large [50]. In this case, the detection and false alarm probabilities can be expressed in terms of Gaussian  $Q$ -functions. We would like to note the rest of the analysis in the chapter does not depend on the specific expressions of the false alarm and detection probabilities. However, numerical results are obtained using (5.5) and (5.6).

## 5.3 State Transition Model and Effective Capacity with CSI at the Receiver only

In this section, we assume that the receiver has perfect CSI and hence perfectly knows the instantaneous values of  $\{h[i]\}$  while the transmitter has no such knowledge. Not knowing the channel conditions, the transmitter sends the information at fixed rates. More specifically, the transmission rate is fixed at  $r_1$  bits/s in the presence of active primary users while the transmission rate is  $r_2$  bits/s when the channel is idle. In this section, we initially construct a state-transition model for cognitive transmission by considering the cases in which the fixed transmission rates are smaller or greater than the instantaneous channel capacity values, and also incorporating the sensing decision and its correctness. In particular, if the fixed rate is smaller than the instantaneous channel capacity, we assume that reliable communication is achieved and the channel is in the ON state. Otherwise, we declare that outage has occurred and the channel is in the OFF state. Note that information has to be retransmitted in such a case. In the following, we provide a detailed description of the state transition model. Subsequently, we identify, through effective capacity, the maximum throughput that can be achieved in the described state-transition model when the system is subject to QoS constraints.

### 5.3.1 State Transition Model

Regarding the decision of channel sensing and its correctness, we have the following four possible scenarios:

1. Channel is busy, detected as busy (correct detection),
2. Channel is busy, detected as idle (miss-detection),

3. Channel is idle, detected as busy (false alarm),
4. Channel is idle, detected as idle (correct detection).

In each scenario, we have two states, namely ON and OFF, depending on whether or not the fixed-transmission rate exceeds the instantaneous channel capacity. In order to identify these states, we have to first determine the instantaneous channel capacity values. Note that if the channel is detected as busy, the secondary transmitter sends the information with power  $\bar{P}_1$ . Otherwise, it transmits with a larger power,  $\bar{P}_2$ . Considering the interference  $s_p$  caused by the primary users as additional Gaussian noise, we can express the instantaneous channel capacities in the above four scenarios as follows:

$$C_1 = B \log_2(1 + \text{SNR}_1 z(i)) \text{ (channel busy, detected busy)} \quad (5.7)$$

$$C_2 = B \log_2(1 + \text{SNR}_2 z(i)) \text{ (channel busy, detected idle)} \quad (5.8)$$

$$C_3 = B \log_2(1 + \text{SNR}_3 z(i)) \text{ (channel idle, detected busy)} \quad (5.9)$$

$$C_4 = B \log_2(1 + \text{SNR}_4 z(i)) \text{ (channel idle, detected idle)}. \quad (5.10)$$

where  $\text{SNR}_i$  for  $i = 1, 2, 3, 4$  denotes the average SNR values in each possible scenario. These SNR expressions are

$$\begin{aligned} \text{SNR}_1 &= \frac{\bar{P}_1}{B(\sigma_n^2 + \sigma_{s_p}^2)}, & \text{SNR}_2 &= \frac{\bar{P}_2}{B(\sigma_n^2 + \sigma_{s_p}^2)}, \\ \text{SNR}_3 &= \frac{\bar{P}_1}{B\sigma_n^2}, & \text{and } \text{SNR}_4 &= \frac{\bar{P}_2}{B\sigma_n^2}. \end{aligned} \quad (5.11)$$

Note that in scenarios 1 and 3, the channel is detected as busy and hence the transmission rate is  $r_1$ . On the other hand, the transmission rate is  $r_2$  in scenarios 2 and 4. If these fixed rates are below the instantaneous capacity values, i.e., when

$r_1 < C_1, C_3$  or  $r_2 < C_2, C_4$ , the cognitive transmission is considered to be in the ON state and reliable communication is achieved at these rates. On the other hand, when  $r_1 \geq C_1, C_3$  or  $r_2 \geq C_2, C_4$ , outage occurs and the transmission is in the OFF state. In this state, reliable communication is not attained, and hence, the information has to be resent. It is assumed that a simple automatic repeat request (ARQ) mechanism is incorporated in the communication protocol to acknowledge the reception of data and to ensure that erroneous data is retransmitted. This state-transition model with 8 states is depicted in Figure 5.1 where the labels of the states are placed on the bottom-right corner. In states 1, 3, 5, and 7, the transmission is in the ON state, and  $r_1(T - N)$  bits in states 1 and 5, and  $r_2(T - N)$  bits in states 3 and 7 are transmitted and successfully received<sup>2</sup>. The effective transmission rate is zero in the OFF states.

Next, we determine the state-transition probabilities. We use  $p_{ij}$  to denote the transition probability from state  $i$  to state  $j$ . Due to the block fading assumption, state transitions occur every  $T$  seconds. When the channel is busy and detected as busy, the probability of staying in the ON state, which is topmost ON state in Fig. 5.1, is expressed as follows:

$$p_{11} = \rho P_d P\{r_1 < C_1(i + TB) \mid r_1 < C_1(i)\} = \rho P_d P\{z(i + TB) > \alpha_1 \mid z(i) > \alpha_1\} \quad (5.12)$$

where

$$\alpha_1 = \frac{2^{\frac{r_1}{B}} - 1}{\text{SNR}_1}, \quad (5.13)$$

---

<sup>2</sup>Note that the transmission stays in each state for the frame duration of  $T$  seconds. However, since  $N$  seconds are allocated to channel sensing, data transmission occurs over a duration of  $T - N$  seconds.

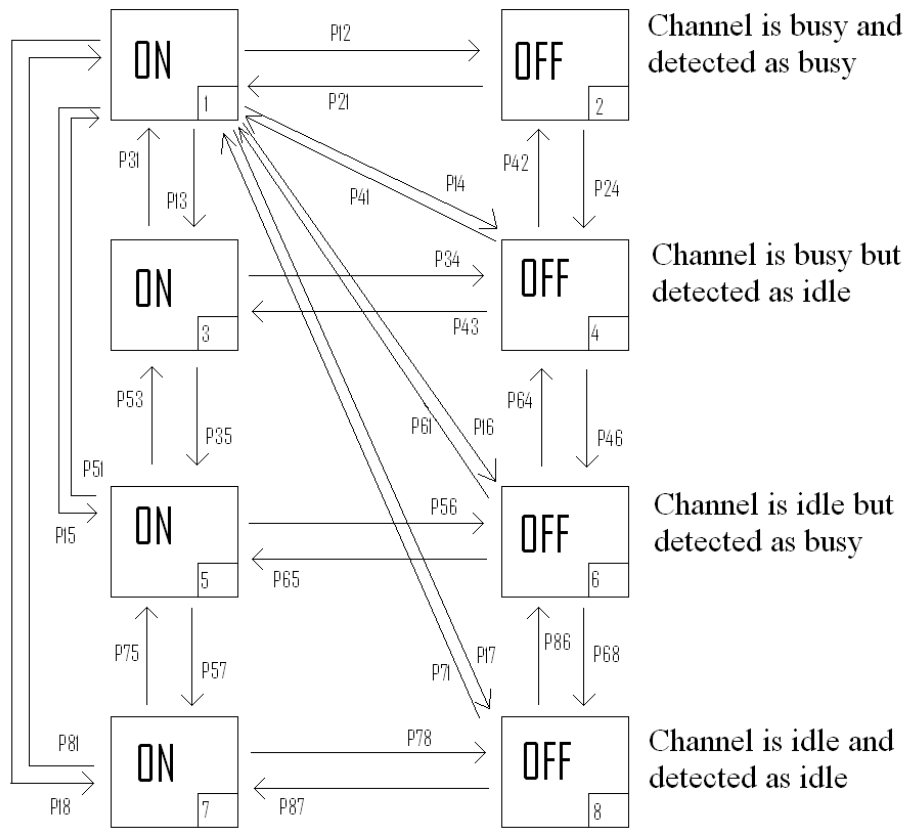


Figure 5.1: State transition model for the cognitive radio channel. The numbered label for each state is given on the bottom-right corner of the box representing the state.



$\rho$  is the prior probability of channel being busy, and  $P_d$  is the probability of detection as defined in (5.6). Note that (5.12) is obtained under the assumption that the primary user activity is independent from frame to frame, leading to the expression which depends only on the prior probability  $\rho$ . Note further that  $p_{11}$  in general depends on the joint distribution of  $(z(i + TB), z(i))$ . However, since fading changes independently from one block to another in the block-fading model, we can further simplify  $p_{11}$  and write it as

$$p_{11} = \rho P_d P\{z[i + TB] > \alpha_1\} = \rho P_d P\{z > \alpha_1\}$$

from which we can immediately see that the transition probability  $p_{11}$  does not depend on the original state. Hence, due to the block fading assumption, we can express

$$p_{i1} = p_1 = \rho P_d P\{z > \alpha_1\} \quad \text{for } i = 1, 2, \dots, 8. \quad (5.14)$$

Similarly, the remaining transition probability expressions become

$$\begin{aligned} p_{i2} = p_2 &= \rho P_d P\{z < \alpha_1\}, & p_{i3} = p_3 &= \rho(1 - P_d) P\{z > \alpha_2\}, \\ p_{i4} = p_4 &= \rho(1 - P_d) P\{z < \alpha_2\}, & p_{i5} = p_5 &= (1 - \rho) P_f P\{z > \alpha_3\}, \\ p_{i6} = p_6 &= (1 - \rho) P_f P\{z < \alpha_3\}, & p_{i7} = p_7 &= (1 - \rho)(1 - P_f) P\{z > \alpha_4\}, \\ p_{i8} = p_8 &= (1 - \rho)(1 - P_f) P\{z < \alpha_4\} \quad \text{for } i = 1, 2, \dots, 8. \end{aligned} \quad (5.15)$$

where  $\alpha_2 = \frac{2^{\frac{r_2}{B}} - 1}{\text{SNR}_2}$ ,  $\alpha_3 = \frac{2^{\frac{r_1}{B}} - 1}{\text{SNR}_3}$ ,  $\alpha_4 = \frac{2^{\frac{r_2}{B}} - 1}{\text{SNR}_4}$ , and  $P_f$  is the false alarm probability.

Now, the  $8 \times 8$  state transition probability matrix can be expressed as

$$R = \begin{bmatrix} p_{1,1} & p_{1,2} & \cdot & \cdot & p_{1,8} \\ \cdot & \cdot & \cdot & \cdot & \cdot \\ \cdot & \cdot & \cdot & \cdot & \cdot \\ p_{8,1} & p_{8,2} & \cdot & \cdot & p_{8,8} \end{bmatrix} = \begin{bmatrix} p_1 & p_2 & \cdot & \cdot & p_8 \\ \cdot & \cdot & \cdot & \cdot & \cdot \\ \cdot & \cdot & \cdot & \cdot & \cdot \\ p_1 & p_2 & \cdot & \cdot & p_8 \end{bmatrix}. \quad (5.16)$$

Note that the rows of  $R$  are identical, and therefore  $R$  is a matrix of unit rank.

### 5.3.2 Effective Capacity

In this section, we identify the maximum throughput that the cognitive radio channel with the aforementioned state-transition model can sustain under statistical QoS constraints imposed in the form of buffer or delay violation probabilities. Wu and Negi in [83] defined the effective capacity as the maximum constant arrival rate that can be supported by a given channel service process while also satisfying a statistical QoS requirement specified by the QoS exponent  $\theta$ . If we define  $Q$  as the stationary queue length, then  $\theta$  is defined as the decay rate of the tail distribution of the queue length  $Q$ :

$$\lim_{q \rightarrow \infty} \frac{\log P(Q \geq q)}{q} = -\theta. \quad (5.17)$$

Hence, we have the following approximation for the buffer violation probability for large  $q_{max}$ :  $P(Q \geq q_{max}) \approx e^{-\theta q_{max}}$ . Therefore, larger  $\theta$  corresponds to more strict QoS constraints, while the smaller  $\theta$  implies looser constraints. In certain settings, constraints on the queue length can be linked to limitations on the delay and hence delay-QoS constraints. It is shown in [51] that  $P\{D \geq d_{max}\} \leq c\sqrt{P\{Q \geq q_{max}\}}$  for constant arrival rates, where  $D$  denotes the steady-

state delay experienced in the buffer. In the above formulation,  $c$  is a positive constant,  $q_{\max} = ad_{\max}$  and  $a$  is the source arrival rate. Therefore, effective capacity provides the maximum arrival rate when the system is subject to statistical queue length or delay constraints in the forms of  $P(Q \geq q_{\max}) \leq e^{-\theta q_{\max}}$  or  $P\{D \geq d_{\max}\} \leq c e^{-\theta a d_{\max}/2}$ , respectively. Since the average arrival rate is equal to the average departure rate when the queue is in steady-state [21], effective capacity can also be seen as the maximum throughput in the presence of such constraints.

In practical applications, the value of  $\theta$  depends on the statistical characterization of the arrival and service processes, bounds on delay or buffer lengths, and target values of the delay or buffer length violation probabilities. In [74], Tang and Zhang described a methodology to determine the value of  $\theta$  (see [74, Section III.B]), and also provided numerical and simulation results that demonstrate how the effective capacity formulation can be used to solve a resource allocation problem in audio and video applications to satisfy given QoS requirements (see [74, Section IV]).

The effective capacity for a given QoS exponent  $\theta$  is given by

$$-\lim_{t \rightarrow \infty} \frac{1}{\theta t} \log_e \mathbb{E}\{e^{-\theta S(t)}\} = -\frac{\Lambda(-\theta)}{\theta} \quad (5.18)$$

where  $\Lambda(\theta) = \lim_{t \rightarrow \infty} \frac{1}{t} \log_e \mathbb{E}\{e^{\theta S(t)}\}$  is a function that depends on the logarithm of the moment generating function of  $S(t)$ ,  $S(t) = \sum_{k=1}^t r(k)$  is the time-accumulated service process, and  $\{r(k), k = 1, 2, \dots\}$  is defined as the discrete-time, stationary and ergodic stochastic service process. Note that the service rate is  $r(k) = r_1(T - N)$  if the cognitive system is in state 1 or 5 at time  $k$ . Similarly, the service rate is  $r(k) = r_2(T - N)$  in states 3 and 7. In all the OFF states,

fixed transmission rates exceed the instantaneous channel capacities and reliable communication is not possible. Therefore, the service rates in these states are effectively zero.

In the next result, we provide the effective capacity for the cognitive radio channel and state transition model described in the previous section.

**Theorem 1** *For the cognitive radio channel with the state transition model given in Section 5.3.1, the normalized effective capacity in bits/s/Hz is given by*

$$R_E(\text{SNR}, \theta) = \max_{r_1, r_2 \geq 0} -\frac{1}{\theta TB} \log_e \left\{ (p_1 + p_5)e^{-(T-N)\theta r_1} + (p_3 + p_7)e^{-(T-N)\theta r_2} + p_2 + p_4 + p_6 + p_8 \right\} \quad (5.19)$$

where  $T$  is the frame duration over which the fading stays constant,  $N$  is the sensing duration,  $r_1$  and  $r_2$  are fixed transmission rates, and  $p_i$  for  $i = 1, \dots, 8$  are the transition probabilities expressed in (5.14)–(5.15).

*Proof:* See Appendix A. □

One of the key steps in obtaining the effective capacity expression in (5.19) is the observation that the matrix  $R$  is of unit rank, which arises due to the assumptions that the primary user activity and fading are changing independently from frame to frame. On the other hand, having a correlation structure would lead to a practically more appealing model that takes into account the bursty nature of these processes. We note that in treating such a model, the general structure of the formulations will be preserved. For instance, when the primary user activity and fading are modeled as Markov processes, the only change occurs in the transition probability matrix  $R$  which is no longer of unit rank. In this case, effective

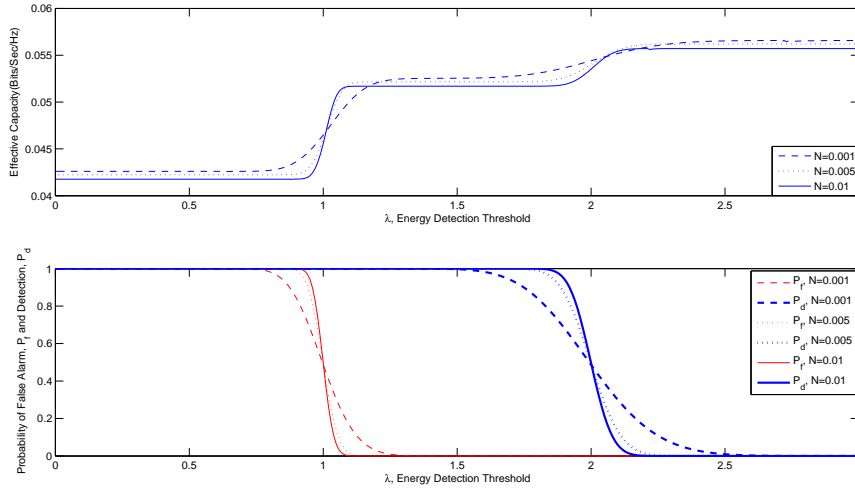


Figure 5.2: Effective Capacity and  $P_f - P_d$  v.s. Channel Detection Threshold  $\lambda$ .  $\theta = 0.01$ .

capacity can be expressed in terms of  $sp(\phi(\theta)R)$ , the maximum of the absolute values of the eigenvalues of the matrix  $\phi(\theta)R$ .

We would like to note that the effective capacity expression in (5.19) is obtained for a given sensing duration  $N$ , detection threshold  $\lambda$ , and QoS exponent  $\theta$ . In the next section, we investigate the impact of these parameters on the effective capacity through numerical analysis.

### 5.3.3 Numerical Results

In this section, we present the numerical results. While the above analysis is valid for any fading distribution with finite variance, we assume in the numerical results that the fading coefficients are zero-mean Gaussian random variables with unit variance. Hence, we consider a Rayleigh fading environment. In Figure 5.2, we plot the effective capacity as a function of the detection threshold value  $\lambda$  for different sensing durations  $N$ . At the same time, we compare the false alarm and

detection probabilities. The channel bandwidth is 100 kHz. We assume that the duration of the block is  $T = 0.1$  seconds. The average input SNR values when the channel is detected correctly are  $\text{SNR}_1 = 0$  dB and  $\text{SNR}_4 = 10$  dB for busy and idle channels, respectively. The QoS exponent is  $\theta = 0.01$ . The channel is assumed to be busy with an average probability of  $\rho = 0.1$ . As we see in Fig. 5.2, the effective capacity is increasing with increasing  $\lambda$ . However, at the same time, as  $\lambda$  increases, the probabilities of false alarm and detection are getting smaller. For instance, when  $\lambda \approx 1$ , the false alarm probabilities start diminishing, which in turn increases the effective capacity values significantly. If  $\lambda$  is increased beyond 2, we observe that the detection probabilities start decreasing, causing increasing disturbance to the primary users. But, since the secondary user assumes that the channel is idle in the case of miss detection and transmits at a higher power level, we again see an increase in the effective capacity. Therefore, this increase occurs at the cost of increased interference to the primary users, which can be limited by imposing a lower bound on the detection probability. In Fig. 5.2, we further observe that as the duration of channel sensing  $N$  increases, the false alarm and detection probabilities decrease with sharper slopes. On the other hand, we note that having a larger  $N$  decreases the effective capacity values outside the range of  $\lambda$  values at which transitions in the false alarm and detection probabilities occur. This is due to the fact that as  $N$  increases, less time is available for data transmission. Finally, we remark that if the threshold value  $\lambda$  is taken between 1.2 and 1.7, the probabilities of false alarm and detection are 0 and 1, respectively, and the channel effective capacity is approximately 0.052 bits/sec/Hz. Such a favorable situation arises because of the large number of samples  $NB$  used for channel sensing. If  $B$  or  $N$  is decreased significantly, false alarm and detection probabilities decrease with much smaller slopes, avoiding the possibility of realizing the above

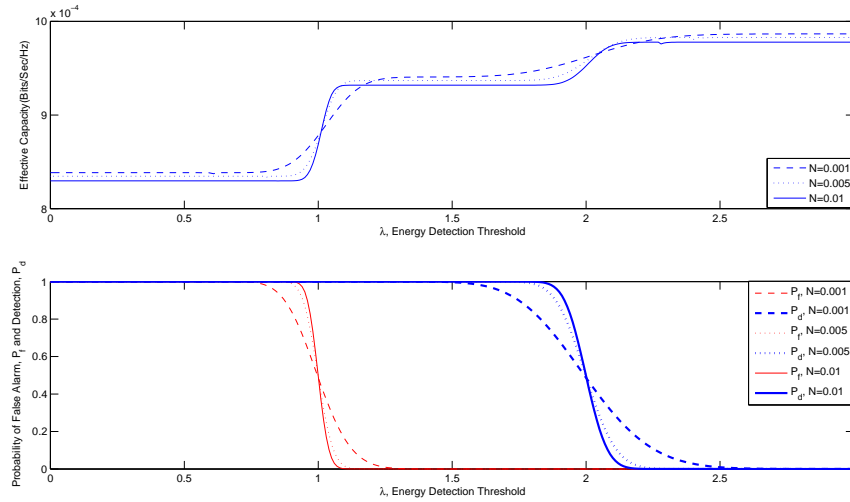


Figure 5.3: Effective Capacity and  $P_f - P_d$  v.s. Channel Detection Threshold  $\lambda$ .  $\theta = 1$ .

favorable scenario.

In Figure 5.3, all parameters other than  $\theta$  are kept the same as the ones used in Fig. 5.2 while the QoS exponent is increased to  $\theta = 1$ . Note that since the false alarm and detection probabilities do not depend on  $\theta$ , we have the same results as in Fig. 5.2. Additionally, similar trends are observed in the effective capacity curves. However, since higher  $\theta$  values mean more strict QoS limitations, we observe much smaller effective capacity values in Fig. 5.3.

In Figure 5.4, we plot the effective capacity as a function of the channel sensing duration, where we consider three different values of the channel detection threshold. The input SNR values are the same as the ones used in the previous figures and  $\theta = 0.01$ . We observe that when  $\lambda = 0.4$  and hence the threshold is small, both the false alarm and detection probabilities are high. Since false alarms happen frequently, effective capacity is small and gets smaller with increasing  $N$ . On the other hand, if  $\lambda = 2.2$ , false alarm and detection probabilities are low and

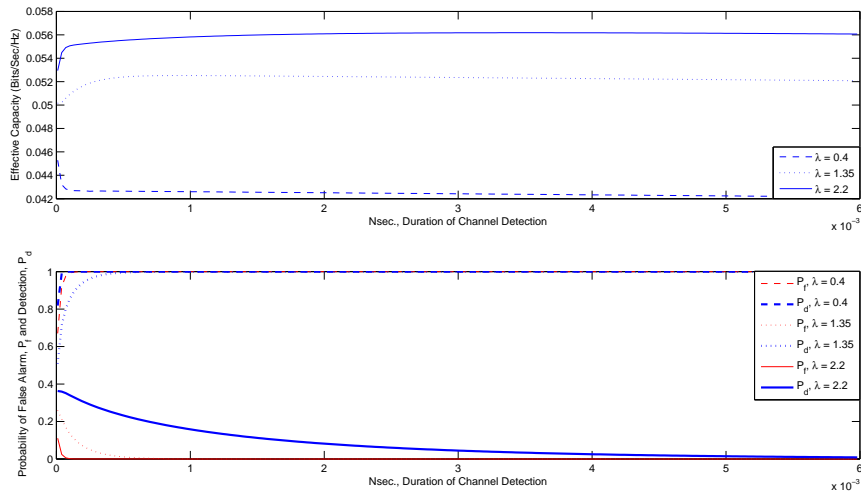


Figure 5.4: Effective Capacity and  $P_f - P_d$  v.s. Channel Sensing Duration,  $N$ .  $\theta = 0.01$ .

decrease with increasing  $N$ . Hence, the secondary transmitter frequently assumes that the channel is idle and transmits with high power. As a result, the effective capacity is high. However, as remarked before, high interference is caused to the primary users. We further note that the effective capacity achieves its maximum value at  $N \approx 0.0035$  above which the effective capacity starts decreasing as less time is allocated to data transmission. When  $\lambda = 1.35$ , detection probabilities approach 1 and false alarm probabilities decrease to zero with increasing  $N$ . Hence, the channel is sensed reliably and disturbance to primary users is minimal. On the other hand, the effective capacity is smaller than that achieved when  $\lambda = 2.2$ .

In Figure 5.5, we plot the optimal transmission rates  $r_1$  and  $r_2$  with which the data is sent through the channel when the channel is busy and idle, respectively, as a function of the channel sensing duration  $N$  for different values of channel occupancy probability  $\rho$ . We set  $\lambda = 1.35$ . As we can see, the optimal transmission rates  $r_2$  for different values of  $\rho$  converge when the detection probability is



1. Similarly, the optimal transmission rates  $r_1$  for different values of the channel occupation probabilities converge when the false alarm probability is 0. Hence, the optimal rates are independent of  $\rho$  when the false alarm and detection probabilities are 0 and 1, respectively.

In Figure 5.6, with the assumption that the primary users' activities are known perfectly (i.e., there is no sensing error), we display the effective capacity and optimal data transmission rates obtained at different channel occupation probabilities  $\rho$  as a function of the QoS exponent  $\theta$ . In the upper part of the figure, we notice that the effective capacity is decreasing with increasing  $\theta$  and increasing primary user activity in the channel. We also observe that as  $\theta$  increases and hence more strict QoS are imposed, the sensitivity of the effective capacity to  $\rho$  decreases. In the lower part of Fig. 5.6, we plot the optimal data transmission rates. The dashed line shows the rates when the channel is empty whereas the solid line gives the rates used when the channel is occupied by the primary users. Here, we observe that while the optimal data transmission rates are decreasing with increasing  $\theta$ , they are independent of  $\rho$  and hence the primary users' activity in the channel.

## 5.4 State Transition Model and Effective Capacity with CSI at Both the Receiver and Transmitter

In this section, we assume that both the transmitter and the receiver have perfect CSI, and hence perfectly know the instantaneous values of  $\{h[i]\}$ <sup>3</sup>. With this as-

---

<sup>3</sup>Channel knowledge can be acquired at the receiver through training-based transmission schemes and can be fed back to the transmitter. In general, these operations require additional resources. However, the cost of channel estimation and feedback is not addressed in this chapter to simplify the analysis. We would like to refer to [65] where estimation schemes are explicitly considered and effective capacity is investigated in the presence of imperfect channel knowledge. Moreover, we would like to note that the assumption of perfect CSI is accurate in slow-fading

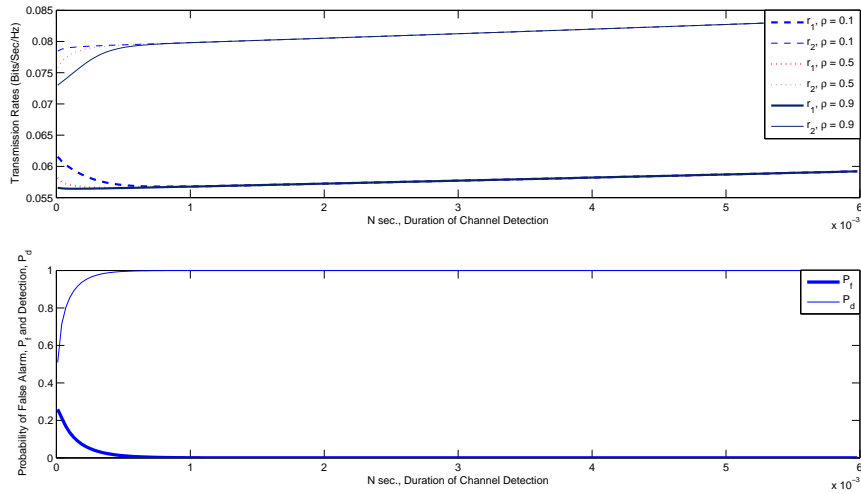


Figure 5.5: Optimal Data Transmission Rates and  $P_f - P_d$  v.s. Channel Sensing Duration  $N$ .  $\theta = 0.01$ .

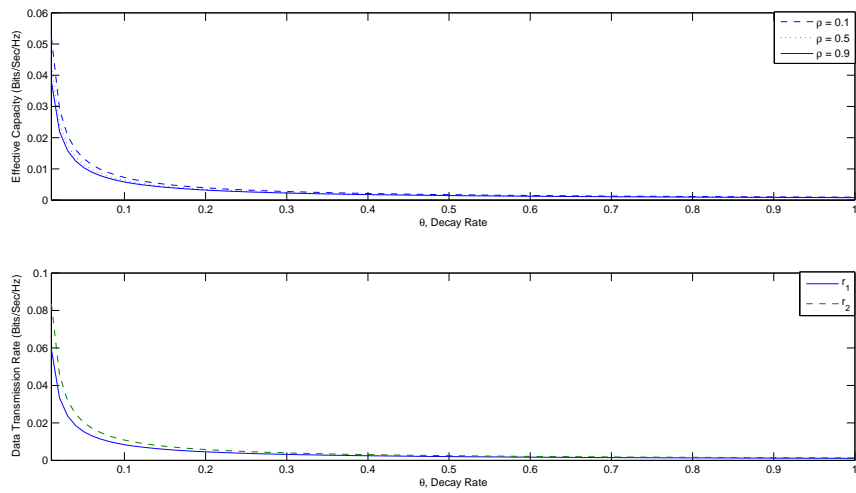


Figure 5.6: Effective Capacity and Optimal Data Transmission Rates v.s. QoS exponent  $\theta$

sumption, as a major difference from Section 5.3, we now allow the transmitter to adapt its rate and power with respect to the channel conditions. In particular, we assume that the transmitter sends the information at the rate that is equal to the instantaneous channel capacity value, and employs the normalized power adaptation policies  $\mu_1(\theta, z(i)) = \frac{P_1(\theta, z(i))}{\bar{P}_1}$  when the channel is busy, and  $\mu_2(\theta, z(i)) = \frac{P_2(\theta, z(i))}{\bar{P}_2}$  when the channel is idle. Note that the power adaptation schemes are normalized by the average power constraints  $\bar{P}_1$  and  $\bar{P}_2$ , and they depend on the QoS exponent  $\theta$  and the instantaneous channel state  $z(i) = |h(i)|^2$ . Note further that the power adaptation policies need to satisfy the average power constraints:

$$\mathbb{E}_z\{\mu_1(\theta, z)\} = \int_0^\infty \mu_1(\theta, z) f(z) dz \leq 1$$

and

$$\mathbb{E}_z\{\mu_2(\theta, z)\} = \int_0^\infty \mu_2(\theta, z) f(z) dz \leq 1 \quad (5.20)$$

where  $f(z)$  denotes the probability density function (pdf) of  $z = |h|^2$ .

### 5.4.1 State Transition Model

With respect to the decision of channel sensing, we still have the four possible channel scenarios outlined at the beginning of Section 5.3.1. Below, we first specify the instantaneous capacity values (denoted by  $C$ ) and the transmission rates (denoted by  $r$ ) used by the transmitter in each possible scenario together with the state in which the channel is, and then we provide a detailed description of the

---

scenarios. In this chapter, we assume that the channel fading coefficients stay constant over a duration of  $TB$  symbols. Hence, close-to-perfect CSI can be obtained when  $TB$  is large.

channel states:

1. Channel is busy and is detected as busy.  $C_1(i) = B \log_2(1 + \mu_1(\theta, z(i))z(i)\text{SNR}_1)$  and  $r_1(i) = C_1(i)$ . The channel is ON.
2. Channel is busy but is detected as idle.  $C_2(i) = B \log_2(1 + \mu_2(\theta, z(i))z(i)\text{SNR}_2)$  and  $r_2(i) > C_2(i)$ . The channel is OFF.
3. Channel is idle but is detected as busy.  $C_3(i) = B \log_2(1 + \mu_1(\theta, z(i))z(i)\text{SNR}_3)$  and  $r_1(i) < C_3(i)$ . The channel is ON.
4. Channel is idle and is detected as idle.  $C_4(i) = B \log_2(1 + \mu_2(\theta, z(i))z(i)\text{SNR}_4)$  and  $r_2(i) = C_4(i)$ . The channel is ON.

SNR expressions above are the same as that defined in (5.11). Note that, in contrast to the analysis in Section 5.3.1, we in this section have only one state (either ON or OFF) for each scenario. We now describe these states. If the channel is detected as busy, the secondary transmitter sends the data at the instantaneous rate

$$r_1(i) = B \log_2(1 + \mu_1(\theta, z(i))z(i)\text{SNR}_1) \quad (5.21)$$

where  $\mu_1(\theta, z(i))$  is the power adaptation policy in this case. Depending on the channel's true state being busy or idle (scenarios 1 or 3 above),  $r_1(i)$  is either equal to the instantaneous channel capacity as in scenario 1 or less than that as in scenario 3. Hence, in both cases, reliable transmission can be attained at the rate of  $r_1(i)$ , and the channels are ON. When the channel is detected as idle, the data transmission rate is

$$r_2(i) = B \log_2(1 + \mu_2(\theta, z(i))z(i)\text{SNR}_4). \quad (5.22)$$

If the channel is actually idle,  $r_2(i)$  is equal to the instantaneous channel capacity, and therefore the channel is in the ON state as in scenario 4. On the other hand, if the channel is busy but detected as idle as in scenario 2 above,  $r_2(i)$  is greater than the channel capacity because the transmitter does not take into account the interference caused by the primary users. Hence, this becomes the only case in which the channel is in the OFF state. Similarly as before, we assume that outage occurs in this state and reliable transmission can not be provided. The information has to be resent with the assistance of an ARQ mechanism.

In summary, we have three ON states and one OFF state under the assumptions of this section. These states correspond to states 1, 4, 5, and 7 of Fig. 5.1. Therefore, the state transition model in this section can be obtained by keeping these states and eliminating states 2, 3, 6, and 8 in the state-transition model in Fig. 5.1. Note that as another major difference from the state-transition model in Section 5.3.1, the transmission rates in each state are now random processes. Therefore, in this new model, the transition probabilities depend only on the detection probabilities and the prior probability of channel being busy,  $\rho$ . These probabilities can be expressed as

$$p_{i1} = p_1 = \rho P_d, \quad p_{i4} = p_4 = \rho(1 - P_d), \quad p_{i5} = p_5 = (1 - \rho)P_f,$$

and

$$p_{i7} = p_7 = (1 - \rho)(1 - P_f), \tag{5.23}$$

for  $i = 1, 4, 5,$  and  $7$ .

### 5.4.2 Effective Capacity

The following result provides the effective capacity expression when the transmitter, having perfect CSI, employs rate and power adaptation during transmission.

**Theorem 2** *For the cognitive radio channel with power and rate adaptation at the transmitter and with the state transition model described in Section 5.4.1, the normalized effective capacity in bits/s/Hz is given by*

$$R_E(\text{SNR}, \theta) = \max_{\substack{\mu_1(\theta, z): \mathbb{E}_z\{\mu_1(\theta, z)\} \leq 1 \\ \mu_2(\theta, z): \mathbb{E}_z\{\mu_2(\theta, z)\} \leq 1}} - \frac{1}{\theta TB} \log_e \left[ (\rho P_d + (1 - \rho) P_f) \mathbb{E}_z \{ e^{-(T-N)\theta r_1} \} \right. \\ \left. + (1 - \rho)(1 - P_f) \mathbb{E}_z \{ e^{-(T-N)\theta r_2} \} + \rho(1 - P_d) \right] \quad (5.24)$$

where the expectations are with respect to  $z$ , and  $r_1 = B \log_2(1 + \mu_1(\theta, z)z\text{SNR}_1)$  and  $r_2 = B \log_2(1 + \mu_2(\theta, z)z\text{SNR}_4)$ .

*Proof:* See Appendix B. □

Having obtained the expression for the effective capacity, we now derive the optimal power adaptation strategies that maximize the effective capacity.

**Theorem 3** *The optimal power adaptation policies that maximize the effective capacity are given by*

$$\mu_1(\theta, z) = \begin{cases} \frac{1}{\text{SNR}_1} \left( \frac{1}{\gamma_1^{a+1}} \frac{1}{z^{a+1}} - \frac{1}{z} \right), & z > \gamma_1 \\ 0, & \text{otherwise} \end{cases} \quad (5.25)$$

and

$$\mu_2(\theta, z) = \begin{cases} \frac{1}{\text{SNR}_4} \left( \frac{1}{\gamma_2^{a+1}} \frac{1}{z^{a+1}} - \frac{1}{z} \right), & z > \gamma_2 \\ 0, & \text{otherwise.} \end{cases} \quad (5.26)$$

where  $a = (T - N)B\theta / \log_e 2$ .  $\gamma_1$  and  $\gamma_2$  are the threshold values in the power adaptation policies and they can be found from the average power constraints in (5.20) through numerical techniques.

*Proof:* See Appendix C. □

The optimal power allocation schemes identified in Theorem 3 are similar to that given in [76]. However, in the cognitive radio channel, we have two allocation schemes depending on the presence or absence of active primary users. Note that the optimal power allocation in the presence of active users,  $\mu_1(\theta, z(i)) = \frac{P_1(\theta, z(i))}{\bar{P}_1}$ , has to be performed under a more strict average power constraint since  $\bar{P}_1 < \bar{P}_2$ . Note also that under certain fading conditions, we might have  $\mu_1(\theta, z(i)) > \bar{P}_1$ , causing more interference to the primary users. Therefore, it is also of interest to apply only rate adaptation and use fixed-power transmission in which case we have  $\mu_1(\theta, z(i)) = \mu_2(\theta, z(i)) = 1$ . We can immediately see from the result of Theorem 2 that the effective capacity of fixed-power/variable-rate transmission is

$$R_E(\text{SNR}, \theta) = -\frac{1}{\theta TB} \log_e \left[ (\rho P_d + (1 - \rho) P_f) \mathbb{E}_z \{ e^{-(T-N)\theta r_1} \} + (1 - \rho)(1 - P_f) \mathbb{E}_z \{ e^{-(T-N)\theta r_2} \} + \rho(1 - P_d) \right] \quad (5.27)$$

where  $r_1 = B \log_2(1 + z\text{SNR}_1)$  and  $r_2 = B \log_2(1 + z\text{SNR}_4)$ .

### 5.4.3 Numerical Results

In Figure 5.7, we plot the effective capacities of the three transmission schemes, namely, fixed-power/fixed-rate transmission (solid line), variable-power/variable-rate transmission (dashed-line), and fixed-power/variable-rate transmission (dotted-line), discussed heretofore in the chapter, as a function of the detection threshold  $\lambda$ . We note that the optimal power adaptation is employed in the variable-power scheme. In this figure, all the parameters are the same as in Fig. 5.2 discussed in Section 5.3. Hence,  $\theta = 0.01$ . When we compare variable-rate/variable-power and variable-rate/fixed-power schemes, we immediately notice, as expected, that variable-rate/variable-power outperforms the latter one for all  $\lambda$  values. However, the difference in the effective capacity values reduces as  $\lambda$  is increased beyond  $\approx 2$  where detection probability starts diminishing. Additionally, we observe that for  $\lambda \geq 2$ , fixed-rate/fixed-power scheme starts outperforming the variable schemes. Note that when the detection probability is small, miss-detections occur frequently. In variable schemes, recall that the transmission enters the OFF state in cases of miss-detection in which the channel is detected as idle but is actually busy, and hence a degradation in the performance is expected. This is also the reason for why the effective capacity of the variable schemes is decreasing for  $\lambda$  values greater than 1.5 where the detection probability has also started getting smaller than 1. Note that this is in stark contrast to the behavior exhibited by the fixed-rate/fixed-power scheme. We finally note that the variable schemes perform better than the fixed-rate/fixed-power transmission when the detection probabilities are relatively high (or equivalently when  $\lambda < \approx 2$ ), and also as before, an decrease in the false alarm probability increases the rates.

Figure 5.8 plots the effective capacities of different transmission schemes as a



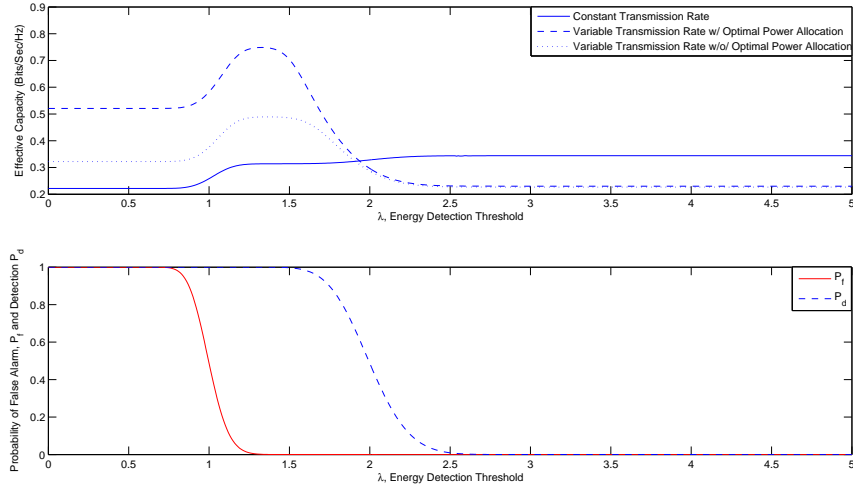


Figure 5.7: Effective Capacity and  $P_f - P_d$  for different schemes v.s. Energy Detection Threshold,  $\lambda$ .  $\theta = 0.01$ .

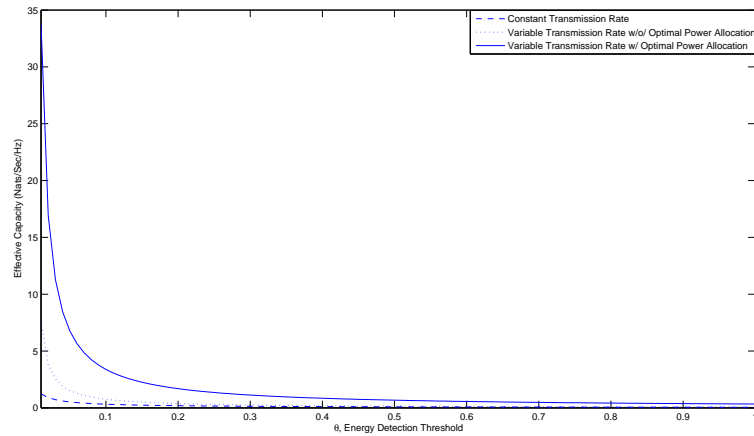


Figure 5.8: Effective Capacity for different schemes v.s. QoS exponent  $\theta$

function of the QoS exponent  $\theta$  under the assumption of perfect channel detection i.e., the probability of false alarm is 0 and the probability of detection is 1. As expected, effective capacity values are decreasing with increasing  $\theta$  values. Since the plot is obtained under perfect channel sensing, the transmission strategy with variable power and rate outperforms the other two schemes for all  $\theta$  values. On the other hand, we interestingly note that the gains attained through adapting the power and rate tend to diminish with increasing  $\theta$ . Hence, QoS constraints have a significant impact in this respect.

## 5.5 Conclusion

In this chapter, we have analyzed the effective capacity of cognitive radio channels in order to identify the performance levels and to determine the interactions between throughput and channel sensing parameters in the presence of QoS constraints. We have initially constructed a state-transition model for cognitive transmission and then obtained expressions for the effective capacity. This analysis is conducted for fixed-power/fixed-rate, fixed-power/variable-rate, and variable-power/variable-rate transmission schemes under different assumptions on the availability of CSI at the transmitter. Through numerical results, we have investigated the impact of channel sensing duration and threshold, detection and false alarm probabilities, and QoS limitations on the throughput. Several insightful observations are made. We have noted that the effective capacity in general increases with decreasing false alarm probabilities. On the other hand, we have remarked that diminishing detection probabilities have a different effect in fixed-rate and variable-rate schemes. We have seen that variable schemes outperform fixed-rate transmission methods if the detection probabilities are sufficiently high.

Otherwise, fixed-power/fixed-rate transmission should be preferred. We have observed that both the effective capacity and transmission rates get smaller with increasing  $\theta$ . We have also noted that the gains through adapting rate and power diminish as  $\theta$  increases and hence QoS constraints become more stringent.

## Chapter 6

# Cognitive Radio Transmission under QoS Constraints and Interference

## Limitations

In this chapter, the performance of cognitive transmission under QoS constraints and interference limitations is studied. Cognitive SUs are assumed to initially perform sensing over multiple frequency bands (or equivalently channels) to detect the activities of primary users. Subsequently, they perform transmission in a single channel at variable power and rates depending on the channel sensing decisions and the fading environment. A state transition model is constructed to model this cognitive operation. Statistical limitations on the buffer lengths are imposed to take into account the QoS constraints of the cognitive SUs. Under such QoS constraints and limitations on the interference caused to the primary users, the maximum throughput is identified by finding the effective capacity of the cognitive radio channel. Optimal power allocation strategies are obtained and the optimal channel selection criterion is identified. The intricate interplay

between effective capacity, interference and QoS constraints, channel sensing parameters and reliability, fading, and the number of available frequency bands is investigated through numerical results.

## 6.1 Cognitive Channel Model and Channel Sensing

In this chapter, we consider a cognitive radio system in which SUs sense  $M$  channels and choose one channel for data transmission. We assume that channel sensing and data transmission are conducted in frames of duration  $T$  seconds. In each frame,  $N$  seconds is allocated for channel sensing while data transmission occurs in the remaining  $T - N$  seconds. Transmission power and rate levels depend on the primary users' activities. If all of the channels are detected as busy, transmitter selects one channel with a certain criterion, and sets the transmission power and rate to  $P_{k,1}(i)$  and  $r_{k,1}(i)$ , respectively, where  $k \in \{1, 2, \dots, M\}$  is the index of the selected channel and  $i = 1, 2, \dots$  denotes the time index. Note that if  $P_{k,1}(i) = 0$ , transmitter stops sending information when it detects primary users in all channels. If at least one channel is sensed to be idle, data transmission is performed with power  $P_{k,2}(i)$  and at rate  $r_{k,2}(i)$ . If multiple channels are detected as idle, then one idle channel is selected again considering a certain criterion.

The discrete-time channel input-output relation between the secondary transmitter and receiver in the  $i^{\text{th}}$  symbol duration in the  $k^{\text{th}}$  channel is given by

$$y_k(i) = h_k(i)x_k(i) + n_k(i) \quad i = 1, 2, \dots, \quad (6.1)$$

if the primary users are absent. On the other hand, if primary users are present

in the channel, we have

$$y_k(i) = h_k(i)x_k(i) + s_{k,p}(i) + n_k(i) \quad i = 1, 2, \dots, \quad (6.2)$$

where  $x_k(i)$  and  $y_k(i)$  denote the complex-valued channel input and output, respectively. In (6.1) and (6.2),  $h_k(i)$  is the channel fading coefficient between the cognitive transmitter and the receiver. We assume that  $h_k(i)$  has a finite variance, i.e.,  $\sigma_{h_k}^2 < \infty$ , but otherwise has an arbitrary distribution. We define  $z_k(i) = |h_k(i)|^2$ . We consider a block-fading channel model and assume that the fading coefficients stay constant for a block of duration  $T$  seconds and change from one block to another independently in each channel. In (6.2),  $s_{k,p}(i)$  represents the active primary user's faded signal arriving at the secondary receiver in the  $k^{\text{th}}$  channel, and has a variance  $\sigma_{s_{k,p}}^2(i)$ .  $n_k(i)$  models the additive thermal noise at the receiver, and is a zero-mean, circularly symmetric, complex Gaussian random variable with variance  $\mathbb{E}\{|n_k(i)|^2\} = \sigma_{n_k}^2$  for all  $i$ . We assume that the bandwidth of the  $k^{\text{th}}$  channel is  $B_k$ .

In the absence of detailed information on primary users' transmission policies, energy-based detection methods are favorable for channel sensing. Knowing that wideband channels exhibit frequency selective features, we can divide the band into channels and estimate each received signal through its discrete Fourier transform (DFT) [67]. The channel sensing can be formulated as a hypothesis testing problem between the noise  $n_k(i)$  and the signal  $s_{k,p}(i)$  in noise. Noting that there are  $NB_k$  complex symbols in a duration of  $N$  seconds in each channel with bandwidth  $B_k$ , the hypothesis test in channel  $k$  can mathematically be expressed as

follows:

$$\begin{aligned}\mathcal{H}_{k,0} & : y_k(i) = n_k(i), \quad i = 1, \dots, NB_k \\ \mathcal{H}_{k,1} & : y_k(i) = s_{k,p}(i) + n_k(i), \quad i = 1, \dots, NB_k.\end{aligned}\tag{6.3}$$

For the above detection problem, the optimal Neyman-Pearson detector is given by [63]

$$Y_k = \frac{1}{NB_k} \sum_{i=1}^{NB_k} |y_k(i)|^2 \underset{\mathcal{H}_{k,0}}{\overset{\mathcal{H}_{k,1}}{\geq}} \gamma_k.\tag{6.4}$$

We assume that  $s_{k,p}(i)$  has a circularly symmetric complex Gaussian distribution with zero-mean and variance  $\sigma_{s_{k,p}}^2$ . Assuming further that  $\{s_{k,p}(i)\}$  are i.i.d., we can immediately conclude that the test statistic  $Y_k$  is chi-square distributed with  $2NB_k$  degrees of freedom. In this case, the probabilities of false alarm and detection can be established as follows:

$$P_{k,f} = Pr(Y_k > \gamma_k | \mathcal{H}_{k,0}) = 1 - P\left(\frac{NB_k \gamma_k}{\sigma_{n_k}^2}, NB_k\right)\tag{6.5}$$

$$P_{k,d} = Pr(Y_k > \gamma_k | \mathcal{H}_{k,1}) = 1 - P\left(\frac{NB_k \gamma_k}{\sigma_{n_k}^2 + \sigma_{s_{k,p}}^2}, NB_k\right)\tag{6.6}$$

where  $P(x, a)$  denotes the regularized lower gamma function and is defined as  $P(x, a) = \frac{\gamma(x, a)}{\Gamma(a)}$  where  $\gamma(x, a)$  is the lower incomplete gamma function and  $\Gamma(a)$  is the Gamma function. In Figure 6.1, the probability of detection,  $P_d$ , and the probability of false alarm,  $P_f$ , are plotted as a function of the energy detection threshold,  $\gamma$ , for different values of channel detection duration. Note that the bandwidth is  $B = 10\text{kHz}$  and the block duration is  $T = 0.1\text{s}$ . We can see that when the detection threshold is low,  $P_d$  and  $P_f$  tend to be 1, which means that the secondary user, always assuming the existence of an active primary user, transmits with power  $P_1(i)$  and rate  $r_1(i)$ . On the other hand, when the detection threshold is high,  $P_d$  and

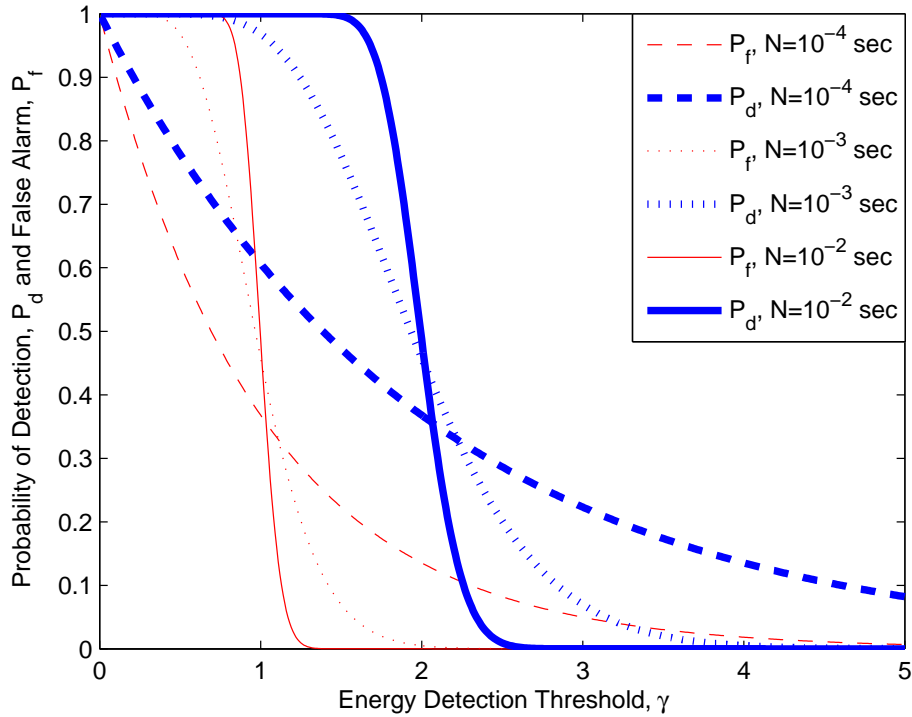


Figure 6.1: Probability of Detection  $P_d$  and False Alarm  $P_f$  vs. Energy Detection Threshold

$P_f$  are close to zero, which means that the secondary user, being unable to detect the activity of the primary users, always transmits with power  $P_2(i)$  and rate  $r_2(i)$ , possibly causing significant interference. The main purpose is to keep  $P_d$  as close to 1 as possible and  $P_f$  as close to 0 as possible. Therefore, we have to keep the detection threshold in a reasonable interval. Note that the duration of detection is also important since increasing the number of channel samples used for sensing improves the quality of channel detection.

In the hypothesis testing problem in (6.3), another approach is to consider  $Y_k$  as Gaussian distributed, which is accurate if  $NB_k$  is large [50]. In this case, the detection and false alarm probabilities can be expressed in terms of Gaussian  $Q$ -



functions. We would like to note the rest of the analysis in the chapter does not depend on the specific expressions of the false alarm and detection probabilities. However, numerical results are obtained using (6.5) and (6.6).

## 6.2 State Transition Model

We assume that both the secondary receiver and transmitter have perfect CSI, and hence perfectly know the realizations of the fading coefficients  $\{h_k(i)\}$ . We further assume that the wideband channel is divided into channels, each with bandwidth that is equal to the coherence bandwidth  $B_c$ . Therefore, we henceforth have  $B_k = B_c$ . With this assumption, we can suppose that independent flat fading is experienced in each channel. In order to further simplify the setting, we consider a symmetric model in which fading coefficients are identically distributed in different channels. Moreover, we assume that the background noise and primary users' signals are also identically distributed in different channels and hence their variances  $\sigma_n^2$  and  $\sigma_{s_p}^2$  do not depend on  $k$ , and the prior probabilities of each channel being occupied by the primary users are the same and equal to  $\rho$ . In channel sensing, the same energy threshold,  $\gamma$ , is applied in each channel. Finally, in this symmetric model, the transmission power and rate policies when the channels are idle or busy are the same for each channel. Due to the consideration of a symmetric model, we in the subsequent analysis drop the subscript  $k$  in the expressions for the sake of brevity.

First, note that we have the following four possible scenarios considering the correct detections and errors in channel sensing:

*Scenario 1:* All channels are detected as busy, and channel used for transmission is actually busy.

*Scenario 2:* All channels are detected as busy, and channel used for transmission is actually idle.

*Scenario 3:* At least one channel is detected as idle, and channel used for transmission is actually busy.

*Scenario 4:* At least one channel is detected as idle, and channel used for transmission is actually idle.

In each scenario, we have one state, namely either ON or OFF, depending on whether or not the instantaneous transmission rate exceeds the instantaneous channel capacity. Considering the interference  $s_p(i)$  caused by the primary users as additional Gaussian noise, we can express the instantaneous channel capacities in the above four scenarios as follows:

$$\text{Scenario 1: } C_1(i) = B_c \log_2(1 + \text{SNR}_1(i)).$$

$$\text{Scenario 2: } C_2(i) = B_c \log_2(1 + \text{SNR}_2(i)).$$

$$\text{Scenario 3: } C_3(i) = B_c \log_2(1 + \text{SNR}_3(i)).$$

$$\text{Scenario 4: } C_4(i) = B_c \log_2(1 + \text{SNR}_4(i)).$$

Above, we have defined

$$\begin{aligned} \text{SNR}_1(i) &= \frac{P_1(i)z(i)}{B_c (\sigma_n^2 + \sigma_{s_p}^2)}, & \text{SNR}_2(i) &= \frac{P_1(i)z(i)}{B_c \sigma_n^2}, \\ \text{SNR}_3(i) &= \frac{P_2(i)z(i)}{B_c (\sigma_n^2 + \sigma_{s_p}^2)}, & \text{SNR}_4(i) &= \frac{P_2(i)z(i)}{B_c \sigma_n^2}. \end{aligned} \quad (6.7)$$

Note that  $z(i) = |h(i)|^2$  denotes the fading power. In scenarios 1 and 2, the secondary transmitter detects all channels as busy and transmits the information

at rate

$$r_1(i) = B_c \log_2 (1 + \text{SNR}_1(i)). \quad (6.8)$$

On the other hand, in scenarios 3 and 4, at least one channel is sensed as idle and the transmission rate is

$$r_2(i) = B_c \log_2 (1 + \text{SNR}_4(i)), \quad (6.9)$$

since the transmitter, assuming the channel as idle, sets the power level to  $P_2(i)$  and expects that no interference from the primary transmissions will be experienced at the secondary receiver (as seen by the absence of  $\sigma_{s_p}^2$  in the denominator of  $\text{SNR}_4$ ).

In scenarios 1 and 2, transmission rate is less than or equal to the instantaneous channel capacity. Hence, reliable transmission at rate  $r_1(i)$  is attained and channel is in the ON state. Similarly, the channel is in the ON state in scenario 4 in which the transmission rate is  $r_2(i)$ . On the other hand, in scenario 3, transmission rate exceeds the instantaneous channel capacity (i.e.,  $r_2(i) > C_3(i)$ ) due to miss-detection. In this case, reliable communication cannot be established, and the channel is assumed to be in the OFF state. Note that the effective transmission rate in this state is zero, and therefore information needs to be retransmitted. We assume that this is accomplished through a simple ARQ mechanism.

For this cognitive transmission model, we initially construct a state transition model. While the ensuing discussion describes this model, Figure 6.2 provides a depiction. As seen in Fig. 6.2, there are  $M + 1$  ON states and 1 OFF state. The single OFF state is the one experienced in scenario 3. The first ON state, which is the top leftmost state in Fig. 6.2, is a combined version of the ON states in scenarios 1 and 2 in both of which the transmission rate is  $r_1(i)$  and the

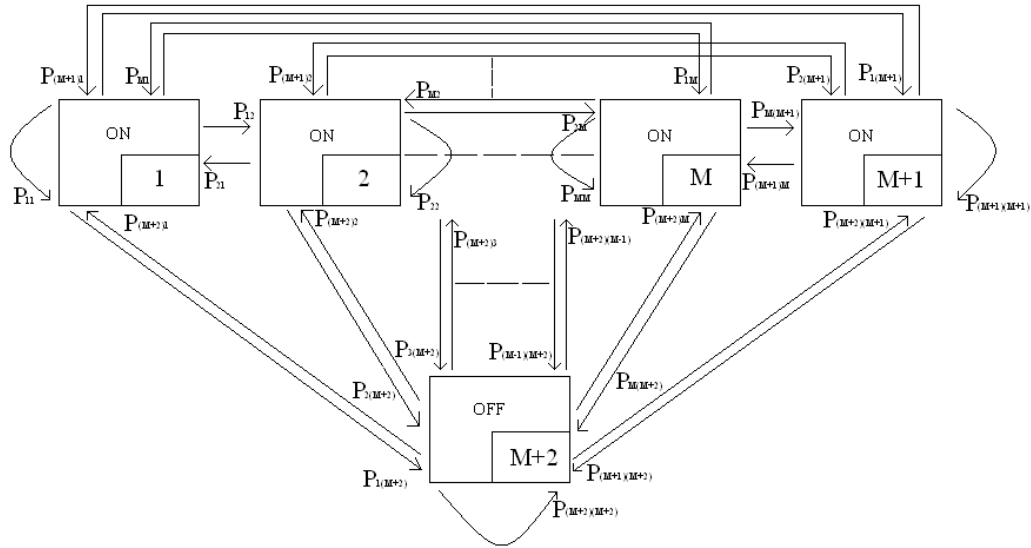


Figure 6.2: State transition model for the cognitive radio channel. The numbered label for each state is given on the lower-right corner of the box representing the state.

transmission power is  $P_1(i)$ . Note that all the channels are detected as busy in this first ON state. The remaining ON states labeled 2 through  $(M + 1)$  can be seen as the expansion of the ON state in scenario 4 in which at least one channel is detected as idle and the channel chosen for transmission is actually idle. More specifically, the  $k^{\text{th}}$  ON state for  $k = 2, 3, \dots, M + 1$  is the ON state in which  $k - 1$  channels are detected as idle and the channel chosen for transmission is idle. Note that the transmission rate is  $r_2(i)$  and the transmission power is  $P_2(i)$  in all ON states labeled 2 through  $(M + 1)$ .

Next, we characterize the state transition probabilities. State transitions occur every  $T$  seconds. We can easily see that the probability of staying in the first ON state, in which all channels are detected as busy, is expressed as follows:

$$p_{11} = \alpha^M \quad (6.10)$$

where  $\alpha = \rho P_d + (1 - \rho) P_f$  is the probability that channel is detected as busy, and  $P_d$  and  $P_f$  are the probabilities of detection and false alarm, respectively as defined in (6.6). Recall that  $\rho$  denotes the probability that a channel is busy (i.e., there are active primary users in the channel). It is important to note that the transition probability in (6.10) is obtained under the assumptions that the primary user activity is independent among the channels and also from one block to another. Indeed, under the assumption of independence over the blocks, the state transition probabilities do not depend on the originating state and hence we have

$$p_{11} = p_{21} = \cdots = p_{(M+1)1} = p_{(M+2)1} = \alpha^M \triangleq p_1 \quad (6.11)$$

where we have defined  $p_1 = p_{i1}$  for all  $i = 1, 2, \dots, M + 2$ . Similarly, we can obtain for  $k = 2, 3, \dots, M + 1$ ,

$$p_{1k} = p_{2k} = \cdots = p_{(M+1)k} = p_{(M+2)k} = P \left( \begin{array}{l} (k-1) \text{ out of } M \\ \text{channels are} \\ \text{detected as idle} \end{array} \text{ and } \begin{array}{l} \text{the channel chosen} \\ \text{for transmission} \\ \text{is actually idle} \end{array} \right) \quad (6.12)$$

$$= \underbrace{\binom{M}{k-1} \alpha^{M-k+1} (1-\alpha)^{k-1}}_{\text{probability that } (k-1) \text{ out of } M \text{ channels are detected as idle}} \times \underbrace{\frac{(1-\rho)(1-P_f)}{1-\alpha}}_{\text{probability that the channel chosen for transmission is actually idle given that it is detected as idle}} \quad (6.13)$$

$$= \frac{M!}{(M-k+1)!(k-1)!} \alpha^{M-k+1} (1-\alpha)^{k-2} (1-\rho) (1-P_f) \quad (6.14)$$

$$\triangleq p_k \quad (6.15)$$

Now, we can easily observe that the transition probabilities for the OFF state are

$$p_{1(M+2)} = p_{2(M+2)} = \cdots = p_{(M+1)(M+2)} = p_{(M+2)(M+2)} \quad (6.16)$$

$$\begin{aligned} &= 1 - \sum_{k=1}^{M+1} p_{1k} \\ &= \sum_{k=1}^M \frac{M!}{(M-k)!k!} \alpha^{M-k} (1-\alpha)^{k-1} \rho(1-P_d) \\ &\triangleq p_{M+2}. \end{aligned} \quad (6.17)$$

Then, we can easily see that the  $(M+2) \times (M+2)$  state transition probability matrix can be expressed as

$$R = \begin{bmatrix} p_{1,1} & \cdot & \cdot & p_{1,M+2} \\ \cdot & & & \cdot \\ \cdot & & & \cdot \\ p_{M+2,1} & \cdot & \cdot & p_{M+2,M+2} \end{bmatrix} = \begin{bmatrix} p_1 & \cdot & \cdot & p_{M+2} \\ \cdot & & & \cdot \\ \cdot & & & \cdot \\ p_1 & \cdot & \cdot & p_{M+2} \end{bmatrix}$$

Note that  $R$  has a rank of 1. Note also that in each frame duration of  $T$  seconds,  $r_1(k)(T-N)$  bits are transmitted and received in state 1, and  $r_2(k)(T-N)$  bits are transmitted and received in states 2 through  $M+1$ , while the transmitted number of bits is assumed to be zero in state  $M+2$ .

### 6.3 Interference Power Constraints

In this section, we consider interference power constraints to limit the transmission powers of the SUs and provide protection to primary users. In particular, we assume that the transmission power of the SUs is constrained in such a way that the average interference power on the primary receiver is limited.

Note that interference to the primary users is caused in scenarios 1 and 3. In scenario 1, the channel is busy, and the secondary user, detecting the channel as busy, transmits at power level  $P_1$ . Consequently, the instantaneous interference power experienced by the primary user is  $P_1 z_{sp}$  where  $z_{sp} = |h_{sp}(i)|^2$  is the magnitude-square of the fading coefficient of the channel between the secondary transmitter and the primary user. Note also that the probability of being in scenario 1 (i.e., the probability of detecting all channels busy and having the chosen transmission channel as actually busy) is  $\alpha^{M-1} \rho P_d$ , as can be easily seen through an analysis similar to that in (6.13).

In scenario 3, the secondary user, detecting the channel as idle, transmits at power  $P_2$  although the channel is actually busy. In this case, the instantaneous interference power is  $P_2 z_{sp}$ . Since we consider power adaption, transmission power levels  $P_1$  and  $P_2$  in general vary with  $z_{sp}$  and also with  $z$ , which is the power of the fading coefficient between the secondary transmitter and secondary receiver in the chosen transmission channel. Hence, in both scenarios, the instantaneous interference power levels depend on both  $z_{sp}$  and  $z$  whose distributions depend on the criterion with which the transmission channel is chosen and the number of available channels from which the selection is performed. For this reason, it is necessary in scenario 3 to separately consider the individual cases with different number of idle-detected channels. We have  $M$  such cases. For instance, in the  $k^{th}$  case for  $k = 1, 2, \dots, M$ , we have  $k$  channels detected as idle and the channel chosen out of these  $k$  channels is actually busy. The probability of the  $k^{th}$  case can be easily found to be  $\frac{M!}{(M-k)!k!} \alpha^{M-k} (1 - \alpha)^{k-1} \rho(1 - P_d)$ .

Following the above discussion, we can now express the average interference

constraints as follows:

$$\underbrace{\alpha^{M-1}\rho P_d}_{\text{probability of scenario 1}} \underbrace{E\{P_1 z_{sp}\}}_{\text{average interference in scenario 1}} + \sum_{k=1}^M \underbrace{\frac{M!}{(M-k)!k!} \alpha^{M-k} (1-\alpha)^{k-1} \rho(1-P_d)}_{\text{probability of the } k^{\text{th}} \text{ case of scenario 3}} \underbrace{E_k\{P_2 z_{sp}\}}_{\text{average interference in the } k^{\text{th}} \text{ case of scenario 3}} \leq I_{avg} \quad (6.18)$$

Note from above that  $I_{avg}$  is the constraint on the interference averaged over the distributions of  $z$  and  $z_{sp}$  (through the expectations), and also averaged over the probabilities of different scenarios and cases. It is important to note that the term  $E_k\{P_2 z_{sp}\}$ , as discussed above, depends in general on the number of idle-detected channels,  $k$ . This dependence is indicated through the subscript  $k$ .

In a system with more strict requirements on the interference, the following individual interference constraints can be imposed:

$$E\{P_1 z_{sp}\} \leq I_0 \quad \text{and} \quad E_k\{P_2 z_{sp}\} \leq I_k \quad \text{for } k = 1, 2, \dots, M. \quad (6.19)$$

If, for instance,  $I_0 = I_1 = I_2 = \dots = I_M$ , then interference averaged over fading is limited by the same constraint regardless of which scenario is being realized. As considered in [58], by appropriately choosing the values of  $I_0$  and  $I_k$  in (6.19), we can provide primary users a minimum rate guarantee for a certain percentage of the time in a Rayleigh fading environment through the following outage



constraints:

$$Pr \left\{ \log_2 \left( 1 + \frac{P_{pri} z_p(i)}{P_1(i) z_{sp}(i) + \sigma_{n_p}^2 B_c} \right) \leq R_{min} \right\} \leq P_1^{out}, \quad (6.20)$$

$$Pr \left\{ \log_2 \left( 1 + \frac{P_{pri} z_p(i)}{P_2(i) z_{sp}(i) + \sigma_{n_p}^2 B_c} \right) \leq R_{min} \right\} \leq P_{2,k}^{out}, \quad \text{for } k = 1, 2, \dots, M. \quad (6.21)$$

$P_1^{out}$  and  $P_{2,k}^{out}$  can be seen as the outage constraints in scenario 1 and in the  $k^{th}$  case of scenario 3, respectively. In the above formulations,  $R_{min}$  is the required minimum transmission rate to be provided to the primary users with outage probabilities  $P_1^{out}$  and  $P_{2,k}^{out}$ , and  $z_p(i) = |h_p(i)|^2$  where  $h_p$  is the fading coefficient of the channel between the primary transmitter and primary receiver.  $\sigma_{n_p}^2$  is the variance of the zero-mean, circularly symmetric, complex Gaussian thermal noise at the primary receiver.  $P_{pri}$  is the transmission power of the primary transmitter. Under the assumption that  $z_p$  is an exponential random variable (i.e., we have a Rayleigh fading channel between the primary transmitter and receiver), the outage probability in (6.20) can be expressed as follows:

$$\begin{aligned} Pr \left\{ \log_2 \left( 1 + \frac{P_{pri} z_p(i)}{P_1(i) z_{sp}(i) + \sigma_{n_p}^2 B_c} \right) \leq R_{min} \right\} \\ = Pr \left\{ z_p \leq \frac{2^{R_{min}} - 1}{P_{pri}} \left( P_1(i) z_{sp}(i) + \sigma_{n_p}^2 B_c \right) \right\} \end{aligned} \quad (6.22)$$

$$= E \left\{ 1 - e^{-\frac{2^{R_{min}} - 1}{P_{pri}} (P_1(i) z_{sp}(i) + \sigma_{n_p}^2 B_c)} \right\} \quad (6.23)$$

$$\leq 1 - e^{-\frac{2^{R_{min}} - 1}{P_{pri}} (E \{ P_1(i) z_{sp}(i) \} + \sigma_{n_p}^2 B_c)} \quad (6.24)$$

where (6.23) is obtained by performing integration with respect to the probability density function (pdf) of  $z_p$  in the evaluation of the probability expression in (6.22). As a result, the expectation in (6.23) is with respect to the remaining random components  $P_1$  and  $z_{sp}$ . Finally, the inequality in (6.24) follows from the concavity of the function  $1 - e^{-x}$  and Jensen's inequality. From (6.24), we can immediately see that if we impose

$$E \{P_1 z_{sp}\} \leq \Phi_1 = -\frac{\log_e (1 - P_1^{out})}{\frac{2^{R_{min}} - 1}{P_{pri}}} - \sigma_{n_p}^2 B_c, \quad (6.25)$$

then the constraint in (6.20) will be satisfied. A similar discussion follows for (6.21) as well.

In the subsequent parts of the chapter, we assume that an average interference power constraint in the form given in (6.18) is imposed.

## 6.4 Effective Capacity

In this section, we identify the maximum throughput that the cognitive radio channel with the aforementioned state-transition model can sustain under interference power constraints and statistical QoS limitations imposed in the form of buffer or delay violation probabilities. Recall that the effective capacity for a given QoS exponent  $\theta$  is given by

$$-\lim_{t \rightarrow \infty} \frac{1}{\theta t} \log_e E\{e^{-\theta S(t)}\} = -\frac{\Lambda(-\theta)}{\theta} \quad (6.26)$$

where  $S(t) = \sum_{k=1}^t r(k)$  is the time-accumulated service process, and  $\{r(k), k = 1, 2, \dots\}$  is defined as the discrete-time, stationary and ergodic stochastic service

process. Note that  $\Lambda(\theta)$  is the asymptotic log-moment generating function of  $S(t)$ , and is given by

$$\Lambda(\theta) = \lim_{t \rightarrow \infty} \frac{1}{t} \log E \left[ e^{\theta S(t)} \right]. \quad (6.27)$$

The service rate according to the model described in Section 6.2 is  $r(k) = r_1(k)(T - N)$  if the cognitive system is in state 1 at time  $k$ . Similarly, the service rate is  $r(k) = r_2(k)(T - N)$  in the states between 2 and  $M + 1$ . In the OFF state, instantaneous transmission rate exceeds the instantaneous channel capacity and reliable communication can not be achieved. Therefore, the service rate in this state is effectively zero.

In the next result, we provide the effective capacity for the cognitive radio channel and state transition model described in the previous section.

**Theorem 4** *For the cognitive radio channel with the state transition model given in Section 6.2, the normalized effective capacity (in bits/s/Hz) under the average interference power constraint (6.18) is given by*

$$\begin{aligned} R_E(\text{SNR}, \theta) = & -\frac{1}{\theta T B_c} \max_{\substack{\alpha^{M-1} \rho P_d E \{P_1 z_{sp}\} \\ + \sum_{k=1}^M \alpha^{M-k} (1-\alpha)^{k-1} \rho (1-P_d) \frac{M!}{(M-k)! k!} E_k \{P_2 z_{sp}\} \\ \leq I_{avg}}} \log_e \left( p_1 E \left\{ e^{-(T-N)\theta r_1} \right\} \right. \\ & \left. + \sum_{k=1}^M p_{k+1} E_k \left\{ e^{-(T-N)\theta r_2} \right\} + p_{M+2} \right). \end{aligned} \quad (6.28)$$

Above,  $p_k$  for  $k = 1, 2, \dots, M + 2$  denote the state transition probabilities defined in (6.11), (6.15), and (6.17) in Section 6.2. Note also that the maximization is with respect to the power adaptation policies  $P_1$  and  $P_2$ .

*Remark:* In the effective capacity expression (6.28), the expectation  $E \{P_1 z_{sp}\}$  in the constraint and  $E \left\{ e^{-(T-N)\theta r_1} \right\}$  are with respect to the joint distribution of

$(z, z_{sp})$  of the channel selected for transmission when all channels are detected busy. The expectations  $E_k \{P_2 z_{sp}\}$  and  $E_k \{e^{-(T-N)\theta r_2}\}$  are with respect to the joint distribution of  $(z, z_{sp})$  of the channel selected for transmission when  $k$  channels are detected as idle.

*Proof:* See Appendix D.  $\square$

We would like to note that the effective capacity expression in (6.28) is obtained for a given sensing duration  $N$ , detection threshold  $\gamma$ , and QoS exponent  $\theta$ . In the next section, we investigate the impact of these parameters on the effective capacity through numerical analysis. Before the numerical analysis, we first identify below the optimal power adaptation policies that the SUs should employ.

**Theorem 5** *The optimal power adaptations for the SUs under the constraint given in (6.18) are*

$$P_1 = \begin{cases} \frac{\mu_1}{z} \left[ \left( \frac{z}{z_{sp} \beta_1 \lambda} \right)^{\frac{1}{c+1}} - 1 \right], & \frac{z}{z_{sp}} \geq \beta_1 \lambda \\ 0, & \text{otherwise} \end{cases}, \quad (6.29)$$

and

$$P_2 = \begin{cases} \frac{\mu_2}{z} \left[ \left( \frac{z}{z_{sp} \beta_2 \lambda} \right)^{\frac{1}{c+1}} - 1 \right], & \frac{z}{z_{sp}} \geq \beta_2 \lambda \\ 0, & \text{otherwise} \end{cases}, \quad (6.30)$$

where  $\mu_1 = B_c(\sigma_n^2 + \sigma_{sp}^2)$ ,  $\mu_2 = \sigma_n^2 B_c$ ,  $c = B_c(T - N)\theta / \log_e 2$ ,  $\beta_1 = \frac{\mu_1 \rho P_d}{c\alpha}$  and  $\beta_2 = \frac{\rho(1-P_d)\mu_2}{c(1-\rho)(1-P_f)}$ .  $\lambda$  is a parameter whose value can be found numerically by satisfying the constraint (6.18) with equality.

*Proof:* See Appendix E.  $\square$

Now, using the optimal transmission policies given in (6.29) and (6.30), we can

express the effective capacity as follows:

$$R_E(\text{SNR}, \theta) = -\frac{1}{\theta T B_c} \log_e \left( p_1 E_{\beta_1 \lambda} \left\{ \left( \frac{z}{z_{sp} \beta_1 \lambda} \right)^{-\frac{c}{c+1}} \right\} + \sum_{k=1}^M p_{k+1} E_{k, \beta_2 \lambda} \left\{ \left( \frac{z}{z_{sp} \beta_2 \lambda} \right)^{-\frac{c}{c+1}} \right\} + p_{M+2} \right). \quad (6.31)$$

Above, the subscripts  $\beta_1 \lambda$  and  $\beta_2 \lambda$  in the expectations denote that the lower limits of the integrals are equal these values and not to zero. For instance,  $E_{\beta_1 \lambda} \left\{ \left( \frac{z}{z_{sp} \beta_1 \lambda} \right)^{-\frac{c}{c+1}} \right\} = \int_{\beta_1 \lambda}^{\infty} \left( \frac{x}{\beta_1 \lambda} \right)^{-\frac{c}{c+1}} f_{\frac{z}{z_{sp}}}(x) dx$ .

Until now, we have not specified the criterion with which the transmission channel is selected from a set of available channels. In (6.31), we can easily observe that the effective capacity depends only on the channel power ratio  $\frac{z}{z_{sp}}$ , and is increasing with increasing  $\frac{z}{z_{sp}}$  due to the fact that the terms  $\left( \frac{z}{z_{sp} \beta_1 \lambda} \right)^{-\frac{c}{c+1}}$  and  $\left( \frac{z}{z_{sp} \beta_2 \lambda} \right)^{-\frac{c}{c+1}}$  are monotonically decreasing functions of  $\frac{z}{z_{sp}}$ . Therefore, the criterion for choosing the transmission band among multiple busy bands unless there is no idle band detected, or among multiple idle bands if there are idle bands detected should be based on this ratio of the channel gains. Clearly, the strategy that maximizes the effective capacity is to choose the channel (or equivalently the frequency band) with the highest ratio of  $\frac{z}{z_{sp}}$ . This is also intuitively appealing as we want to maximize  $z$  to improve the secondary transmission and at the same time minimize  $z_{sp}$  to diminish the interference caused to the primary users. Maximizing  $\frac{z}{z_{sp}}$  provides us the right balance in the channel selection.

We define  $x = \max_{i \in \{1, 2, \dots, M\}} \frac{z_i}{z_{sp, i}}$  where  $\frac{z_i}{z_{sp, i}}$  is the ratio of the gains in the  $i^{\text{th}}$  channel. Assuming that these ratios are independent and identically distributed

in different channels, we can express the pdf of  $x$  as

$$f_x(x) = M f_{\frac{z}{z_{sp}}}(x) \left[ F_{\frac{z}{z_{sp}}}(x) \right]^{M-1}, \quad (6.32)$$

where  $f_{\frac{z}{z_{sp}}}$  and  $F_{\frac{z}{z_{sp}}}$  are the pdf and cumulative distribution function (cdf), respectively, of  $\frac{z}{z_{sp}}$ , the gain ratio in one channel. Now, the expectation  $E_{\beta_1\lambda} \left\{ \left( \frac{z}{z_{sp}\beta_1\lambda} \right)^{-\frac{c}{c+1}} \right\}$ , which arises under the assumption that all channels are detected busy and the transmission channel is selected among these  $M$  channels, can be evaluated with respect to the distribution in (6.32).

Similarly, we define  $x_k = \max_{i \in \{1, 2, \dots, k\}} \frac{z_i}{z_{sp,i}}$  for  $k = 1, \dots, M$ . The pdf of  $x_k$  can be expressed as follows:

$$f_{x_k}(x) = k f_{\frac{z}{z_{sp}}}(x) \left[ F_{\frac{z}{z_{sp}}}(x) \right]^{k-1} \quad k = 1, 2, \dots, M. \quad (6.33)$$

The expectation  $E_{k, \beta_2\lambda} \left\{ \left( \frac{z}{z_{sp}\beta_2\lambda} \right)^{-\frac{c}{c+1}} \right\}$  can be evaluated using the distribution in (6.33). Finally, after some calculations, we can write the effective capacity in integral form as

$$\begin{aligned} R_E(SNR, \theta) = & -\frac{1}{\theta TB_c} \log_e \left\{ M \alpha^M \int_{\beta_1\lambda}^{\infty} f_{\frac{z}{z_{sp}}}(x) \left[ F_{\frac{z}{z_{sp}}}(x) \right]^{M-1} \left[ \frac{\beta_1\lambda}{x} \right]^{\frac{c}{c+1}} dx \right. \\ & + (1 - \rho)(1 - P_f) M \int_{\beta_2\lambda}^{\infty} f_{\frac{z}{z_{sp}}}(x) \left[ \alpha + (1 - \alpha) F_{\frac{z}{z_{sp}}}(x) \right]^{M-1} \left[ \frac{\beta_2\lambda}{x} \right]^{\frac{c}{c+1}} dx \\ & \left. + p_{M+2} \right\}. \end{aligned} \quad (6.34)$$

## 6.5 Numerical Results

In this section, we present numerical results for the effective capacity as a function of the channel sensing reliability (i.e., detection and false alarm probabilities) and the average interference constraints. Throughout the numerical results, we assume that QoS parameter is  $\theta = 0.1$ , block duration is  $T = 1\text{s}$ , channel sensing duration is  $N = 0.1\text{s}$ , and the prior probability of each channel being busy is  $\rho = 0.1$ .

Before the numerical analysis, we first provide expressions for the probabilities of operating in each one of the four scenarios described in Section 6.2. These probabilities are also important metrics in analyzing the performance. We have

$$\begin{aligned}
 P\{\text{secondary system is in scenario 1}\} &= P_{S_1} \\
 &= \alpha^{M-1} \rho P_d, \\
 P\{\text{secondary system is in scenario 2}\} &= P_{S_2} \\
 &= \alpha^{M-1} (1 - \rho) P_f, \\
 P\{\text{secondary system is in scenario 3}\} &= P_{S_3} \\
 &= \underbrace{\sum_{k=1}^M \binom{M}{k} \alpha^{M-k} (1 - \alpha)^k}_{\text{probability that at least one channel is detected as idle}} \underbrace{\frac{\rho(1 - P_d)}{1 - \alpha}}_{\substack{\text{probability that} \\ \text{the channel chosen} \\ \text{for transmission} \\ \text{is actually busy} \\ \text{given that it is} \\ \text{detected as idle}}} \\
 &= \frac{(1 - \alpha^M) \rho (1 - P_d)}{1 - \alpha}, \\
 P\{\text{secondary system is in scenario 4}\} &= P_{S_4} \\
 &= \frac{(1 - \alpha^M) (1 - \rho) (1 - P_f)}{1 - \alpha}. \tag{6.35}
 \end{aligned}$$

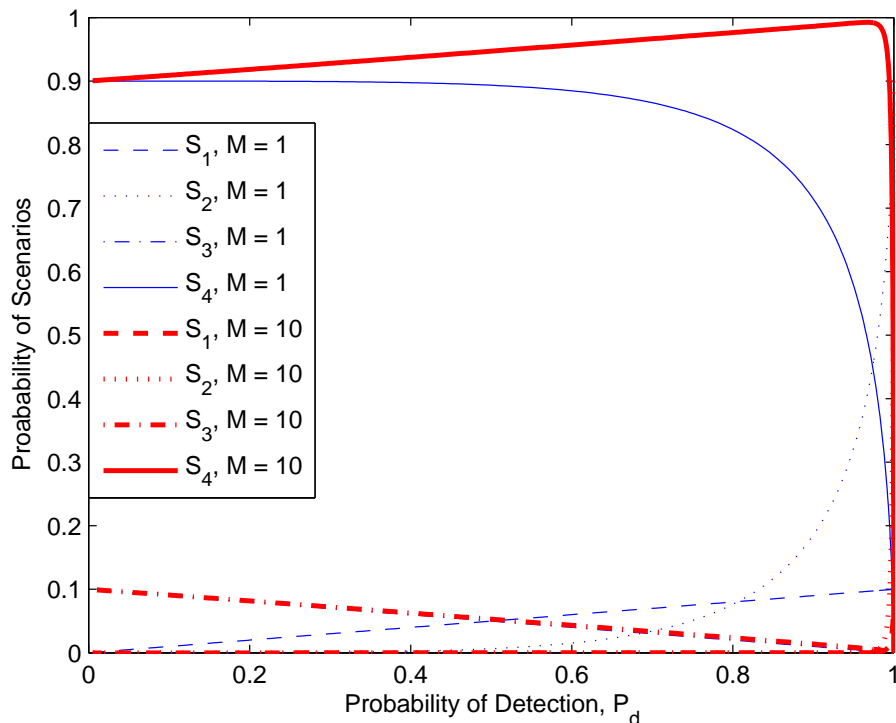


Figure 6.3: Probability of different scenarios vs. probability of detection  $P_d$  for different number of channels  $M$ .

In Figure 6.3, we plot these probabilities as a function of the detection probability  $P_d$  for two cases in which the number of channels is  $M = 1$  and  $M = 10$ , respectively. As expected, we observe that  $P_{S_1}$  and  $P_{S_2}$  decrease with increasing  $M$ . We also see that  $P_{S_3}$  and  $P_{S_4}$  are assuming small values when  $P_d$  is very close to 1. Note from Fig. 6.1 that as  $P_d$  approaches 1, the false alarm probability  $P_f$  increases as well.

### 6.5.1 Rayleigh Fading

The analysis in the preceding sections apply for arbitrary joint distributions of  $z$  and  $z_{sp}$  under the mild assumption that they have finite means (i.e., fading has



finite average power). In this subsection, we consider a Rayleigh fading scenario in which the power gains  $z$  and  $z_{sp}$  are exponentially distributed. We assume that  $z$  and  $z_{sp}$  are mutually independent and each has unit-mean. Then, the pdf and cdf of  $\frac{z}{z_{sp}}$  can be expressed as follows:

$$f_{\frac{z}{z_{sp}}}(x) = \frac{1}{(x+1)^2} \quad x \geq 0 \quad \text{and} \quad F_{\frac{z}{z_{sp}}}(x) = \frac{x}{x+1} \quad x \geq 0. \quad (6.36)$$

In Fig. 6.4, we plot the effective capacity vs. probability of detection,  $P_d$ , for different number of channels when the average interference power constraint normalized by the noise power is  $\bar{I}_{avg}(dB) = 10 \log_{10} \left( \frac{I_{avg}}{\sigma_{n_p}^2 B_c} \right) = 0dB$ , where  $\sigma_{n_p}^2$  is the noise variance at the primary user. We observe that with increasing  $P_d$ , the effective capacity is increasing due to the fact more reliable detection of the activity primary users leads to fewer miss-detections and hence the probability of scenario 3 or equivalently the probability of being in state  $M+2$ , in which the transmission rate is effectively zero, diminishes. We also interestingly see that the highest effective capacity is attained when  $M=1$ . Hence, SUs seem to not benefit from the availability of multiple channels. This is especially pronounced for high values of  $P_d$ . Although several factors and parameters are in play in determining the value of the effective capacity, one explanation for this observation is that the probabilities of scenarios 1 and 2, in which the SUs transmit with power  $P_1$ , decrease with increasing  $M$ , while the probabilities of scenarios 3 and 4 increase as seen in (6.35). Note that in scenario 3, no reliable communication is possible and transmission rate is effectively zero. In Fig. 6.5, we display similar results when  $\bar{I}_{avg} = -10dB$ . Hence, SUs operate under more stringent interference constraints. In this case, we note that  $M=2$  gives the highest throughput while the performance with  $M=1$  is strictly suboptimal.

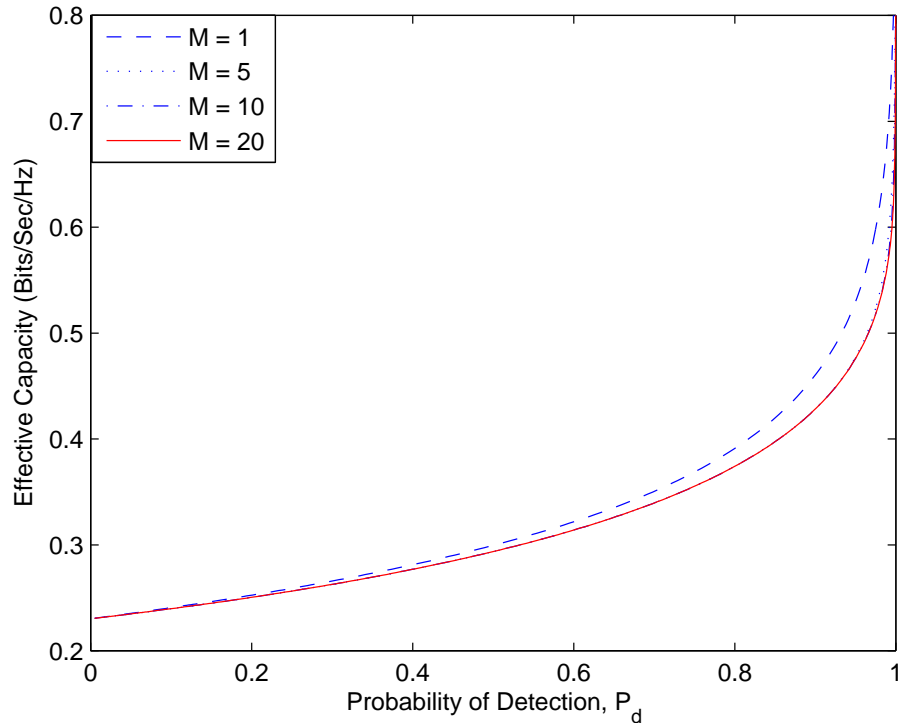


Figure 6.4: Effective capacity vs. probability of detection  $P_d$  for different number of channels  $M$  when  $\bar{I}_{avg} = 0$  dB.

In Fig. 6.6, we show the effective capacities as a function  $\bar{I}_{avg}$  (dB) for different values of  $M$  when  $P_d = 0.9$  and  $P_f = 0.2$ . Confirming our previous observation, we notice that as the interference constraint gets more strict and hence  $\bar{I}_{avg}$  becomes smaller, a higher value of  $M$  is needed to maximize the effective capacity. For instance,  $M = 10$  channels are needed when  $\bar{I}_{avg} < -30$ dB. On the other hand, for approximately  $\bar{I}_{avg} > -6$ dB, having  $M = 1$  gives the highest throughput.

Above, we have remarked that increasing the number of available channels from which the transmission channel is selected provides no benefit or can even degrade the performance of SUs under certain conditions. On the other hand, it is important to note that increasing  $M$  always brings a benefit to the primary

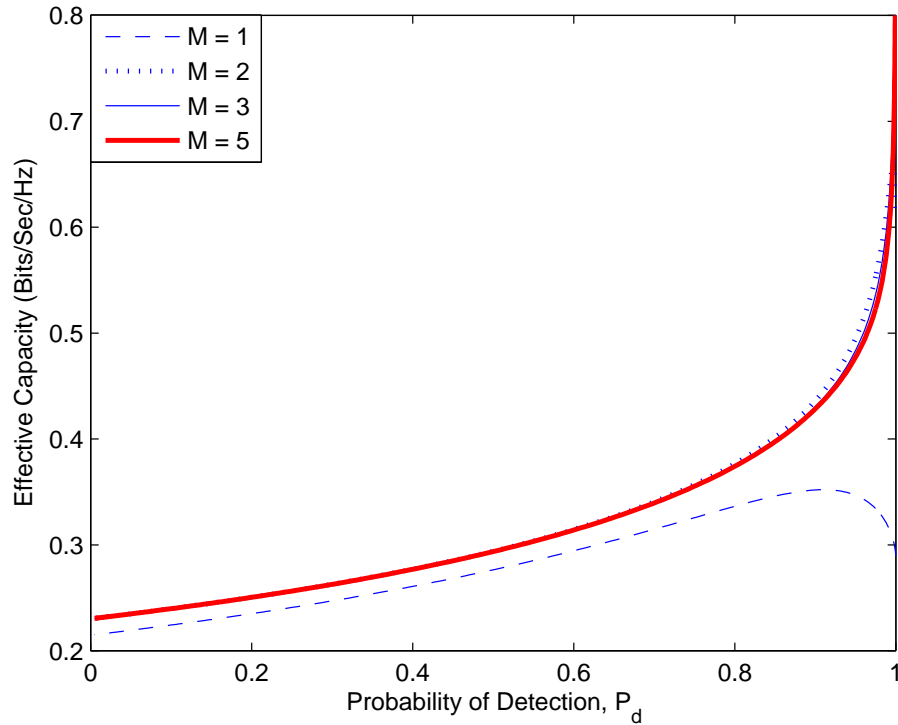


Figure 6.5: Effective capacity vs. probability of detection  $P_d$  for different number of channels  $M$  when  $\bar{I}_{avg} = -10$  dB.

users in the form of decreased probability of interference. In order to quantify this type of gain, we consider below the probability that the channel selected for transmission is actually busy and hence the primary user in this channel experiences interference:

$$P_{int} = P \left( \begin{array}{l} \text{channel selected} \\ \text{for transmission} \\ \text{is actually busy} \end{array} \right) = P \left( \begin{array}{l} \text{channel selected} \\ \text{for transmission} \\ \text{is actually busy} \end{array} \text{ and } \begin{array}{l} \text{all channels are} \\ \text{detected as busy} \end{array} \right) \\ + P \left( \begin{array}{l} \text{channel selected} \\ \text{for transmission} \\ \text{is actually busy} \end{array} \text{ and } \begin{array}{l} \text{at least one channel} \\ \text{is detected as idle} \end{array} \right) \quad (6.37)$$

$$= P_{S_1} + P_{S_3} \quad (6.38)$$

$$= \rho \frac{1 - \alpha^M - P_d + P_d \alpha^{M-1}}{1 - \alpha}. \quad (6.39)$$

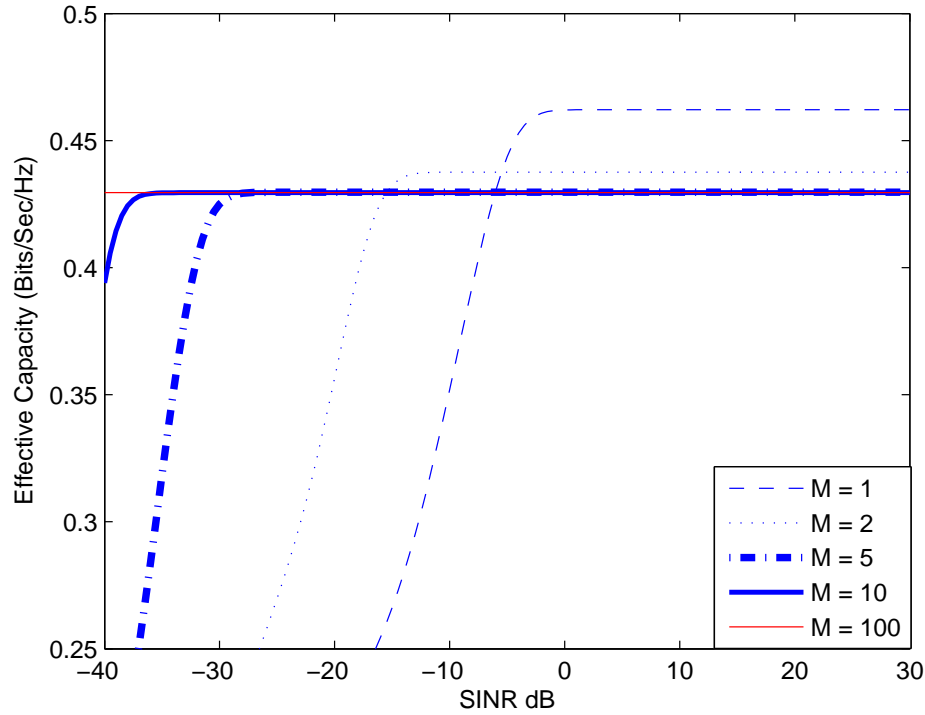


Figure 6.6: Effective capacity vs.  $\bar{I}_{avg}$  for different values of  $M$  when  $P_d = 0.9$  and  $P_f = 0.2$  in the Rayleigh fading channel.

Note that  $P_{int}$  depends on  $P_d$  and also  $P_f$  through  $\alpha = \rho P_d + (1 - \rho)P_f$ . It can be easily seen that this interference probability  $P_{int}$  decreases with increasing  $M$  when  $P_d > P_f$ . As  $M$  goes to infinity, we have  $\lim_{M \rightarrow \infty} P_{int} = \rho \frac{1 - P_d}{1 - \alpha}$ . Indeed, in this asymptotic regime,  $P_{int}$  becomes zero with perfect detection (i.e., with  $P_d = 1$ ). Note that SUs transmit (if  $P_1 > 0$ ) even when all channels are detected as busy. As  $M \rightarrow \infty$ , the probability of such an event vanishes. Also, having  $P_d = 1$  enables the SUs to avoid scenario 3. Hence, interference is not caused to the primary users.

In Fig. 6.7, we plot  $P_{int}$  vs. the detection probability for different values of  $M$ . We also display how the false alarm probability evolves as  $P_d$  varies from 0 to 1.

It can be easily seen that while  $P_{int} = \rho$  when  $M = 1$ , a smaller  $P_{int}$  is achieved for higher values of  $M$  unless  $P_d = 1$ . On the other hand, as also discussed above, we immediately note that  $P_{int}$  monotonically decreases to 0 as  $P_d$  increases to 1 when  $M$  is unbounded (i.e.,  $M \rightarrow \infty$ ).

### 6.5.2 Nakagami Fading

Nakagami fading occurs when multipath scattering with relatively large delay-time spreads occurs. Therefore, Nakagami distribution matches some empirical data better than many other distributions do. With this motivation, we also consider Nakagami fading in our numerical results. The pdf of the Nakagami- $m$  random variable  $y = |h|$  is given by  $f_y(y) = \frac{2}{\Gamma(m)} \left(\frac{m}{2\sigma_y^2}\right)^m y^{2m-1} e^{-\frac{my^2}{2\sigma_y^2}}$  where  $m$  is the number of degrees of freedom. If both  $z_{sp}$  and  $z$  have the same number of degrees of freedom, we can express the pdf of  $x = \frac{z}{z_{sp}}$  as follows:

$$f_x(x) = \frac{\Gamma(2m)x^{m-1}}{(x+1)^{2m}\Gamma(m)^2}. \quad (6.40)$$

Note also that Rayleigh fading is a special case of Nakagami fading when  $m = 1$ . In our experiments, we consider the case in which  $m = 3$ . Now, we can express the cdf of  $x$  for  $m = 3$  as

$$F_x(x) = 1 + \frac{15}{(x+1)^4} - \frac{10}{(x+1)^3} - \frac{6}{(x+1)^4}. \quad (6.41)$$

In Fig. 6.8, we plot effective capacity vs.  $\bar{I}_{avg}$  (dB) for different values of  $M$  when  $P_d = 0.9$  and  $P_f = 0.2$ . Here, we again observe results similar to those in Fig. 6.6. We obtain higher throughput by sensing more than one channel in the presence of strict interference constraints on cognitive radios.

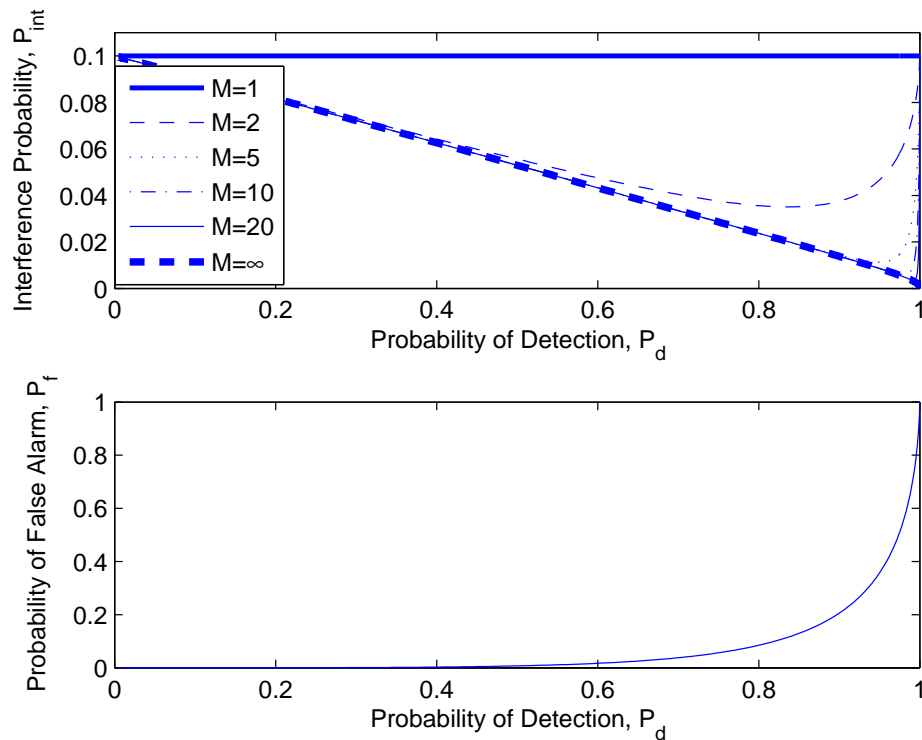


Figure 6.7:  $P_{int}$  vs. correct detection probability  $P_d$  for different number of channels  $M$  in the upper figure. False alarm probability  $P_f$  vs. correct detection probability  $P_d$  in the lower figure.

## 6.6 Conclusion

In this chapter, we have studied the performance of cognitive transmission under QoS constraints and interference limitations. We have considered a scenario in which SUs sense multiple channels and then select a single channel for transmission with rate and power that depend on both sensing decisions and fading. We have constructed a state transition model for this cognitive operation. We have meticulously identified possible scenarios and states in which the SUs operate. These states depend on sensing decisions, true nature of the channels' being busy or idle, and transmission rates being smaller or greater than the instantaneous

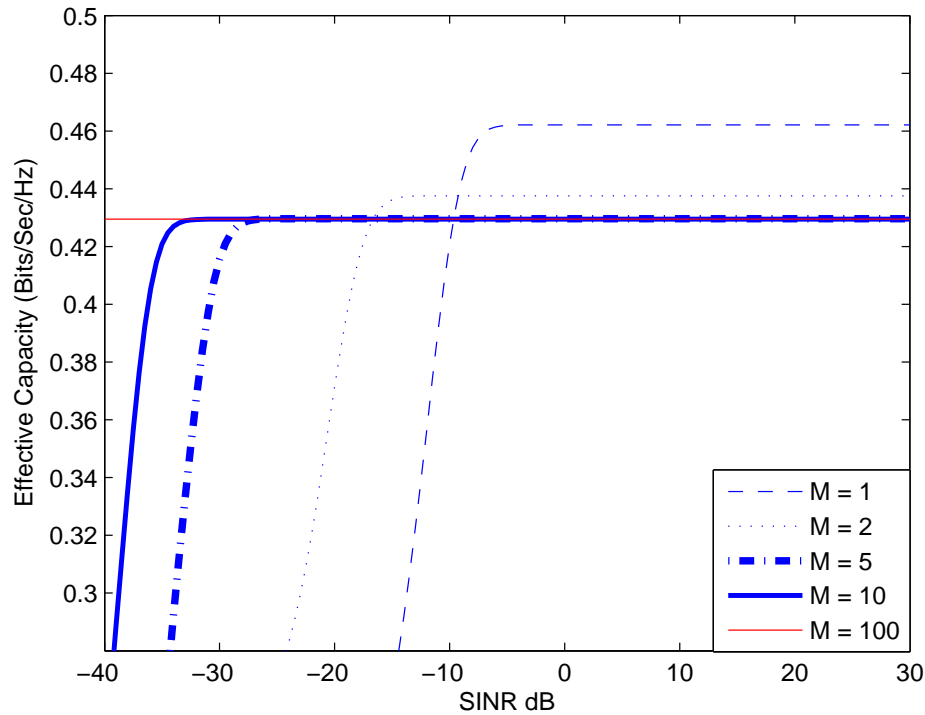


Figure 6.8: Effective capacity vs.  $\bar{I}_{avg}$  for different values of  $M$  when  $P_d = 0.9$  and  $P_f = 0.2$  in the Nakagami- $m$  fading channel with  $m = 3$ .

channel capacity values. We have formulated and imposed an average interference constraint on the SUs. Under such interference constraints and also statistical QoS limitations in the form of buffer constraints, we have obtained the maximum throughput through the effective capacity formulation. Therefore, we have effectively analyzed the performance in a practically appealing setting in which both the primary and SUs are provided with certain service guarantees. We have determined the optimal power adaptation strategies and the optimal channel selection criterion in the sense of maximizing the effective capacity. We have had several interesting observations through our numerical results. We have shown that improving the reliability of channel sensing expectedly increases the throughput.

We have noted that sensing multiple channels is beneficial only under relatively strict interference constraints. At the same time, we have remarked that sensing multiple channels can decrease the chances of interfering with a primary user.



## Chapter 7

# Performance Analysis of Cognitive Radio Systems under QoS

## Constraints and Channel Uncertainty

In this chapter, performance of cognitive transmission over time-selective flat fading channels is studied under QoS constraints and channel uncertainty. Cognitive SUs are assumed to initially perform channel sensing to detect the activities of the primary users, and then attempt to estimate the channel fading coefficients through training. Energy detection is employed for channel sensing, and different MMSE estimation methods are considered for channel estimation. In both channel sensing and estimation, erroneous decisions can be made, and hence, channel uncertainty is not completely eliminated. In this setting, performance is studied and interactions between channel sensing and estimation are investigated. Following the channel sensing and estimation tasks, SUs engage in data transmission. Transmitter, being unaware of the channel fading coefficients, is assumed to send the data at fixed power and rate levels that depend on the channel

sensing results. Under these assumptions, a state-transition model is constructed by considering the reliability of the transmissions, channel sensing decisions and their correctness, and the evolution of primary user activity which is modeled as a two-state Markov process. In the data transmission phase, an average power constraint on the SUs is considered to limit the interference to the primary users, and statistical limitations on the buffer lengths are imposed to take into account the QoS constraints of the secondary traffic. The maximum throughput under these statistical QoS constraints is identified by finding the effective capacity of the cognitive radio channel. Numerical results are provided for the power and rate policies.

## 7.1 Cognitive Channel Model

We consider a cognitive channel model in which a secondary transmitter sends information to a secondary receiver. Initially, the SUs perform channel sensing. Then, depending on the channel sensing results, the secondary transmitter selects pilot symbol and data transmission power policy. Note that the pilot symbol is used for the estimation of the channel fading coefficients. We assume that channel sensing, channel estimation, and data transmission are performed in frames of total duration  $T$  seconds. In each frame, the first  $N$  seconds is allocated for channel sensing. Following the channel sensing, a single pilot symbol is employed to enable the secondary receiver to estimate the channel fading coefficient. Then, data transmission is performed. The allocation of the frame duration to these tasks is depicted in Figure 7.1.

Pilot symbol and data symbol powers, and transmission rates depend on the channel sensing results, i.e., if the channel is sensed to be busy (correct detection

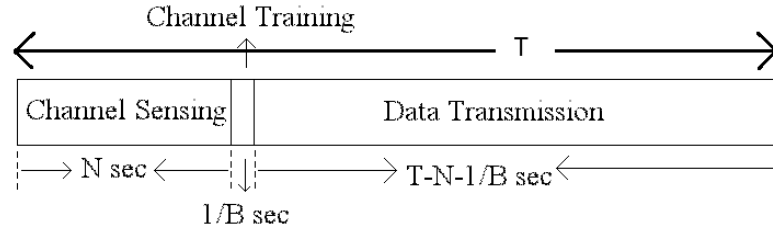


Figure 7.1: Transmission frame consisting of channel sensing, channel training and data transmission. Total frame duration is  $T$ . First  $N$  seconds is allocated to channel sensing. Following channel sensing, a single pilot symbol is sent in the training phase. Under the assumption that the symbol rate is  $B$  complex symbols per second, a single pilot has a duration of  $1/B$  seconds, where  $B$  denotes the bandwidth. The remaining time of  $T - N - 1/B$  seconds is used for data transmission.

of busy case or false alarm), the average transmission power and transmission rate are set to  $\bar{P}_1$  and  $r_1$ , respectively. If, on the other hand, the channel is sensed to be idle (misdetection or correct detection of idle case), the average transmission power and transmission rate are set to  $\bar{P}_2$  and  $r_2$ , respectively. Note that if  $\bar{P}_1 = 0$ , the secondary transmitter stops the transmission when the primary users are sensed to be active.

The discrete-time channel input-output relation between the secondary transmitter and receiver in the  $i^{\text{th}}$  symbol duration is given by

$$y_i = h_i x_i + n_i \quad i = 1, 2, \dots, \quad (7.1)$$

if the primary users are inactive. On the other hand, if the primary users are

using the channel, we have

$$y_i = h_i x_i + n_i + s_i \quad i = 1, 2, \dots, \quad (7.2)$$

where  $x_i$  and  $y_i$  denote the complex-valued channel input and output, respectively. In (7.1) and (7.2),  $h_i$  represents the fading coefficient between the secondary transmitter and receiver. The fading coefficients are zero-mean, circularly symmetric, complex Gaussian distributed with variance  $\mathbb{E}\{|h_i|^2\} = \sigma_h^2$ . In (7.1) and (7.2),  $\{n_i\}$  is a sequence of additive thermal random noise samples at the secondary receiver, that are zero-mean, circularly symmetric, complex Gaussian distributed with variance  $\mathbb{E}\{|n_i|^2\} = \sigma_n^2$  for all  $i$ . In (7.2),  $s_i$  denotes the sum of active primary users' faded signals arriving at the secondary receiver. We denote the variance of  $s_i$  as  $\sigma_s^2$ . Note also that since the bandwidth is  $B$ , symbol rate is assumed to be  $B$  complex symbols per second.

We consider block-fading and assume that the fading coefficients  $\{h_i\}$  stay constant within each frame of  $T$  seconds and change independently from one frame to another. We also assume that the activity of the primary users stay the same in each frame. However, a two-state Markov model is employed to model the transitions of the activity of the primary users between the frames.

## 7.2 Channel Sensing

Energy-detection methods are considered to be well-suited for channel sensing if the transmission policies of primary users are not known. We can formulate the channel sensing as a hypothesis testing problem between the noise  $n_i$  and the signal  $s_i$  in noise. Since the bandwidth is  $B$ , there are  $NB$  complex symbols in a

duration of  $N$  seconds. Now, the hypothesis testing problem can mathematically be expressed as follows:

$$\mathcal{H}_0 : y_i = n_i, \quad i = 1, 2, \dots, NB \quad (7.3)$$

$$\mathcal{H}_1 : y_i = n_i + s_i, \quad i = 1, 2, \dots, NB.$$

We assume that  $s_i$  has a circularly symmetric complex Gaussian distribution<sup>1</sup> with zero-mean and variance  $\sigma_s^2$ . Furthermore, as in [50], we assume that the signal samples  $\{s_i\}$  are i.i.d.. Under these assumptions, the optimal Neyman-Pearson detector for the above hypothesis problem is given by [63]

$$Y = \frac{1}{NB} \sum_{i=1}^{NB} |y_i|^2 \underset{\mathcal{H}_0}{\underset{\mathcal{H}_1}{\geq}} \lambda \quad (7.4)$$

where  $\lambda$  is the detection threshold. Observing that  $Y$  is chi-squared distributed with  $2NB$  degrees of freedom, we can establish the probabilities of false alarm and detection as follows:

$$P_f = \Pr\{Y > \lambda \mid \mathcal{H}_0\} = 1 - P\left(\frac{NB\lambda}{\sigma_n^2}, NB\right) \quad (7.5)$$

$$P_d = \Pr\{Y > \lambda \mid \mathcal{H}_1\} = 1 - P\left(\frac{NB\lambda}{\sigma_n^2 + \sigma_s^2}, NB\right) \quad (7.6)$$

where  $P(x, y)$  denotes the regularized gamma function and is defined as  $P(x, y) = \frac{\gamma(x, y)}{\Gamma(y)}$  where  $\gamma(x, y)$  is the lower incomplete gamma function and  $\Gamma(y)$  is the Gamma function.

Above, we have considered an i.i.d. scenario. If  $\{s_i\}$  are correlated and if the

---

<sup>1</sup>Note that if the signals are being received in a rich multipath environment or the number of active primary users is large, the simplifying Gaussian assumption for the distribution of  $s_i$  has high accuracy. Moreover, if, for example the primary users are employing frequency or phase modulation,  $s_i$  in the presence of even a single primary user in flat fading Rayleigh channel will be Gaussian distributed.

correlation structure is known by the cognitive users, then the optimal detector computes, as the test statistic, the quadratic form  $\mathbf{y}^\dagger \mathbf{K} \mathbf{y}$  where  $\mathbf{y}$  is the vector of  $NB$  received signal samples  $\{y_i\}_{i=1}^{NB}$ , and  $\mathbf{K}$  is a matrix that depends on the covariance matrix of the primary user signal samples  $\{s_i\}_{i=1}^N$  [63, Case III.B.4]. If  $\{s_i\}$  are identically distributed, then the false alarm and detection probabilities are again expressed in terms of the regularized lower gamma function and are in the same form as in (7.5) and (7.6) (see [63, Equation III.B.96]).

In the hypothesis testing problem given in (7.3), another approach is to consider  $Y$  as Gaussian distributed, which is accurate if  $NB$  is large [50]. In this case, the detection and false alarm probabilities can be expressed in terms of Gaussian  $Q$ -functions. We would like to note that the rest of the analysis in the chapter does not depend on the specific expressions of the false alarm and detection probabilities. However, numerical results are obtained using (7.5) and (7.6).

A similar hypothesis-testing formulation for channel sensing is also studied in [2] and is provided in this chapter as well for the completeness of the discussion.

### 7.3 Pilot Symbol-Assisted Transmission

After channel sensing is performed, the secondary transmitter sends the pilot symbol to enable the receiver to estimate the channel fading coefficient. In this section, we consider several channel estimation methods. As emphasized earlier, channel estimation has dependence on channel sensing results. Regarding the channel sensing result and its correctness, we have the following four possible scenarios:

1. *Scenario 1*: Channel is busy, detected as busy (correct detection),

2. *Scenario 2*: Channel is busy, detected as idle (miss-detection),
3. *Scenario 3*: Channel is idle, detected as busy (false alarm),
4. *Scenario 4*: Channel is idle, detected as idle (correct detection).

Note that the secondary transmitter sends data with average power  $\bar{P}_1$  if the channel is sensed as busy, whereas the transmitter sends data with average power  $\bar{P}_2$  if the channel is detected to be idle. Since fading stays constant in each frame, it is enough to send only one pilot symbol in each frame<sup>2</sup>. Therefore, the first  $N$  seconds of a frame duration  $T$  seconds is spared to sense the channel, a single pilot symbol is sent following channel sensing, and  $(T - N)B - 1$  data symbols are transmitted after the pilot symbol<sup>3</sup>. In each frame, the average input power is

$$\frac{1}{T} \sum_{i=(lT+N)B}^{(l+1)TB-1} \mathbb{E} \left\{ |x_i|^2 \right\} = \bar{P}_1 \quad l = 0, 1, 2, \dots, \quad (7.7)$$

when activity is sensed in the channel, whereas the average input power is

$$\frac{1}{T} \sum_{i=(lT+N)B}^{(l+1)TB-1} \mathbb{E} \left\{ |x_i|^2 \right\} = \bar{P}_2 \quad l = 0, 1, 2, \dots, \quad (7.8)$$

when the channel is sensed to be idle. Above,  $l$  denotes the frame index. From the average power constraints, we see that the total energy allocated to the pilot and data symbols is limited in one frame by  $T\bar{P}_1$  or  $T\bar{P}_2$  when the channel is busy or idle, respectively.

---

<sup>2</sup>Since MMSE estimation depends only on the pilot power and not on the number of pilot symbols, a single pilot symbol with optimized power is sufficient.

<sup>3</sup>Since the symbol rate is  $B$  symbols per second, we have  $(T - N)B$  symbols in a duration of  $T - N$  seconds. Among these symbols, the first symbol is a pilot symbol and the remaining  $(T - N)B - 1$  symbols are the data symbols.

We assume that, depending on the capabilities of the transmitters and the energy resources they are equipped with, there exists peak constraints on the average powers, e.g.,

$$\bar{P}_1 \leq \bar{P}_{peak} \quad \text{and} \quad \bar{P}_2 \leq \bar{P}_{peak}. \quad (7.9)$$

Additionally, note that the secondary transmitter transmits with an average power  $\bar{P}_1$  in scenario 1 and with an average power  $\bar{P}_2$  in scenario 2. In both scenarios, primary users are active in the channel and experience interference due to the transmission of the SUs. In order to limit the interference and protect the primary users, we impose the following constraint on  $\bar{P}_1$  and  $\bar{P}_2$ :

$$P_d \bar{P}_1 + (1 - P_d) \bar{P}_2 \leq \bar{P}_{avg} \quad (7.10)$$

where  $P_d$  is the probability of detection and  $(1 - P_d)$  is the probability of miss-detection, and  $P_d$  and  $1 - P_d$  can be regarded as the probabilities of scenarios 1 and 2, respectively. In the following, we describe how  $\bar{P}_{avg}$  can be related to the interference constraints. Let us denote the fading coefficient between the secondary transmitter and primary receiver as  $h_{sp}$ . Now, the average interference experienced by the primary user can be expressed as

$$\mathbb{E}\{P_d \bar{P}_1 |h_{sp}|^2 + (1 - P_d) \bar{P}_2 |h_{sp}|^2\} = (P_d \bar{P}_1 + (1 - P_d) \bar{P}_2) \mathbb{E}\{|h_{sp}|^2\} \leq I_{avg} \quad (7.11)$$

where  $I_{avg}$  can be regarded as the average interference constraint. We assume that the realizations of  $h_{sp}$  are not known at the secondary transmitter and hence the secondary transmitter cannot adapt its transmission according to  $h_{sp}$ . However, if the statistics of  $h_{sp}$  (e.g., the mean of  $|h_{sp}|^2$  is known), then the secondary



transmitter can choose  $P_{avg} = \frac{I_{avg}}{\mathbb{E}\{|h_{sp}|^2\}}$  in order to satisfy (7.11).

Finally, we would like to note that in the perfect detection case in which  $P_d = 1$ , there are no miss-detections and (7.10) specializes to  $\bar{P}_1 \leq \bar{P}_{avg}$ . Hence, expectedly, only  $\bar{P}_1$ , which is the transmission power when the channel is sensed as busy, is affected by the interference constraints, and we have  $\bar{P}_2 \leq \bar{P}_{peak}$ . If  $P_d < 1$ , miss-detections should also be considered. In such cases, the SUs do not detect the active primary users and transmit at power  $\bar{P}_2$ . Hence,  $\bar{P}_2$  should also be considered in interference control as formulated in (7.10).

### 7.3.1 Training Phase

In the channel training phase, the pilot symbol power is set depending on the sensing result. If the channel is detected as busy, the power of pilot symbol is set to  $P_{tb} = \eta \bar{P}_1 T$ . On the other hand, the pilot power is  $P_{ti} = \eta \bar{P}_2 T$  when no activity is detected.  $\eta$  is the fraction of the total power allocated to the pilot symbol.

For the scenarios described at the beginning of this section, the corresponding received signals in the training phase are given by the following:

1. *Scenario 1:*  $y_{(lT+N)B} = h_l \sqrt{P_{tb}} + n_{(lT+N)B} + s_{(lT+N)B}$ ,
2. *Scenario 2:*  $y_{(lT+N)B} = h_l \sqrt{P_{ti}} + n_{(lT+N)B} + s_{(lT+N)B}$ ,
3. *Scenario 3:*  $y_{(lT+N)B} = h_l \sqrt{P_{tb}} + n_{(lT+N)B}$ ,
4. *Scenario 4:*  $y_{(lT+N)B} = h_l \sqrt{P_{ti}} + n_{(lT+N)B}$ .

Above,  $h_l$  denotes the channel fading coefficients in the  $l^{th}$  block. The fading coefficients are estimated via MMSE estimation, which provides the following

estimates for each scenario:

$$\text{Scenario 1: } \hat{h}_{l,m-mmse} = \frac{\sqrt{P_{tb}}\sigma_h^2}{P_{tb}\sigma_h^2 + \sigma_n^2 + \sigma_s^2} y_{(lT+N)B}, \quad (7.12)$$

$$\text{Scenario 2: } \hat{h}_{l,m-mmse} = \frac{\sqrt{P_{ti}}\sigma_h^2}{P_{ti}\sigma_h^2 + \sigma_n^2} y_{(lT+N)B}, \quad (7.13)$$

$$\text{Scenario 3: } \hat{h}_{l,m-mmse} = \frac{\sqrt{P_{tb}}\sigma_h^2}{P_{tb}\sigma_h^2 + \sigma_n^2 + \sigma_s^2} y_{(lT+N)B}, \quad (7.14)$$

$$\text{Scenario 4: } \hat{h}_{l,m-mmse} = \frac{\sqrt{P_{ti}}\sigma_h^2}{P_{ti}\sigma_h^2 + \sigma_n^2} y_{(lT+N)B}. \quad (7.15)$$

From above, we see that the estimate expressions in scenarios 1 and 3 in which the channel is detected as busy are the same. So are the expressions in scenarios 2 and 4 in which the channel is detected as idle. Hence, the receiver has two estimation rules depending on whether the channel is sensed as busy or idle. Note that the MMSE formulation is obtained under the assumption that the primary users' signal  $s$  is Gaussian distributed with mean zero and variance  $\sigma_s^2$ . It is also important to note that the above MMSE estimates are affected by the channel sensing results. For instance, in scenario 2, the channel is busy but the receiver senses the channel as idle. Based on this sensing result, the receiver assumes that the noise variance is  $\sigma_n^2$  rather than the actual value  $\sigma_n^2 + \sigma_s^2$ , and multiplies the observation  $y_{(lT+N)B}$  by  $\frac{\sqrt{P_{ti}}\sigma_h^2}{P_{ti}\sigma_h^2 + \sigma_n^2}$  instead of  $\frac{\sqrt{P_{ti}}\sigma_h^2}{P_{ti}\sigma_h^2 + \sigma_n^2 + \sigma_s^2}$ . Hence, in the computation of the MMSE estimate, the receiver treats its channel sensing decision as the true decision. Hence, if the sensing decision is erroneous, the MMSE estimate is obtained for a mismatched channel. For this reason, we call these estimates as *mismatched MMSE* estimates and use the subscript  $m - mmse$ . Note that from the receiver's perspective, the variance of the noise is random taking two possible values,  $\sigma_n^2$  and  $\sigma_n^2 + \sigma_s^2$ . In the presence of uncertainty in the noise statistics, the true MMSE

estimate is given by the following result.

**Theorem 6** *Given the channel sensing decision and the observation  $y$  in the training phase, the receiver obtains the MMSE estimate through the following formulation:*

$$\begin{aligned}\hat{h}_{mmse} &= \mathbb{E}\{h|y\} = \Pr\{\sigma^2 = \sigma_n^2 | y\} \frac{\sqrt{P_t}\sigma_h^2}{P_t\sigma_h^2 + \sigma_n^2}y + \Pr\{\sigma^2 \\ &= \sigma_n^2 + \sigma_s^2 | y\} \frac{\sqrt{P_t}\sigma_h^2}{P_t\sigma_h^2 + \sigma_n^2 + \sigma_s^2}y\end{aligned}\quad (7.16)$$

where

$$\Pr\{\sigma^2 = \sigma_n^2 | y\} = \frac{\Pr\{\sigma^2 = \sigma_n^2\}f(y|\sigma^2 = \sigma_n^2)}{f(y)}$$

and similarly

$$\Pr\{\sigma^2 = \sigma_n^2 + \sigma_s^2 | y\} = \frac{\Pr\{\sigma^2 = \sigma_n^2 + \sigma_s^2\}f(y|\sigma^2 = \sigma_n^2 + \sigma_s^2)}{f(y)}.$$

In the above formulation, we have

$$\Pr\{\sigma^2 = \sigma_n^2\} = \begin{cases} \frac{aP_f}{aP_f + bP_d} & \text{if the channel is detected busy} \\ \frac{a(1-P_f)}{a(1-P_f) + b(1-P_d)} & \text{if the channel is detected idle} \end{cases} \quad (7.17)$$

$$\Pr\{\sigma^2 = \sigma_n^2 + \sigma_s^2\} = \begin{cases} \frac{bP_d}{aP_f + bP_d} & \text{if the channel is detected busy} \\ \frac{b(1-P_d)}{a(1-P_f) + b(1-P_d)} & \text{if the channel is detected idle} \end{cases} \quad (7.18)$$

$$f(y|\sigma^2 = \sigma_n^2) = \frac{1}{\pi(P_t\sigma_h^2 + \sigma_n^2)} e^{-\frac{|y|^2}{P_t\sigma_h^2 + \sigma_n^2}} \quad (7.19)$$

$$f(y|\sigma^2 = \sigma_n^2 + \sigma_s^2) = \frac{1}{\pi(P_t\sigma_h^2 + \sigma_n^2 + \sigma_s^2)} e^{-\frac{|y|^2}{P_t\sigma_h^2 + \sigma_n^2 + \sigma_s^2}} \quad (7.20)$$

$$\begin{aligned}f(y) &= \Pr\{\sigma^2 = \sigma_n^2\}f(y|\sigma^2 = \sigma_n^2) \\ &\quad + \Pr\{\sigma^2 = \sigma_n^2 + \sigma_s^2\}f(y|\sigma^2 = \sigma_n^2 + \sigma_s^2)\end{aligned}\quad (7.21)$$

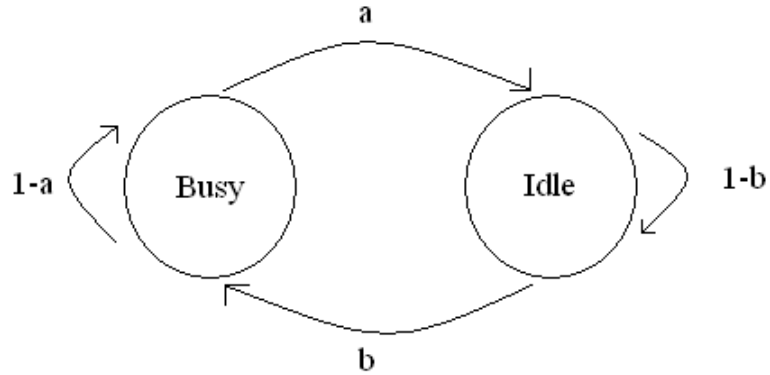


Figure 7.2: Two-state Markov model for the primary user activity.

In (7.17) and (7.18),  $P_d$  and  $P_f$  denote the detection and false-alarm probabilities, respectively, and  $a$  and  $b$  are the transition probabilities in the two-state Markov model of the primary user activity (depicted in Fig. 7.2 and described in detail in Section 7.4). Note also that  $P_t$  denotes the power of the pilot symbol and is equal to  $P_{tb}$  if the channel is detected busy and equal to  $P_{ti}$  if the channel is detected idle.

*Proof:* See Appendix F. □

It can be immediately seen that as in the mismatched MMSE case, we again have two estimation rules depending on the channel sensing result. Note that the statistical characterization (e.g., finding the variance or more generally the distribution) of the MMSE estimate in Theorem 6 is a difficult task and can only be done through numerical analysis. It is also computationally intensive for the receiver to obtain this estimate. Another strategy is to obtain the linear MMSE

estimate. Note that given the observation  $y$ , the linear MMSE estimate is given by

$$\begin{aligned}
\hat{h}_{l-mmse} &= \frac{\mathbb{E}\{hy^*\}}{\mathbb{E}\{|y|^2\}}y \\
&= \frac{\sqrt{P_t}\sigma_h^2}{\mathbb{E}\{|y|^2\}}y & (7.22) \\
&= \frac{\sqrt{P_t}\sigma_h^2}{\Pr\{\sigma^2 = \sigma_n^2\}\mathbb{E}\{|y|^2 \mid \sigma^2 = \sigma_n^2\} + \Pr\{\sigma^2 = \sigma_n^2 + \sigma_s^2\}\mathbb{E}\{|y|^2 \mid \sigma^2 = \sigma_n^2 + \sigma_s^2\}}y \\
&= \frac{\sqrt{P_t}\sigma_h^2}{\Pr\{\sigma^2 = \sigma_n^2\}(P_t\sigma_h^2 + \sigma_n^2) + \Pr\{\sigma^2 = \sigma_n^2 + \sigma_s^2\}(P_t\sigma_h^2 + \sigma_n^2 + \sigma_s^2)}y & (7.23)
\end{aligned}$$

where  $\Pr\{\sigma^2 = \sigma_n^2\}$  and  $\Pr\{\sigma^2 = \sigma_n^2 + \sigma_s^2\}$  are given in (7.17) and (7.18). Similarly, as in Theorem 6,  $P_t$  is either equal to  $P_{tb}$  or  $P_{ti}$  depending whether the channel is detected as busy or idle.

It is interesting to note that if channel sensing results are perfect, i.e.,  $P_d = 1$  and  $P_f = 0$ , all estimation methods discussed above converge.

### 7.3.2 Data Transmission Phase

Now, we can express the fading coefficients as follows

$$h_l = \hat{h}_l + \tilde{h}_l \quad (7.24)$$

where  $\tilde{h}_l$  is the estimation error. Consequently, the input-output relationship in the data transmission phase of the  $l^{\text{th}}$  frame can be written as

$$y_i = \hat{h}_l x_i + \tilde{h}_l x_i + n_i + s_i \quad (lT + N)B + 1 \leq i \leq (l + 1)TB - 1 \quad (7.25)$$

if the channel is busy, and

$$y_i = \hat{h}_l x_i + \tilde{h}_l x_i + n_i \quad (lT + N)B + 1 \leq i \leq (l + 1)TB - 1 \quad (7.26)$$

if the channel is idle.

Note that the mismatched MMSE estimates in (7.12) – (7.15) and linear MMSE estimate in (7.23) can be written as  $\hat{h} = Ky$  where  $K$  is a constant that depends on the channel sensing result and  $y$  is the received signal in the training phase. Since  $y$  is a Gaussian random variable,  $\hat{h}_l$  and  $\tilde{h}_l$  are zero-mean circularly symmetric complex Gaussian random variables in these cases. The variance of the channel estimates is  $\sigma_h^2 = K^2 \mathbb{E}\{|y|^2\}$ . In particular, we have the following variance expressions for the mismatched MMSE estimates in different scenarios:

$$\begin{aligned} \text{Scenario 1: } \sigma_{\hat{h}_{l,m-mmse}}^2 &= \frac{P_{tb}\sigma_h^4}{P_{tb}\sigma_h^2 + \sigma_n^2 + \sigma_s^2}, \\ \text{Scenario 2: } \sigma_{\tilde{h}_{l,m-mmse}}^2 &= \frac{P_{ti}\sigma_h^4}{(P_{ti}\sigma_h^2 + \sigma_n^2)^2} (P_{ti}\sigma_h^2 + \sigma_n^2 + \sigma_s^2), \\ \text{Scenario 3: } \sigma_{\hat{h}_{l,m-mmse}}^2 &= \frac{P_{tb}\sigma_h^4}{(P_{tb}\sigma_h^2 + \sigma_n^2 + \sigma_s^2)^2} (P_{tb}\sigma_h^2 + \sigma_n^2), \\ \text{Scenario 4: } \sigma_{\tilde{h}_{l,m-mmse}}^2 &= \frac{P_{ti}\sigma_h^4}{P_{ti}\sigma_h^2 + \sigma_n^2}. \end{aligned}$$

In all scenarios, the variance of the estimation error in both mismatch and linear MMSE can be written as

$$\sigma_{\hat{h}_l}^2 = (1 - 2K\sqrt{P_t})\sigma_h^2 + \sigma_{\tilde{h}_l}^2. \quad (7.27)$$

Again,  $P_t$  is either  $P_{tb}$  or  $P_{ti}$  depending on whether the channel is sensed as busy or idle, respectively. In true MMSE, since the estimate and error are uncorrelated,

we have  $\sigma_{\hat{h}_l}^2 = \sigma_h^2 - \sigma_{\hat{h}_l}^2$ .

## 7.4 State Transition Model

In this section, we construct a state-transition model for cognitive transmission. In order to identify this model, we first consider the transmission rates that can be supported by the channel. In the presence of channel uncertainty, it is generally difficult to characterize the channel capacity, which is the maximum transmission rate at which reliable communications can be established [34]. Therefore, most studies work with lower bounds on the channel capacity. One common technique employed in deriving an achievable rate expression is to regard the error in the channel estimate as another source of Gaussian noise. Since Gaussian noise is the worst uncorrelated noise, this assumption leads to a lower bound [37]. On the other hand, the achievable rate expressions obtained using this approach are good measures of the rates supported in communication systems that operate as if the channel estimate were perfect (i.e., in systems where Gaussian codebooks designed for known channels are used, and scaled nearest neighbor decoding is employed at the receiver) [48].

Considering the channel estimation results and interference  $s$  caused by the primary users, we have the following achievable rate expressions as lower bounds

to the instantaneous channel capacities in the above four scenarios:

$$\begin{aligned}
\text{Scenario 1: } R_1 &= \frac{(T-N)B-1}{T} \log \left( 1 + \text{SNR}_1 |w_l|^2 \right) \\
\text{Scenario 2: } R_2 &= \frac{(T-N)B-1}{T} \log \left( 1 + \text{SNR}_2 |w_l|^2 \right) \\
\text{Scenario 3: } R_3 &= \frac{(T-N)B-1}{T} \log \left( 1 + \text{SNR}_3 |w_l|^2 \right) \\
\text{Scenario 4: } R_4 &= \frac{(T-N)B-1}{T} \log \left( 1 + \text{SNR}_4 |w_l|^2 \right)
\end{aligned} \tag{7.28}$$

where

$$\begin{aligned}
\text{SNR}_1 &= \frac{P_{db} \sigma_{\hat{h}_1}^2}{P_{db} \sigma_{\hat{h}_1}^2 + \sigma_n^2 + \sigma_s^2}, & \text{SNR}_2 &= \frac{P_{di} \sigma_{\hat{h}_1}^2}{P_{di} \sigma_{\hat{h}_2}^2 + \sigma_n^2 + \sigma_s^2} \\
\text{SNR}_3 &= \frac{P_{db} \sigma_{\hat{h}_1}^2}{P_{db} \sigma_{\hat{h}_3}^2 + \sigma_n^2}, & \text{and } \text{SNR}_4 &= \frac{P_{di} \sigma_{\hat{h}_1}^2}{P_{di} \sigma_{\hat{h}_4}^2 + \sigma_n^2}.
\end{aligned} \tag{7.29}$$

These lower bounds are obtained by assuming that  $\tilde{h}_l x_i$  and  $s_i$  are Gaussian distributed which is the worst-case noise. Above, we have defined  $\hat{h}_l = w_l \sigma_{\tilde{h}_l}$ . Note that  $w_l$  is a standard complex Gaussian random variable with zero mean and unit variance, i.e.,  $w_l \sim \mathcal{CN}(0, 1)$ , in mismatched and linear MMSE. Hence,  $z_l = |w_l|^2$  has an exponential distribution with mean 1.  $P_{db}$  and  $P_{di}$  are the data symbols powers when the channel is busy and idle, respectively, and they can be written as

$$P_{db} = \frac{\bar{P}_1 T - P_{tb}}{(T-N)B-1} \quad \text{and} \quad P_{di} = \frac{\bar{P}_2 T - P_{ti}}{(T-N)B-1}. \tag{7.30}$$

While the receiver attempts to learn the channel through training, we assume that the transmitter is unaware of the channel conditions and transmits the information at fixed rates  $r_1$  and  $r_2$ , depending on the channel being sensed as busy or idle, respectively. Therefore, the transmission rate is  $r_1$  in scenarios 1 and 3, and



$r_2$  in scenarios 2 and 4. If these rates are below the achievable rate expressions provided in (7.28), i.e., if  $r_1 < R_1, R_3$  or  $r_2 < R_2, R_4$ , the transmission is considered to be in the ON state and reliable communication is achieved at these rates. On the other hand, if  $r_1 \geq R_1, R_3$  or  $r_2 \geq R_2, R_4$ , then we assume that outage occurs and reliable communication can not be achieved. In such a case, the channel is in the OFF state. To ensure the reception of correct data, a simple ARQ mechanism needs to be incorporated in the communication protocol in the OFF state.

From the above discussion, we see that in each scenario we have two states, namely ON and OFF, depending on whether or not the fixed-transmission rate exceeds the instantaneous rate that the channel can support. Therefore, overall we have eight states. Fig. 5.1 depicts the state transition model for the cognitive radio transmission considering all possible scenarios related to the channel sensing decisions and their correctness, and the reliability of the transmissions. The labels for the states are provided on the bottom-right corner of the box representing the state.

The transition probabilities in this state-transition model depend on the channel fading coefficients, the fixed transmission rates, and the primary user activity. Recall that we consider block-fading and assume that the fading coefficients stay constant throughout the frame and change independently from one frame to another. We also assume that primary user activity does not change within each frame. However, we employ a two-state Markov model to describe the transition of the primary user activity between the frames. This Markov model is depicted in Fig. 7.2. Busy state indicates that the channel is occupied by the primary users, and idle state indicates that there is no primary user present in the channel. Probability of transitioning from busy state to idle state is denoted by  $a$ , and the probability of transitioning from idle state to busy state is denoted by  $b$ . Note

that, by our assumption, state transitions happen every  $T$  seconds, which is the frame duration.

Next, we determine the state transition probabilities. Let us first consider in detail the probability of staying in the topmost ON state in Fig. 5.1. This probability, denoted by  $p_{11}$ , is given by

$$p_{11} = \Pr \left\{ \begin{array}{l} \text{channel is busy and is detected busy,} \\ \text{and } r_1 < R_1(l) \text{ in the } l^{\text{th}} \text{ frame} \end{array} \middle| \begin{array}{l} \text{channel is busy and is detected busy,} \\ \text{and } r_1 < R_1(l-1) \text{ in the } (l-1)^{\text{th}} \text{ frame} \end{array} \right\} \quad (7.31)$$

$$\begin{aligned} &= \Pr \left\{ \begin{array}{l} \text{channel is busy} \\ \text{in the } l^{\text{th}} \text{ frame} \end{array} \middle| \begin{array}{l} \text{channel is busy} \\ \text{in the } (l-1)^{\text{th}} \text{ frame} \end{array} \right\} \times \Pr \left\{ \begin{array}{l} \text{channel is detected busy} \\ \text{in the } l^{\text{th}} \text{ frame} \end{array} \middle| \begin{array}{l} \text{channel is busy} \\ \text{in the } l^{\text{th}} \text{ frame} \end{array} \right\} \\ &\quad \times \Pr \{r_1 < R_1(l) \mid r_1 < R_1(l-1)\} \end{aligned} \quad (7.32)$$

$$= (1-a) P_d \Pr \{r_1 < R_1(l) \mid r_1 < R_{1-1}(l)\} \quad (7.33)$$

$$= (1-a) P_d \Pr \{z_l > \alpha_1 \mid z_{l-1} > \alpha_1\} \quad (7.34)$$

$$= (1-a) P_d \Pr \{z_l > \alpha_1\} \quad (7.35)$$

$$= (1-a) P_d \Pr \{z > \alpha_1\} \quad (7.36)$$

where

$$\alpha_1 = \frac{2^{\frac{r_1 T}{(T-N)B-1}} - 1}{\text{SNR}_1}, \quad (7.37)$$

$P_d$  is the probability of detection in channel sensing,  $r_1$  is the fixed transmission rate in scenario 1, and  $R_1(l)$  denotes the achievable rate expression in scenario 1 in the  $l^{\text{th}}$  frame. Above, (7.32) is obtained by using the chain rule of probability<sup>4</sup> and noting the following facts. Channel being busy in the  $l^{\text{th}}$  frame depends only on channel being busy in the  $(l-1)^{\text{th}}$  frame and not on the other events in the condition. Moreover, since channel sensing is performed individually in each frame without any dependence on the channel sensing decision and primary

---

<sup>4</sup>Consider the events  $A, B, C$ , and  $D$ . Using the chain rule, the conditional probability  $\Pr(A \cap B \cap C \mid D)$  can be written as  $\Pr(A \cap B \cap C \mid D) = \Pr(A \mid D) \times \Pr(B \mid A \cap D) \times \Pr(C \mid A \cap B \cap D)$ .

user activity in the previous frame, channel being detected as busy in the  $l^{\text{th}}$  frame depends only on the event that the channel is actually busy in the  $l^{\text{th}}$  frame. Finally, the event  $\{r_1 < R_1(l)\}$  is related to the channel fading coefficients and hence possibly depends on the event  $\{r_1 < R_1(l-1)\}$  through the dependence of fading coefficients between frames. (7.33) follows by realizing that the first probability in (7.32) is equal to  $(1-a)$ , the probability of staying in the busy state in the Markov model given for primary user activity, and noticing that the second probability is equal to  $P_d$ , the detection probability in channel sensing. (7.34) is obtained by noting that the event  $\{r_1 < R_1(l) = \frac{(T-N)B-1}{T} \log(1 + \text{SNR}_1 |w_l|^2)\}$  is equivalent to the event  $\{z_l > \alpha_1\}$  where  $z_l = |w_l|^2$  and  $\alpha_1$  is defined in (7.37). (7.35) follows from the fact that  $z_l$  and  $z_{l-1}$  are independent due to the block-fading assumption. Finally, (7.36) is obtained by noting that fading coefficients and their estimates are identically distributed in each frame and hence the index  $l$  in  $z_l$  can be dropped.

Similarly, the probabilities for transitioning from any state to state 1 (topmost ON state) can be expressed as

$$\begin{aligned} p_{b1} = p_{11} = p_{21} = p_{31} = p_{41} &= (1-a)P_d \Pr\{z > \alpha_1\}, \\ p_{i1} = p_{51} = p_{61} = p_{71} = p_{81} &= bP_d \Pr\{z > \alpha_1\}. \end{aligned} \quad (7.38)$$

Note that we have common expressions for the transition probabilities in cases in which the originating state has a busy channel (i.e., states 1, 2, 3, and 4) and in cases in which the originating state has an idle channel (i.e., states 5, 6, 7, and 8).

In a similar manner, the remaining transition probabilities are given by the following:

For all  $b \in \{1, 2, 3, 4\}$  and  $i \in \{5, 6, 7, 8\}$ ,

$$\begin{aligned}
p_{b2} &= (1-a)P_d \Pr\{z \leq \alpha_1\}, & p_{i2} &= bP_d \Pr\{z \leq \alpha_1\}, \\
p_{b3} &= (1-a)(1-P_d) \Pr\{z > \alpha_2\}, & p_{i3} &= b(1-P_d) \Pr\{z > \alpha_2\}, \\
p_{b4} &= (1-a)(1-P_d) \Pr\{z \leq \alpha_2\}, & p_{i4} &= b(1-P_d) \Pr\{z \leq \alpha_2\}, \\
p_{b5} &= aP_f \Pr\{z > \alpha_3\}, & p_{i5} &= (1-b)P_f \Pr\{z > \alpha_3\}, \\
p_{b6} &= aP_f \Pr\{z \leq \alpha_3\}, & p_{i6} &= (1-b)P_f \Pr\{z \leq \alpha_3\}, \\
p_{b7} &= a(1-P_f) \Pr\{z > \alpha_4\}, & p_{i7} &= (1-b)(1-P_f) \Pr\{z > \alpha_4\}, \\
p_{b8} &= a(1-P_f) \Pr\{z \leq \alpha_4\}, & p_{i8} &= (1-b)(1-P_f) \Pr\{z \leq \alpha_4\},
\end{aligned} \tag{7.39}$$

where  $\alpha_2 = \frac{2^{\frac{r_2 T}{(T-N)B-1}} - 1}{\text{SNR}_2}$ ,  $\alpha_3 = \frac{2^{\frac{r_1 T}{(T-N)B-1}} - 1}{\text{SNR}_3}$ , and  $\alpha_4 = \frac{2^{\frac{r_2 T}{(T-N)B-1}} - 1}{\text{SNR}_4}$ . Note that since  $b \in \{1, 2, 3, 4\}$  is the index of the states with busy channels, we above have, for instance,  $p_{b2} = p_{12} = p_{22} = p_{32} = p_{42}$ .

Now, we can easily see that the  $8 \times 8$  state transition matrix can be expressed as

$$R = \begin{bmatrix} p_{1,1} & \cdot & \cdot & p_{1,8} \\ \cdot & & & \cdot \\ p_{4,1} & \cdot & \cdot & p_{4,8} \\ p_{5,1} & \cdot & \cdot & p_{5,8} \\ \cdot & & & \cdot \\ p_{8,1} & \cdot & \cdot & p_{8,8} \end{bmatrix} = \begin{bmatrix} p_{b1} & \cdot & \cdot & p_{b8} \\ \cdot & & & \cdot \\ p_{b1} & \cdot & \cdot & p_{b8} \\ p_{i1} & \cdot & \cdot & p_{i8} \\ \cdot & & & \cdot \\ p_{i1} & \cdot & \cdot & p_{i8} \end{bmatrix}. \tag{7.40}$$

Note that  $R$  has a rank of 2. Finally, we also note that  $Tr_1$  and  $Tr_2$  bits are transmitted and received in the ON states 1 and 5, and 3 and 7, respectively, while the transmitted number of bits is assumed to be zero in the OFF states (i.e., in states 2, 4, 6, and 8).

## 7.5 Effective Capacity

In this section, we identify the maximum throughput that the cognitive radio channel with the aforementioned state-transition model can sustain under statistical QoS constraints imposed in the form of buffer or delay violation probabilities. Recall that the effective capacity for a given QoS exponent  $\theta$  is given by

$$-\lim_{t \rightarrow \infty} \frac{1}{\theta t} \log_e \mathbb{E}\{e^{-\theta S(t)}\} \triangleq -\frac{\Lambda(-\theta)}{\theta} \quad (7.41)$$

where  $\Lambda(\theta) = \lim_{t \rightarrow \infty} \frac{1}{t} \log_e \mathbb{E}\{e^{\theta S(t)}\}$  is a function that depends on the logarithm of the moment generating function of  $S(t)$ ,  $S(t) = \sum_{k=1}^t r(k)$  is the time-accumulated service process, and  $\{r(k), k = 1, 2, \dots\}$  is defined as the discrete-time, stationary and ergodic stochastic service process. Note that the service rate is  $r(k) = Tr_1$  if the cognitive system is in state 1 or 5 at time  $k$ . Similarly, the service rate is  $r(k) = Tr_2$  in states 3 and 7. In all the OFF states, fixed transmission rates exceed the instantaneous achievable rates, and outage occurs. Therefore, the service rates in these states are effectively zero.

In the next result, we provide the effective capacity for the cognitive radio channel and state transition model described in the previous section.

**Theorem 7** For the cognitive radio channel with the state transition model given in Section 7.4, the normalized effective capacity in bits/s/Hz is given by

$$\begin{aligned}
R_E(\text{SNR}, \theta) = & \max_{\substack{r_1, r_2 \geq 0 \\ \mathbf{P}_1 \leq \mathbf{P}_{peak} \text{ and } \mathbf{P}_2 \leq \mathbf{P}_{peak} \\ P_d \bar{P}_1 + (1 - P_d) \bar{P}_2 \leq \bar{P}_{avg}}} -\frac{1}{\theta T B} \log_e \\
& \frac{1}{2} \left[ (p_{b1} + p_{i5})e^{-\theta T r_1} + (p_{b3} + p_{i7})e^{-\theta T r_2} + p_{b2} + p_{b4} + p_{i6} + p_{i8} \right] \\
& + \frac{1}{2} \left\{ \left[ (p_{b1} - p_{i5})e^{-\theta T r_1} + (p_{b3} - p_{i7})e^{-\theta T r_2} + p_{b2} + p_{b4} - p_{i6} - p_{i8} \right]^2 \right. \\
& \left. + 4 \left( p_{i1}e^{-\theta T r_1} + p_{i3}e^{-\theta T r_2} + p_{i2} + p_{i4} \right) \left( p_{b5}e^{-\theta T r_1} + p_{b7}e^{-\theta T r_2} + p_{b6} + p_{b8} \right) \right\}^{\frac{1}{2}}
\end{aligned} \tag{7.42}$$

where  $T$  is the frame duration over which the fading stays constant,  $r_1$  and  $r_2$  are fixed transmission rates, and  $p_{bk}$  and  $p_{ik}$  for  $k = 1, \dots, 8$ ,  $b = 1, 2, 3, 4$ , and  $i = 5, 6, 7, 8$  are the transition probabilities expressed in (7.38) and (7.39).

*Proof:* See Appendix G. □

## 7.6 Numerical Results

In this section, we present the numerical results. In our simulations, we assume that the fading coefficients are zero-mean Gaussian random variables with unit variance,  $\sigma_h^2 = 1$ . Note also that in all of the simulations we assume  $T = 0.1$  seconds,  $N = 0.01$  seconds,  $B = 1000$  Hz,  $\sigma_n^2 = 1$ ,  $\sigma_s^2 = 1$ ,  $\theta = 0.1$ ,  $a = 0.9$ ,  $b = 0.1$ , and  $\eta = 0.1$ . Unless stated otherwise, we assume in the numerical results that mismatch MMSE with estimates given in (7.12) – (7.15) is employed in the training phase. Moreover, we set  $\mathbf{P}_{peak} = 10$  dB.

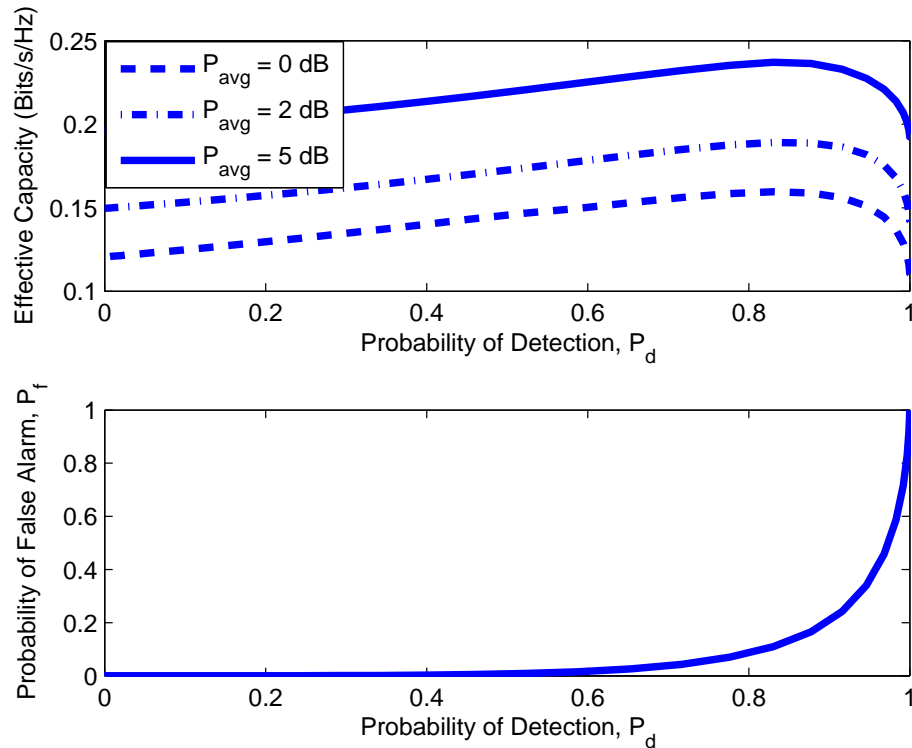


Figure 7.3: Upper Figure: Effective capacity vs. detection probability  $P_d$  for different values of  $\bar{P}_{avg}$ . Lower Figure: False alarm probability  $P_f$  vs.  $P_d$ .

In Figure 7.3, we display the optimal effective capacity as a function of the probability of detection,  $P_d$ , for different values of  $\bar{P}_{avg}$ . As expected, with increasing  $\bar{P}_{avg}$ , the effective capacity value increases. Note also that probability of false alarm  $P_f$  is displayed in the second half of Fig. 7.3. It is clear that the maximum effective capacity values are obtained when  $P_d$  is close to 0.9. As  $P_d$  further increases and approaches 1, we notice in the lower plot in Fig. 7.3 that false-alarm probability increases to 1 as well. Hence, the SUs start to regard the channel busy all the time and performance degradations are experienced because of not being able to take advantage of idle channel states. In Fig. 7.4, the optimal values of  $\bar{P}_1$  and  $\bar{P}_2$  for different values of  $\bar{P}_{avg}$  are displayed again as a function of  $P_d$ . Recall

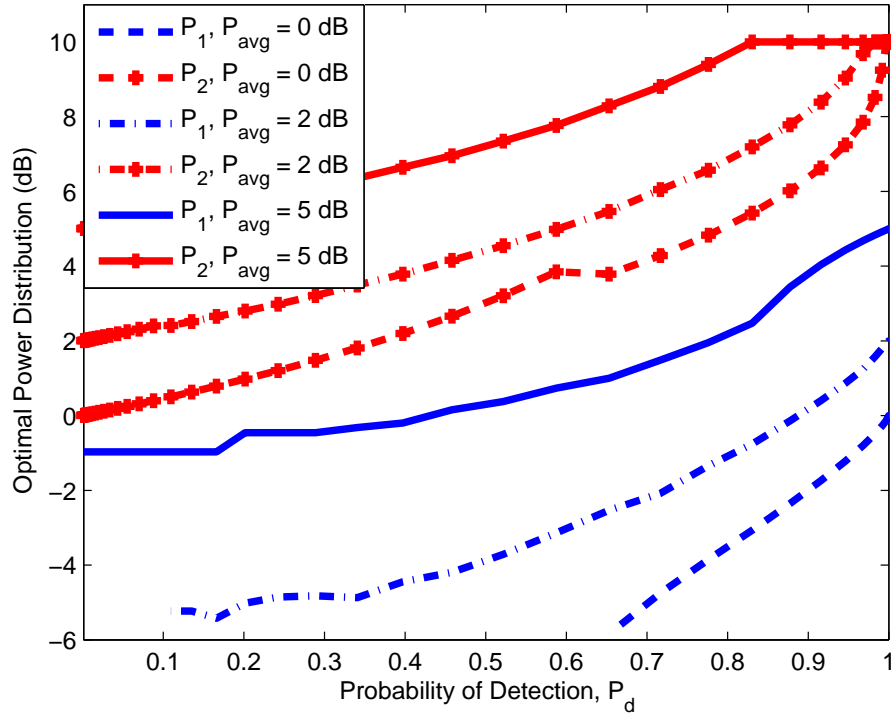


Figure 7.4: Optimal values of  $\bar{P}_1$  and  $\bar{P}_2$  vs. detection probability  $P_d$  for different values of  $\bar{P}_{avg}$ .

that  $\bar{P}_1$  and  $\bar{P}_2$  are the transmission power levels when the channel is sensed as busy and idle, respectively. First, we note that generally the power levels increase with increasing detection probability values. Also, we see in the figure that  $\bar{P}_2$  is generally larger than  $\bar{P}_1$ . Hence, more power is allocated to cases in which the channel is detected as idle. As  $P_d$  increases, we note from (7.10) that the constraint on  $\bar{P}_2$  relaxes since  $\bar{P}_2$  is multiplied by a smaller weight  $(1 - P_d)$ . Consequently,  $\bar{P}_2$  increases. Indeed, as  $P_d \rightarrow 1$ , the only constraint on  $\mathbf{P}_2$  is  $\mathbf{P}_2 \leq \mathbf{P}_{peak} = 10$  dB. Hence, the optimal value is  $\mathbf{P}_2 = \mathbf{P}_{peak}$ , and we actually observe in the figure that all  $\mathbf{P}_2$  curves converge to 10 dB as  $P_d$  approaches 1. On the other hand, as  $P_d \rightarrow 1$ , (7.10) becomes  $\mathbf{P}_1 \leq \mathbf{P}_{avg}$ . Since  $\mathbf{P}_{avg} < \mathbf{P}_{peak} = 10$  dB, the only active constraint



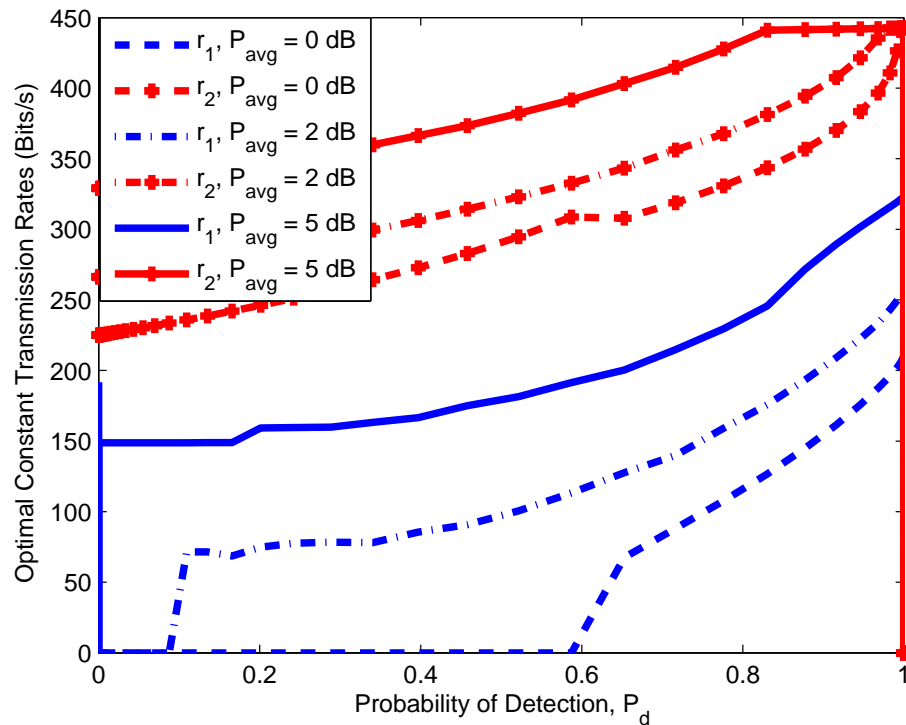


Figure 7.5: Optimal values of  $r_1$  and  $r_2$  vs. detection probability  $P_d$  for different values of  $\bar{P}_{avg}$ .

on  $\mathbf{P}_1$  is  $\mathbf{P}_1 \leq \mathbf{P}_{avg}$  and it is noted in the figure that  $\mathbf{P}_1$  approaches the optimal value  $\mathbf{P}_{avg}$  as  $P_d$  increases to 1. On the other hand, we interestingly observe that for relatively low values of  $\mathbf{P}_{avg}$  (e.g.,  $\mathbf{P}_{avg} = 0, 2$  dB), we have  $\mathbf{P}_1 = 0$  if  $P_d$  is below a certain threshold. Hence, no transmission is performed when the channel is sensed as busy. As  $P_d$  further decreases and approaches 0, the SUs always miss the primary user activities, and (7.10) becomes  $\mathbf{P}_2 \leq \mathbf{P}_{avg}$ , which is, similarly as discussed above, is the only active constraint for  $\mathbf{P}_2$ . Indeed,  $\mathbf{P}_2$  curves approach the corresponding  $\mathbf{P}_{avg}$  values as  $P_d \rightarrow 0$ .

In Fig. 7.5, we show the optimal fixed transmission rates  $r_1$  and  $r_2$  as a function of  $P_d$  for different values of  $\bar{P}_{avg}$ . Note that the optimal transmission rates are

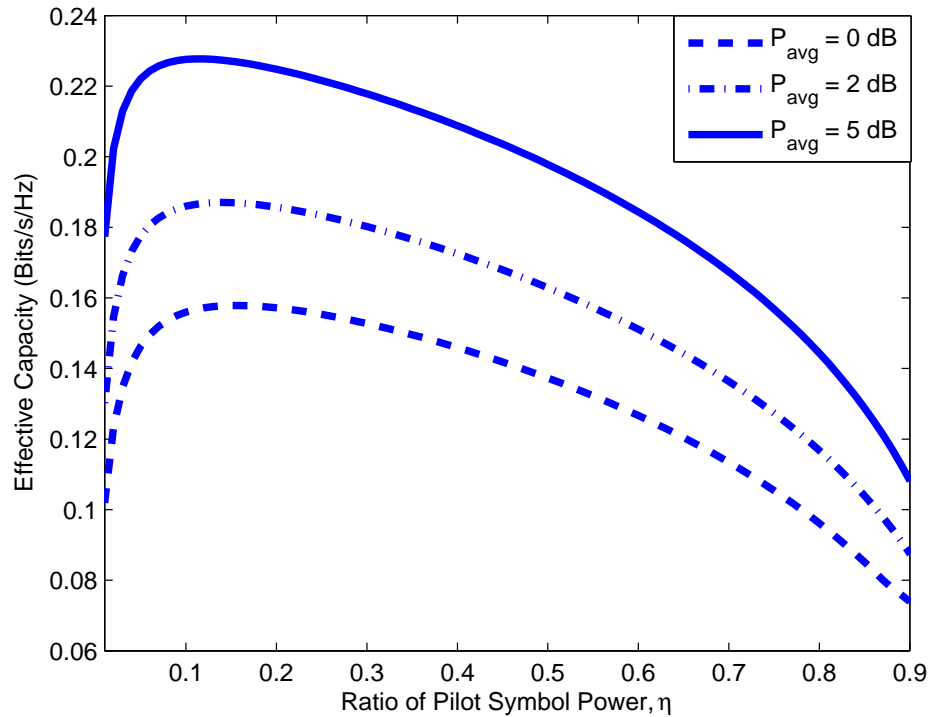


Figure 7.6: Effective capacity vs.  $\eta$ , the fraction of total power allocated to the pilot symbol, for different values of  $\bar{P}_{avg}$ .

obtained at optimal power levels. We observe that  $r_2$ , the transmission rate when the channel is detected as idle, is larger than  $r_1$ . In general, we note similar trends as in Fig. 7.4.

In Fig. 7.6, we plot the effective rate as a function of  $\eta$ , the fraction of the total power allocated to the pilot symbol. We again consider three different average power levels. When the average power levels are 0, 2, and 5 dB, the optimal fractions are  $\eta = 0.16, 0.14$ , and  $0.11$ , respectively. In this figure, we have  $P_d = 0.92$  and  $P_f = 0.24$ . Hence, these are the optimal training power levels in the presence of channel sensing errors. In Fig. 7.7, the optimal transmission rates are plotted as a function of  $\eta$ . It is observed that at all average power levels, the optimal

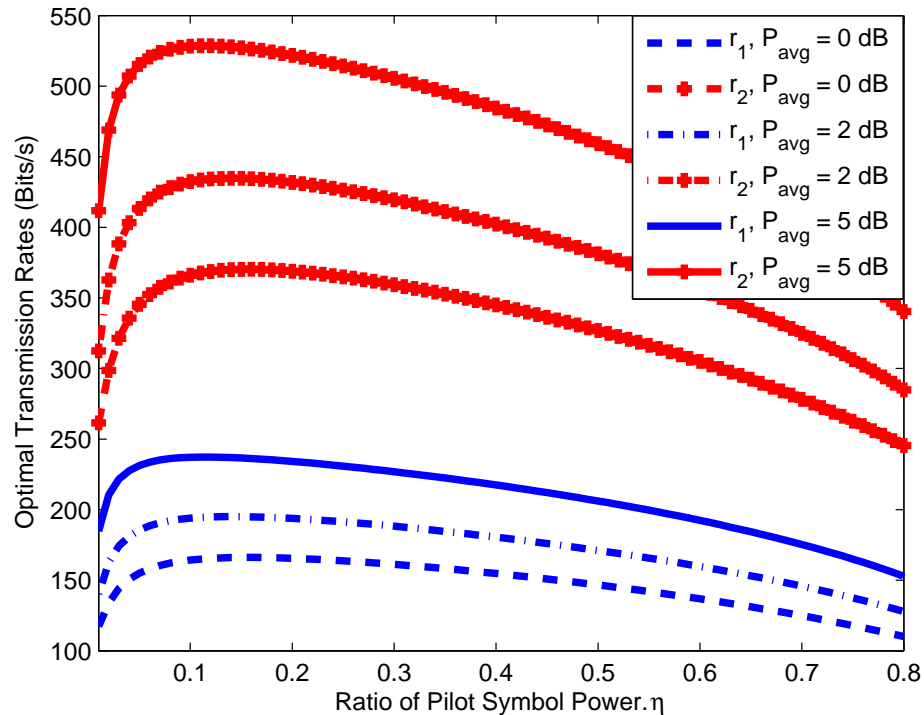


Figure 7.7: Optimal values of  $r_1$  and  $r_2$  vs.  $\eta$ , the fraction of total power allocated to the pilot symbol, for different values of  $P_{avg}$ .

transmission rate when the channel is sensed to be idle, i.e.,  $r_2$ , is higher than the optimal transmission rate when the channel is detected as busy, i.e.,  $r_1$ . In Fig. 7.8,  $P_1$  and  $P_2$  are plotted as a function of  $\eta$ . It is observed that  $P_2$  is higher than  $P_1$  at all average power levels and for all values of  $\eta$ . Note that the optimal power distributions are obtained for constant  $P_d$  and  $P_f$ . Finally, we plot in Fig. 7.9  $\eta$  vs.  $P_d$ , and observe that the fraction of power allocated to training increases with increasing  $P_d$ .

Heretofore in the numerical results, we have assumed that mismatched MMSE is employed at the receiver. In Figures 7.10 and 7.11, we compare the effective capacity values obtained using mismatched MMSE and linear MMSE techniques.

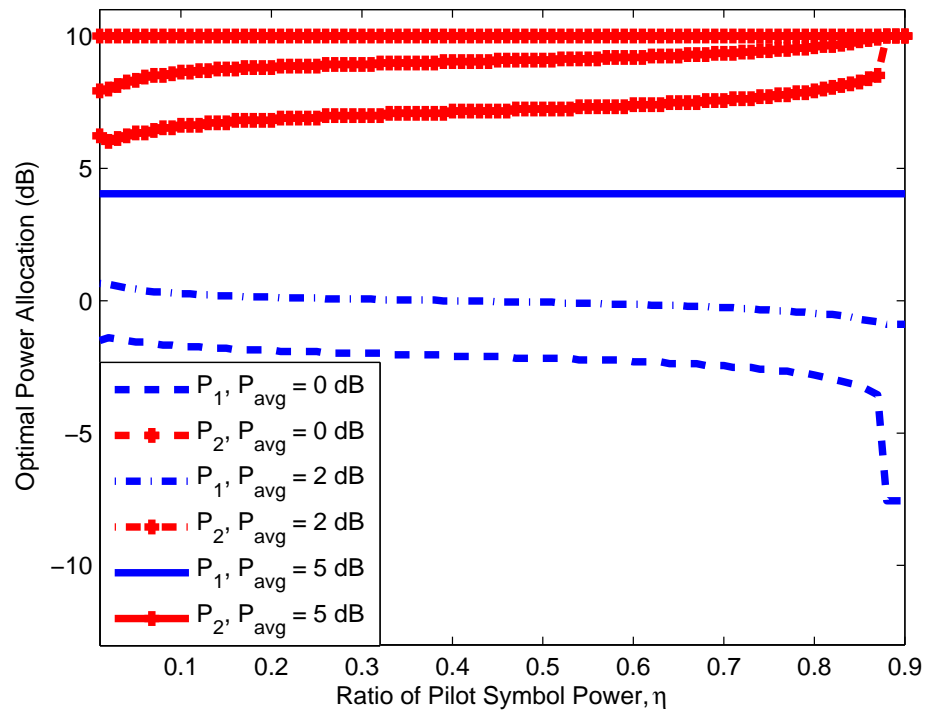


Figure 7.8: Optimal values of  $\bar{P}_1$  and  $\bar{P}_2$  vs.  $\eta$ , the fraction of total power allocated to the pilot symbol, for different values of  $\bar{P}_{avg}$ .

In Fig. 7.10, we plot the effective capacity vs.  $\bar{P}_{avg}$  curve. We notice that linear MMSE provides a slightly better performance for low  $\bar{P}_{avg}$ . The performance gap vanishes as  $\bar{P}_{avg}$  increases. In Fig. 7.11, a similar conclusion is also reached. In this figure, we also observe that linear MMSE provides gains especially when the detection probability  $P_d$  is high. Note that this is another interesting observation indicating the strong interactions between channel sensing and channel estimation.

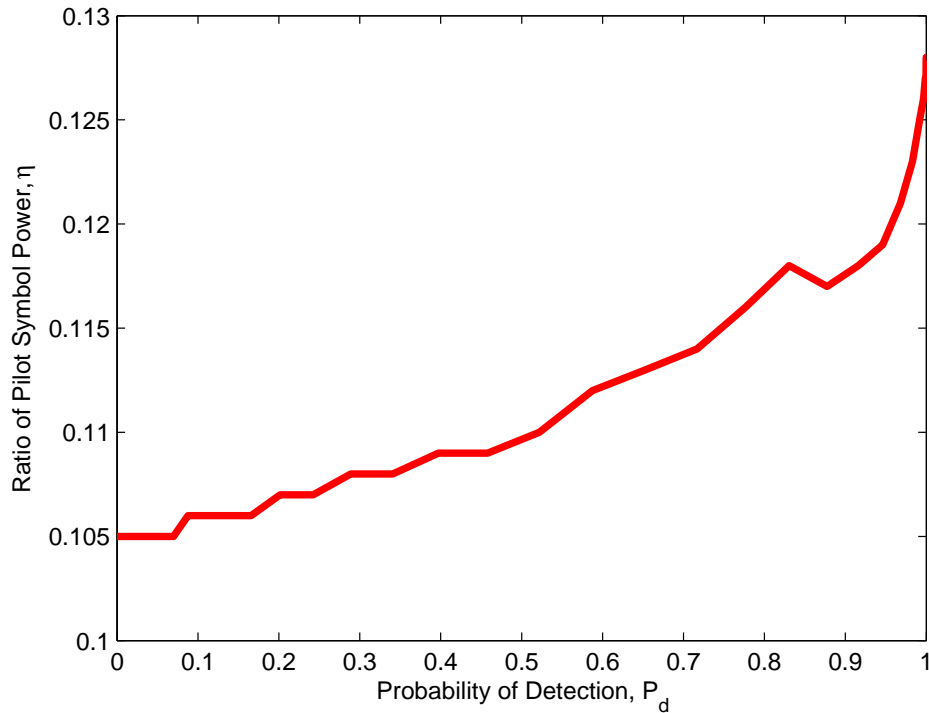


Figure 7.9:  $\eta$ , the fraction of total power allocated to the pilot symbol, vs detection probability  $P_d$ .  $P_{avg} = 5$  dB.

## 7.7 Conclusion

In this chapter, we have analyzed the effective capacity of cognitive radio channels in the presence of QoS constraints, channel uncertainty, and transmission power limitations. We have considered a system model in which the cognitive SUs initially perform channel sensing and estimation, and subsequently transmit data. Channel sensing is done through energy detection and is formulated as a hypothesis testing problem. We have considered different estimation techniques, namely, mismatched MMSE, linear MMSE, and MMSE, in the training phase. In this setting, we have identified the interactions between channel sensing and estimation. In particular, we have noted that sensing errors lead to degradations

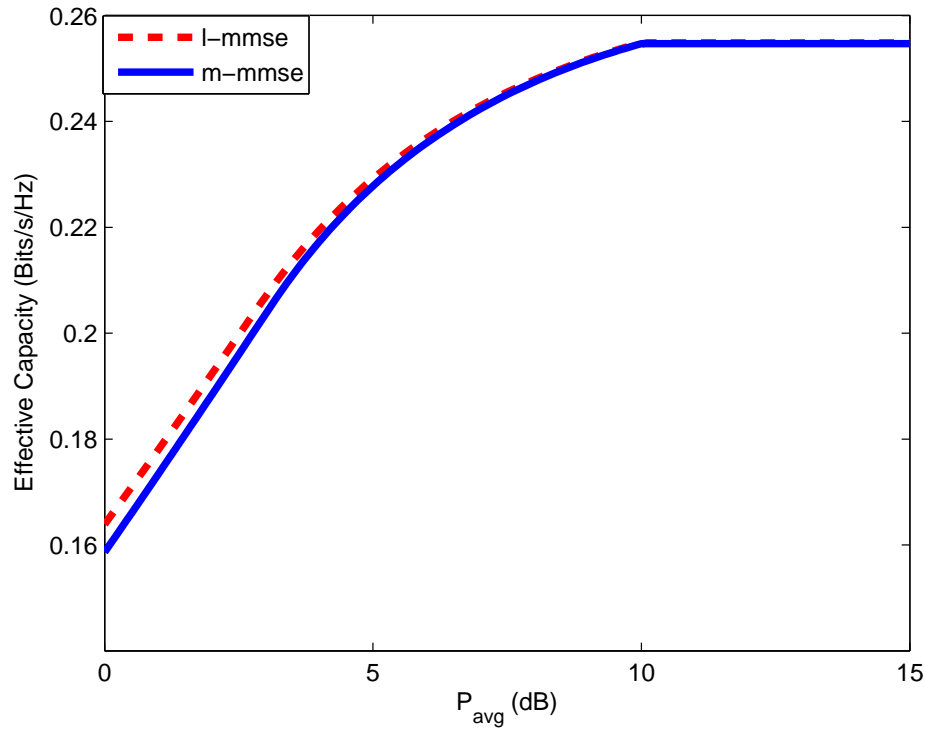


Figure 7.10: Effective Capacity vs.  $\bar{P}_{avg}$  when  $m - mmse$  and  $l - mmse$  estimation techniques are employed.

in the estimation results. We have also shown that imperfections in sensing complicate MMSE estimation, and suboptimal techniques such as mismatched and linear MMSE enable tractable analysis.

In the data transmission phase, we have assumed that the transmitter, not being aware of the channel conditions, send the data at fixed power and rate. We have further assumed that these transmission parameters depend on whether the channel is sensed as busy or idle. For this cognitive operation, we have constructed a state-transition model by considering the reliability of the transmissions, channel sensing decisions and their correctness, and the evolution of primary user activity which is modeled as a two-state Markov process. We have

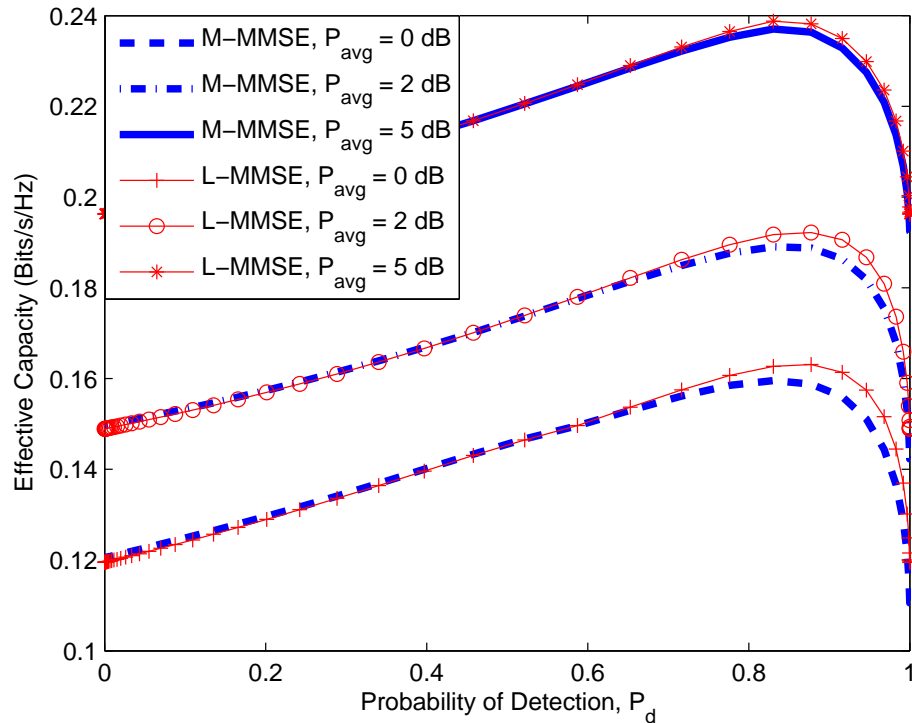


Figure 7.11: Effective capacity vs. detection probability  $P_d$  for different values of  $\bar{P}_{avg}$  when  $m - mmse$  and  $l - mmse$  estimation techniques are employed.

formulated the transition probabilities in this model. Then, for the constructed state-transition model, we have obtained an expression for the effective capacity and identified the maximum throughput in the presence of buffer constraints. We have performed a numerical analysis and shown the impact of several parameters such as detection and false probabilities, average power constraints, training power value, on the performance. We have determined the optimal transmission power and rate levels. We have also compared the performances of linear and mismatched MMSE estimation methods.

## Chapter 8

# On the Transmission Capacity Limits of Cognitive MIMO Channels

In this chapter, throughput of cognitive MIMO systems operating under QoS constraints is studied. It is assumed that transmission power and the covariance of the input signal vector are varied depending on the sensed activities of primary users in the system. Considering the reliability of the transmission and channel sensing results, a state-transition model is provided. Effective capacity is determined, and expressions for the first and second derivatives of the effective capacity are obtained at SNR=0. The minimum bit energy requirements in the presence of QoS limitations are identified.

### 8.1 Channel Model and Power Constraint

We consider a cognitive MIMO channel model and assume that the secondary transmitter and receiver are equipped with  $M$  and  $N$  antennas, respectively. In a



flat fading channel, we can express the channel input-output relation as

$$\mathbf{y} = \mathbf{H}\mathbf{x} + \mathbf{n} + \mathbf{s} \quad (8.1)$$

if the primary users are active in the channel, and as

$$\mathbf{y} = \mathbf{H}\mathbf{x} + \mathbf{n} \quad (8.2)$$

if the primary users are absent. Above,  $\mathbf{x}$  denotes the  $M \times 1$ -dimensional transmitted signal vector, and  $\mathbf{y}$  denotes the  $N \times 1$ -dimensional received signal vector. In (8.1) and (8.2),  $\mathbf{n}$  is an  $N \times 1$ -dimensional zero-mean Gaussian random vector with a covariance matrix  $\mathbb{E}\{\mathbf{n}\mathbf{n}^\dagger\} = \sigma_n^2 \mathbf{I}$  where  $\mathbf{I}$  is the identity matrix. In (8.1),  $\mathbf{s}$  is an  $N \times 1$ -dimensional vector of the sum of active primary users' faded signals arriving at the secondary receiver. Considering that the vector  $\mathbf{s}$  can have correlated components, we express its covariance matrix as  $\mathbb{E}\{\mathbf{s}\mathbf{s}^\dagger\} = N\sigma_s^2 \mathbf{K}_s$  where  $\sigma_s^2$  is the variance of each component of  $\mathbf{s}$  and  $\text{tr}(\mathbf{K}_s) = 1$ . Finally, in (8.1) and (8.2),  $\mathbf{H}$  denotes the  $N \times M$  dimensional random channel matrix whose components are the fading coefficients between the corresponding antennas at the secondary transmitting and receiving ends. We consider a block-fading scenario and assume that the realization of the matrix  $\mathbf{H}$  remains fixed over a block duration of  $T$  seconds and changes independently from one block to another.

We assume that the SUs initially perform channel sensing to detect the activities of primary users, and then depending on the channel sensing results, they choose the transmission strategy. More specifically, if the channel is sensed as busy, the transmitted signal vectors is  $\mathbf{x}_1$ . Otherwise, the signal is  $\mathbf{x}_2$ . In order to control the interference caused to the primary users, the average transmission

power levels can be different. The average energy constraint on the channel input is

$$\mathbb{E}\{\|\mathbf{x}_1\|^2\} \leq \frac{P_1}{B} \quad (8.3)$$

if the channel is sensed as busy. On the other hand, if the channel is detected to be idle, the energy constraint becomes

$$\mathbb{E}\{\|\mathbf{x}_2\|^2\} \leq \frac{P_2}{B}. \quad (8.4)$$

In (8.3) and (8.4),  $B$  is the bandwidth of the system.

Directionality of the transmitted signal vectors might also be different depending on the channel sensing results. We define the normalized input covariance matrix of  $\mathbf{x}_1$

$$\mathbf{K}_{x_1} = \frac{\mathbb{E}\{\mathbf{x}_1\mathbf{x}_1^\dagger\}}{P_1/B} \quad (8.5)$$

if the channel is busy, and  $\mathbf{x}_2$  as

$$\mathbf{K}_{x_2} = \frac{\mathbb{E}\{\mathbf{x}_2\mathbf{x}_2^\dagger\}}{P_2/B} \quad (8.6)$$

if the channel is idle. Note that the trace of normalized covariance matrices are bounded by

$$\text{tr}(\mathbf{K}_{x_1}) \leq 1 \quad (8.7)$$

and

$$\text{tr}(\mathbf{K}_{x_2}) \leq 1. \quad (8.8)$$

We consider a practical scenario in which errors such as miss-detections and false-alarms possibly occur in channel sensing. We denote the correct-detection and false-alarm probabilities by  $P_d$  and  $P_f$ , respectively. We note the following

two cases. When the primary users are active and this activity is sensed correctly (which happens with probability  $P_d$ ), then the SUs transmit with average power  $P_1$ . On the other hand, if the primary user activity is missed in sensing (which occurs with probability  $1 - P_d$ ), the SUs send the information with average power  $P_2$ . In both cases, primary users experience interference. In order to limit the average interference, we impose the following power constraint

$$P_d P_1 + (1 - P_d) P_2 \leq P. \quad (8.9)$$

Now, we define the average SNR as

$$\text{SNR} = \frac{\mathbb{E}\{\|\mathbf{x}\|^2\}}{\mathbb{E}\{\|\mathbf{n}\|^2\}} = \frac{P}{NB\sigma_n^2} \quad (8.10)$$

where  $\mathbb{E}\{\|\mathbf{x}\|^2\} = P_d \mathbb{E}\{\|\mathbf{x}_1\|^2\} + (1 - P_d) \mathbb{E}\{\|\mathbf{x}_2\|^2\}$ . Also, we assume  $P_1 = \mu P$  and  $P_2 = \nu P$  where  $\mu$  and  $\nu$  are some positive numbers, and rewrite (8.9) as

$$P_d \mu P + (1 - P_d) \nu P \leq P, \quad (8.11)$$

and we obtain

$$P_d \mu + (1 - P_d) \nu \leq 1. \quad (8.12)$$

Note that, to maximize the channel throughput, we have to choose optimal  $\mu$  and  $\nu$  values.

## 8.2 State Transition Model and Channel Throughput Metrics

### 8.2.1 State Transition

We assume that both the secondary transmitter and receiver have perfect CSI and hence perfectly know the instantaneous values of  $\{\mathbf{H}\}$  in each transmission block. More specifically, the secondary transmitter sends the information with optimized data vectors. Moreover, depending on channel sensing results and their correctness, we have four scenarios:

1. Channel is busy, detected as busy (correct detection),
2. Channel is busy, detected as idle (miss-detection),
3. Channel is idle, detected as busy (false alarm),
4. Channel is idle, detected as idle (correct detection).

Using the notation  $\mathbb{E}\{(\mathbf{s} + \mathbf{n})(\mathbf{s} + \mathbf{n})^\dagger\} = \mathbb{E}\{\mathbf{s}\mathbf{s}^\dagger\} + \mathbb{E}\{\mathbf{n}\mathbf{n}^\dagger\} = \sigma_n^2 \mathbf{K}_z$  where  $\text{tr}(\mathbf{K}_z) = \frac{N(\sigma_s^2 + \sigma_n^2)}{\sigma_n^2}$ , we can express the instantaneous channel capacities in the above four scenarios as follows:

$$\begin{aligned}
 C_1 &= B \max_{\substack{\mathbf{K}_{x_1} \succeq 0 \\ \text{tr}(\mathbf{K}_{x_1}) \leq 1}} \log_2 \det \left[ \mathbf{I} + \frac{\mu P}{B \sigma_n^2} \mathbf{H} \mathbf{K}_{x_1} \mathbf{H}^\dagger \mathbf{K}_z^{-1} \right] \\
 &= B \max_{\substack{\mathbf{K}_{x_1} \succeq 0 \\ \text{tr}(\mathbf{K}_{x_1}) \leq 1}} \log_2 \det \left[ \mathbf{I} + \mu N \text{SNR} \mathbf{H} \mathbf{K}_{x_1} \mathbf{H}^\dagger \mathbf{K}_z^{-1} \right],
 \end{aligned}$$

$$\begin{aligned}
C_2 &= B \max_{\substack{\mathbf{K}_{x_2} \succeq 0 \\ \text{tr}(\mathbf{K}_{x_2}) \leq 1}} \log_2 \det \left[ \mathbf{I} + \frac{\nu P}{B\sigma_n^2} \mathbf{H} \mathbf{K}_{x_2} \mathbf{H}^\dagger \mathbf{K}_z^{-1} \right] \\
&= B \max_{\substack{\mathbf{K}_{x_2} \succeq 0 \\ \text{tr}(\mathbf{K}_{x_2}) \leq 1}} \log_2 \det \left[ \mathbf{I} + \nu N_{\text{SNR}} \mathbf{H} \mathbf{K}_{x_2} \mathbf{H}^\dagger \mathbf{K}_z^{-1} \right], \\
C_3 &= B \max_{\substack{\mathbf{K}_{x_1} \succeq 0 \\ \text{tr}(\mathbf{K}_{x_1}) \leq 1}} \log_2 \det \left[ \mathbf{I} + \frac{\mu P}{B\sigma_n^2} \mathbf{H} \mathbf{K}_{x_1} \mathbf{H}^\dagger \right] \\
&= B \max_{\substack{\mathbf{K}_{x_1} \succeq 0 \\ \text{tr}(\mathbf{K}_{x_1}) \leq 1}} \log_2 \det \left[ \mathbf{I} + \mu N_{\text{SNR}} \mathbf{H} \mathbf{K}_{x_1} \mathbf{H}^\dagger \right], \\
C_4 &= B \max_{\substack{\mathbf{K}_{x_2} \succeq 0 \\ \text{tr}(\mathbf{K}_{x_2}) \leq 1}} \log_2 \det \left[ \mathbf{I} + \frac{\nu P}{B\sigma_n^2} \mathbf{H} \mathbf{K}_{x_2} \mathbf{H}^\dagger \right] \\
&= B \max_{\substack{\mathbf{K}_{x_2} \succeq 0 \\ \text{tr}(\mathbf{K}_{x_2}) \leq 1}} \log_2 \det \left[ \mathbf{I} + \nu N_{\text{SNR}} \mathbf{H} \mathbf{K}_{x_2} \mathbf{H}^\dagger \right]. \tag{8.13}
\end{aligned}$$

We note that since  $\mathbf{K}_z$  is a positive definite matrix and its eigenvalues are greater than or equal to 1,  $\mathbf{K}_z^{-1}$  is a positive definite matrix with eigenvalues  $1 \geq \lambda_i \geq \frac{\sigma_n^2}{N(\sigma_n^2 + \sigma_s^2)}$ .

The secondary transmitter is assumed to send the data at two different rates depending on the sensing results. If the channel is detected as busy, the transmission rate is

$$r_1 = B \max_{\substack{\mathbf{K}_{x_1} \succeq 0 \\ \text{tr}(\mathbf{K}_{x_1}) \leq 1}} \log_2 \det \left[ \mathbf{I} + \mu N_{\text{SNR}} \mathbf{H} \mathbf{K}_{x_1} \mathbf{H}^\dagger \mathbf{K}_z^{-1} \right], \tag{8.14}$$

and if the channel is detected as idle, the transmission rate is

$$r_2 = B \max_{\substack{\mathbf{K}_{x_2} \succeq 0 \\ \text{tr}(\mathbf{K}_{x_2}) \leq 1}} \log_2 \det \left[ \mathbf{I} + \nu N_{\text{SNR}} \mathbf{H} \mathbf{K}_{x_2} \mathbf{H}^\dagger \right]. \tag{8.15}$$

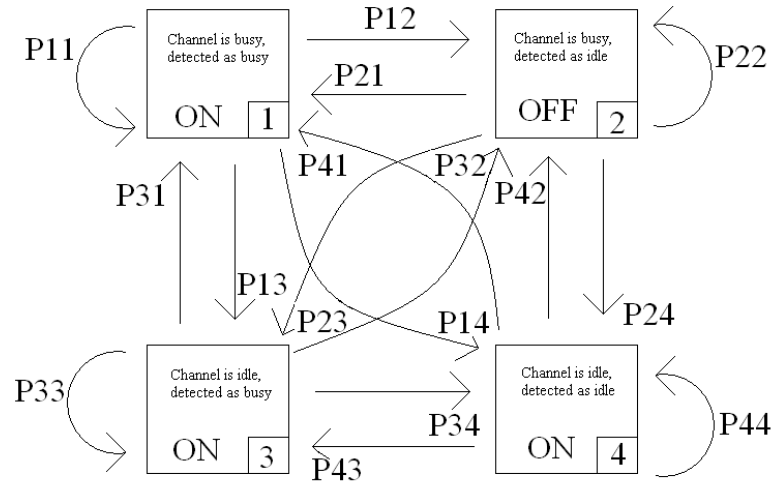


Figure 8.1: State transition model for the cognitive radio channel. The numbered label for each state is given on the bottom-right corner of the box representing the state.

Furthermore, note that in scenarios 1 and 4, transmission occurs at the rate of instantaneous channel capacity, i.e.,  $r_1 = C_1$  in scenario 1 and  $r_2 = C_4$  in scenario 4. In scenario 3, the transmission rate is less than the capacity, i.e.,  $r_1 \leq C_3$ , and in scenario 2, we have the transmission rate exceeding the channel capacity, i.e.,  $r_2 > C_2$ , that is because sensing has not detected the active primary users successfully and their interference on the SUs' signals are not taken into account.

In all scenarios except 2, communication is performed reliably. Hence, the transmission rate is effectively zero, and retransmission is required in Scenario 2. These four scenarios or equivalently states are depicted in Figure 8.1. As described above, the channel is ON in states 1, 3, and 4 and OFF in state 2.

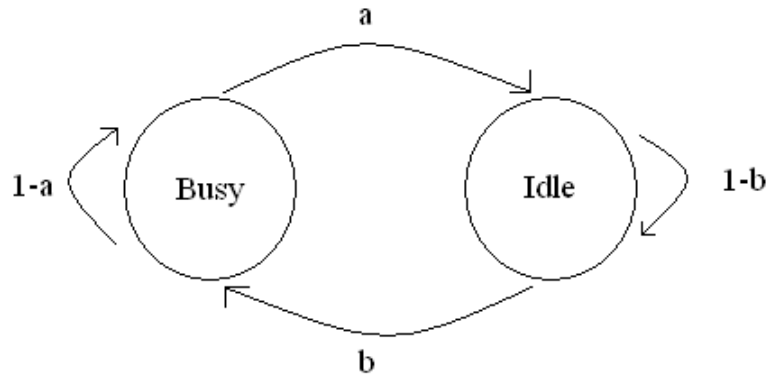


Figure 8.2: Two-state Markov model for the primary user activity.

Next, we determine the state-transition probabilities. We use  $p_{ij}$  to denote the transition probability from state  $i$  to state  $j$  as seen in Fig. 8.1. Due to the block fading assumption, state transitions occur every  $T$  seconds. We also assume that primary user activity does not change within each frame. And, we consider a two-state Markov model to describe the transition of the primary user activity between the frames. This Markov model is depicted in Figure 8.2. Busy state indicates that the channel is occupied by the primary users, and idle state indicates that there is no primary user present in the channel. Probability of transitioning from busy state to idle state is denoted by  $a$ , and the probability of transitioning from idle state to busy state is denoted by  $b$ . Note that, by our assumption, state transitions happen every  $T$  seconds, which is the frame duration. Let us first consider in detail the probability of staying in the topmost ON state in Fig. 8.1.

This probability, denoted by  $p_{11}$ , is given by

$$p_{11} = P \left\{ \begin{array}{l} \text{channel is busy and is detected busy} \\ \text{in the } l^{\text{th}} \text{ frame} \end{array} \middle| \begin{array}{l} \text{channel is busy and is detected busy} \\ \text{in the } (l-1)^{\text{th}} \text{ frame} \end{array} \right\} \quad (8.16)$$

$$\begin{aligned} &= P \left\{ \begin{array}{l} \text{channel is busy} \\ \text{in the } l^{\text{th}} \text{ frame} \end{array} \middle| \begin{array}{l} \text{channel is busy} \\ \text{in the } (l-1)^{\text{th}} \text{ frame} \end{array} \right\} \times P \left\{ \begin{array}{l} \text{channel is detected busy} \\ \text{in the } l^{\text{th}} \text{ frame} \end{array} \middle| \begin{array}{l} \text{channel is busy} \\ \text{in the } l^{\text{th}} \text{ frame} \end{array} \right\} \\ &= (1-a)P_d \end{aligned} \quad (8.17)$$

where  $P_d$  is the probability of detection in channel sensing. Channel being busy in the  $l^{\text{th}}$  frame depends only on channel being busy in the  $(l-1)^{\text{th}}$  frame and not on the other events in the condition. Moreover, since channel sensing is performed individually in each frame without any dependence on the channel sensing decision and primary user activity in the previous frame, channel being detected as busy in the  $l^{\text{th}}$  frame depends only on the event that the channel is actually busy in the  $l^{\text{th}}$  frame.

Similarly, the probabilities for transitioning from any state to state 1 (topmost ON state) can be expressed as

$$p_{b1} = p_{11} = p_{21} = (1-a)P_d \quad \text{and} \quad p_{i1} = p_{31} = p_{41} = bP_d. \quad (8.18)$$

Note that we have common expressions for the transition probabilities in cases in which the originating state has a busy channel (i.e., states 1 and 2) and in cases in which the originating state has an idle channel (i.e., states 3 and 4).

In a similar manner, the remaining transition probabilities are given by the following:

$$\text{For all } b \in \{1, 2\} \text{ and } i \in \{3, 4\},$$



$$\begin{aligned}
p_{b2} &= (1-a)(1-P_d), \quad \text{and} \quad p_{i2} = b(1-P_d), \\
p_{b3} &= aP_f, \quad \text{and} \quad p_{i3} = (1-b)P_f, \\
p_{b4} &= a(1-P_f), \quad \text{and} \quad p_{i4} = (1-b)(1-P_f).
\end{aligned} \tag{8.19}$$

Now, we can easily see that the  $4 \times 4$  state transition matrix can be expressed as

$$R = \begin{pmatrix} p_{11} & \cdot & \cdot & p_{14} \\ p_{21} & \cdot & \cdot & p_{24} \\ p_{31} & \cdot & \cdot & p_{34} \\ p_{41} & \cdot & \cdot & p_{44} \end{pmatrix} = \begin{pmatrix} p_{b1} & \cdot & \cdot & p_{b4} \\ p_{b1} & \cdot & \cdot & p_{b4} \\ p_{i1} & \cdot & \cdot & p_{i4} \\ p_{i1} & \cdot & \cdot & p_{i4} \end{pmatrix}. \tag{8.20}$$

### 8.2.2 Effective Capacity

Recall that the effective capacity for a given QoS exponent  $\theta$  is given by

$$-\lim_{t \rightarrow \infty} \frac{1}{\theta t} \log_e \mathbb{E}\{e^{-\theta S(t)}\} = -\frac{\Lambda(-\theta)}{\theta} \tag{8.21}$$

where  $\Lambda(\theta) = \lim_{t \rightarrow \infty} \frac{1}{t} \log_e \mathbb{E}\{e^{\theta S(t)}\}$  is a function that depends on the logarithm of the moment generating function of  $S(t)$ ,  $S(t) = \sum_{k=1}^t r(k)$  is the time-accumulated service process, and  $\{r(k), k = 1, 2, \dots\}$  is defined as the discrete-time, stationary and ergodic stochastic service process. Note that the service rate in each transmission block is  $r(k) = Tr_1$  if the cognitive system is in Scenario 1 or 3 at time  $k$ . Similarly, the service rate is  $r(k) = Tr_2$  in Scenario 4. In the OFF state in Scenario 2, the service rate is effectively zero.

Considering the effective rates in each scenario and the probabilities of the

scenarios, we can write the following theorem.

**Theorem 8** *For the cognitive radio channel with the aforementioned state transition model, the normalized effective capacity in bits/s/Hz/dimension is given by*

$$\begin{aligned}
C_E(\text{SNR}, \theta) = & \max_{\substack{\mu, \nu \geq 0 \\ P_d \mu + (1 - P_d) \nu \leq 1}} \\
& - \frac{1}{\theta T B N} \log_e \mathbb{E} \left\{ \frac{1}{2} \left[ (p_{b1} + p_{i3}) e^{-\theta T r_1} + p_{i4} e^{-\theta T r_2} + p_{b2} \right] \right. \\
& + \frac{1}{2} \left\{ \left[ (p_{b1} - p_{i3}) e^{-\theta T r_1} - p_{i4} e^{-\theta T r_2} + p_{b2} \right]^2 \right. \\
& \left. \left. + 4 \left( p_{i1} e^{-\theta T r_1} + p_{i2} \right) \left( p_{b3} e^{-\theta T r_1} + p_{b4} e^{-\theta T r_2} \right) \right\}^{1/2} \right\} \quad (8.22)
\end{aligned}$$

where  $T$  is the frame duration over which the fading stays constant,  $r_1$  and  $r_2$  are the transmission rates, and  $\{p_{b1, b2, b3, b4, i1, i2, i3, i4}\}$  are the state transition probabilities.

*Proof:* See Appendix H. □

Note that above we have assumed that  $\mathbf{H}$  and  $\mathbf{K}_z$  are perfectly known at the transmitter. If, on the other hand, only statistical information related to  $\mathbf{H}$  are known at the transmitter, then the input covariance matrix can be chosen to maximize the effective capacity. In that case, the normalized effective capacity will be

expressed as

$$\begin{aligned}
C_E(\text{SNR}, \theta) = & \max_{\substack{\mu, \nu \geq 0 \\ P_d \mu + (1 - P_d) \nu \leq 1}} \max_{\substack{\mathbf{K}_{x_1}, \mathbf{K}_{x_2} \succeq 0 \\ \text{tr}(\mathbf{K}_{x_1}), \text{tr}(\mathbf{K}_{x_2}) \leq 1}} \\
& - \frac{1}{\theta TBN} \log_e \mathbb{E} \left\{ \frac{1}{2} [(p_{b1} + p_{i3}) \Theta_{r_1} + p_{i4} \Theta_{r_2} + p_{b2}] \right. \\
& + \frac{1}{2} \left\{ [(p_{b1} - p_{i3}) \Theta_{r_1} - p_{i4} \Theta_{r_2} + p_{b2}]^2 \right. \\
& \left. \left. + 4(p_{i1} \Theta_{r_1} + p_{i2})(p_{b3} \Theta_{r_1} + p_{b4} \Theta_{r_2}) \right\}^{1/2} \right\} \text{bits/s/Hz/dimension}
\end{aligned} \tag{8.23}$$

where  $\Theta_{r_1} = e^{-\theta TB \log_2 \det[\mathbf{I} + \mu N \text{SNR} \mathbf{H} \mathbf{K}_{x_1} \mathbf{H}^\dagger \mathbf{K}_z^{-1}]}$  and  $\Theta_{r_2} = e^{-\theta TB \log_2 \det[\mathbf{I} + \nu N \text{SNR} \mathbf{H} \mathbf{K}_{x_2} \mathbf{H}^\dagger]}$ .

For given input covariance matrices  $\mathbf{K}_{x_1}$  and  $\mathbf{K}_{x_2}$ , and for given  $\mu$  and  $\nu$ , we express the effective rate as

$$\begin{aligned}
R_E(P_1, P_2, \theta) = & - \frac{1}{\theta TBN} \log_e \mathbb{E} \left\{ \frac{1}{2} [(p_{b1} + p_{i3}) \Theta_{r_1} + p_{i4} \Theta_{r_2} + p_{b2}] \right. \\
& + \frac{1}{2} \left\{ [(p_{b1} - p_{i3}) \Theta_{r_1} - p_{i4} \Theta_{r_2} + p_{b2}]^2 \right. \\
& \left. \left. + 4(p_{i1} \Theta_{r_1} + p_{i2})(p_{b3} \Theta_{r_1} + p_{b4} \Theta_{r_2}) \right\}^{1/2} \right\} \text{bits/s/Hz/dimension.}
\end{aligned} \tag{8.24}$$

### 8.2.3 Ergodic Capacity

As  $\theta$  vanishes, the QoS constraints become loose and it can be easily verified that the effective capacity approaches the ergodic channel capacity, i.e.,

$$\lim_{\theta \rightarrow 0} C_E(\text{SNR}, \theta) = \frac{1}{N(a+b)} \max_{\substack{\mu, \nu \geq 0 \\ P_d \mu + (1-P_d) \nu \leq 1}} \max_{\substack{\mathbf{K}_{x_1}, \mathbf{K}_{x_2} \succeq 0 \\ \text{tr}(\mathbf{K}_{x_1}), \text{tr}(\mathbf{K}_{x_2}) \leq 1}} \mathbb{E} \left\{ (bP_d + aP_f) \det \left[ \mathbf{I} + \mu N \text{SNR} \mathbf{H} \mathbf{K}_{x_1} \mathbf{H}^\dagger \mathbf{K}_z^{-1} \right] + a(1 - P_f) \det \left[ \mathbf{I} + \nu N \text{SNR} \mathbf{H} \mathbf{K}_{x_2} \mathbf{H}^\dagger \right] \right\}. \quad (8.25)$$

Note that in the ergodic capacity expression (8.25), the maximum ergodic capacity achieved in Scenario 2 is 0, because the SUs don't know that primary users are active in the channel, and then the maximum capacity aimed can not be realized.

## 8.3 Effective Capacity in the Low-Power Regime

### 8.3.1 First and Second Derivative of the Effective Capacity

In this section, we study the effective capacity in the low-SNR regime and investigate the impact of the QoS constraints. First, we consider the following second-order expansion of the effective capacity under different assumptions on the degree of channel state information:

$$C_E(\text{SNR}, \theta) = \dot{C}_E(0, \theta) \text{SNR} + \ddot{C}_E(0, \theta) \frac{\text{SNR}^2}{2} + o(\text{SNR}^2) \quad (8.26)$$

where  $\dot{C}_E(0, \theta)$  and  $\ddot{C}_E(0, \theta)$  denote the first and second derivatives of the effective capacity with respect to SNR at SNR=0.

We define a new function

$$f(\text{SNR}, \theta) = \frac{1}{2} \left[ (p_{b1} + p_{i3}) e^{-\theta Tr_1} + p_{i4} e^{-\theta Tr_2} + p_{b2} \right] + \frac{1}{2} \times \underbrace{\left\{ \left[ (p_{b1} - p_{i3}) e^{-\theta Tr_1} - p_{i4} e^{-\theta Tr_2} + p_{b2} \right]^2 + 4 (p_{i1} e^{-\theta Tr_1} + p_{i2}) (p_{b3} e^{-\theta Tr_1} + p_{b4} e^{-\theta Tr_2}) \right\}^{1/2}}_{\chi}, \quad (8.27)$$

and we can write the effective rate as

$$R_E(\text{SNR}, \theta) = D \log_e \mathbb{E} [f(\text{SNR}, \theta)] \quad (8.28)$$

where  $D = -\frac{1}{\theta TBN}$ . The derivative of the effective rate will be

$$\dot{R}_E(\text{SNR}, \theta) = \frac{D}{\mathbb{E} [f(\text{SNR}, \theta)]} \mathbb{E} [\dot{f}(\text{SNR}, \theta)] \quad (8.29)$$

where

$$\dot{f}(\text{SNR}, \theta) = -\theta T \alpha(\text{SNR}, \theta) \dot{r}_1 e^{-\theta Tr_1} - \theta T \beta(\text{SNR}, \theta) \dot{r}_2 e^{-\theta Tr_2}, \quad (8.30)$$

and

$$\alpha(\text{SNR}, \theta) = \frac{1}{2} (p_{b1} + p_{i3}) + \frac{(p_{b1} - p_{i3}) [(p_{b1} - p_{i3}) e^{-\theta Tr_1} - p_{i4} e^{-\theta Tr_2} + p_{b2}]}{2\chi} + \frac{p_{i1} (p_{b3} e^{-\theta Tr_1} + p_{b4} e^{-\theta Tr_2}) + p_{b3} (p_{i1} e^{-\theta Tr_1} + p_{i2})}{\chi}$$

and  $\beta(\text{SNR}, \theta) = \frac{1}{2} p_{i4} - \frac{p_{i4} [(p_{b1} - p_{i3}) e^{-\theta Tr_1} - p_{i4} e^{-\theta Tr_2} + p_{b2}]}{2\chi} + \frac{p_{b4} (p_{i1} e^{-\theta Tr_1} + p_{i2})}{\chi}$ . Note that we can write  $r_1$  and  $r_2$  as

$$r_1 = \frac{B}{\log_e 2} \sum_i \log_e [1 + \mu N_{\text{SNR}} \lambda_i(\Phi_1)] \quad (8.31)$$

and

$$r_2 = \frac{B}{\log_e 2} \sum_i \log_e [1 + \nu N \text{SNR} \lambda_i(\Phi_2)] \quad (8.32)$$

where  $\Phi_1 = \mathbf{H}\mathbf{K}_{x_1}\mathbf{H}^\dagger\mathbf{K}_z^{-1}$  and  $\Phi_2 = \mathbf{H}\mathbf{K}_{x_2}\mathbf{H}^\dagger$ , and  $\lambda_i$  is the eigenvalue of the matrices given in the parentheses. Now, we can write the derivatives of  $r_1$  and  $r_2$  as

$$\dot{r}_1 = \frac{B}{\log_e 2} \sum_i \frac{\mu N \lambda_i(\Phi_1)}{1 + \mu N \text{SNR} \lambda_i(\Phi_1)} \quad (8.33)$$

and

$$\dot{r}_2 = \frac{B}{\log_e 2} \sum_i \frac{\nu N \lambda_i(\Phi_2)}{1 + \nu N \text{SNR} \lambda_i(\Phi_2)}. \quad (8.34)$$

Noting that the function  $f(\text{SNR}, \theta)$  evaluated at  $\text{SNR}=0$  is 1, i.e.,  $f(0, \theta) = 1$ , and  $\alpha(0, \theta)$  and  $\beta(0, \theta)$  are constant values which we denote as  $\bar{\alpha}$  and  $\bar{\beta}$ , respectively, we can easily see that the value of the first derivative of the effective rate at  $\text{SNR}=0$  is

$$\dot{R}_E(0, \theta) = \frac{1}{\log_e 2} \mathbb{E} [\bar{\alpha} \mu \text{tr}\{\Phi_1\} + \bar{\beta} \nu \text{tr}\{\Phi_2\}]. \quad (8.35)$$

Note that by definition,  $\mathbf{K}_{x_1}$  and  $\mathbf{K}_{x_2}$  are positive semi-definite Hermitian matrices. As Hermitian matrices,  $\mathbf{K}_{x_1}$  and  $\mathbf{K}_{x_2}$  can be written as follows

$$\mathbf{K}_{x_1} = \mathbf{U}_1 \Lambda_1 \mathbf{U}_1^\dagger = \sum_{i=1}^M \lambda_{1,i} \mathbf{u}_{1,i} \mathbf{u}_{1,i}^\dagger \quad (8.36)$$

and

$$\mathbf{K}_{x_2} = \mathbf{U}_2 \Lambda_2 \mathbf{U}_2^\dagger = \sum_{i=1}^M \lambda_{2,i} \mathbf{u}_{2,i} \mathbf{u}_{2,i}^\dagger \quad (8.37)$$

where  $\mathbf{U}_1$  and  $\mathbf{U}_2$  are the unitary matrices,  $\{\mathbf{u}_{1,i}\}$  and  $\{\mathbf{u}_{2,i}\}$  are the column vectors of  $\mathbf{U}_1$  and  $\mathbf{U}_2$ , respectively.  $\Lambda_1$  and  $\Lambda_2$  are the real diagonal matrices with diagonal components  $\{\lambda_{1,i}\}$  and  $\{\lambda_{2,i}\}$ , respectively. Since  $\mathbf{K}_{x_1}$  and  $\mathbf{K}_{x_2}$  are positive semi-definite, we have  $\lambda_{1,i} \geq 0$  and  $\lambda_{2,i} \geq 0$ . Furthermore, since all the available

energy should be used for transmission, we have  $\mathbf{tr}(\mathbf{K}_{x_1}) = \sum_{i=1}^M \lambda_{1,i} = 1$  and  $\mathbf{tr}(\mathbf{K}_{x_2}) = \sum_{i=1}^M \lambda_{2,i} = 1$ .

Now, we can write

$$\begin{aligned}
\dot{R}_E(0, \theta) &= \frac{1}{\log_e 2} \mathbb{E} \left[ \bar{\alpha} \mu \mathbf{tr}(\mathbf{H} \mathbf{K}_{x_1} \mathbf{H}^\dagger \mathbf{K}_z^{-1}) + \bar{\beta} \nu \mathbf{tr}(\mathbf{H} \mathbf{K}_{x_2} \mathbf{H}^\dagger) \right] \\
&= \frac{1}{\log_e 2} \mathbb{E} \left[ \bar{\alpha} \mu \mathbf{tr}(\mathbf{H} \mathbf{K}_{x_1} \mathbf{H}^\dagger \mathbf{U}_z \Lambda_z \mathbf{U}_z^\dagger) + \bar{\beta} \nu \mathbf{tr}(\mathbf{H} \mathbf{K}_{x_2} \mathbf{H}^\dagger) \right] \\
&= \frac{1}{\log_e 2} \mathbb{E} \left[ \bar{\alpha} \mu \mathbf{tr}(\Lambda_z^{1/2} \mathbf{U}_z^\dagger \mathbf{H} \mathbf{K}_{x_1} \mathbf{H}^\dagger \mathbf{U}_z \Lambda_z^{1/2}) + \bar{\beta} \nu \mathbf{tr}(\mathbf{H} \mathbf{K}_{x_2} \mathbf{H}^\dagger) \right] \\
&= \frac{1}{\log_e 2} \sum_{i=1}^M \left\{ \lambda_{1,i} \bar{\alpha} \mu \mathbb{E} [\mathbf{tr}(\Lambda_z^{1/2} \mathbf{U}_z^\dagger \mathbf{H} \mathbf{u}_{1,i} \mathbf{u}_{1,i}^\dagger \mathbf{H}^\dagger \mathbf{U}_z \Lambda_z^{1/2})] + \lambda_{2,i} \bar{\beta} \nu \mathbb{E} [\mathbf{tr}(\mathbf{H} \mathbf{u}_{2,i} \mathbf{u}_{2,i}^\dagger \mathbf{H}^\dagger)] \right\} \\
&= \frac{1}{\log_e 2} \sum_{i=1}^M \left\{ \lambda_{1,i} \bar{\alpha} \mu \mathbb{E} [\mathbf{tr}(\mathbf{u}_{1,i}^\dagger \mathbf{H}^\dagger \mathbf{U}_z \Lambda_z^{1/2} \Lambda_z^{1/2} \mathbf{U}_z^\dagger \mathbf{H} \mathbf{u}_{1,i})] + \lambda_{2,i} \bar{\beta} \nu \mathbb{E} [\mathbf{tr}(\mathbf{u}_{2,i}^\dagger \mathbf{H}^\dagger \mathbf{H} \mathbf{u}_{2,i})] \right\} \\
&= \frac{1}{\log_e 2} \sum_{i=1}^M \left\{ \lambda_{1,i} \bar{\alpha} \mu \mathbb{E} [\mathbf{tr}(\mathbf{u}_{1,i}^\dagger \mathbf{H}^\dagger \mathbf{K}_z^{-1} \mathbf{H} \mathbf{u}_{1,i})] + \lambda_{2,i} \bar{\beta} \nu \mathbb{E} [\mathbf{tr}(\mathbf{u}_{2,i}^\dagger \mathbf{H}^\dagger \mathbf{H} \mathbf{u}_{2,i})] \right\} \\
&\leq \frac{1}{\log_e 2} \left\{ \bar{\alpha} \mu \mathbb{E} \left[ \lambda_{\max}(\mathbf{H}^\dagger \mathbf{K}_z^{-1} \mathbf{H}) \right] + \bar{\beta} \nu \mathbb{E} \left[ \lambda_{\max}(\mathbf{H}^\dagger \mathbf{H}) \right] \right\} \tag{8.38}
\end{aligned}$$

where  $\lambda_{\max}(\mathbf{H}^\dagger \mathbf{K}_z^{-1} \mathbf{H})$  and  $\lambda_{\max}(\mathbf{H}^\dagger \mathbf{H})$  denote the maximum eigenvalues of the matrices  $\mathbf{H}^\dagger \mathbf{K}_z^{-1} \mathbf{H}$  and  $\mathbf{H}^\dagger \mathbf{H}$ . The upper bound in (8.38) can be achieved by choosing the normalized input covariance matrices as

$$\mathbf{K}_{x_1} = \mathbf{u}_1 \mathbf{u}_1^\dagger \tag{8.39}$$

and

$$\mathbf{K}_{x_2} = \mathbf{u}_2 \mathbf{u}_2^\dagger \tag{8.40}$$

where  $\mathbf{u}_1$  and  $\mathbf{u}_2$  are the unit-norm eigenvectors that correspond to the maximum

eigenvalues  $\lambda_{\max}(\mathbf{H}^\dagger \mathbf{K}_z^{-1} \mathbf{H})$  and  $\lambda_{\max}(\mathbf{H}^\dagger \mathbf{H})$ . This lets us conclude that

$$\dot{C}_E(0, \theta) = \frac{1}{\log_e 2} \left\{ \bar{\alpha} \mu \mathbb{E} \left[ \lambda_{\max}(\mathbf{H}^\dagger \mathbf{K}_z^{-1} \mathbf{H}) \right] + \bar{\beta} \nu \mathbb{E} \left[ \lambda_{\max}(\mathbf{H}^\dagger \mathbf{H}) \right] \right\}. \quad (8.41)$$

It is worth to mention the multiplicities of  $\lambda_{\max}(\mathbf{H}^\dagger \mathbf{K}_z^{-1} \mathbf{H})$  and  $\lambda_{\max}(\mathbf{H}^\dagger \mathbf{H})$  which are  $l_1 \geq 1$  and  $l_2 \geq 1$ , and input-covariance matrices can be given in the following forms:

$$\mathbf{K}_{x_1} = \sum_{i=1}^{l_1} \kappa_{1i} \mathbf{u}_{1,i} \mathbf{u}_{1,i}^\dagger \quad (8.42)$$

and

$$\mathbf{K}_{x_2} = \sum_{i=1}^{l_2} \kappa_{2i} \mathbf{u}_{2,i} \mathbf{u}_{2,i}^\dagger \quad (8.43)$$

where  $\kappa_{1i}, \kappa_{2i} \in [0, 1]$  and  $\sum_{i=1}^{l_1} \kappa_{1i} = 1$  and  $\sum_{i=1}^{l_2} \kappa_{2i} = 1$ , and  $\{\mathbf{u}_{1,i}\}$  and  $\{\mathbf{u}_{2,i}\}$  are the orthonormal eigenvectors that span the maximal-eigenvalue eigenspaces of  $\mathbf{H}^\dagger \mathbf{K}_z^{-1} \mathbf{H}$  and  $\mathbf{H}^\dagger \mathbf{H}$ , respectively. As for the second derivative, we differentiate  $\dot{R}_E(\text{SNR}, \theta)$  in (8.29) with respect to SNR once more. However, mathematically it is tractable, and it is hard to obtain a definite solution. Therefore, we will consider a special case where  $a + b = 1$ . Now, we obtain

$$\ddot{R}_E(\text{SNR}, \theta) = \frac{D}{\mathbb{E} [f(\text{SNR}, \theta)]} \mathbb{E} [\ddot{f}(\text{SNR}, \theta)] - \frac{D}{\mathbb{E}^2 [f(\text{SNR}, \theta)]} \mathbb{E}^2 [\dot{f}(\text{SNR}, \theta)] \quad (8.44)$$

where

$$\dot{f}(\text{SNR}, \theta) = -\theta T(aP_f + bP_d) \dot{r}_1 e^{-\theta \text{Tr}_1} - \theta T a(1 - P_f) \dot{r}_2 e^{-\theta \text{Tr}_2} \quad (8.45)$$



and

$$\begin{aligned} \ddot{f}(\text{SNR}, \theta) = & \theta^2 T^2 (bP_d + aP_f) \dot{r}_1^2 e^{-\theta T r_1} + \theta^2 T^2 a(1 - P_f) \dot{r}_2^2 e^{-\theta T r_2} \\ & - \theta T (bP_d + aP_f) \ddot{r}_1 e^{-\theta T r_1} - \theta T a(1 - P_f) \ddot{r}_2 e^{-\theta T r_2}. \end{aligned} \quad (8.46)$$

Now, we can write the second derivatives of  $r_1$  and  $r_2$  as

$$\ddot{r}_1 = -\frac{B}{\log_e 2} \sum_i \frac{\mu^2 N^2 \lambda_i^2(\Phi_1)}{[1 + \mu N \text{SNR} \lambda_i(\Phi_1)]^2} \quad (8.47)$$

and

$$\ddot{r}_2 = -\frac{B}{\log_e 2} \sum_i \frac{\nu^2 N^2 \lambda_i^2(\Phi_2)}{[1 + \nu N \text{SNR} \lambda_i(\Phi_2)]^2}. \quad (8.48)$$

We can easily see that when SNR goes to 0, we can express the first and second derivatives of  $f(\text{SNR}, \theta)$

$$\dot{f}(0, \theta) = -\frac{(bP_d + aP_f)\theta T B N \mu}{\log_e 2} \text{tr}\{\Phi_1\} - \frac{a(1 - P_f)\theta T B N \nu}{\log_e 2} \text{tr}\{\Phi_2\} \quad (8.49)$$

and

$$\begin{aligned} \ddot{f}(0, \theta) = & \frac{\ell_1 \theta T B N^2 \mu^2}{\log_e 2} \text{tr}\{\Phi_1^\dagger \Phi_1\} + \frac{\ell_2 \theta T B N^2 \nu^2}{\log_e 2} \text{tr}\{\Phi_2^\dagger \Phi_2\} \\ & + \frac{\ell_1 \theta^2 T^2 B^2 N^2 \mu^2}{\log_e^2 2} \text{tr}^2\{\Phi_1\} + \frac{\ell_2 \theta^2 T^2 B^2 N^2 \nu^2}{\log_e^2 2} \text{tr}^2\{\Phi_2\}, \end{aligned} \quad (8.50)$$

and  $\ell_1 = (bP_d + aP_f)$  and  $\ell_2 = a(1 - P_f)$ . We know  $f(0, \theta) = 1$ . Then, we write

$$\ddot{R}(0, \theta) = \frac{1}{\theta T B N} \left\{ \mathbb{E}^2 [\dot{f}(0, \theta)] - \mathbb{E} [\dot{f}(0, \theta)] \right\}. \quad (8.51)$$

We can easily verify that

$$\mathbb{E} \{ \text{tr}(\Phi_1) \} = \mathbb{E} \left\{ \text{tr}(\mathbf{H}\mathbf{K}_{x_1}\mathbf{H}^\dagger\mathbf{K}_z^{-1}) \right\} = \mathbb{E} \left\{ \lambda_{\max}(\mathbf{H}^\dagger\mathbf{K}_z^{-1}\mathbf{H}) \right\} \quad (8.52)$$

$$\mathbb{E} \{ \text{tr}(\Phi_2) \} = \mathbb{E} \left\{ \text{tr}(\mathbf{H}\mathbf{K}_{x_2}\mathbf{H}^\dagger) \right\} = \mathbb{E} \left\{ \lambda_{\max}(\mathbf{H}^\dagger\mathbf{H}) \right\} \quad (8.53)$$

and

$$\begin{aligned} \mathbb{E} \left\{ \text{tr}(\Phi_1^\dagger\Phi_1) \right\} &= \mathbb{E} \left\{ \text{tr}(\mathbf{K}_z^{-1}\mathbf{H}\mathbf{K}_{x_1}\mathbf{H}^\dagger\mathbf{H}\mathbf{K}_{x_1}\mathbf{H}^\dagger\mathbf{K}_z^{-1}) \right\} \\ &= \mathbb{E} \left\{ \text{tr}(\mathbf{K}_z^{-1}\mathbf{K}_z^{-1}\mathbf{H}\mathbf{K}_{x_1}\mathbf{H}^\dagger\mathbf{H}\mathbf{K}_{x_1}\mathbf{H}^\dagger) \right\} \end{aligned} \quad (8.54)$$

$$\geq \mathbb{E} \left\{ \text{tr}(\mathbf{K}_z^{-1}\mathbf{H}\mathbf{K}_{x_1}\mathbf{H}^\dagger\mathbf{K}_z^{-1}\mathbf{H}\mathbf{K}_{x_1}\mathbf{H}^\dagger) \right\} \quad (8.55)$$

$$= \mathbb{E} \left\{ \sum_{i,j}^{l_1} \kappa_{1i}\kappa_{1j} \text{tr}(\mathbf{K}_z^{-1}\mathbf{H}\mathbf{u}_i\mathbf{u}_i^\dagger\mathbf{H}^\dagger\mathbf{K}_z^{-1}\mathbf{H}\mathbf{u}_j\mathbf{u}_j^\dagger\mathbf{H}^\dagger) \right\} \quad (8.56)$$

$$= \mathbb{E} \left\{ \sum_i^{l_1} \kappa_{1i}^2 \text{tr}(\mathbf{K}_z^{-1}\mathbf{H}\mathbf{u}_i\mathbf{u}_i^\dagger\mathbf{H}^\dagger\mathbf{K}_z^{-1}\mathbf{H}\mathbf{u}_i\mathbf{u}_i^\dagger\mathbf{H}^\dagger) \right\} \quad (8.57)$$

$$= \mathbb{E} \left\{ \sum_i^{l_1} \kappa_{1i}^2 \lambda_{\max}(\mathbf{H}^\dagger\mathbf{K}_z^{-1}\mathbf{H}) \text{tr}(\mathbf{K}_z^{-1}\mathbf{H}\mathbf{u}_i\mathbf{u}_i^\dagger\mathbf{H}^\dagger) \right\} \quad (8.58)$$

$$= \mathbb{E} \left\{ \sum_i^{l_1} \kappa_{1i}^2 \lambda_{\max}(\mathbf{H}^\dagger\mathbf{K}_z^{-1}\mathbf{H}) \text{tr}(\mathbf{u}_i^\dagger\mathbf{H}^\dagger\mathbf{K}_z^{-1}\mathbf{H}\mathbf{u}_i) \right\} \quad (8.59)$$

$$= \mathbb{E} \left\{ \sum_i^{l_1} \kappa_{1i}^2 \lambda_{\max}^2(\mathbf{H}^\dagger\mathbf{K}_z^{-1}\mathbf{H}) \right\} \quad (8.60)$$

$$= \mathbb{E} \left\{ \lambda_{\max}^2(\mathbf{H}^\dagger\mathbf{K}_z^{-1}\mathbf{H}) \sum_i^{l_1} \kappa_{1i}^2 \right\} \quad (8.61)$$

$$\geq \frac{1}{l_1} \mathbb{E} \left\{ \lambda_{\max}^2(\mathbf{H}^\dagger\mathbf{K}_z^{-1}\mathbf{H}) \right\} \quad (8.62)$$

where (8.55) comes from the fact that if  $A, B \in M_n$  are Hermitian,  $\text{tr}(AB)^2 \leq \text{tr}(A^2B^2)$  [38, Chap. 4, Problem 4.1.11]. (8.56) and (8.57) follow from the fact that  $\{\mathbf{u}_{1i}\}$  are the eigenvectors that correspond to  $\lambda_{\max}(\mathbf{H}^\dagger\mathbf{K}_z^{-1}\mathbf{H})$  and hence

$\mathbf{u}_{1,i}^\dagger \mathbf{H}^\dagger \mathbf{K}_z^{-1} \mathbf{H} \mathbf{u}_{1,j} = 0$  if  $i \neq j$ , which comes from the orthonormality of  $\{\mathbf{u}_{1,i}\}$ . Finally, (8.62) follows from the properties that  $\kappa_{1i} \in [0, 1]$  and  $\sum_{i=1}^{l_1} \kappa_{1i} = 1$ , and the fact that  $\sum_{i=1}^{l_1} \kappa_{1i}^2$  is minimized by choosing  $\kappa_{1i} = \frac{1}{l_1}$ , that leads us to the lower bound  $\sum_{i=1}^{l_1} \kappa_{1i}^2 \geq \frac{1}{l_1}$ . Same procedure can be applied to  $\mathbb{E} \{ \text{tr}(\Phi_2^\dagger \Phi_2) \}$ , and we can easily see that

$$\begin{aligned} \mathbb{E} \{ \text{tr}(\Phi_2^\dagger \Phi_2) \} &= \mathbb{E} \{ \text{tr}(\mathbf{H} \mathbf{K}_{x_1} \mathbf{H}^\dagger \mathbf{H} \mathbf{K}_{x_1} \mathbf{H}^\dagger) \} \\ &= \mathbb{E} \left\{ \sum_{i,j}^{l_2} \kappa_{2,i} \kappa_{2,j} \text{tr}(\mathbf{H} \mathbf{u}_{2,i} \mathbf{u}_{2,i}^\dagger \mathbf{H}^\dagger \mathbf{H} \mathbf{u}_{2,j} \mathbf{u}_{2,j}^\dagger \mathbf{H}^\dagger) \right\} \end{aligned} \quad (8.63)$$

$$= \mathbb{E} \left\{ \sum_i^{l_2} \kappa_{2,i}^2 \text{tr}(\mathbf{H} \mathbf{u}_{2,i} \mathbf{u}_{2,i}^\dagger \mathbf{H}^\dagger \mathbf{H} \mathbf{u}_{2,i} \mathbf{u}_{2,i}^\dagger \mathbf{H}^\dagger) \right\} \quad (8.64)$$

$$= \mathbb{E} \left\{ \sum_i^{l_2} \kappa_{2,i}^2 \lambda_{\max}(\mathbf{H}^\dagger \mathbf{H}) \text{tr}(\mathbf{H} \mathbf{u}_{2,i} \mathbf{u}_{2,i}^\dagger \mathbf{H}^\dagger) \right\} \quad (8.65)$$

$$= \mathbb{E} \left\{ \sum_i^{l_2} \kappa_{2,i}^2 \lambda_{\max}(\mathbf{H}^\dagger \mathbf{H}) \text{tr}(\mathbf{u}_{2,i}^\dagger \mathbf{H}^\dagger \mathbf{H} \mathbf{u}_{2,i}) \right\} \quad (8.66)$$

$$= \mathbb{E} \left\{ \sum_i^{l_2} \kappa_{2,i}^2 \lambda_{\max}^2(\mathbf{H}^\dagger \mathbf{H}) \right\} \quad (8.67)$$

$$= \mathbb{E} \left\{ \lambda_{\max}^2(\mathbf{H}^\dagger \mathbf{H}) \sum_i^{l_2} \kappa_{2,i}^2 \right\} \quad (8.68)$$

$$\geq \frac{1}{l_2} \mathbb{E} \left\{ \lambda_{\max}^2(\mathbf{H}^\dagger \mathbf{H}) \right\} \quad (8.69)$$

Now, we can write the second derivative of effective rate as

$$\begin{aligned} \ddot{R}_E(0, \theta) &= \frac{1}{\theta TBN} \left\{ \mathbb{E}^2 \left[ \frac{\ell_1 \theta TBN \mu}{\log_e 2} \mathbf{tr}(\Phi_1) + \frac{\ell_2 \theta TBN \nu}{\log_e 2} \mathbf{tr}(\Phi_2) \right] \right. \\ &\quad - \mathbb{E} \left[ \frac{\ell_1 \theta^2 T^2 B^2 N^2 \mu^2}{\log_e^2 2} \mathbf{tr}^2(\Phi_1) + \frac{\ell_2 \theta^2 T^2 B^2 N^2 \nu^2}{\log_e^2 2} \mathbf{tr}^2(\Phi_2) \right] \\ &\quad \left. - \mathbb{E} \left[ \frac{\ell_1 \theta TBN^2 \mu^2}{\log_e 2} \mathbf{tr}(\Phi_1^\dagger \Phi_1) + \frac{\ell_2 \theta TBN^2 \nu^2}{\log_e 2} \mathbf{tr}(\Phi_2^\dagger \Phi_2) \right] \right\} \end{aligned} \quad (8.70)$$

$$\begin{aligned} &= \frac{\theta TBN}{\log_e^2 2} \mathbb{E}^2 [ \ell_1 \mu \mathbf{tr}(\Phi_1) + \ell_2 \nu \mathbf{tr}(\Phi_2) ] \\ &\quad - \frac{\theta TBN}{\log_e^2 2} \mathbb{E} [ \ell_1 \mu^2 \mathbf{tr}^2(\Phi_1) + \ell_2 \nu^2 \mathbf{tr}^2(\Phi_2) ] \\ &\quad - \frac{N}{\log_e 2} \mathbb{E} [ \ell_1 \mu^2 \mathbf{tr}(\Phi_1^\dagger \Phi_1) + \ell_2 \nu^2 \mathbf{tr}(\Phi_2^\dagger \Phi_2) ] \end{aligned} \quad (8.71)$$

$$\begin{aligned} &\leq \frac{\theta TBN}{\log_e^2 2} \mathbb{E}^2 [ \ell_1 \mu \lambda_{\max}(\mathbf{H}^\dagger \mathbf{K}_z^{-1} \mathbf{H}) + \ell_2 \nu \lambda_{\max}(\mathbf{H}^\dagger \mathbf{H}) ] \\ &\quad - \frac{\theta TBN}{\log_e^2 2} \mathbb{E} [ \ell_1 \mu^2 \lambda_{\max}^2(\mathbf{H}^\dagger \mathbf{K}_z^{-1} \mathbf{H}) + \ell_2 \nu^2 \lambda_{\max}^2(\mathbf{H}^\dagger \mathbf{H}) ] \\ &\quad - \frac{N}{\log_e 2} \mathbb{E} \left[ \frac{\ell_1 \mu^2 \lambda_{\max}^2(\mathbf{H}^\dagger \mathbf{K}_z^{-1} \mathbf{H})}{l_1} + \frac{\ell_2 \nu^2 \lambda_{\max}^2(\mathbf{H}^\dagger \mathbf{H})}{l_2} \right] = \ddot{C}_E(0, \theta) \end{aligned} \quad (8.72)$$

### 8.3.2 Energy Efficiency in the Low-Power Regime

Now, we can analyze the energy efficiency in the low-power regime using the expressions for the first and second derivatives. The minimum bit energy under QoS constraints is given by [81]

$$\frac{E_b}{N_{0_{min}}} = \lim_{\text{SNR} \rightarrow 0} \frac{\text{SNR}}{C_E(\text{SNR})} = \frac{1}{\dot{C}_E(0)}. \quad (8.73)$$

At  $\frac{E_b}{N_{0min}}$ , the slope  $\mathcal{S}_0$  of the spectral efficiency versus  $E_b/N_0$  (in dB) curve is defined as [81]

$$\mathcal{S}_0 \lim_{\frac{E_b}{N_0} \downarrow \frac{E_b}{N_{0min}}} \frac{C_E \left( \frac{E_b}{N_0} \right)}{10 \log_{10} \frac{E_b}{N_0} - 10 \log_{10} \frac{E_b}{N_{0min}}} 10 \log_{10} 2. \quad (8.74)$$

Considering the expression for normalized effective capacity, the wideband slope can be found from [81]

$$\mathcal{S}_0 = \frac{2 [\dot{C}_E(0)]^2}{-\ddot{C}_E(0)} \log_e 2 \quad \text{bits/s/Hz/(3 dB)/receive antenna.} \quad (8.75)$$

Applying the results (8.41) and (8.72) to the above formulation, we obtain

$$\frac{E_b}{N_{0min}} = \frac{\log_e 2}{\ell_1 \mu \mathbb{E} [\lambda_{max}(\mathbf{H}^\dagger \mathbf{K}_z^{-1} \mathbf{H})] + \ell_2 \nu \mathbb{E} [\lambda_{max}(\mathbf{H}^\dagger \mathbf{H})]} \quad (8.76)$$

$$\mathcal{S}_0 = \frac{2\mathbb{E}^2 [\ell_1 \mu \alpha + \ell_2 \nu \beta]}{\theta TBN \{ \mathbb{E} [\ell_1 \mu^2 \alpha^2 + \ell_2 \nu^2 \beta^2] - \mathbb{E}^2 [\ell_1 \mu \alpha + \ell_2 \nu \beta] \} + N \mathbb{E} \left[ \frac{\ell_1 \mu^2 \alpha^2}{l_1} + \frac{\ell_2 \nu^2 \beta^2}{l_2} \right]} \log_e 2 \quad (8.77)$$

where  $\alpha = \lambda_{max}(\mathbf{H}^\dagger \mathbf{K}_z^{-1} \mathbf{H})$  and  $\beta = \lambda_{max}(\mathbf{H}^\dagger \mathbf{H})$ .

When we have equal power allocation, i.e.,  $\mathbf{K}_x = \frac{1}{M} \mathbf{I}$ , and with the assumption that  $\mathbf{s}$  with dimension  $N \times 1$  is a zero-mean Gaussian random vector with a covariance matrix  $\mathbb{E}\{\mathbf{s}\mathbf{s}^\dagger\} = \sigma_s^2 \mathbf{I}$  where  $\mathbf{I}$  is the identity matrix, it can be immediately seen from (8.76) and (8.77) that

$$\frac{E_b}{N_{0min}} = \frac{\log_e 2}{\left( \frac{\ell_1 \mu}{\sigma_s^2} + \ell_2 \nu \right) \mathbb{E} [\text{tr}(\mathbf{H}^\dagger \mathbf{H})]} \quad (8.78)$$

$$\mathcal{S}_0 = \frac{2 \left( \frac{\ell_1 \mu}{\sigma_s^2} + \ell_2 \nu \right)^2 \mathbb{E}^2 \left[ \text{tr}(\mathbf{H}^\dagger \mathbf{H}) \right]}{\Omega} \quad (8.79)$$

where

$$\begin{aligned} \Omega = & \theta T B N \left\{ \left[ \frac{\ell_1 \mu^2}{\sigma_s^4} + \ell_2 \nu^2 \right] \mathbb{E} \left[ \text{tr}^2(\mathbf{H}^\dagger \mathbf{H}) \right] - \left[ \frac{\ell_1 \mu}{\sigma_s^2} + \ell_2 \nu \right]^2 \mathbb{E}^2 \left[ \text{tr}(\mathbf{H}^\dagger \mathbf{H}) \right] \right\} \\ & + N \left[ \frac{\ell_1 \mu^2}{\sigma_s^4} + \ell_2 \nu^2 \right] \mathbb{E} \left[ \text{tr} \left( (\mathbf{H}^\dagger \mathbf{H})^2 \right) \right] \log_e 2. \end{aligned}$$

Now, assuming that  $\mathbf{H}$  has independent zero-mean unit-variance complex Gaussian random entries, we have [54]

$$\begin{aligned} \mathbb{E} \left[ \text{tr}(\mathbf{H}^\dagger \mathbf{H}) \right] &= NM, \quad \mathbb{E} \left[ \text{tr}^2(\mathbf{H}^\dagger \mathbf{H}) \right] = NM(NM + 1), \\ \mathbb{E} \left[ \text{tr} \left( (\mathbf{H}^\dagger \mathbf{H})^2 \right) \right] &= NM(N + M). \end{aligned} \quad (8.80)$$

Using these facts, we can write the following minimum bit energy and wideband slope expressions for the uniform power allocation case

$$\frac{E_b}{N_{0_{min}}} = \frac{\log_e 2}{\left( \frac{\ell_1 \mu}{\sigma_s^2} + \ell_2 \nu \right) NM} \quad (8.81)$$

$$\mathcal{S}_0 = \frac{2 \left( \frac{\ell_1 \mu}{\sigma_s^2} + \ell_2 \nu \right)^2 M^2}{Y} \quad (8.82)$$

where

$$\begin{aligned} Y = & \theta T B \left\{ \left[ \frac{\ell_1 \mu^2}{\sigma_s^4} + \ell_2 \nu^2 \right] M(NM + 1) - \left[ \frac{\ell_1 \mu}{\sigma_s^2} + \ell_2 \nu \right]^2 M^2 \right\} \\ & + \left[ \frac{\ell_1 \mu^2}{\sigma_s^4} + \ell_2 \nu^2 \right] M(N + M) \log_e 2 \end{aligned}$$

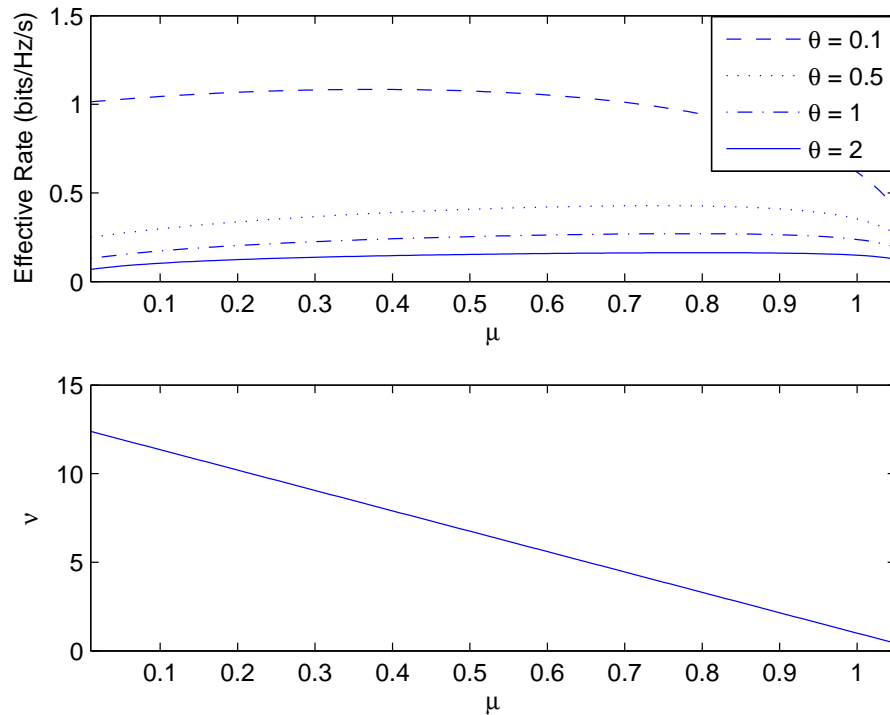


Figure 8.3: Effective Rate and  $\nu$  v.s.  $\mu$  for different Decay Rate,  $\theta$ , values.

## 8.4 Numerical Results

In this section, we numerically show the results obtained in the previous sections. In our simulations, we consider the i.i.d. Rayleigh fading channel where the variables of the channel matrix  $\mathbf{H}$  are i.i.d. zero-mean, unit variance, circularly symmetric Gaussian random variables. Moreover, we assume that input covariance matrix is  $\mathbf{K}_x = \frac{1}{M}\mathbf{I}$  and that variables of received signal coming from primary users are i.i.d. and have a variance  $\sigma_s^2$  so that  $\mathbf{K}_z = \frac{\sigma_s^2 + \sigma_n^2}{\sigma_s^2}\mathbf{I}$ . As the objective

function we consider the effective rate which is given as

$$R_E(\text{SNR}, \theta) = -\frac{1}{\theta TB} \log_e \mathbb{E} \left\{ \ell_1 e^{-\theta TB \log_2 \det \left[ \mathbf{I} + \frac{\mu N \sigma_n^2}{M(\sigma_s^2 + \sigma_n^2)} \text{SNR} \mathbf{H} \mathbf{H}^\dagger \right]} + \ell_2 e^{-\theta TB \log_2 \det \left[ \mathbf{I} + \frac{\nu N}{M} \text{SNR} \mathbf{H} \mathbf{H}^\dagger \right]} + \rho(1 - P_d) \right\} \text{bits/Hz/s.} \quad (8.83)$$

With these assumptions, it will be easy to calculate the effective rate by using expression for the moment generating function of instantaneous mutual information given by Wang and Giannakis in [82, Theorem 1]. After adopting this expression into our effective rate formulation (8.83), we obtain

$$R_E(\text{SNR}, \theta) = -\frac{1}{\theta TB} \log_e \left\{ [bP_d + aP_f] \frac{\det \left[ \mathbf{G} \left( \theta, \frac{\mu \sigma_n^2 \text{SNR}}{\sigma_s^2 + \sigma_n^2} \right) \right]}{\prod_{i=1}^k \Gamma(d+i)} + a(1 - P_f) \frac{\det [\mathbf{G}(\theta, \nu \text{SNR})]}{\prod_{i=1}^k \Gamma(d+i)} + b(1 - P_d) \right\} \text{bits/Hz/s} \quad (8.84)$$

where  $k = \min(M, N)$ ,  $d = \max(M, N) - \min(M, N)$ , and  $\Gamma(\cdot)$  is the Gamma function. Here,  $\mathbf{G}(\theta, \text{SNR})$  is a  $k \times k$  Hankel matrix whose  $(m, n)^{th}$  component is

$$g_{m,n} = \int_0^\infty \left( 1 + \frac{N}{M} \text{SNR} z \right)^{-\theta TB \log_2 e} z^{m+n+d-2} e^{-z} dz \quad m, n = 1, 2, \dots, k. \quad (8.85)$$

In our simulations, we assume  $T = 0.1 \text{sec.}$ ,  $B = 100 \text{Hz}$ ,  $\sigma_n^2 = \sigma_s^2 = 1$ ,  $b = 0.1$ ,  $a = 0.9$ ,  $P_d = 0.92$  and  $P_f = 0.21$ . In Figure 8.3, we plot the effective transmission rate as a function of  $\mu$  for different decay rate values  $\theta$ . As expected, with increasing decay rate the effective rate is decreasing. The course of the maximum effective rate as a function of  $\mu$  is moving towards the high values of  $\mu$  with increasing decay rate values, which means that more power is allocated for



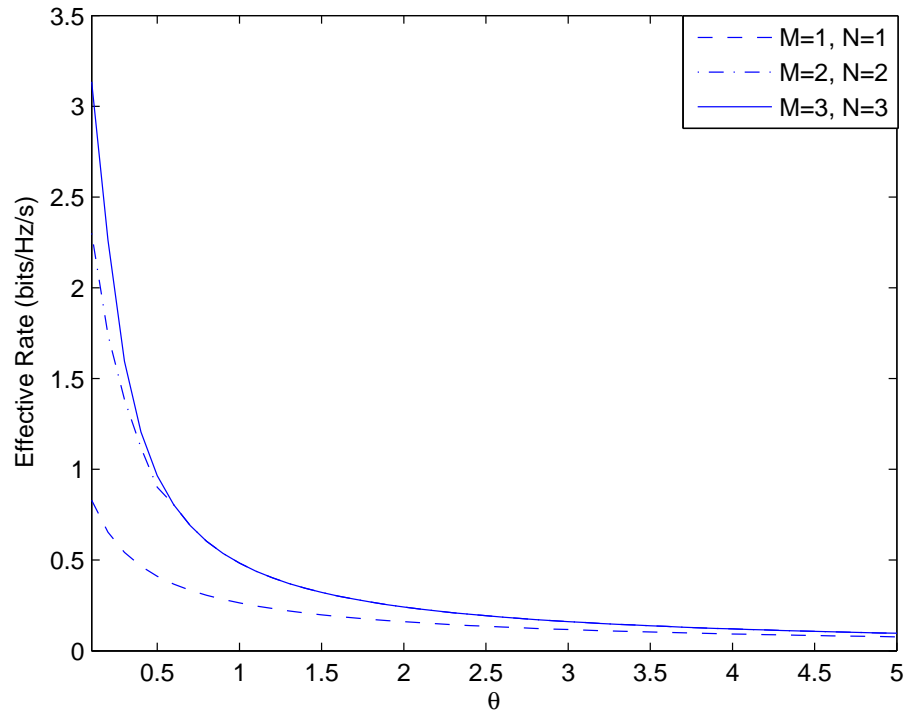


Figure 8.4: Effective Rate v.s. Decay Rate,  $\theta$  for different Number of Antennas,  $M$ .

the case when the primary users are active when there are more stringent buffer constraints. Note that the number of transmit and receive antennas are 1 and 1, respectively, and SNR=0 dB. In Figure 8.4, we plot the effective rate as a function of decay rate  $\theta$  for different values of transmit and receive antennas when, again, SNR=0 dB. Due to increasing buffer constraint levels, the effective rate is decreasing for all antenna cases, and at high  $\theta$  values, the increase due to more number of antennas in effective rate is considerably decreasing and becoming same for all cases. In Figure 8.5 and Figure 8.6, we display the effective rate as a function of SNR for different values of decay rates. In Fig. 8.5 the number of antennas at both receiver and transmitter ends is 1, whereas in Fig. 8.6 it is 3 at both ends. It can be easily observed that at high SNR values, the number of antennas does not

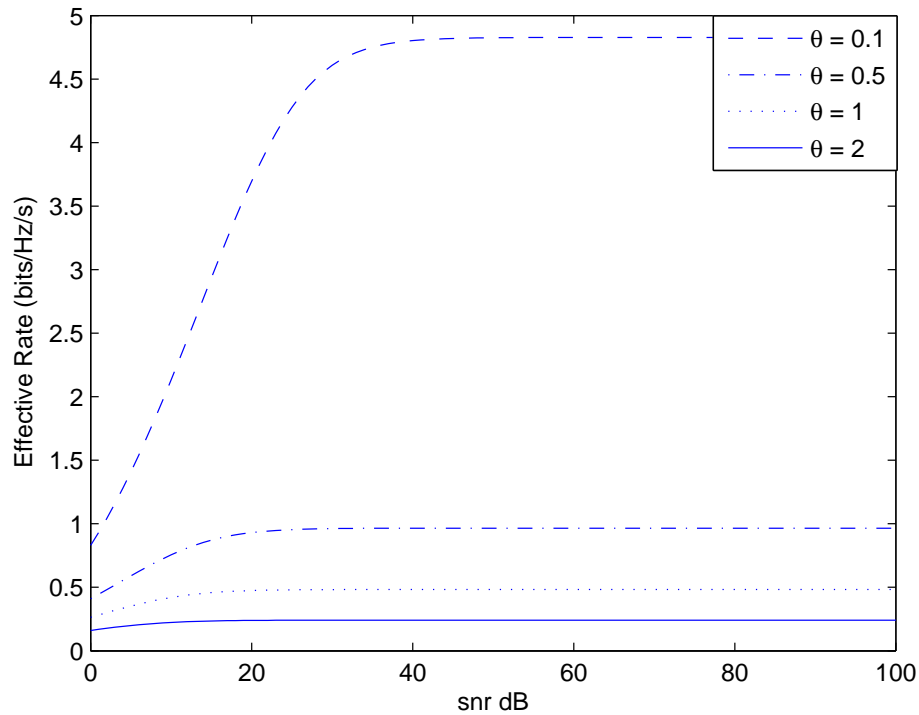


Figure 8.5: Effective Rate v.s. SNR for different values of Decay Rate,  $\theta M = 1$ .

improve the effective transmission rates. On the other hand, at lower SNR values, the number of antennas gains importance. At stringent delay constraints, using more antennas at lower SNR values is more beneficial for the SUs under power limitations.

## 8.5 Conclusion

In this chapter, we investigated the performance levels of cognitive MIMO wireless communication systems under queuing and delay constraints. We considered the effective rate as our objective performance metric and studied in the low-power regime. We obtained the expressions for the first and second derivatives

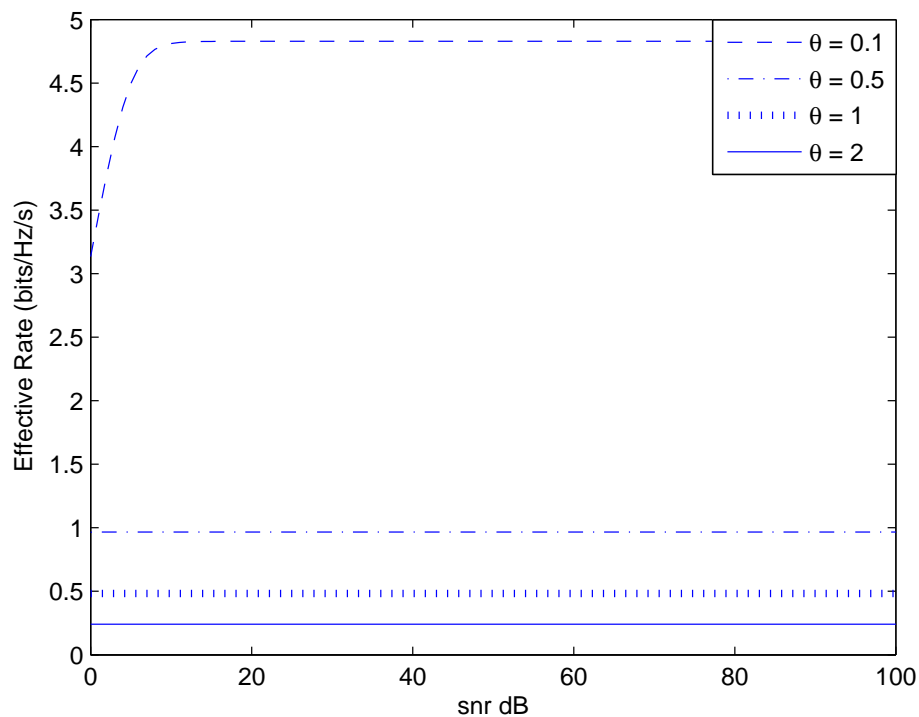


Figure 8.6: Effective Rate v.s. SNR for different values of Decay Rate,  $\theta$   $M=3$ .

of effective capacity. We observe that the first derivative does not depend on the decay rate but it is affected by the power allocation rates for the cases when the channel is busy and the case when the channel is idle. On the other hand, the second derivative is a function of decay rate  $\theta$ . We also demonstrated the minimum bit energy requirements under the QoS constraints. Finally, we displayed the numerical results that show the course of effective transmission rate.

# Appendix A

## Proof of Theorem 1

In [20, Chap. 7, Example 7.2.7], it is shown for Markov modulated processes that

$$\frac{\Lambda(\theta)}{\theta} = \frac{1}{\theta} \log_e sp(\phi(\theta)R) \quad (\text{A.1})$$

where  $sp(\phi(\theta)R)$  is the spectral radius (i.e., the maximum of the absolute values of the eigenvalues) of the matrix  $\phi(\theta)R$ ,  $R$  is the transition matrix of the underlying Markov process, and  $\phi(\theta) = \text{diag}(\phi_1(\theta), \dots, \phi_M(\theta))$  is a diagonal matrix whose components are the moment generating functions of the processes in  $M$  states. The rates supported by the cognitive radio channel with the state transition model described in the previous section can be seen as a Markov modulated process and hence the setup considered in [20] can be immediately applied to our setting. Note that the transmission rates are non-random and fixed in each state in the cognitive channel. More specifically, the possible rates are  $r_1(T - N)$ ,  $r_2(T - N)$ , and 0 for which the moment generating functions are  $e^{\theta r_1(T - N)}$ ,  $e^{\theta r_2(T - N)}$ , and 1, respectively. Therefore, we have  $\phi(\theta) = \text{diag}\{e^{(T - N)\theta r_1}, 1, e^{(T - N)\theta r_2}, 1, e^{(T - N)\theta r_1}, 1, e^{(T - N)\theta r_2}, 1\}$ .

Then, using (5.16), we can write

$$\phi(\theta)R = \begin{bmatrix} \phi_1(\theta)p_1 & \cdot & \cdot & \cdot & \phi_1(\theta)p_8 \\ \phi_2(\theta)p_1 & \cdot & \cdot & \cdot & \phi_2(\theta)p_8 \\ \phi_3(\theta)p_1 & \cdot & \cdot & \cdot & \phi_3(\theta)p_8 \\ \cdot & \cdot & \cdot & \cdot & \cdot \\ \phi_8(\theta)p_1 & \cdot & \cdot & \cdot & \phi_8(\theta)p_8 \end{bmatrix} = \begin{bmatrix} e^{(T-N)\theta r_1}p_1 & \cdot & \cdot & \cdot & e^{(T-N)\theta r_1}p_8 \\ p_1 & \cdot & \cdot & \cdot & p_8 \\ e^{(T-N)\theta r_2}p_1 & \cdot & \cdot & \cdot & e^{(T-N)\theta r_2}p_8 \\ \cdot & \cdot & \cdot & \cdot & \cdot \\ p_1 & \cdot & \cdot & \cdot & p_8 \end{bmatrix} \quad (\text{A.2})$$

Since  $\phi(\theta)R$  is a matrix with unit rank, we can readily find that

$$\begin{aligned} sp(\phi(\theta)R) &= \text{trace}(\phi(\theta)R) \\ &= \phi_1(\theta)p_1 + \dots + \phi_8(\theta)p_8 \end{aligned} \quad (\text{A.3})$$

$$= (p_1 + p_5)e^{(T-N)\theta r_1} + (p_3 + p_7)e^{(T-N)\theta r_2} + p_2 + p_4 + p_6 + p_8. \quad (\text{A.4})$$

Then, combining (A.4) with (A.1) and (5.18), we obtain the expression inside the maximization on the right-hand side of (5.19). Note that this expression is the effective capacity for given values of fixed transmission rates  $r_1$  and  $r_2$ , and can be maximized by choosing the optimal values of  $r_1$  and  $r_2$ . This maximization leads to the effective capacity formula given in (5.19).

## Appendix B

### Proof of Theorem 2

The proof is very similar to the proof of Theorem 1. The only differences are that we now have four states and the service processes (or equivalently the transmission rates) are random processes that depend on  $z$ . As described in Section 5.4.1, the rates are  $r_1(i)$  in states 1 and 5,  $r_2(i)$  in state 7, and zero in state 4. Therefore, the corresponding moment generating functions are  $\phi_1(\theta) = \phi_5(\theta) = \mathbb{E}_z\{e^{(T-N)\theta r_1}\}$ ,  $\phi_7(\theta) = \mathbb{E}_z\{e^{(T-N)\theta r_2}\}$ , and  $\phi_4(\theta) = 1$ , where the expectations are with respect to  $z$ . Using the same approach as in the proof of Theorem 1, we can easily find that

$$\frac{\Lambda(\theta)}{\theta} = \frac{1}{\theta} \log_e \left[ (p_1 + p_5) \mathbb{E}_z\{e^{(T-N)\theta r_1}\} + p_7 \mathbb{E}_z\{e^{(T-N)\theta r_2}\} + p_4 \right] \quad (\text{B.1})$$

$$= \frac{1}{\theta} \log_e \left[ (\rho P_d + (1 - \rho) P_f) \mathbb{E}_z\{e^{(T-N)\theta r_1}\} + (1 - \rho)(1 - P_f) \mathbb{E}_z\{e^{(T-N)\theta r_2}\} + \rho(1 - P_d) \right]. \quad (\text{B.2})$$

Combining the expression in (B.2) with (5.18), and maximizing over all possible power adaptation schemes leads to (5.24).

## Appendix C

### Proof of Theorem 3

Since logarithm is a monotonic function, the optimal power adaptation policies can also be obtained from the following minimization problem

$$\min_{\substack{\mu_1(\theta, z): \mathbb{E}_z\{\mu_1(\theta, z)\} \leq 1 \\ \mu_2(\theta, z): \mathbb{E}_z\{\mu_2(\theta, z)\} \leq 1}} (\rho P_d + (1 - \rho)P_f) \mathbb{E}_z\{e^{-(T-N)\theta r_1}\} + (1 - \rho)(1 - P_f)\mathbb{E}_z\{e^{-(T-N)\theta r_2}\}. \quad (\text{C.1})$$

It is clear that the objective function in (C.1) is strictly convex and the constraint functions in (5.20) are linear with respect to  $\mu_1(\theta, z)$  and  $\mu_2(\theta, z)$  [76, Appendix I]. Then, forming the Lagrangian function and setting the derivatives of the Lagrangian with respect to  $\mu_1(\theta, z)$  and  $\mu_2(\theta, z)$  equal to zero, we obtain

$$\left\{ \lambda_1 - a\text{SNR}_1 z [\rho P_d + (1 - \rho)P_f] [1 + \mu_1(\theta, z)z\text{SNR}_1]^{-a-1} \right\} f(z) = 0 \quad (\text{C.2})$$

$$\left\{ \lambda_2 - a\text{SNR}_4 z (1 - \rho) (1 - P_f) [1 + \mu_2(\theta, z)z\text{SNR}_4]^{-a-1} \right\} f(z) = 0 \quad (\text{C.3})$$

where  $\lambda_1$  and  $\lambda_2$  are the Lagrange multipliers. Defining  $\gamma_1 = \frac{\lambda_1}{[\rho P_d + (1 - \rho)P_f] a\text{SNR}_1}$  and  $\gamma_2 = \frac{\lambda_2}{(1 - \rho)(1 - P_f) a\text{SNR}_4}$ , and solving (C.2) and (C.3), we obtain optimal power

policies given in (5.25) and (5.26). Since in general all available transmission power should be used, the values of the Lagrange multipliers  $\lambda_1$  and  $\lambda_2$  and hence the values of  $\gamma_1$  and  $\gamma_2$  can be numerically obtained from the relations  $\mathbb{E}_z\{\mu_1(\theta, z)\} = 1$  and  $\mathbb{E}_z\{\mu_2(\theta, z)\} = 1$ .



## Appendix D

### Proof of Theorem 4

In [20, Chap. 7, Example 7.2.7], it is shown for Markov modulated processes that

$$\frac{\Lambda(\theta)}{\theta} = \frac{1}{\theta} \log_e sp(\phi(\theta)R) \quad (\text{D.1})$$

where  $sp(\phi(\theta)R)$  is the spectral radius (i.e., the maximum of the absolute values of the eigenvalues) of the matrix  $\phi(\theta)R$ ,  $R$  is the transition matrix of the underlying Markov process, and  $\phi(\theta) = \text{diag}(\phi_1(\theta), \dots, \phi_{M+2}(\theta))$  is a diagonal matrix whose components are the moment generating functions of the processes in given states. The rates supported by the cognitive radio channel with the state transition model described in the previous section can be seen as a Markov modulated process and hence the setup considered in [20] can be immediately applied to our setting. Since the processes in the states are time-varying transmission rates, we can easily find that

$$\phi(\theta) = \text{diag} \left\{ E \left\{ e^{(T-N)\theta r_1} \right\}, E_1 \left\{ e^{(T-N)\theta r_2} \right\}, \dots, E_M \left\{ e^{(T-N)\theta r_2} \right\}, 1 \right\}. \quad (\text{D.2})$$

Then, we have

$$\phi(\theta)R = \begin{bmatrix} \phi_1(\theta)p_1 & \cdot & \cdot & \phi_1(\theta)p_{M+2} \\ \cdot & & & \cdot \\ \cdot & & & \cdot \\ \phi_{M+2}(\theta)p_1 & \cdot & \cdot & \phi_{M+2}(\theta)p_{M+2} \end{bmatrix}.$$

Since  $\phi(\theta)R$  is a matrix with unit rank, we can readily find that

$$\begin{aligned} sp(\phi(\theta)R) &= \text{trace}(\phi(\theta)R) \\ &= \phi_1(\theta)p_1 + \phi_2(\theta)p_2 + \cdots + \phi_{M+1}(\theta)p_{M+1} + \phi_{M+2}(\theta)p_{M+2} \quad (\text{D.3}) \\ &= p_1 E \left\{ e^{(T-N)\theta r_1} \right\} + p_2 E_1 \left\{ e^{(T-N)\theta r_2} \right\} + \cdots + p_{M+1} E_M \left\{ e^{(T-N)\theta r_2} \right\} \\ &\quad + p_{M+2}. \quad (\text{D.4}) \end{aligned}$$

Then, combining (D.4) with (D.1) and (6.26), normalizing the expression with  $TB_c$  in order to have the effective capacity in the units of bits/s/Hz, and considering the maximization over power adaptation policies, we reach to the effective capacity formula given in (6.28).

# Appendix E

## Proof of Theorem 5

Since logarithm is a monotonic function, the optimal power adaptation policies can also be obtained from the following minimization problem:

$$\begin{aligned} & \min_{\substack{\alpha^{M-1} \rho P_d E\{P_1 z_{sp}\} \\ + \sum_{k=1}^M \alpha^{M-k} (1-\alpha)^{k-1} \rho (1-P_d) \frac{M!}{(M-k)! k!} E_k\{P_2 z_{sp}\} \\ \leq I_{avg}}} p_1 E\left\{e^{-(T-N)\theta r_1}\right\} + \sum_{k=1}^M p_{k+1} E_k\left\{e^{-(T-N)\theta r_2}\right\} \end{aligned} \quad (\text{E.1})$$

It is clear that the objective function in (E.1) is strictly convex and the constraint function in (6.18) is linear with respect to  $P_1$  and  $P_2$ <sup>1</sup>. Then, forming the Lagrangian function and setting the derivatives of the Lagrangian with respect to  $P_1$  and  $P_2$  equal to zero, we obtain:

$$\left[ \frac{\lambda \rho P_d z_{sp}}{\alpha} - \frac{c z}{\mu_1} \left( 1 + \frac{z P_1}{\mu_1} \right)^{-c-1} \right] \alpha^M f(z, z_{sp}) = 0 \quad (\text{E.2})$$

---

<sup>1</sup>Strict convexity follows from the strict concavity of  $r_1$  and  $r_2$  in (6.8) and (6.9) with respect to  $P_1$  and  $P_2$  respectively, strict convexity of the exponential function, and the fact that the nonnegative weighted sum of strictly convex functions is strictly convex [15, Section 3.2.1].

and

$$\left[ \lambda \rho (1 - P_d) z_{sp} - \frac{c(1 - \rho)(1 - P_f)z}{\mu_2} \left( 1 + \frac{zP_2}{\mu_2} \right)^{-c-1} \right] \times \sum_{k=1}^M \alpha^{M-k} (1 - \alpha)^{k-1} \frac{M!}{(M-k)!k!} f_k(z, z_{sp}) = 0 \quad (\text{E.3})$$

where  $\lambda$  is the Lagrange multiplier. Above,  $f(z, z_{sp})$  denotes the joint distribution of  $(z, z_{sp})$  of the channel selected for transmission when all channels are detected busy. Hence, in this case, the transmission channel is chosen among  $M$  channels. Similarly,  $f_k(z, z_{sp})$  denotes the joint distribution when  $k$  channels are detected idle, and the transmission channel is selected out of these  $k$  channels. Defining  $\beta_1 = \frac{\mu_1 \rho P_d}{c\alpha}$  and  $\beta_2 = \frac{\rho(1-P_d)\mu_2}{c(1-\rho)(1-P_f)}$ , and solving (E.2) and (E.3), we obtain the optimal power policies given in (6.29) and (6.30).

# Appendix F

## Proof of Theorem 6

In the cognitive scenario we are considering, the signal received by the receiver in the training phase is

$$y = \begin{cases} \sqrt{P_t}h + n + s & \text{if the channel is busy} \\ \sqrt{P_t}h + n & \text{if the channel is idle} \end{cases}. \quad (\text{F.1})$$

Note that we assume that  $n$  and  $s$  are independent complex Gaussian random variables with zero-mean and variances  $\sigma_n^2$  and  $\sigma_s^2$ , respectively. Therefore, the variance of the noise component<sup>1</sup> is either  $\sigma_n^2 + \sigma_s^2$  or  $\sigma_n^2$ , depending on whether the channel is busy or idle. Since the receiver does not perfectly know the state of the primary user activity and only has a guess through channel sensing, the noise variance,  $\sigma^2$ , is random taking two values:  $\sigma_n^2 + \sigma_s^2$  and  $\sigma_n^2$ . Now, the MMSE

---

<sup>1</sup>Noise component is  $n + s$  when the channel is busy, and  $n$  when the channel is idle.

estimate in the presence of uncertainty in the noise statistics is obtained as follows:

$$\hat{h}_{mmse} = \mathbb{E}\{h|y\} \quad (\text{F.2})$$

$$= P(\sigma^2 = \sigma_n^2 | y)\mathbb{E}\{h | y, \sigma^2 = \sigma_n^2\} + P(\sigma^2 = \sigma_n^2 + \sigma_s^2 | y)\mathbb{E}\{h | y, \sigma^2 = \sigma_n^2 + \sigma_s^2\} \quad (\text{F.3})$$

$$= P\{\sigma^2 = \sigma_n^2 | y\} \frac{\sqrt{P_t}\sigma_h^2}{P_t\sigma_h^2 + \sigma_n^2}y + P\{\sigma^2 = \sigma_n^2 + \sigma_s^2 | y\} \frac{\sqrt{P_t}\sigma_h^2}{P_t\sigma_h^2 + \sigma_n^2 + \sigma_s^2}y. \quad (\text{F.4})$$

Above, (F.3) is obtained by using the following property of conditional expectation:  $\mathbb{E}\{X | Y\} = \mathbb{E}\{\mathbb{E}\{X | Y, Z\} | Y\}$  where the outer expectation on the right-hand side is with respect to the conditional distribution of  $Z$  given  $Y$ . In our setting,  $Z$  is the noise variance. Hence, the above formulation indicates that we can find the MMSE estimate by evaluating the average of the MMSE estimates with fixed noise variances with respect to the conditional distribution of the noise variance given the observation. This is indeed what is done in (F.3).

(F.4) is obtained by noting that once the noise variance is fixed, the MMSE estimates in a Gaussian setting are given by  $\mathbb{E}\{h | y, \sigma^2 = \sigma_n^2\} = \frac{\sqrt{P_t}\sigma_h^2}{P_t\sigma_h^2 + \sigma_n^2}y$  and  $\mathbb{E}\{h | y, \sigma^2 = \sigma_n^2 + \sigma_s^2\} = \frac{\sqrt{P_t}\sigma_h^2}{P_t\sigma_h^2 + \sigma_n^2 + \sigma_s^2}y$ .

Next, we provide the expressions for the conditional probabilities using Bayes' rule:

$$P\{\sigma^2 = \sigma_n^2 | y\} = \frac{P\{\sigma^2 = \sigma_n^2\}f(y|\sigma^2 = \sigma_n^2)}{f(y)}$$

and

$$P\{\sigma^2 = \sigma_n^2 + \sigma_s^2 | y\} = \frac{P\{\sigma^2 = \sigma_n^2 + \sigma_s^2\}f(y|\sigma^2 = \sigma_n^2 + \sigma_s^2)}{f(y)}.$$

Given the value of the noise variance  $\sigma^2$ ,  $y$  is conditionally Gaussian distributed with zero mean and variance  $\sigma^2$ , as can be immediately seen from the relations in (F.1). These conditional Gaussian distributions are provided in (7.19) and (7.20) in Section 7.3.1.  $f(y)$  is the average of the conditional distributions and hence is given by (7.21). The prior probability of the noise variance depends on the channel sensing result. For instance, let us assume that the channel is detected as busy. Then,

$$P\{\sigma^2 = \sigma_n^2\} = P\{\text{channel is idle} \mid \text{channel is detected busy}\} \quad (\text{F.5})$$

$$= \frac{P\{\text{channel is idle}\}P\{\text{channel is detected busy} \mid \text{channel is idle}\}}{P\{\text{channel is detected busy}\}} \quad (\text{F.6})$$

$$= \frac{P\{\text{channel is idle}\}P\{\text{channel is detected busy} \mid \text{channel is idle}\}}{P\{\text{channel is idle}\}P\{\text{channel is detected busy} \mid \text{channel is idle}\} + P\{\text{channel is busy}\}P\{\text{channel is detected busy} \mid \text{channel is busy}\}} \quad (\text{F.7})$$

$$= \frac{\frac{a}{a+b}P_f}{\frac{a}{a+b}P_f + \frac{b}{a+b}P_d} \quad (\text{F.8})$$

$$= \frac{aP_f}{aP_f + bP_d} \quad (\text{F.9})$$

Note that having  $\sigma^2 = \sigma_n^2$  means that there are no primary users in the channel and hence channel is idle. By our assumption, channel is detected as busy. Therefore,  $P\{\sigma^2 = \sigma_n^2\}$  is equal to the conditional probability  $P\{\text{channel is idle} \mid \text{channel is detected busy}\}$ . Then, the expression in (F.9) is obtained by noting that  $P\{\text{channel is idle}\} = \frac{a}{a+b}$  and  $P\{\text{channel is busy}\} = \frac{b}{a+b}$ , which can be derived easily from the two-state Markov chain used for primary user activity, and by realizing that  $P\{\text{channel is detected busy} \mid \text{channel is idle}\}$  is the false alarm probability  $P_f$  and  $P\{\text{channel is detected busy} \mid \text{channel is busy}\}$  is the detection probability  $P_d$ . The expressions in (7.17) and (7.18) for the other cases are obtained using a similar approach.

# Appendix G

## Proof of Theorem 7

In [20, Chap. 7, Example 7.2.7], it is shown for Markov modulated processes that

$$\frac{\Lambda(\theta)}{\theta} = \frac{1}{\theta} \log_e sp(\phi(\theta)R) \quad (\text{G.1})$$

where  $sp(\phi(\theta)R)$  is the spectral radius or the maximum of the absolute values of the eigenvalues of the matrix  $\phi(\theta)R$ ,  $R$  is the transition matrix of the underlying Markov process, and  $\phi(\theta) = \text{diag}(\phi_1(\theta), \dots, \phi_M(\theta))$  is a diagonal matrix whose components are the moment generating functions of the processes in  $M$  states ( $M = 8$  in our case). The rates supported by the cognitive radio channel with the state transition model described in the previous section can be seen as a Markov modulated process and hence the setup considered in [20] can be immediately applied to our setting. Note that the transmission rates are non-random and fixed in each state in the cognitive channel. More specifically, the possible rates are  $Tr_1$ ,  $Tr_2$ , and 0 for which the moment generating functions are  $e^{\theta Tr_1}$ ,  $e^{\theta Tr_2}$ , and 1, respectively. Therefore, we have  $\phi(\theta) = \text{diag}\{e^{\theta Tr_1}, 1, e^{\theta Tr_2}, 1, e^{\theta Tr_1}, 1, e^{\theta Tr_2}, 1\}$ .



Then, using (7.40), we can write

$$\phi(\theta)R = \begin{bmatrix} \phi_1(\theta)p_{b1} & \cdot & \cdot & \phi_1(\theta)p_{b8} \\ \cdot & & & \cdot \\ \phi_3(\theta)p_{b1} & \cdot & \cdot & \phi_3(\theta)p_{b8} \\ \phi_4(\theta)p_{b1} & \cdot & \cdot & \phi_4(\theta)p_{b8} \\ \phi_5(\theta)p_{i1} & \cdot & \cdot & \phi_5(\theta)p_{i8} \\ \cdot & & & \cdot \\ \phi_8(\theta)p_{i1} & \cdot & \cdot & \phi_8(\theta)p_{i8} \end{bmatrix}. \quad (\text{G.2})$$

Since  $\phi(\theta)R$  is a matrix with rank 2, we can readily find that [80]

$$\begin{aligned} sp(\phi(\theta)R) &= \frac{1}{2} \left[ \phi_1(\theta)p_{b1} + \dots + \phi_4(\theta)p_{b4} + \phi_5(\theta)p_{i5} + \dots + \phi_8(\theta)p_{i8} \right] \\ &\quad + \frac{1}{2} \left\{ \left[ \phi_1(\theta)p_{b1} + \dots + \phi_4(\theta)p_{b4} - \phi_5(\theta)p_{i5} - \dots - \phi_8(\theta)p_{i8} \right]^2 \right. \\ &\quad \left. + 4 \left( \phi_1(\theta)p_{i1} + \dots + \phi_4(\theta)p_{i4} \right) \left( \phi_5(\theta)p_{b5} + \dots + \phi_8(\theta)p_{b8} \right) \right\}^{\frac{1}{2}} \\ &= \frac{1}{2} \left[ (p_{b1} + p_{i5})e^{\theta Tr_1} + (p_{b3} + p_{i7})e^{\theta Tr_2} + p_{b2} + p_{b4} + p_{i6} + p_{i8} \right] \\ &\quad + \frac{1}{2} \left\{ \left[ (p_{b1} - p_{i5})e^{\theta Tr_1} + (p_{b3} - p_{i7})e^{\theta Tr_2} + p_{b2} + p_{b4} - p_{i6} - p_{i8} \right]^2 \right. \\ &\quad \left. + 4 \left( p_{i1}e^{\theta Tr_1} + p_{i3}e^{\theta Tr_2} + p_{i2} + p_{i4} \right) \left( p_{b5}e^{\theta Tr_1} + p_{b7}e^{\theta Tr_2} + p_{b6} + p_{b8} \right) \right\}^{\frac{1}{2}}. \end{aligned} \quad (\text{G.3})$$

Then, combining (G.3) with (G.1) and (7.41), we obtain the expression inside the maximization on the right-hand side of (7.42). Note that this expression is the effective capacity for given values of fixed transmission rates  $r_1$  and  $r_2$  and of

average power levels  $\bar{P}_1$  and  $\bar{P}_2$ , and can be maximized by choosing the optimal values of  $r_1$  and  $r_2$  over the optimized power allocation policy. This maximization leads to the effective capacity formula given in (7.42). Note also that we have normalized the effective capacity expression in (7.42) by  $TB$  to have it in the units of bits/s/Hz.

# Appendix H

## Proof of Theorem 8

In [20, Chap. 7, Example 7.2.7], it is shown for Markov modulated processes that

$$\frac{\Lambda(\theta)}{\theta} = \frac{1}{\theta} \log_e sp(\phi(\theta)R) \quad (\text{H.1})$$

where  $sp(\phi(\theta)R)$  is the spectral radius (i.e., the maximum of the absolute values of the eigenvalues) of the matrix  $\phi(\theta)R$ ,  $R$  is the transition matrix of the underlying Markov process, and  $\phi(\theta) = \text{diag}(\phi_1(\theta), \dots, \phi_M(\theta))$  is a diagonal matrix whose components are the moment generating functions of the processes in  $M$  states. The rates supported by the cognitive radio channel with the state transition model described above can be seen as a Markov modulated process and hence the setup considered in [20] can be immediately applied to our setting. Note that the transmission rates are random in each state in the cognitive channel. Therefore, the corresponding moment generating functions are  $\phi_1(\theta) = \phi_3(\theta) = \mathbb{E}\{e^{T\theta r_1}\}$ ,

$\phi_4(\theta) = \mathbb{E}\{e^{T\theta r_2}\}$  and  $\phi_2(\theta) = 1$ . Then, using (8.20), we can write

$$\phi(\theta)R = \begin{bmatrix} \phi_1(\theta)p_{b1} & \cdot & \cdot & \phi_1(\theta)p_{b4} \\ \phi_2(\theta)p_{b1} & & & \phi_2(\theta)p_{b4} \\ \phi_3(\theta)p_{i1} & & & \phi_3(\theta)p_{i4} \\ \phi_4(\theta)p_{i1} & \cdot & \cdot & \phi_4(\theta)p_{i4} \end{bmatrix} = \begin{bmatrix} \mathbb{E}\{e^{T\theta r_1}\}p_{b1} & \cdot & \cdot & \mathbb{E}\{e^{T\theta r_1}\}p_{b4} \\ p_{b1} & & & p_{b4} \\ \mathbb{E}\{e^{T\theta r_1}\}p_{i1} & & & \mathbb{E}\{e^{T\theta r_1}\}p_{i4} \\ \mathbb{E}\{e^{T\theta r_2}\}p_{i1} & & & \mathbb{E}\{e^{T\theta r_2}\}p_{i4} \end{bmatrix} \quad (\text{H.2})$$

Since  $\phi(\theta)R$  is a matrix with rank 2, we can readily find that

$$\begin{aligned} sp(\phi(\theta)R) &= \text{trace}(\phi(\theta)R) \\ &= \frac{1}{2} \{ \phi_1(\theta)p_{b1} + \phi_2(\theta)p_{b2} + \phi_3(\theta)p_{i3} + \phi_4(\theta)p_{i4} \} \\ &\quad + \frac{1}{2} \left\{ [\phi_1(\theta)p_{b1} + \phi_2(\theta)p_{b2} - \phi_3(\theta)p_{i3} - \phi_4(\theta)p_{i4}]^2 \right. \\ &\quad \left. + 4(\phi_1(\theta)p_{i1} + \phi_2(\theta)p_{i2})(\phi_3(\theta)p_{b3} + \phi_4(\theta)p_{b4}) \right\}^{1/2} \\ &= \frac{1}{2} \left\{ (p_{b1} + p_{i3}) \mathbb{E}\{e^{T\theta r_1}\} + p_{i4} \mathbb{E}\{e^{T\theta r_2}\} + p_{b2} \right\} \\ &\quad + \frac{1}{2} \left\{ [(p_{b1} - p_{i3}) \mathbb{E}\{e^{T\theta r_1}\} - p_{i4} \mathbb{E}\{e^{T\theta r_2}\} + p_{b2}]^2 \right. \\ &\quad \left. + 4(p_{i1} \mathbb{E}\{e^{T\theta r_1}\} + p_{i2}) (p_{b3} \mathbb{E}\{e^{T\theta r_1}\} + p_{b4} \mathbb{E}\{e^{T\theta r_2}\}) \right\}^{1/2}. \quad (\text{H.3}) \end{aligned}$$

Then, combining (H.3) with (H.1) and (8.21), we obtain the expression inside the maximization on the right-hand side of (8.22).

# Bibliography

- [1] A. Bdeir I. Abou-Faycal and M. Médard. Power allocation schemes for pilot symbol assisted modulation over rayleigh fading channels with no feedback. In *IEEE International Conference on Communications (ICC)*, volume 2, pages 737–741, Paris, France, June 20–24 2004. [1.2](#)
- [2] S. Akin and M. C. Gursoy. Effective capacity analysis of cognitive radio channels for quality of service provisioning. *IEEE Transaction on Wireless Communications*, 9(11):3354–3364. [1.9](#), [7.2](#)
- [3] S. Akin and M. C. Gursoy. *Performance analysis of cognitive systems under QoS constraints and channel uncertainty*. submitted to the IEEE Transactions on Wireless Communications revised and submitted, October 2010. [1.9](#)
- [4] S. Akin and M. C. Gursoy. Training optimization for gauss-markov rayleigh fading channels. In *Proceedings of the 2007 IEEE International Conference on Communications (ICC)*, Glasgow, Scotland, UK, June 24–28 2007. [1.9](#), [3.3](#)
- [5] S. Akin and M. C. Gursoy. Achievable rates and training optimization for fading relay channels with memory. In *42nd Annual Conference on Information Sciences and Systems (CISS)*, Princeton University, Princeton, NJ, March 14–18 2008. [1.9](#)

- [6] S. Akin and M. C. Gursoy. Pilot-symbol-assisted communications with non-causal and causal wiener filters. In *9th IEEE International Workshop on Signal Processing Advances in Wireless Communications (SPAWC)*, Recife, Brazil, July 6–9 2008. [1.9](#), [4.2](#)
- [7] S. Akin and M. C. Gursoy. Performance analysis of cognitive radio systems under qos constraints and channel uncertainty. In *IEEE Global Communications Conference Exhibition and Industry Forum (GLOBECOM)*, Miami, FL, December 6–10 2010. [1.9](#)
- [8] S. Akin and M. C. Gursoy. Qos analysis of cognitive radio channels with perfect csi at both receiver and transmitter. In *IEEE Wireless Communications and Networking (WCNC)*, Sydney, Australia, April 18–21 2010. [1.9](#)
- [9] S. Akin and M. C. Gursoy. On the performance limits of cognitive mimo channels. In *IEEE Wireless Communications and Networking (WCNC)*, Cancun, Quintana-Roo, Mexico, March 28–31 2011. [1.9](#)
- [10] S. Akin and M.C. Gursoy. Effective capacity analysis of cognitive radio channels for quality of service provisioning. In *Proceedings of the IEEE Global Communications Conference (Globecom)*, Honolulu, HI, November 30–December 4 2009. [1.9](#)
- [11] S. Akin and M.C. Gursoy. Cognitive radio transmission under interference limitations and qos constraints. In *Proceedings of IEEE International Conference on Communications (ICC)*, Capetown, South Africa, May 23–27 2010. [1.9](#), [1](#)
- [12] V. Asghari and S. Aissa. Rate and power adaptation for increasing spectrum efficiency in cognitive radio networks. In *IEEE International Conference on Communications (ICC)*, Dresden, Germany, June 14–18 2009. [1.6](#)

- [13] J. Baltersee, G Fock, and H. Meyr. Achievable rate of mimo channels with data-aided channel estimation and perfect interleaving. *IEEE Journal on Selected Areas in Communications*, 19(12):150–152. [1.2](#)
- [14] J. Baltersee, G Fock, and H. Meyr. An information theoretic foundation of synchronized detection. *IEEE Transactions on Communications*, 49(12):2115–2123. [1.2](#)
- [15] S. Boyd and L. Vandenberghe. *Convex Optimization*. Cambridge University Press, March 2004. [1](#)
- [16] B.Wang, J.Zhang, and L.Zheng. Achievable rates and scaling laws of power constrained wireless sensory relay networks. *IEEE Transactions on Information Theory*, 52(9):4084–4104. [1.2](#)
- [17] J.K. Cavers. An analysis of pilot symbol assisted modulation for rayleigh fading channels. *IEEE Transactions on Vehicular Technology*, 40(4):686–693, November 1991. [1.2](#)
- [18] J.K. Cavers. Pilot assisted symbol modulation and differential detection in fading and delay spread. *IEEE Transactions on Information Theory*, 43(7):2206–2212, July 1995. [1.2](#)
- [19] C.-S. Chang. Stability, queue length, and delay of of deterministic and stochastic queuing networks. *IEEE Transactions on Automatic Control*, 39(5):913–931. [1.5](#)
- [20] C.-S. Chang. *Performance Guarantees in Communication Networks*. Springer, first edition, April 1995. [A, A, D, D, G, G, H, H](#)

- [21] C.-S. Chang and T. Zajic. Effective bandwidths of departure processes from queues with time-varying capacities. In *Proceedings of IEEE Infocom*, Boston, MA, April 2–6 1995. 5.3.2
- [22] Y. Chen, Q. Zhao, and A. Swami. Joint design and separation principle for opportunistic spectrum access. In *Proceedings 40th IEEE Asilomar Conference on Signals, Systems, Computers*, Monterey, CA, October 29–November 1 2006. 1.3, 1.4
- [23] N. Devroye, P. Mitran, and V. Tarokh. Achievable rates in cognitive radio channels. *IEEE Transactions on Information Theory*, 52(5):1813–1827. 1.3
- [24] M. Gabriella di Benedetto, Y. Hua, T. Kaiser, and X. Wang. Cognitive radio technology. *IEEE Signal Processing Magazine*, 25(6):10–198. 1.7
- [25] T. Ericson. A gaussian channel with slow fading. *IEEE Transactions on Information Theory*, 16(3):353–355, May 1970. 1.1
- [26] F. Gao, R. Zhang, Y.-C. Liang, and X. Wang. Design of learning-based mimo cognitive radio systems. *IEEE Transactions on Vehicular Technology*, 59(4):1707–1720. 1.8
- [27] S. Geirhofer, L. Tong, and B. M. Sadler. A measurement-based model for dynamic spectrum access in wlan channels. In *Military Communications Conference*, Washington D.C., October 23–25 2006. 1.3
- [28] A. Ghasemi and E. Sousa. Spectrum sensing in cognitive radio networks: The cooperation-processing tradeoff. *Wireless Communications and Mobile Computing*, 7(9):1049–1060. 1.6



- [29] A. Ghasemi and E. S. Sousa. Spectrum sensing in cognitive radio networks: Requirements, challenges and design trade-offs. *IEEE Communications Magazine*, 46(4):32–39. 1.4
- [30] A. Goldsmith, S. A. Jafar, N. Jindal, and S. Vishwanath. Capacity limits of mimo channels. *IEEE Journal on Selected Areas in Communications*, 21(5):684–702. 1.8
- [31] A.J. Goldsmith and M.S. Alouini. Comparison of fading channel capacity under different csi assumptions. In *Proceedings of IEEE Vehicular Technology Conference (VTC)*, Tokyo, Japan, September 24–28 2000. 1.1
- [32] A.J. Goldsmith and P.P. Varaiya. Capacity of fading channels with channel side information. *IEEE Transactions on Information Theory*, 43(6):1992–1996, November 1997. 1.1
- [33] M. C. Gursoy. *MIMO wireless communications under statistical queuing constraints*. submitted to the *IEEE Transactions on Information Theory*, September 2009. 1.8, 1.9
- [34] M. C. Gursoy. On the capacity and energy efficiency of training-based transmissions over fading channels. *IEEE Transaction on Information Theory*, 55(10):4543–4567. 7.4
- [35] M. C. Gursoy. An energy efficiency perspective on training for fading channels. In *Proceedings of IEEE International Symposium on Information Theory (ISIT)*, Nice, France, June 24–29 2007. 4.2

- [36] M. C. Gursoy, D. Qiao, and S. Velipasalar. Analysis of energy efficiency in fading channel under qos constraints. *IEEE Transactions on Wireless Communications*, 8(8):4252–4263. 1.5
- [37] B. Hassibi and B. M. Hochwald. How much training is needed in multiple-antenna wireless links? *IEEE Transactions on Information Theory*, 49(4):951–963. 1.2, 2.4, 2.4, 4.4, 7.4
- [38] R. A. Horn and C. R. Johnson. *Matrix Analysis*. Cambridge University Press, February 1985. 8.3.1
- [39] J. Mitola III and G. Q. Maguire. Cognitive radio: Making software radios more personal. *IEEE Personal Communications*, 6(4):13–18. 1.3
- [40] H. Jiang, L. Lai, R. Fan, and H. V. Poor. Cognitive radio: How to maximally utilize spectrum opportunities in sequential sensing. In *Global Telecommunications Conference*, New Orleans, LA, November 30–December 4 2008. 1.3, 1.4
- [41] E. A. Jorswieck, R. Mochaourab, and M. Mittelbach. Effective capacity maximization in multi-antenna channels with covariance feedback. In *Proceedings of IEEE International Conference on Communications (ICC)*, Dresden, Germany, June 14–18 2009. 1.8
- [42] A. Jovicic and P. Viswanath. Cognitive radio: An information-theoretic perspective. *IEEE Transactions on Information Theory*, 55(9):3945–3958. 1.3
- [43] Y. Jung and A. M.-C. So. *Optimal Spectrum Sharing in MIMO Cognitive Radio Networks via Semidefinite Programming*. [http : //arxiv.org/PS\\_cache/arxiv/pdf/1006/1006.4225v2.pdf](http://arxiv.org/PS_cache/arxiv/pdf/1006/1006.4225v2.pdf). 1.8

- [44] T. Kailath, A.H. Sayed, and B. Hassibi. *Linear Estimation*. Upper Saddle River, first edition, April 2000. [3.3](#), [3.3](#), [4.2](#)
- [45] H. Kim and K. G. Shin. Efficient discovery of spectrum opportunities with mac-layer sensing in cognitive radio networks. *IEEE Transactions on Mobile Computing*, 7(5):533–545. [1.3](#)
- [46] J.N. Laneman. *Cooperation in wireless networks: Principles and applications*. Springer, ch.1 Cooperative Diversity: Models, Algorithms, and Architectures, first edition, July 2006. [1.2](#)
- [47] J.N. Laneman, D.N.C. Tse, and G.W. Wornel. Cooperative diversity in wireless networks: Efficient protocols and outage behavior. *IEEE Transactions on Information Theory*, 50(12):3062–3080. [1.2](#), [4.5](#)
- [48] A. Lapidoth and S. Shamai (Shitz). Fading channels: How perfect need ‘perfect side information’ be? *IEEE Transaction on Information Theory*, 48(5):1118–1134. [7.4](#)
- [49] W.C.Y. Lee. Estimate of channel capacity in rayleigh fading environment. *IEEE Transactions on Vehicular Technology*, 39(3):187–189, August 1990. [1.1](#)
- [50] Y.-C. Liang, Y. Zheng, E. C. Y. Peh, and A. T. Hoang. Sensing-throughput tradeoff for cognitive radio networks. *IEEE Transactions on Wireless Communications*, 7(4):1326–1337. [1.4](#), [1.6](#), [5.2](#), [5.2](#), [6.1](#), [7.2](#), [7.2](#)
- [51] L. Liu and J.-F. Chamberland. On the effective capacities of multiple-antenna gaussian channels. In *IEEE International Symposium on Information Theory*, Toronto, Canada, July 6–11 2008. [1.8](#), [5.3.2](#)

- [52] L. Liu, P. Parag, J. Tang, W.-Y. Chen, and J.-F. Chamberland. Resource allocation and quality of service evaluation for wireless communication systems using fluid models. *IEEE Transactions on Information Theory*, 53(5):1767–1777. 1.5
- [53] A. Lozano and A. M. Tulino. Capacity of multiple-transmit multiple-receive antenna architectures. *IEEE Transaction on Information Theory*, 48(12):3117–3128. 1.8
- [54] A. Lozano, A. M. Tulino, and S. Verdú. Multiple-antenna capacity in the low-power regime. *IEEE Transaction on Information Theory*, 49(10):2527–2544. 1.8, 8.3.2
- [55] T. L. Marzetta and B. M. Hochwald. Capacity of a mobile multiple-antenna communication link in rayleigh flat fading. *IEEE Transactions on Information Theory*, 45(1):139–157, January 1999. 1.1
- [56] I. Abou-Faycal M. Médard and U. Madhow. Binary adaptive coded pilot symbol assisted modulation over rayleigh fading channels without feedback. *IEEE Transactions on Communications*, 53(6):1036–1046. 1.2, 2.1
- [57] L. Musavian and S. Aissa. Capacity and power allocation for spectrum-sharing communications in fading channels. *IEEE Transactions on Wireless Communications*, 8(1):148–156. 1.6
- [58] L. Musavian and S. Aissa. Quality-of-service based power allocation in spectrum-sharing channels. In *IEEE Global Communication Conference (GlobeCom)*, New Orleans, LA, November 30–December 4 2008. 1.7, 6.3

- [59] L. Musavian and S. Aissa. Adaptive modulation in spectrum-sharing systems with delay constraints. In *IEEE International Conference on Communications (ICC)*, Dresden, Germany, June 14–18 2009. 1.7
- [60] S. Ohno and G.B. Giannakis. Average-rate optimal psam transmissions over time-selective fading channels. *IEEE Transactions on Wireless Communications*, 1(4):712–720. 1.2, 3.3
- [61] N. Devroye P. Mitran and V. Tarokh. On compound channels with side information at the transmitter. *IEEE Transactions on Information Theory*, 52(4):1745–1755. 1.3
- [62] S. M. Perlaza, N. Fawaz, S. Lasaulce, and M. Debbah. From spectrum pooling to space pooling: Opportunistic interference alignment in mimo cognitive networks. *IEEE Transactions on Signal Processing*, 58(7):3728–3741. 1.8
- [63] H. V. Poor. *An Introduction to Signal Detection and Estimation*. Springer-Verlag, second edition, March 1994. 5.2, 5.2, 6.1, 7.2, 7.2
- [64] M. C. Gursoy H. V. Poor and S. Verdú. The noncoherent rician fading channel – Part I : Structure of the capacity-achieving input. *IEEE Transactions on Wireless Communications*, 4(5):2193–2206, September 2005. 1.1
- [65] D. Qiao, M. C. Gursoy, and S. Velipasalar. Energy efficiency in the low-snr regime under queueing constraints and channel uncertainty. In *Proceedings of the IEEE Global Communications Conference (Globecom)*, Honolulu, HI, November 30–December 4 2009. 3
- [66] Z. Quan, S. Cui, H. V. Poor, and A. H. Sayed. Collaborative wideband sensing for cognitive radios. *IEEE Signal Processing Magazine*, 25(6):60–73. 1.3

- [67] Z. Quan, S. Cui, A. H. Sayed, and H. V. Poor. Wideband spectrum sensing in cognitive radio networks. In *Proceedings of IEEE International Conference on Communications*, Beijin, China, May 19–23 2008. [1.6](#), [6.1](#)
- [68] L. Tong B.M. Sadler and M. Dong. Pilot-assisted wireless transmissions. *IEEE Signal Processing Magazine*, 21(6):12–25, November 2004. [1.2](#)
- [69] S. Sandhu, R. U. Nabar, D. A. Gore, and A. Paulraj. Near-optimal selection of transmit antennas for a mimo channel based on shannon capacity. In *Proceedings 34th IEEE Asilomar Confonference on Signals, Systems, Computers*, Pasific Grove, CA, October 29–November 1 2000. [1.8](#)
- [70] M. F. Sencan and M. C. Gursoy. Achievable rates for pilot-assisted transmission over rayleigh fading channels. In *Proceedings of the 40th Annual Conference on Information Science and Systems (CISS)*, Princeton University, Princeton, NJ, March 22–24 2006. [1.2](#)
- [71] O. Simeone, Y. Bar-Ness, and U. Spagnolini. Stable throughput of cognitive radios with and without relaying capability. *IEEE Transactions on Communications*, 55(12):2351–2360. [1.5](#)
- [72] S. Sridharan and S. Vishwanath. On the capacity of a class of mimo cognitive radios. *IEEE Journal of Selected Topics in Signal Processing*, 2(1):103–117. [1.8](#)
- [73] S. Srinivasa, S. A. Jafar, and N. Jindal. On the capacity of the cognitive tracking channel. In *IEEE International Symposium on Information Theory*, Seattle, WA, July 9–14 2006. [1.3](#)

- [74] J. Tang and X. Zhang. Cross-layer-model based adaptive resource allocation for statistical qos guarantees in mobile wireless networks. *IEEE Transactions on Wireless Communications*, 7(6):2318–2328. 1.5, 5.3.2
- [75] J. Tang and X. Zhang. Quality-of-service driven power and rate adaptation for multichannel communications over wireless links. *IEEE Transactions on Wireless Communications*, 6(12):4349–4360. 1.5
- [76] J. Tang and X. Zhang. Quality-of-service driven power and rate adaptation over wireless links. *IEEE Transactions on Wireless Communications*, 6(8):3058–3068. 1.5, 5.4.2, C
- [77] I. E. Telatar. Capacity of multi-antenna gaussian channels. *European Transactions on Telecommunications*, 10(6):585–596. 1.8
- [78] S. Adireddy L. Tong and H. Viswanathan. Optimal placement of training for unknown channels. In *Conference on Information Sciences and Systems (CISS)*, The Johns Hopkins University, Baltimore, MD, March 21–23 2001. 1.2
- [79] I. Abou-Faycal M. D. Trott and S. Shamai (Shitz). The capacity of discrete-time memoryless rayleigh fading channels. *IEEE Transactions on Information Theory*, 47(4):1290–1301, May 2001. 1.1
- [80] S. Venit and R. Katz. Eigenvalues of matrices of low rank. *The College Mathematics Journal*, 31(3):208–210. G
- [81] S. Verdú. Spectral efficiency in the wideband regime. *IEEE Transaction on Information Theory*, 48(6):1319–1343. 8.3.2, 8.3.2, 8.3.2
- [82] Z. Wang and G. B. Giannakis. Outage mutual information of space-time mimo channels. *IEEE Transaction on Information Theory*, 50(4):657–662. 8.4

- [83] D. Wu and R. Negi. Effective capacity: A wireless link model for support of quality of service. *IEEE Transactions on Wireless Communications*, 2(4):630–643. 1.5, 1.9, 5.3.2
- [84] J. Zhang and M.C. Gursoy. Achievable rates and optimal resource allocation for imperfectly-known relay channels. In *Proceedings of 45th Annual Allerton Conference on Communication, Control and Computing*, University of Illinois at Urbana-Champaign, September 26–28 2007. 4.4
- [85] R. Zhang and Y. C. Liang. Exploiting multi-antennas for opportunistic spectrum sharing in cognitive radio networks. *IEEE Journal of Selected Topics in Signal Processing*, 2(1):88–102. 1.8
- [86] Q. Zhao, S. Geirhofer, L. Tong, and B. M. Sadler. Opportunistic spectrum access via periodic channel sensing. *IEEE Transactions on Signal Processing*, 56(2):785–796. 1.3, 1.4
- [87] Q. Zhao and B. Sadler. A survey of dynamic spectrum access. *IEEE Signal Processing Magazine*, 24(3):79–89. 1.3